

**Investigating the biosafety and toxicity of magnetic  
iron oxide nanoparticles *in vitro* and *in vivo***



A thesis submitted for the degree of

Doctor of Philosophy

by

**Ruchira Mann**

College of Health, Medicine and Life Sciences

Brunel University London

February 2021

## **Declaration of work**

I hereby declare that all work undertaken in this thesis is of my own, unless otherwise specified. This thesis has been submitted solely for the degree of Doctor of Philosophy.

Ruchira Mann

## Abstract

Nanoparticles (NPs) are promising tools for a broad range of clinical applications, including therapeutic purposes. The surfaces of NPs can be modified for targeted therapy and a controlled drug release can be achieved with NPs as drug carriers, which is particularly desirable in the treatment of cancer to reduce side effects. However, their biosafety is still of concern due to toxic effects exhibited by NPs. Furthermore, upon administration, NPs will unavoidably come into contact with blood serum proteins and cells of the innate immune system, which is the body's first line of defence. This can result in unwanted clearance of NPs by phagocytic cells such as macrophages, thus reducing their therapeutic efficacy. Here, we aimed to investigate the intracellular fate and toxicity of starch coated fluorescent iron oxide nanoparticles (IONPs) in mouse macrophages by using immunohistochemistry and microscopy techniques. We show that different protein corona compositions on the surface of IONPs can influence their uptake and also show that IONPs can enter cells through more than one endocytic pathway, including macropinocytosis, by using different sized fluorescent dextran molecules as endocytic markers. Through cytokine profiling using qPCR and transcriptome profiling using RNA-sequencing, we investigated the cellular immunotoxicity of IONPs by identifying particular biomarkers and genes which are involved in inflammatory processes. IONP toxicity was studied *in vivo* using zebrafish (*Danio rerio*) embryos as animal models following microinjections of IONPs. Biodistribution of IONPs was studied with confocal microscopy. Macrophages were labelled by microinjecting a high molecular weight dextran to investigate uptake of IONPs by macrophages *in vivo*, which was low. IONPs accumulated mostly in the pericardium and liver at 5dpf and overall a low mortality rate was recorded.

## Table of Contents

<b>Abstract.....</b>	<b>ii</b>
<b>Acknowledgements.....</b>	<b>vi</b>
<b>Abbreviations: .....</b>	<b>vii</b>
<b>1. Introduction.....</b>	<b>1</b>
<b>1.1 Nanomedicine: An Overview .....</b>	<b>2</b>
<b>1.2 Current examples of nanoparticles in drug delivery .....</b>	<b>4</b>
<b>1.3 Nanotherapeutics in cancer and other diseases.....</b>	<b>6</b>
<b>1.4 Iron Oxide Nanoparticles .....</b>	<b>8</b>
<b>1.5 Nanoparticles and the immune system .....</b>	<b>11</b>
<b>1.6 Macrophages and other phagocytes .....</b>	<b>18</b>
<b>1.7 Nanoparticle Uptake Mechanisms .....</b>	<b>21</b>
<b>1.8 Nanoparticle uptake by macrophages .....</b>	<b>27</b>
<b>1.9 Intracellular trafficking of NPs.....</b>	<b>29</b>
<b>1.10 Biomarkers of Nanoparticle immunotoxicity .....</b>	<b>32</b>
<b>1.11 Transcriptome profiling to assess nanoparticle toxicity.....</b>	<b>37</b>
<b>1.12 Animal models to study nanoparticle toxicity .....</b>	<b>38</b>
<b>Aim .....</b>	<b>40</b>
<b>2. Materials and Methods.....</b>	<b>41</b>
<b>2.1 Materials .....</b>	<b>42</b>
<b>2.2 Cell Culture .....</b>	<b>43</b>

2.3 Preparation of cells .....	44
2.4 Preparation and Addition of Nanoparticles.....	44
2.5 Immunofluorescence Staining.....	48
2.5.1 Colocalisation quantification.....	52
2.6 Veronal buffers .....	53
2.7 LysoTracker.....	54
2.8 Dextran: a marker for fluid phase endocytosis .....	54
2.9 Western Blotting .....	55
2.10 Quantitative RT PCR .....	57
2.11 RNA Sequencing and Transcriptome analysis.....	60
2.12 Microinjections in zebrafish ( <i>Danio rerio</i> ) embryos.....	64
2.13. Statistical Analyses .....	70
<b>3. Intracellular Localisation of Iron Oxide Nanoparticles in Mouse Macrophages.....</b>	<b>72</b>
3.1 Introduction.....	73
3.2 Results Using Human Serum .....	78
3.3 Results Using Mouse Serum.....	98
3.4 Discussion .....	126
<b>4. Immunotoxicity of Iron Oxide Nanoparticles.....</b>	<b>133</b>
4.1 Introduction.....	134
4.2 Results.....	137
5.2.2 Investigating the toxicity of IONPs using transcriptome and gene expression analysis ...	144

5.3 Discussion .....	182
<b>5. Zebrafish (<i>Danio rerio</i>) Embryos: A Model to Study Iron Oxide Nanoparticle Toxicity .</b>	<b>189</b>
5.1 Introduction .....	190
5.2 Results .....	197
5.3 Discussion .....	221
<b>6. General Discussion.....</b>	<b>227</b>
<b>7. References.....</b>	<b>235</b>

## Acknowledgements

This thesis would not have been possible without the help, guidance and support of some people.

Firstly, I would like to thank my supervisor, Dr Gudrun Stenbeck, for her utmost support throughout this project over the past few years. She is always been so caring and helpful and was always there when I needed guidance, with her office door always open. This would not have been possible without her support, guidance and expert knowledge and I will be ever so grateful for everything she has taught me, which shaped me into a better researcher. I would also like to thank my second supervisor, Dr Uday Kishore, for his guidance and constructive feedback, which helped me to think about different aspects of my work.

To my parents, who have supported me from day 1 in pursuing my goals, thank you for instilling in me good values and principles which contributed to my journey as a researcher today. Thank you to my brother who makes me laugh once in a while with his good/bad jokes! To my husband Khoshal, thank you for everything. Thank you for supporting me, pushing me to keep going and believing in me. I am truly lucky to have such an amazing and supportive partner like you.

Last but not least, I would like to thank my friends, Saqlain, Aakila and Juhi who helped me through this journey just by being there. And I look forward to our virtual coffee mornings every week! Finally, I am grateful to have studied in such an enjoyable research environment at Brunel University London. I would also like to express my sincere gratitude to my examiners Dr Helinor Johnston and Dr Anthony Tsolaki for providing insightful feedback on my work and challenging me on new aspects of my studies.

## Abbreviations:

- APCs: Antigen presenting cells
- BSA: Bovine serum albumin
- CIE: Clathrin-independent endocytosis
- CMC: Carboxymethyl cellulose
- CME: Clathrin-mediated endocytosis
- CNTs: Carbon nanotubes
- DNA: Deoxyribonucleic acid
- EDTA: Ethylenediaminetetraacetic acid
- EGTA: Ethylene glycol-bis( $\beta$ -aminoethyl ether)-N,N,N',N'-tetraacetic acid
- GO: Gene Ontology
- IFN: Interferon
- Ig: Immunoglobulin
- IL: Interleukin
- IONPs: Iron oxide nanoparticles
- MBL: Mannose-binding lectin
- MHC: Major histocompatibility complex
- NF- $\kappa$ B: Nuclear factor *kappa* B
- NPs: Nanoparticles
- PAMPs: Pathogen associated molecular patterns
- PBS: Phosphate buffered saline
- PCR: Polymerase chain reaction
- PGLA: Poly(lactic-co-glycolic acid)



- PRRs: Pattern recognition receptors
- RNA: Ribonucleic acid
- ROS: Reactive oxygen species
- SDS: Sodium dodecyl sulphate
- SPION: Superparamagnetic iron oxide nanoparticles
- TGF: Transforming growth factor
- TLRs: Toll-like receptors
- TNF: Tumour necrosis factor
- WGA: Wheat germ agglutinin

---

## **1. Introduction**

---

## 1.1 Nanomedicine: An Overview

Delivering therapeutic compounds to a target site is often a major problem in the treatment of many diseases. This can be characterised by factors such as poor biodistribution, limited effectiveness and lack of selectivity. However, these drawbacks can be surpassed by controlling drug delivery to the target sites. Nanoparticles (NPs) are defined as materials with overall dimensions on the nanoscale range, with a size range of 1nm – 100nm. Due to their small size, NPs exhibit unique biological and physiochemical properties which make them desirable for biomedical applications and are thus being explored as drug and gene therapy delivery vehicles. The application of nanotechnology, first described by Professor Noro Taniguchi in 1974 (Kreuter, 2007), in medical research, in the treatment, prevention and diagnosis of diseases can be referred to as nanomedicine. In short, nanomedicine is defined as the application of nanotechnology to medicine. The main purpose of using NPs in the treatment of diseases as drug delivery vehicles is to deliver the intended drug specifically to the target cells in order to avoid numerous side effects that arise from the damage caused to normal and healthy tissues of the body.

Although the study of NPs in the treatment of diseases has made significant contributions to the field of nanomedicine, there are only a handful of NP-conjugated drugs approved for clinical use, in cancer therapeutics and other diseases. This is because several factors and limitations have to be considered when engineering NPs for drug delivery. NPs used for medical applications have to be biocompatible and non-toxic. Undesirable effects of NPs heavily depend on their shape, hydrodynamic size, surface chemistry, dosage, mode of administration, residence time in the bloodstream and reaction with the immune system (Alkilany & Murphy, 2010;

Wahajuddin & Arora, 2012). Furthermore, there are more physiological barriers that can be encountered by NPs upon administration in the bloodstream, thus making the engineering and tailoring of NPs for drug delivery even more challenging. These barriers and potential solutions to overcome those limitations are summarised below in figure 1.1.

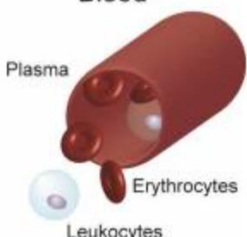


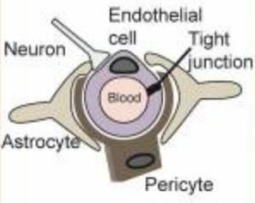
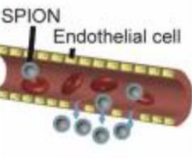
	Blood	Liver and Spleen	Kidneys	Blood-brain Barrier	Extravasation
Barrier					
Restrictions	<ul style="list-style-type: none"> <li>Highly complex fluid</li> <li>Enzyme degradation</li> <li>Immune recognition</li> </ul>	<ul style="list-style-type: none"> <li>Objects larger than 100 nm recognized and removed from circulation</li> </ul>	<ul style="list-style-type: none"> <li>Objects smaller than the 10 nm pores of the glomerulus are filtered out of the blood</li> </ul>	<ul style="list-style-type: none"> <li>Tight junctions between endothelial cells in the brain prevent passive access</li> </ul>	<ul style="list-style-type: none"> <li>Gaps between endothelial cells restrict material escape from the blood</li> </ul>
Strategies	<ul style="list-style-type: none"> <li>PEGylation</li> <li>Zwitterionic polymers</li> <li>Encapsulation of drug or biotherapeutic</li> </ul>	<ul style="list-style-type: none"> <li>Hydrodynamic size less than 100 nm</li> </ul>	<ul style="list-style-type: none"> <li>Hydrodynamic size greater than 10 nm</li> </ul>	<ul style="list-style-type: none"> <li>Osmotically shrink endothelial cells to open junctions</li> <li>Active transport across vasculature</li> </ul>	<ul style="list-style-type: none"> <li>Enhanced permeability and retention effect</li> <li>Hydrodynamic size 30 - 100 nm</li> </ul>

Figure 1.1. **Physiological barriers and restrictions encountered by nanotherapeutics.** This image provides a summary of the barriers and limitations encountered by therapeutic NPs, along with some strategies that can be investigated and explored to overcome these barriers when engineering NPs intended for drug delivery. Image from *Kievit & Zhang, 2011*.

NPs are being extensively studied by scientists across the globe for the diagnosis, prevention and treatment of diseases, including therapeutic interventions. Furthermore, NPs have also been investigated to merge their therapeutic and diagnostic properties, using only one nanomedicine formulation and these formulations are known as nanotheranostics (Rizzo et al., 2013). These nanotheranostics can be used to generate useful data on pharmacokinetics, including drug delivery, release and efficacy and can be indicative of the possibilities of using NPs in personalised medicine (Rizzo et al., 2013). Nanomedicine is proving to be a useful concept in deciphering the pathophysiology of a number of diseases and will

be highly beneficial to patients by improving their lifespan and quality of life. The use of nanomedicines have a number of advantages over the use of standard and conventional drugs (Ventola, 2012). Nanomedicines, especially NPs loaded with a drug of interest, are likely to have longer circulation times than conventional drugs as NPs have reduced hepatic degradation and excretion. The volume of drug distribution of the nanomedicines will also be reduced and hence there will be less of the drug in healthy tissues, leading to reduced side effects in patients. Using nanomedicines, which specifically target the diseased tissue, will also improve site-specific drug delivery, which means that the drug will accumulate more in the pathological site, thus improving the therapeutic index (Bala Tannan *et al.*, 2020).

## **1.2 Current examples of nanoparticles in drug delivery**

NPs have come a long way in the diagnosis and treatment of many diseases, including cancer, where patients would benefit greatly from targeted therapy. For example: a 'hybrid' micellar NP with multifunctional properties has been recently developed. It contains metal NPs useful in MRI detection, quantum dots for fluorescent imaging, polyethylene glycol (PEG) for increased circulation times, the tumour-specific F3 peptide for targeting and doxorubicin as the therapeutic agent (Jain *et al.*, 2012). The 'hybrid' NP formulation showed to be efficient in a mouse model that was implanted with human breast cancer cells (Park *et al.*, 2008). An important evidence of the potential function of gold NPs (GNPs) as a drug delivery mechanism was the use of 5 nm GNPs covalently bound to cetuximab, a monoclonal anti-epidermal growth factor receptor (EGFR) antibody, as a targeted therapy and gemcitabine (an anti-metabolite) as a therapeutic payload investigated in pancreatic cancer (Patra *et al.*, 2010). EGFR is overexpressed in about 60% of pancreatic cancers and the combination of

cetuximab and gemcitabine was investigated in phase II trials for pancreatic cancer. The GNP-cetuximab-gemcitabine nanocomplex was found to be superior to the use of the agents alone or in combination *in vitro* and *in vivo* (Jain, Hirst and O'Sullivan, 2012).

NPs, liposomes, polymers, antibodies and micelles have all been investigated as carrier materials in the field of nanotherapeutics. An example of a nanotherapeutic being studied is for the delivery of paclitaxel (taxol). The study of poly(lactic-co-glycolic acid) (PGLA) NPs in the paclitaxel formulation showed an increase in cytotoxicity to cancer cells as well as an effective therapeutic method *in vivo* using male rat models (Win and Feng, 2006).

In comparison to standard diagnostics methods, there are not many diagnostic imaging methods that are currently using nanomedicine formulations (nanodiagnostics). One example of clinical studies using nanodiagnostics is the usage of Resovist-like iron oxide NPs (IONPs) in the observation of macrophage activity in atherosclerosis, injected cancer vaccines, lymph node metastases and neural stem cells (Rizzo *et al.*, 2013).

The development of nanotechnology in surgery is still under extensive study but as surgical procedures are becoming less invasive, nanotechnology and its application to surgical procedures has immense potential (Singh and Singh, 2013).

Other than diagnostic and therapeutic purposes, NPs have made significant advances in the development of vaccine formulations. The use of NPs in vaccines can be more favourable than conventional vaccines since a number of parameters such as shape, solubility, size and surface chemistry can be precisely controlled (Al-Halifa *et al.*,

2019). For example, a recently developed vaccine against SARS-CoV-2 by BioNtech and Pfizer used NPs as the delivery vehicles to intravenously administer an mRNA-based vaccine (Polack *et al.*, 2020).

### **1.3 Nanotherapeutics in cancer and other diseases**

Nanomedicine as an alternative treatment for cell-based therapeutics is proving to be an effective strategy that is more specific than conventional drugs in a range of diseases such as neurological diseases (for example: multiple sclerosis, Parkinson's disease, Alzheimer's disease), diabetes and cancer (M Samarasinghe *et al.*, 2012). PGLA NPs are being broadly studied as drug delivery vehicles in the treatment of neurological disorders as they are able to cross the blood brain barrier generating promising results (Semete *et al.*, 2010). In addition, PGLA NPs have also shown no signs of cytotoxicity. They are eliminated from the body by first undergoing hydrolysis forming compounds that are metabolised by the citric acid cycle (Semete *et al.*, 2010).

The concept of personalised medicine has received a lot of attention, especially in the treatment of cancer. Similar to how every individual is unique, the cancerous lesions are also unique to the patients and each one will be different in terms of disease onset, progression and treatment efficacy. These can be useful factors to exploit for better clinical management of the disease. Personalised medicine is an individualised therapy, which is designed after considering the unique disease profiles of each patient. Through personalised medicine, clinicians can make fairly accurate predictions on the progression of the disease, effectiveness of therapy and the patient's chances of relapse, all with a maximum therapeutic index and minimal toxicity for the patient (Jackson and Chester, 2015). With advances in sequencing

technologies and completion of the Human Genome Project in 2003, techniques such as genome sequencing, transcriptomic analysis and proteomic analysis are being increasingly used with the aim of identifying specific mutations, biomarkers or pathways associated with a disease to be used as predictive tools for the development of effective treatment plans (Krzyszczuk *et al.*, 2018). This is particularly useful in the treatment of cancer. For example, a recent study showed that whole-genome sequencing of a prostate cancer patient revealed that his cancer was driven by a specific mutation and this provided important information for potential future treatments using a personalised medicine approach (Armstrong *et al.*, 2021). Due to their current limitations in developing the formulation, only a few personalised medicines have been clinically tested, the best example being the identification of the oestrogen receptor (ER) in breast cancer treatment (Ellsworth *et al.*, 2010). These drawbacks mainly include the high failure rate of personalised medicine and identifying valid biomarkers (Liu, 2012). Some therapeutic NPs in the form of liposomes that have been clinically approved for cancer treatment are doxil, myocet and liposomal doxorubicin, which were also the first kind of nanotherapeutics to be clinically approved (Shi *et al.*, 2016). NPs have also been conjugated with ligands specific to the patient with the intention of targeting specific cancer cells in order to have a better treatment efficacy; an example is  $\alpha_v\beta_3$ -targeted paramagnetic NPs to identify angiogenesis sites of melanoma tumours in a non-invasive manner (Schmieder *et al.*, 2005).

Iron oxide nanoparticles (IONPs), due to their magnetic properties, have proven to be useful for magnetic resonance imaging and have been used to monitor cells following



transplants, including neural cells, stem cells as well as bone marrow cells (M Samarasinghe, K Kanwar and R Kanwar, 2012).

Nanomedicine formulations can also be used in regenerative medicine, where the primary focus lies in restoring and maintaining the normal functions of cells, tissues, the extracellular matrix and even organs that have previously been damaged (Engel et al., 2008). Diseases such as osteoporosis, Parkinson's disease, spine injuries, Alzheimer's disease as well as cancer can benefit from regenerative medicine. Regenerative medicine research is still at an early stage and there are two main strategies that scientists are working on. The first one involves using 3D scaffolds to expand stem cells collected from the patient, which are first expanded in vitro and then implanted back into the patient; and the second method is the development of NPs that would send multiple signals to the stem cells in the patient which would subsequently induce the regeneration of the damaged tissue (Engel *et al.*, 2008).

#### **1.4 Iron Oxide Nanoparticles**

Iron oxide nanoparticles (IONPs) are widely desirable for their magnetic and catalytic properties. Magnetic NPs have very unique properties such as high magnetic susceptibility, low Curie temperature, superparamagnetic and high coercivity (Wu et al., 2008). Magnetic NPs are also used in many bioapplications such as detection of biological materials, magnetic bioseparation, clinical diagnosis and therapeutics (Wu, He and Jiang, 2008). For example: IONPs are useful in magnetic fluid hyperthermia treatment (MFH), which is used in the treatment of cancers by specifically heating the area of malignancy, changing the physiology of the cells and inducing apoptosis (Hildebrandt, 2002).

Novel drug delivery vehicles are also being developed using magnetic IONPs and the help of an external magnetic field to target the NPs to a particular site as a strategy in the development of superparamagnetic iron oxide NPs (SPIONs) (Wahajuddin and Arora, 2012). Delivering anticancer drugs with functionalised SPIONs to a specific target site is an area of high interest in the development of cancer treatment strategies; for example: SPION-induced hyperthermia has been used for the localised killing of cancer cells (Wahajuddin and Arora, 2012).

The biological applications of magnetic IONPs require the iron to be in an aqueous salt environment. In order to prevent oxidisation of the iron in this environment, a gold coating on the IONPs can be used, which will however affect their magnetic properties.

The magnetic properties, including large surface area to volume ratio, of IONPs make them one of the most favourable and promising drug delivery vehicles. SPIONs are one of the easiest formulations to produce and have proved to have the least toxicity (Wahajuddin and Arora, 2012). The ability to control magnetic NPs externally by using a magnet is another promising targeting mechanism. Carcinomas that are close to the surface of the skin are highly likely to benefit from magnetic targeting therapy. Despite being so promising, there are only a handful of magnetic NPs used in drug delivery on the market. This is because there are many limitations and more toxicity issues to overcome, before they are clinically safe to be used. Some IONPs that are currently clinically approved or in the clinical trial stage are summarised in the table below.

Generic Name	IONP Coating	Blood half-life	Stage	Reference
<b>Ferumoxtran-10</b>	Dextran	> 24 hours	Clinical trial	(Harisinghani <i>et al.</i> , 2006)
<b>Ferumoxides</b>	Dextran	10 minutes	Clinically approved	(Wang, 2011)
<b>Ferucarbotran</b>	Carboxy-dextran	12 minutes for 60-80nm, 6-8 hours for 20-25nm	Clinically approved	(Wang, 2011; Vellinga <i>et al.</i> , 2009)
<b>Feruglose</b>	PEGylated starch	2 hours	Clinical trial	(Daldrup-Link <i>et al.</i> , 2003)
<b>Ferumoxytol</b>	Carboxymethyl-dextran	10-14 hours	Clinically approved	(Muehe <i>et al.</i> , 2016)
<b>Nanotherm</b>	Aminosilane	-	Clinically approved in Europe	(Maier-Hauff <i>et al.</i> , 2011)

Table 1.1. **Magnetic Iron Oxide Nanoparticles applications in nanomedicine.** This table summarises some IONPs that are currently clinically approved or that are still in the clinical trials phase. Most of the formulations mentioned above are most commonly used as contrast agents such as for lymph node imaging, liver imaging and macrophage imaging. Nanotherm was approved in 2010 in Europe only for glioblastoma therapy. At the time of writing, the literature suggests that the Nanotherm therapy system may soon receive FDA approval in the US for the treatment of prostate cancer.

In this thesis, 100nm spherical magnetic IONPs with a starch coating were used in all studies with the aim of further understanding their biosafety and toxicity. Although many studies have emphasized on the promising nature of IONPs for therapeutic purposes, only a few IONP formulations as mentioned in the table above have been approved for clinical use, suggesting a big gap between paradigm and end-use of IONPs in drug delivery. Despite IONPs being chemically inert (Vallabani and Singh,

2018), there is a need for further studies investigating toxicity of IONPs and their interactions with the immune system in order to develop strategies where maximum therapeutic efficiency is obtained. Currently, all approved IONP formulations are iron oxide-carbohydrate based or colloids using small spherical iron oxide-carbohydrate NPs (Soetaert *et al.*, 2020), emphasizing the potential of spherical NPs. Furthermore, the presence of a carbohydrate coating provides stability to the IONP core with the aim of slowing down the release of Fe in blood or biological media (Auerbach and Ballard, 2010). Other than shape and outer shell coating, the size of IONPs also play a role in determining the bioavailability hence therapeutic efficiency of IONPs. One study has shown that for intracellular drug delivery, the favourable particle size for IONPs is between 10nm – 100nm as these provide the longest blood circulation times (Turrina, Berensmeier and Schwaminger, 2021). Thus, through the studies carried out in this thesis, we aim to contribute to the existing literature by understanding intracellular behaviour and toxicity of 100nm starch coated spherical IONPs.

## **1.5 Nanoparticles and the immune system**

The immune system is an interactive and intricate network consisting of mainly cells and cytokines. Being the body's first line of defence, the immune system has the primary task of detecting foreign substances to protect the host whilst preserving the integrity of the body. Abnormal functioning of the immune system will result in infections, immunodeficiency disorders, autoimmune diseases and can even result in the formation of tumours. The immune system has two different subsystems: the innate immune system and the adaptive immune system.

The innate immune system is usually the first response triggered upon exposure to a foreign substance and phagocytic macrophages will recognise and bind to the

receptors of the foreign substances, which will induce the production of cytokines (figure 1.2) (Mogensen, 2009).

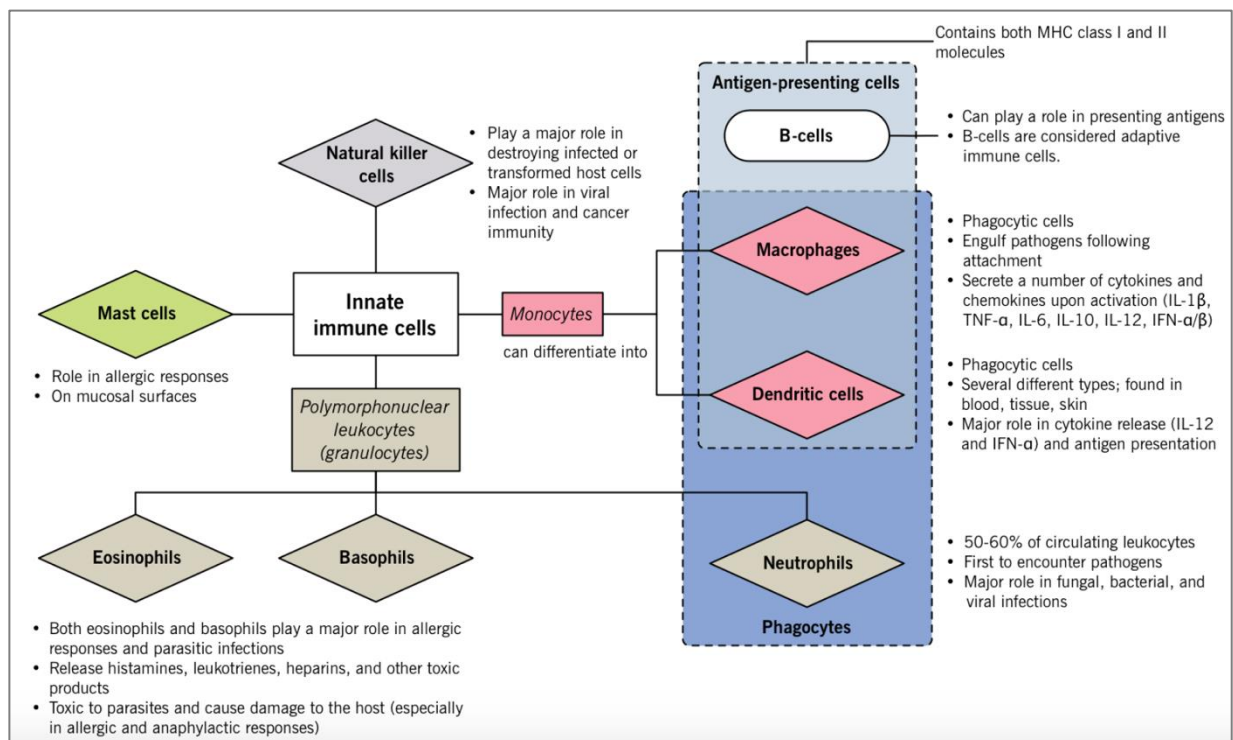


Figure 1.2. **Overview of innate immune cells.** This figure shows the different innate immune cells and their role in the host's immune defence mechanism. The first and main cells involved in the innate immune system are macrophages, which are differentiated from their precursors; monocytes. Cells of the innate immune system such as macrophages and dendritic cells can activate B cells (of the adaptive immune) system through antigen presentation and recognition, thus bridging the link between innate and adaptive immunity. *Image from: Chaudhry, 2016.*

The above figure provides an overview of the cells of the innate immune system and the role they play in innate immunity. Innate immune cells such as monocytes can be activated and differentiate into phagocytic cells such as macrophages and dendritic cells. The activated macrophages will also secrete chemokines, which are proteins that will attract other phagocytes from the bloodstream such as neutrophils and monocytes as they have chemokine receptors on their surface (Charles A Janeway et al., 2001). Cytokines and chemokines are produced by activated macrophages upon exposure to foreign substances, which is the first part of the inflammation process. It can also trigger complement activation. Complement consists of proteins that will be

cleaved into smaller peptides to coat the surface of the foreign substance to be recognised and destroyed by the phagocytic cells (figure 1.3).

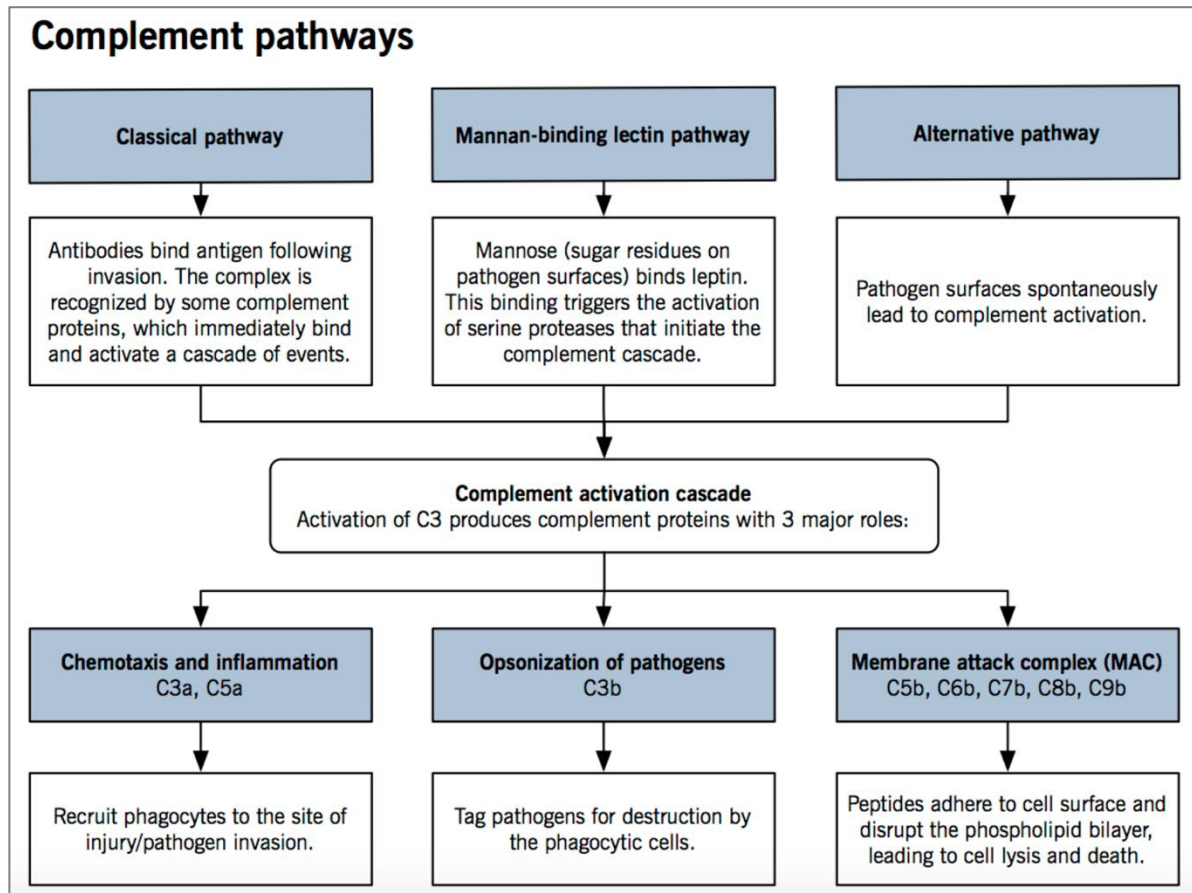


Figure 1.3. **Complement pathway activation.** This figure illustrates the three different pathways through which the complement system can be activated: the classical pathway, mannan-binding lectin pathway and alternative pathway. Although they are activated differently, all three pathway activations converge up to the formation of complement protein C3. *Image from: Chaudhry, 2016.*

The above figure shows an overview of the 3 pathways of the complement system. Regardless of how they are activated, all 3 pathways lead to the formation of the enzyme C3 convertase, which is crucial for the cleavage of other proteases and convertases in order to be able perform specific functions in the clearance of pathogens (figure 1.3). The complement system can be activated through three different pathways: classical pathway, alternative pathway and lectin pathway (figure 1.3). The classical pathway involves the complement C1 protein complex, whose production is initiated by antigen-antibody immune complexes (Noris and Remuzzi,

2013). When C1q molecules bind to the antigen-antibody immune complexes, conformational changes occur in the C1q molecules, which leads to activation and cleavage of other proteases and convertases; for example C1q cleaves C4 and C2 into classical pathway convertase, C4bC2a, which further cleaves C3 convertases into C3a and C3b (Nesargikar et al., 2012). The alternative pathway is not stimulated by antibody-antigen complexes but by lipids, carbohydrates and proteins found on the surface of foreign substances and pathogens (Sarma and Ward, 2011). The alternative pathway is usually constantly active at a low level in the body and involves the protein convertase C3 that undergoes hydrolysis to form C3b, which then coats the surface of the foreign pathogens (Merle et al., 2015).

The lectin pathway bears many similarities to the classical pathways, except for the initial activation stimuli. Instead of C1q in the classical pathway, the lectin pathway is activated when mannose binding lectin (MBL) or ficolin bind to specific carbohydrate patterns on the surface of foreign pathogens (Sarma and Ward, 2011). MBL-associated serine proteases (MASP), similar to C1 in the classical pathway, cleave C2 and C4 forming C3 convertase, which is further cleaved into C3a and C3b (Nesargikar, Spiller and Chavez, 2012).

Studies have shown that carbon nanotubes can trigger complement activation via the classical and alternative pathways in a human monocytic cell line, although higher activation via the classical pathway was observed, which may depend on the coating of the carbon nanotubes (Pondman *et al.*, 2014). The activation of complement also showed an increased uptake by phagocytic cells.

The innate immune system of a host provides immediate defence against foreign substances and in contrast to the adaptive immune system, does not provide long-lasting immunity. The adaptive immune system provides long-lasting immunity against

infections and diseases by developing an immunological memory through the differentiation of activated B lymphocytes into memory cells. Activation of the adaptive immune system to some extent depends on the innate immune response as it is the first inflammatory response in the body. The adaptive immune system is usually activated a few days after the innate immune response if the innate immune system was unable to destroy all the pathogens. The adaptive immune response is much more specific to a particular pathogen (Chaplin, 2010). There are two main types of adaptive immune responses: humoral immunity, which is antibody-mediated (depends on B lymphocytes/cells) and cell-mediated immunity, which depends on T lymphocytes/cells (figure 1.4). The figure below provides an overview of the cells involved in adaptive immunity and how they differentiate into specialised cells to perform particular functions.



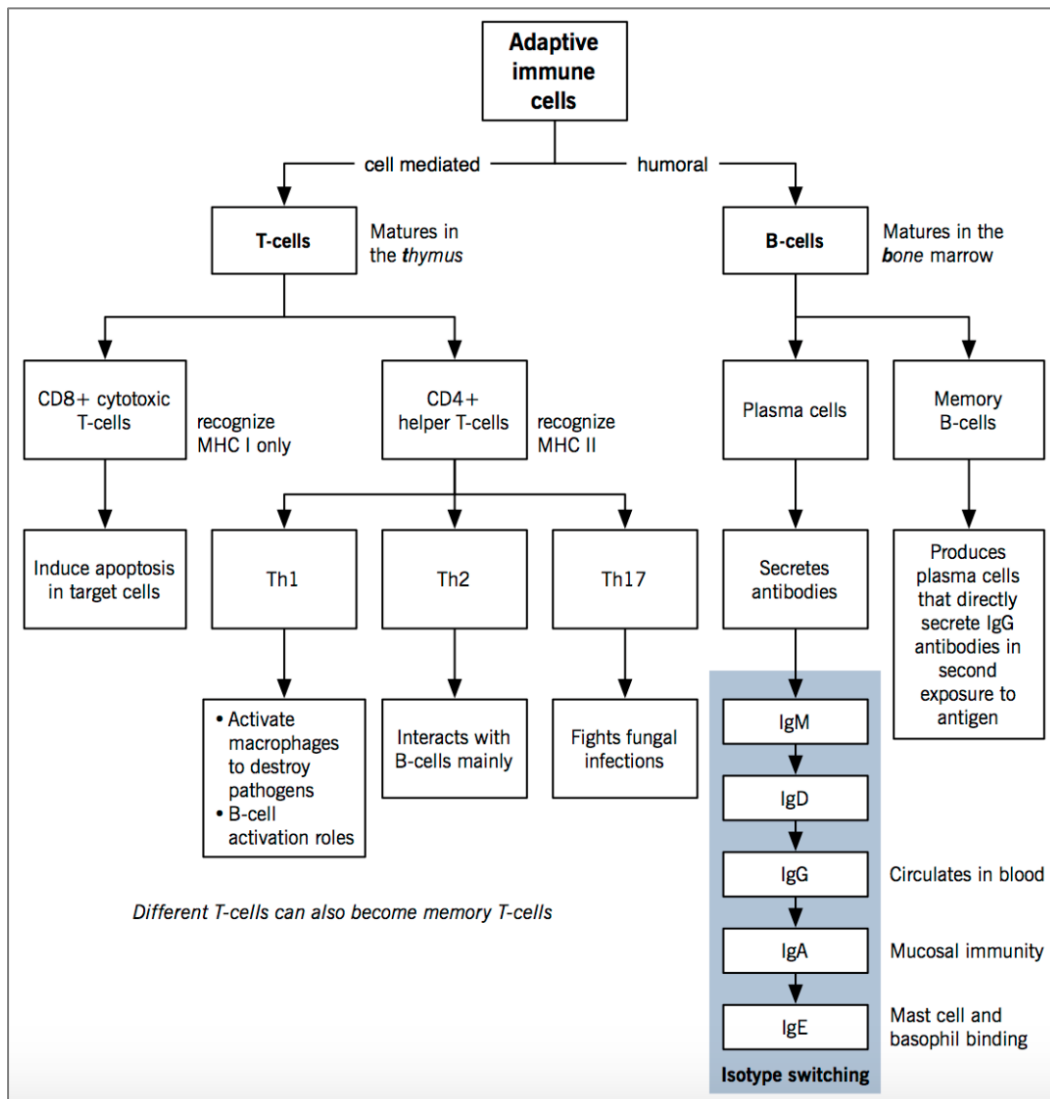


Figure 1.4. **Adaptive immune system overview.** This image shows a summary of the adaptive immune system, the cells involved and the responses triggered. The two main cells of adaptive immunity are B lymphocytes and T lymphocytes, which can differentiate into different cells and they all play important roles in the clearance of pathogens from the body as well as the development of an immunological memory against specific pathogens. *Image from: Chaudhry, 2016.*

During humoral immunity, activated B cells secrete immunoglobulins which are specific to the foreign antigen (Chaplin, 2010). The presence of these antigens is responsible for the production of the antibodies. When the antibodies bind to the antigens, the pathogen becomes inactivated because the antibody-antigen binding has blocked their ability to bind to host cell receptors (Charles A Janeway *et al.*, 2001). The binding of antibodies to the antigens on the pathogen's surface also act as

'markers' to make it easier for the pathogens to be ingested and destroyed by phagocytes; this process is called opsonisation.

During cell-mediated immunity, the main cells involved are the T lymphocytes that will either kill the infected cells directly or will help macrophages to phagocytose the infected cell. Cytotoxic T cells (CD8<sup>+</sup> T cells) will directly kill the infected cells that display the foreign antigen on the surface of a host cell (example: a host cell infected with a virus) (Alberts *et al.*, 2002). Helper T cells (CD4<sup>+</sup> T cells) can help in activating B cells to produce antibodies as well as help to activate cytotoxic T cells to directly kill infected cells (Alberts *et al.*, 2002) (figure 1.4).

When engineered NPs are administered to the body, there is a high probability that they will encounter the immune system and subsequently trigger an immune response with both wings of the immune system; the innate and adaptive immune response. The immune response activated will depend on the physiochemical properties of the NPs (Kononenko *et al.*, 2015). Other than the complement system, NPs can also activate the mononuclear phagocyte system (MPS) to some extent, which leads to their ingestion by phagocytes (Gustafson *et al.*, 2015). The phagocytes, being the body's 'professional eaters', may try to engulf the NPs and eliminate them as they normally would upon exposure to microbes, as described above.

Understanding these factors and how they may disturb the host's immune system is important in the study of toxicology and development of nanotherapeutics. Many studies have shown that the body's exposure to NPs can activate the complement system and trigger inflammatory or allergic reactions (Szebeni, 2014). Although NPs are known to be potentially toxic for the body, engineering the NPs and their properties

may result in either evading the immune system or intentionally targeting the immune system (Dobrovolskaia et al., 2016).

For example: nanoliposomes can be modified to have different effects on the immune system. The literature shows two main types of nanoliposome formulations that elicit different immune responses: one that stimulates an immune response to an antigen inside the nanoliposome and the second formulation incorporates a polymer coat on the nanoliposome in order to avoid being recognised by the immune system (Zolnik et al., 2010). A handful of liposome-based drug carriers have been approved for the treatment of cancer and some infections, while more liposome-based formulations are being investigated for therapeutic vaccines (Zolnik *et al.*, 2010).

The past few decades have shown tremendous advances in the understanding of interactions between NPs and the immune system, however a number of questions on the interactions and how they can be exploited remain unanswered. Understanding physiochemical properties of NPs and their modifications is also crucial to determine the effects they will have on the immune system.

## **1.6 Macrophages and other phagocytes**

Phagocytes or phagocytic cells are important cells of the immune system that protect the body against foreign substances by ingesting the foreign substances and eliminating them through a process called phagocytosis. Phagocytosis is a unique phenomenon of the immune system for clearing foreign pathogens. Phagocytosis is not only important for the killing of foreign pathogens but also important for the removal of apoptotic cells and cellular debris from necrosis. A number of targets, ligands and phagocytic receptors are recognised by phagocytic cells to initiate the process of

phagocytosis. Aside from phagocytosis, macrophages can also help in initiating the activation of the adaptive immune system as they are important antigen-presenting cells, which are recognised by T cells.

Phagocytes can be classified into two classes; 'professional' or 'non-professional' phagocytes and these are determined by the efficacy of phagocytosis. Professional phagocytes include monocytes, macrophages, neutrophils, dendritic cells, mast cells whereas non-professional phagocytes include epithelial cells (Aderem and Underhill, 1999).

The main phagocytes described in this chapter are macrophages, which are blood cells formed in the bone marrow. Monocytes are macrophage precursors and upon differentiation, they become activated macrophages upon encounter with pathogens and cytokines (Mosser and Edwards, 2008). Activated macrophages can be polarised into two types of macrophages: classically activated macrophages (M1 macrophages) through the secretion of IFN- $\gamma$  and alternatively activated macrophages (M2 macrophages) through the secretion of IL-4 (Martinez and Gordon, 2014). M1 macrophages display pro-inflammatory characteristics and mainly function in pathogen-killing, whereas M2 macrophages are involved in tissue repair through cell proliferation (Orecchioni *et al.*, 2019).

As mentioned previously, macrophages are professional phagocytes of the immune system and can detect foreign bodies through specific ligand-receptor interactions such as toll-like receptors (TLRs) and pattern recognition receptors (PRRs) (Richards and Endres, 2014). These interactions and activation of the receptors are the driving force for the foreign bodies to be engulfed by the macrophages (Karavitis and Kovacs, 2011). Receptor activation leads to the formation of a phagosome in the macrophage.

The phagosome ultimately fuses with late endosomes and finally with lysosomes forming a hybrid-like organelle called a phagolysosome through a series of fission and fusion events (Aderem and Underhill, 1999). In the phagolysosomes, an environment with already limited nutrition, enzymes, reactive oxygen species (ROS) and reactive nitrogen species (RNS) will degrade and kill the pathogen (Slauch, 2011).

Neutrophils are another type of phagocytic cells, which are also found in the bloodstream and are important for protecting the body against foreign substances and in wound healing. Neutrophils are one of the first immune cells to be recruited at sites of acute inflammation through chemotaxis, where they can eliminate foreign pathogens through different mechanisms including phagocytosis, degranulation (this involves the secretion of anti-microbial solutes) and the formation of neutrophil extracellular traps (Mayadas, Cullere and Lowell, 2014). These traps are made up of chromatin and proteins and act as a 'net' to trap pathogens for elimination as well as preventing the spread of foreign pathogens by acting as a barrier. At the same time neutrophils are able to secrete cytokines, which recruit and activate other phagocytes (Kolaczkowska and Kubes, 2013). Neutrophils are able to recognise and ingest foreign pathogens when they are opsonised by antibodies and can eliminate and kill pathogens through their oxidative burst mechanism.

Dendritic cells (DCs) are also classified as important phagocytes, however unlike other phagocytes, dendritic cells do not have the primary function of phagocytosis but they are very effective antigen-presenting cells. They are also known as professional antigen-presenting cells (APCs). DCs are mainly responsible to alert the immune system of invading pathogens by processing antigens from foreign pathogens and

presenting them on their cell surface to be recognised by T lymphocytes, which are then activated (Savina and Amigorena, 2007). DCs are able to present the processed antigens through two receptors: MHC class I and MHC class II molecules which are present on the surface of DCs. Activation of T lymphocytes initiates the adaptive immune response and the body's immunological memory as described in section 1.5.

## **1.7 Nanoparticle Uptake Mechanisms**

Since NPs have been discovered as being able to be internalised by cells, they have been the prime focus of many scientists for target therapies. Nanomedicines encounter a number of obstacles before being internalised by cells, thus the most efficient mechanism to get the NPs across the cell and plasma membrane has to be identified for specific nanomedicines, particularly those intended for intracellular targeting. The plasma membrane maintains a complex integrity due to its important role in cell-cell communications, cell division and cell adhesion (Kraft, 2013). To a certain extent, these functions of the plasma membrane are carefully regulated by the process of endocytosis (Kumari, MG and Mayor, 2010). During endocytosis part of the plasma membrane invaginates and new intracellular vesicles are formed translocating substances, such as proteins, extracellular fluids and lipids, across the plasma membrane and into the cell (Saheki and De Camilli, 2012). Different types of substances (proteins, fluids, etc.) will be internalised into the cells through different mechanisms, as shown below (figure 1.5).

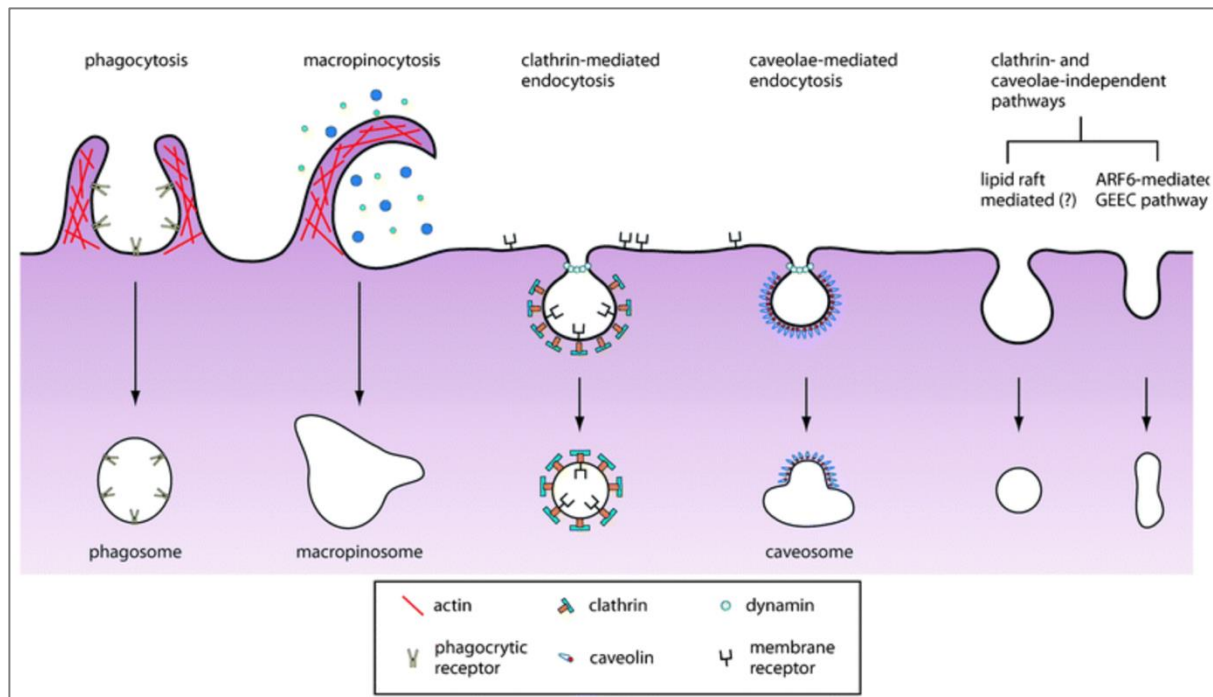


Figure 1.5. **Endocytic pathways at the plasma membrane**. The above figure shows the different endocytic pathways through which various substances including NPs can be internalised. Physical and chemical properties of particles, molecules or protein determine the mechanism of endocytosis. *Image from: Chou et al., 2011.*

Endocytosis can be classified into two main types: phagocytosis and pinocytosis. Pinocytosis, which is internalisation of mostly fluids, can be further categorised into four sub-types: clathrin-mediated endocytosis, caveolae-mediated endocytosis, clathrin/caveolae-independent endocytosis and macropinocytosis. All these pathways are not present in every cell type but the endocytosis pathway will have a major role in the intracellular fate and trafficking of internalised particles. However, in all endocytic pathways, there are important intracellular organelles that play crucial roles, which include early endosomes, late endosomes and lysosomes. Early endosomes are thought of as sorting organelles, where internalised particles or substances are sorted to be either degraded in the lysosome/late endosomes, to be transported back to the trans-Golgi network or if they are to undergo recycling back to the plasma membrane (Jovic et al., 2010). Examples of proteins specific to early endosomes are Rab5 and Rab4, which are small GTP-binding proteins.

Late endosomes are mainly involved in the recycling and degradation (delivery to lysosomes) of the internalised substances. Recycling can either be in the form of direct recycling to the plasma membrane or indirect recycling through recycling endosomes (Scott et al., 2014). Late endosomes also mediate the transport of lysosomal components between lysosomes and the trans-Golgi network (Huotari and Helenius, 2011). Examples of proteins localised to late endosomes are Rab 7, Rab 9 and Rab 11. Lysosomes are membrane-bound organelles that receive substances that are to be degraded from the early/late endosomes. To help in the degradation of the substances, lysosomes constantly maintain a low pH and contain acid hydrolases, which are involved in the hydrolysis and hence, degradation of the substances (Luzio et al., 2007).

Clathrin-mediated endocytosis (CME) is one of the most studied endocytosis pathways in eukaryotic cells and is important for the uptake of nutrients, membrane recycling, and intracellular signalling (Kirchhausen, 2000). Over fifty different proteins are required to regulate the formation of vesicles at the plasma membrane (Popova et al., 2013). The participation of all these proteins causes a slight dip to be formed at the surface of the plasma membrane, following which a spherical clathrin-coated vesicle is formed (Macro et al., 2012). To release the clathrin-coated vesicle from the plasma membrane, specific proteins, called dynamins assemble around the neck of the vesicle in a ring-like structure (Traub & Bonifacino, 2013; Popova et al., 2013). Once released from the plasma membrane, the clathrin coat on the vesicle is removed by auxilins and chaperons such as Hsc70 (Yameen *et al.*, 2014). The uncoated vesicle can now fuse with early endosomes where the content may be degraded or recycled back to the plasma membrane. CME is the main endocytic pathway for receptor-



mediated uptake of NPs (Yameen *et al.*, 2014). The uptake mechanism of NPs is highly dependent on the physical properties of the NPs such as size, surface charge and shape. Certain NPs, particularly ones that are made from polylactic-co-polyethylene glycol, with sizes approximately 100nm were shown to be taken into the cell through CME (Harush-Frenkel *et al.*, 2007). Furthermore, PGLA NPs have also been shown to mainly take the CME pathway of internalisation (Vasir and Labhassetwar, 2008). However, there have been no studies yet that show a direct link between 100nm sized NPs (of different coatings) and CME.

Clathrin-independent endocytosis (CIE) is another endocytic pathway that plays a role in processes such as cell polarisation, plasma membrane repair, intracellular signalling and cell spreading (Sandvig *et al.*, 2008). CIE does not require the coating on the vesicle that is required for CME. CIE does involve vesicle formation on the surface of the plasma membrane that is mainly dependent on the presence of actin and actin-associated proteins (Mayor and Pagano, 2007). CIE can be further classified into three sub-types, which are categorised by the type of proteins involved: RhoA-dependent CIE, Cdc42-dependent CIE and Arf-6-dependent CIE (Mayor *et al.*, 2014). Following vesicle formation, the cargos that enter the cell are delivered to early endosomes first and following the sorting process, they are transported to the lysosomes or late endosomes to be degraded or recycled back to the plasma membrane (Hansen and Nichols, 2009). Specific NPs, particularly self-branched and trisaccharide-substituted (glycosylated) chitosan oligomers (SBTCO) NPs, have been shown to be mainly endocytosed through CIE pathways (Garaiova *et al.*, 2012).

Caveolae-mediated endocytosis involves structures called caveolae. Caveolae play a part in many processes including protein endocytosis, signal transduction and cholesterol homeostasis (Parton and Simons, 2007). Caveolae are small plasma membrane invaginations (of 50-100nm) and are present in a number of cells and tissues including fibroblasts, endothelial cells, smooth muscle cells and adipocytes (Cohen et al., 2004). Caveolae are coated mainly by caveolins; particularly Cav1, Cav2 and Cav3 (Parton and Simons, 2007). Other proteins that coat the caveolae are known as cavins and they also contribute to the formation of caveolae (Parton and del Pozo, 2013). Caveolin proteins have the ability to oligomerise and this process is important in the generation of the endocytic vesicle (Cohen *et al.*, 2004). The internalised material is transported to caveosomes before being sorted to lysosomes, the Golgi apparatus or the endoplasmic reticulum, depending on the endocytosed material (Kiss and Botos, 2009).

Macropinocytosis is the fourth endocytic pathway classified under pinocytosis. Macropinocytosis is an actin-dependent endocytic pathway and involves the formation of large vesicles called macropinosomes (Lim and Gleeson, 2011). Macropinocytosis is generally the preferred uptake route of larger substances such as bacteria, viruses, apoptotic cell fragments and large amounts of extracellular fluids (Zeineddine and Yerbury, 2015). Macropinocytosis mainly internalises large substances and fluids, generating vesicles  $>1\mu\text{m}$  in diameter whereas phagocytosis involves the uptake of particles that are  $>0.5\mu\text{m}$  in diameter (Cardelli, 2001). Macropinocytosis also plays an important part in the process of antigen presentation of MHC class II molecules (Sallusto et al., 1995). Macropinocytosis is mainly triggered by growth factors but it can also be triggered by particles such as apoptotic bodies, bacteria, viruses and

necrotic cells (Zeineddine and Yerbury, 2015). The formation of the macropinosome vesicle is promoted by actin polymerisation and actin-mediated ruffling, which occurs following the activation of receptor tyrosine kinases such as epidermal growth factor receptors (Kerr and Teasdale, 2009). Once the macropinosomes are formed containing the trapped solute and soluble substances, the macropinosomes undergo a maturation process (Lim and Gleeson, 2011). The maturation involves extensive tubulation of the macropinosomes, which then become more spherical as they migrate centripetally towards the late endosomes/lysosomes (Lim and Gleeson, 2011). The contents of the macropinosomes are then either recycled back to the plasma membrane or degraded in the late endosomes/lysosomes.

Phagocytosis (described in section 1.4) is a type of endocytosis specific for foreign pathogens, which are translocated across the cell membrane and into the phagosome. The uptake of NPs by macrophages through phagocytosis requires attractive forces, which can be in the form of electrostatic forces, Van der Waals forces, hydrophobic/hydrophilic forces or ionic forces, and occurs between the NPs and cell surface (Weissleder et al., 2014). NP uptake by phagocytosis can also occur through receptor mediated recognition of opsonins that are present on the surface of the NPs (Weissleder, Nahrendorf and Pittet, 2014). Different drug delivery particle shapes have been investigated for their ability to inhibit phagocytosis and the results have shown that phagocytosis can be reduced or even inhibited by using more elongated drug delivery particles made with high aspect ratios (Champion and Mitragotri, 2009).

Many particles that are of small micron sizes are able to be internalised into cells via micropinocytosis (Gratton *et al.*, 2008). NPs can be endocytosed into macrophages

as well as in cancer cells through micropinocytosis; these are the two main types of cells that have the highest uptake of NPs (Weissleder et al., 2014). However, most of the literature suggests that in principle NPs are internalised into cells through the many different endocytic pathways. Understanding these uptake pathways and the ability to control the endocytic pathway taken by NPs is important in mediating their intracellular fate and the biological response that the NPs will trigger, which will also help in understanding the overall physiological effect in response to NPs.

### **1.8 Nanoparticle uptake by macrophages**

Macrophages, as described in section 1.6, have very important functions in protecting the host against foreign bodies and NPs are endocytosed by macrophages, due to their naturally high endocytic activity. As a result of this, NPs are common tools used in the imaging and study of macrophages.

Macrophages can recognise opsonised particles and specific surface and biological patterns that are most likely to be present on the surface of NPs, which will determine their fate (Etheridge *et al.*, 2013). However, how the phagocytes interact with the surface of the NPs, which determines their endocytic pathway, intracellular fate and removal, is not clearly understood (Gustafson et al., 2015). NPs are mostly recognised by macrophages through the proteins that are adsorbed on their surface. Exploiting this recognition will help tremendously in the making of NPs for therapeutic purposes as they may remain in the circulation for longer (Dobrovolskaia et al., 2008). An example of these protein recognitions is the positively charged collagen domains of the scavenger receptors on the surface of macrophages that have been shown to facilitate internalisation of negatively charged nanomaterials (Gustafson *et al.*, 2015). NP surface size and shape can contribute to changes in the conformation of adsorbed

proteins; for example: lysozymes are small enzymes that have been shown to adsorb to silica NPs of almost any size (Gustafson *et al.*, 2015). Bovine serum albumin (BSA) on the other hand adsorbs to NPs especially those with rough surfaces; for example: a study showed that with an increase in BSA adsorption, there was a decrease in cellular uptake of rough gold NPs compared to smooth gold NPs (Albanese *et al.*, 2010). These protein adsorptions on the surface of NPs may form specific patterns that contribute to their recognition by macrophages.

Macrophage surface receptors such as TLRs, Fc receptors, mannose receptors and scavenger receptors play an important role in the uptake of NPs (Gustafson *et al.*, 2015). TLRs are important receptors of the innate immune system and are involved in the detection of 'foreign' material through the recognition of PAMPS (pathogen associated molecular patterns) and a study investigating the involvement of TLRs in titanium dioxide (TiO<sub>2</sub>) NP uptake has found that TLR4 in particular played a role in the uptake of TiO<sub>2</sub> NPs in human cell lines and triggered an inflammation response (Chen, Kanehira and Taniguchi, 2013). Fc receptors are cell surface receptors for the Fc part of immunoglobulin and have a major role in linking the innate and adaptive immune responses by binding to the Fc portion of the antibodies (Nimmerjahn and Ravetch, 2007). A study identified that NP surfaces adsorbed with Fc molecules increased the cellular uptake of these particles more than the endocytosis of molecular IgG (Vilasaliu *et al.*, 2012). Mannose receptors are glycoprotein endocytic receptors that binds to carbohydrate domains of microbes and endogenous ligands (Pawde *et al.*, 2020). Jain *et al.*, 2008 demonstrated that gelatine NP surface deposited with mannose significantly increased the uptake of the NPs compared to the unmodified gelatine NPs. Scavenger receptors are PRRs and they can recognise and bind to a

number of ligands such as pathogens, lipoproteins and foreign particles which are negatively charged (Shannahan, Bai and Brown, 2015). Upon binding to these ligands, cellular uptake is promoted and pro-inflammatory responses can also be induced (Shannahan, Bai and Brown, 2015).

NPs that have been tailored to specifically target Fc receptors and mannose receptors were shown to be internalised quicker than those targeting scavenger receptors (Taylor *et al.*, 2005), suggesting that these two receptors are more effective in the endocytosis of NPs. Macrophages are also able to internalise NPs without bound serum proteins, which further suggests that the four receptors mentioned above can independently recognise the NPs without the help of protein coating, unless it is a non-specific endocytic pathway such as macropinocytosis (Dutta *et al.*, 2007). Understanding the interactions between surface receptors on macrophages and NPs is crucial in the engineering of NPs for drug delivery or other therapeutic purposes.

### **1.9 Intracellular trafficking of NPs**

After endocytosis and uptake of NPs across the plasma membrane, their intracellular trafficking determines their intracellular fate in the cell, which in turn determines the therapeutic efficacy and cellular toxicity of NPs (Peñaloza *et al.*, 2017). Once internalised, the NPs will first come into contact with membrane-bound early endosomes, which are intracellular vesicles that bud off the plasma membrane following the endocytosis of NPs (Foroozandeh and Aziz, 2018).

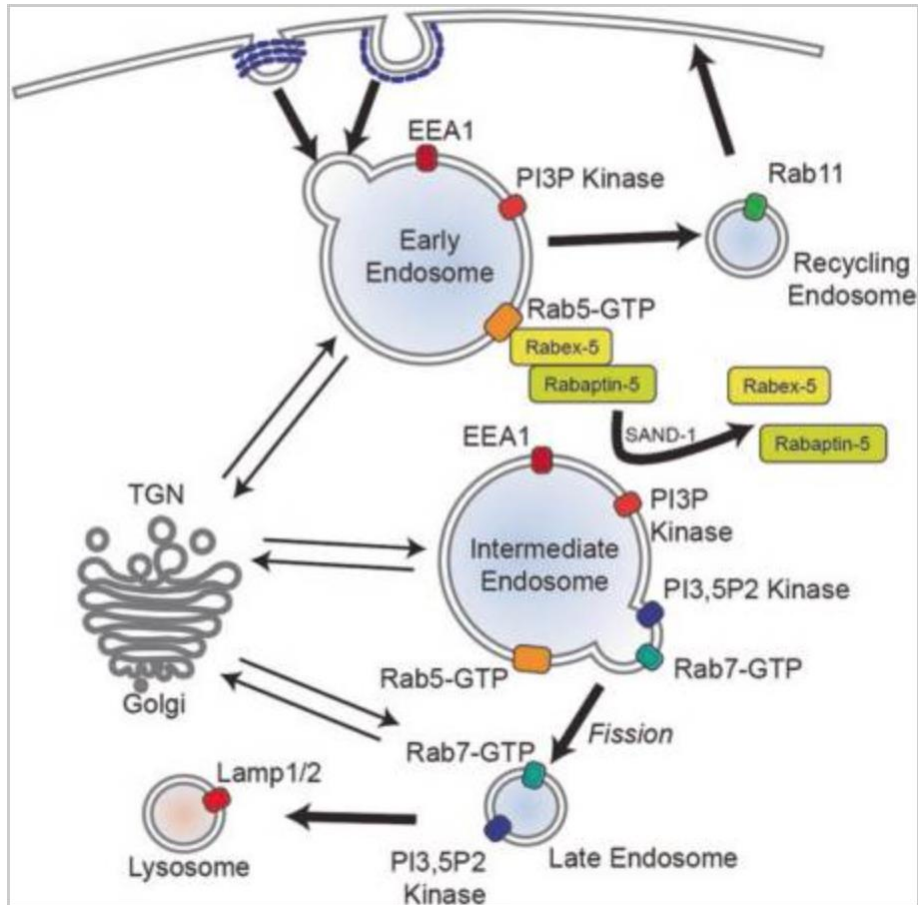


Figure 1.6. **Overview of intracellular trafficking of endocytosed material.** The above figure shows an overview of the intracellular trafficking of internalised cargo molecules and particular proteins involved in the trafficking at each stage. Vesicles with the cargo molecule bud off from the plasma membrane to fuse with early endosomes, with the involvement of particular proteins such as Rab5-GTP, PI3P Kinase and EEA1. Recycling endosomes are formed through fission of early endosomes and carry cargo molecules to be recycled back to the plasma membrane. Early endosomes give rise to late endosomes through maturation and differentiation, which can deliver cargo molecules to lysosomes or alternatively fuse with lysosomes for the ultimate purpose of degradation. During the maturation of early endosomes, proteins can also be transported back and forth to the trans-Golgi network. *Reference and image from: Kaur & Lakkaraju, 2018.*

Endosomes formed at the plasma membrane are key players in controlling recycling and degradation of internalised molecules/particles and thus endosomes can be classified into early endosomes, late endosomes or recycling endosomes (Scott, Vacca and Gruenberg, 2014) (see figure 1.6 above for summary).

Early endosomes carry cargo molecules/particles internalised from extracellular surroundings through endocytosis and the main function of early endosomes is to then

sort those cargo molecules/particles either into recycling compartments to be taken back to the plasma membrane or into degradative compartments such as the lysosomes where the cargo molecule/particle is degraded (Kaur and Lakkaraju, 2018). Through the fission of early endosomes into smaller recycling endosomes, certain cargo molecules such as ligands, lipids and plasma membrane proteins are transported back to the plasma membrane by these recycling endosomes (Kaur and Lakkaraju, 2018). Recycling endosomes are likely to traffic cargo molecules to be recycled to the plasma membrane via different trafficking pathways depending on the individual cargo molecule in the vesicle and much about the mechanisms regulating these pathways is yet to be understood but a number of these may operate via microtubule-based pathways (Goldenring, 2015).

Late endosomes are formed by the differentiation and maturation of early endosomes which can transport the molecule/particle to the lysosomes where they are degraded (Huotari and Helenius, 2011). Late endosomes can also fuse with lysosomes to form endolysosomes where the enclosed molecules/particles are degraded by hydrolytic enzymes (Foroozandeh and Aziz, 2018). Lysosomes are acidic organelles where degradation of proteins, lipids and polysaccharides occur in a cell, although some NPs are able to evade the endosome before lysosomal degradation by being released into the cytoplasm, which is a feature particularly of interest in cytosolic drug delivery (Martens *et al.*, 2014). One study investigated the intracellular trafficking of different sized polystyrene NPs (Sandin *et al.*, 2012). The study found that small NPs (40nm) are trafficked through Rab5 and are quickly transferred to late endosomes (Rab9) before finally localising to lysosomes (using Rab7 as a marker). They also showed that larger sized NPs (100nm) are also trafficked through the same endosomes but at



a slower rate than the smaller NPs. Due to a lack of sufficient colocalisation of NPs, with Rab 11 (a marker for recycling endosomes), Sandin *et al.* (2012) also reported that the recycling of NPs to the plasma membrane is unlikely, although some NPs manage to access the recycling endosomes. Other studies using Silica NPs have observed similar fate and trafficking patterns of NPs in lymphoid and myeloid cells (Sola *et al.*, 2021). The current literature contains gaps for the studies of intracellular trafficking of IONPs and further studies need to be carried out to broaden the understanding of the trafficking of IONPs, particularly if they are to be used for intracellular targeting.

Autophagy is another degradation pathway in cells which can contribute to the intracellular fate of NPs and this pathway can also be a result of toxic effects induced NPs (Wang *et al.*, 2017). Autophagy is a process mediated by an organelle called autophagosome, during which components of the cytoplasm are targeted for degradation by lysosomes and recycled (Wang *et al.*, 2017). Thus, studying the intracellular fate of NPs is especially important if the NPs are intended to be used as drug delivery vehicles and depending on whether they are recycled or degraded can bring their therapeutic efficiency and cytotoxicity into question.

### **1.10 Biomarkers of Nanoparticle immunotoxicity**

Toxic effects of NPs differ between different types of NPs, particularly depending on physical and chemical properties, as mentioned previously. Regardless of these characteristics, upon administration, NPs will undoubtedly encounter components of the immune system, especially the innate immune system as it is the host's first line of defence against 'foreign' material. NPs can interact with the innate immune system

to either enhance the immune response, triggering a pro-inflammatory response, or suppress the immune response resulting in an anti-inflammatory response (Elsabahy and Wooley, 2013). Depending on their intended purpose, NPs can be designed to specifically induce proinflammatory or anti-inflammatory responses in the body, however, concerns arise when administered NPs interact with the immune system in an undesirable way, resulting in unwanted pathologies such as hypersensitivity reactions and inflammation (figure 1.7) (Zolnik *et al.*, 2010). Furthermore, the inflammation response against NPs can significantly alter the residence times of NPs in the body, which can in turn affect their bioavailability and therapeutic efficacy. For example, one study showed that human properdin opsonised carbon nanotubes generated a high pro-inflammatory response and an increased uptake in human macrophages, suggesting that the clearance of NPs by the immune system can be influenced by the local synthesis of complement proteins, regardless of whether there is activation of the complement system (Kouser *et al.*, 2018).

Immunosuppressive effects exhibited by NPs can be favourable for a decreased risk of autoimmune reactions but on the other hand a suppressed immune system can be favourable for the growth of cancerous cells (Ngobili and Daniele, 2016). A study investigating the immunosuppressive effects of carbon nanotubes (CNTs) showed that administration of CNTs through inhalation suppressed the function of B cells, increased Transforming growth factor (TGF)- $\beta$  secretion, and triggered the secretion of the anti-inflammatory cytokine IL-10, leading to immunosuppressive effects (Mitchell *et al.*, 2009). On the other end of the spectrum, unintended immunostimulatory effects exhibited by NPs can result in the development of

autoimmune reactions such hypersensitivity reactions or more severe reactions such as anaphylactic shocks, as seen in the figure below (Zolnik *et al.*, 2010).

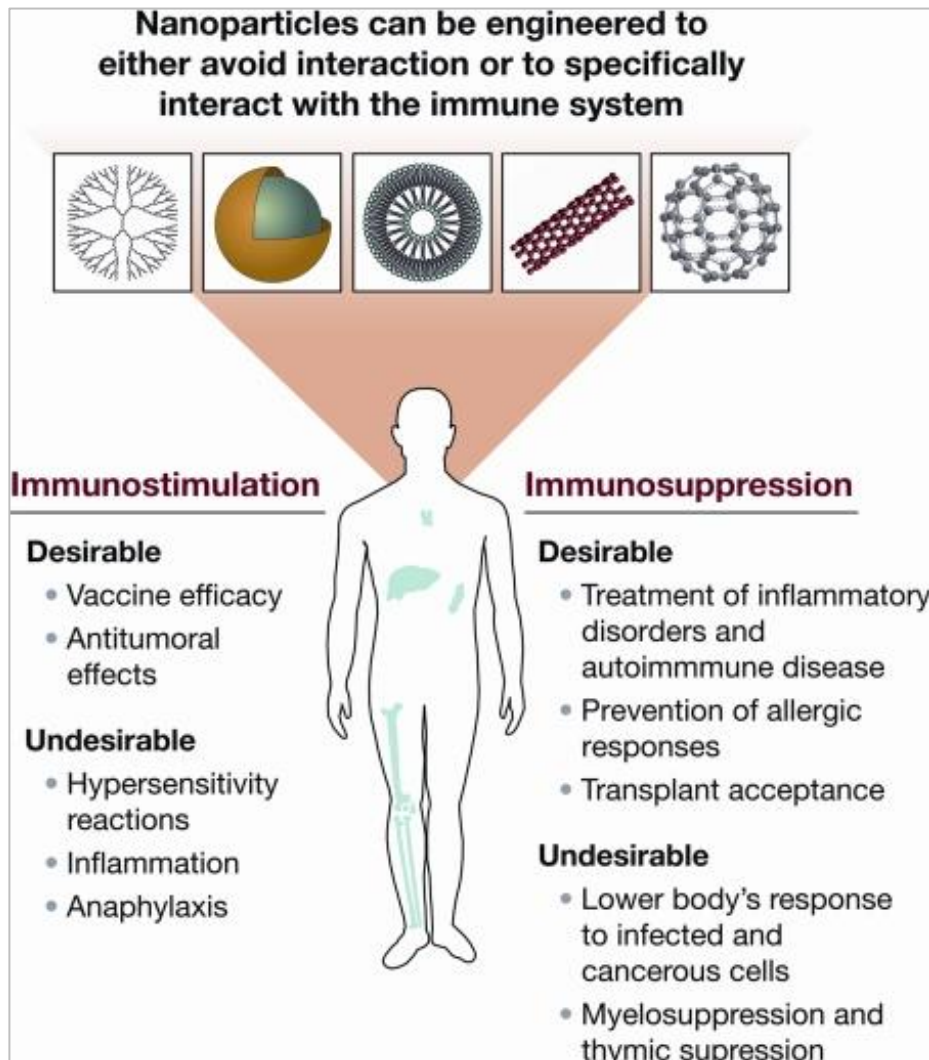


Figure 1.7. **Interactions of nanoparticles with the immune system.** The above image shows the different effects that can occur upon nanoparticle interaction with the immune system, which are important factors to be considered during the development of nanotherapeutics. Administered NPs can either enhance or suppress normal immune function, which can result in unwanted effects and pathologies. *Image from: Zolnik et al., 2010.*

Cytokines are powerful tools in immunotoxicity studies and can be used as biomarkers to study pro-inflammatory and anti-inflammatory effects of NPs. Cytokines give a good indication of immunomodulatory effects and NP inflammation-mediated toxicity (Elsabahy and Wooley, 2013). Furthermore, some studies showed that heating the tissue with magnetic IONPs, under the appropriate conditions can further enhance the

immune response which benefits cancer treatment (Grauer *et al.*, 2019). Cytokines are small pleiotropic proteins secreted by immune cells during an immune response and secretion of pro-inflammatory cytokines results in immune cell activation and production of other inflammatory cytokines whereas secretion of anti-inflammatory cytokines counteracts the action of pro-inflammatory cytokines, suppressing the immune response (Kany, Vollrath and Relja, 2019). Some studies reported that IONPs can interact with immune cells *in vitro* and increase oxidative stress, thus inducing apoptosis (Dobrovolskaia, Germolec and Weaver, 2009). Currently, the biodistribution, metabolism and excretion of NPs is still not fully understood, mainly owing to the lack of successful techniques and methods to measure NPs in tissues. However, multiple studies have reported the frequent accumulation of various NP types in unwanted organs (Ganapathy, Moghe and Roth, 2015). Furthermore, studies have provided evidence that show metal NPs can cause sub-lethal effects in zebrafish including oxidative stress, respiratory toxicity and disturbances to trace elements in tissues (BJ and RD, 2011).

Activated macrophages are one of the main immune cells which secrete cytokines. Upon exposure to a pathogen or 'danger signal' they act as a communicating mechanism to link the innate and adaptive immune system (Arango Duque and Descoteaux, 2014). Some of the pro-inflammatory cytokines secreted by macrophages are IL-1, TNF (tumour necrosis factor), IL-6, IL-12 and IL-12 (Arango Duque and Descoteaux, 2014). One study investigated the interactions of 5-8nm magnetite NPs and immune cells in mouse models and reported a dose-dependent increase of pro-inflammatory cytokines IL-6, IL-1 and TNF- $\alpha$  in the blood (Park *et al.*, 2010). TNF is one of the pleiotropic cytokines, which means it can act on different

signalling pathways and is known to be involved in apoptosis, activation of stress-activated protein kinases and NF- $\kappa$ B activation (Zhang and An, 2007). *In vitro* and *in vivo* studies have shown that NF- $\kappa$ B activation and pro-inflammatory cytokine production (such as IL-8, IL-6, TNF- $\alpha$  and IL-1 $\beta$ ) were triggered by carbon nanotubes and metallic NPs (Pujalté *et al.*, 2011). Other studies have shown that complement deposited carbon nanotubes downregulated TNF- $\alpha$  and IL-1 $\beta$ , and upregulated IL-12 levels in a human monocytic cell line (Pondman *et al.*, 2016). The same study also identified IL-10, which is a potent anti-inflammatory cytokine, to mediate a key role in the immunomodulatory effects during NP interaction with immune cells.

Overexpression of pro-inflammatory cytokines can lead to inflammation related pathologies, for instance, normal secretion of IL-6 is important during inflammation by promoting the differentiation and development of T cells, however abnormal IL-6 upregulation is linked to many inflammatory diseases such as Crohn's disease and rheumatoid arthritis (Nishimoto and Kishimoto, 2004). Moreover, overexpression of pro-inflammatory cytokines such as IL-1 $\beta$ , TNF- $\alpha$  and IL-6 are involved in pathological and neuropathic pain (Zhang and An, 2007). Additionally, one study showed that aberrant IL-8 expression is involved in acute lung injury (Allen and Kurdowska, 2014). Anti-inflammatory cytokines are immunosuppressive and control the actions of pro-inflammatory cytokines. Some examples of potent anti-inflammatory cytokines are IL-10, IL-4, IL-11, IL-13 and IL-1 receptor antagonist (Opal and DePalo, 2000). IL-10 is the most potent of them and can suppress the effects of pro-inflammatory cytokines such as IL-1, IL-6 and TNF- $\alpha$  (Gibson *et al.*, 2013). TGF- $\beta$  also has anti-inflammatory effects by suppressing cytokine functions such as IL-1, IL-6, IL-2 and TNF- $\alpha$  and also acts as an antagonist for the production of nitric oxide in macrophages, which is increased in neuropathic pain (Echeverry *et al.*, 2009).

Hence, an effective immune response is carefully regulated by the intricate network of cytokines. Abnormal cytokine expression levels can lead to diseases, including autoimmune reactions and tumour progression. Thus, studying the effects of nanoparticle exposure on cytokine expression levels is a key part of immunotoxicity studies of NPs.

### **1.11 Transcriptome profiling to assess nanoparticle toxicity**

A transcriptome consists of all RNAs transcribed by cells or tissues at a particular physiological condition or developmental stage (Yang *et al.*, 2020). High-throughput sequencing (HTS) technologies such as RNA sequencing or microarray technologies can be used to understand diseases at a molecular level and identify pathways affected following treatments by analysing gene transcription levels (Yang *et al.*, 2020). Identifying the molecular responses to NP exposure is a powerful approach which can contribute to the understanding of toxic effects exhibited by NPs and can also open new premises for the development of targeted therapies. For example, through RNA sequencing a study has shown that high doses of silicon dioxide NPs inhibited the transcription of specific genes that may be involved in neurotoxicity and apoptosis (Sun *et al.*, 2017). Another study used RNA sequencing to study the toxicity of iron sulphide NPs in adult zebrafish and identified that exposure to iron sulphide NPs caused significant changes in gene expression in the liver cells relating to inflammatory responses, oxidative stress, detoxification and DNA damage/repair (Zheng, Lu and Zhao, 2018).

Other than toxicity, transcriptome profiling can also be used to identify pathways activated in the cellular uptake of NPs. For example, through RNA sequencing, a study

identified that nanosilicates were taken up by human mesenchymal stem cells through clathrin-mediated endocytosis (Carrow *et al.*, 2018a). Furthermore, other studies identified that gold NPs triggered oxidative stress, which lead to physical damage of neurons and lack of cell-to-cell communication, thus identifying the neurotoxicity of gold NPs through the use of RNA sequencing (Mo *et al.*, 2020). Transcriptome profiling allows researchers to identify changes at the base level and it can provide good indication of toxicity of NPs on a wider range of pathways, which can be translated to pathological conditions. Moreover, identifying changes in gene expression can provide great insights into identifying new strategies for therapeutic and diagnostic targets. Hence, transcriptome profiling is a useful tool in studying the toxicity of NPs at a molecular level.

### **1.12 Animal models to study nanoparticle toxicity**

Several animal models are used to assess toxicity of NPs on a physiological level, the most common models being mice, rats and zebrafish (*Danio rerio*). The literature shows that zebrafish have traditionally been for aquatic toxicity testing and in the last decade, zebrafish have been characterised as established animal models to study NP toxicity (Chakraborty *et al.*, 2016). In addition, nowadays many countries are adopting the “Three R’s” principle in animal research, which stand for Replacement, Reduction and Refinement, encouraging the use of alternative animal models (Tonelli *et al.*, 2020). Thus, zebrafish are becoming increasingly popular for toxicity studies both in the embryonic and adult stage, each of them having special and desirable characteristics for research purposes. Some advantages of using zebrafish in research are their small size, embryo transparency, quick development, high reproducibility and low maintenance costs compared to other animal models (Strähle

*et al.*, 2012). Furthermore, zebrafish embryos are desirable replacements for the study of early developmental stages since the embryos are likely to suffer less pain or even no pain at all (Strähle *et al.*, 2012). Additionally, following gene mapping in zebrafish, it was found that the zebrafish genome displays approximately 75% similarity with the human genome which makes zebrafish an even more desirable animal model (Chakraborty *et al.*, 2016a).

Toxicity in zebrafish can be studied through hatching analysis, malformations of embryos, behavioural studies, immunotoxicity, genotoxicity, breeding patterns and measurement of mortality rate (Cassar *et al.*, 2020). Moreover, zebrafish embryos/larvae lack adaptive immunity for the first 4 weeks and solely rely on their innate immune system during early development (Trede *et al.*, 2004), making them particularly attractive models to immunologists. Thus, zebrafish as an animal model are proving to be a strong tool for toxicity studies *in vivo*.



## Aim

The aim of this thesis is to study the intracellular fate and toxicity of IONPs. We are particularly interested in the intracellular trafficking of IONPs in macrophages and the innate immune responses triggered by IONPs following uptake by macrophages. Furthermore, zebrafish (*danio rerio*) embryos we used as *in vivo* models to assess the biodistribution and toxicity of IONPs. We also aimed to label macrophages *in vivo* to study IONP distribution and uptake by macrophages in zebrafish. We hypothesise that IONPs behave differently when a protein corona is adsorbed to their surface compared to unmodified IONPs, affecting their uptake and inflammatory responses triggered.

---

## **2. Materials and Methods**

---

## **2.1 Materials**

All buffers and solutions in this section were prepared as stated below, unless otherwise specified.

### **Magnetic iron oxide nanoparticles (IONPs)**

Product code: nano-screenMAG-D/R, purchased from the manufacturer Chemicell.  
IONPs stock concentration: 25 mg/ml (in aqueous dispersion). Particle size: 100nm.

### **Phosphate Buffer Saline (PBS) (ThermoScientific)**

PBS was prepared using Oxoid™ Phosphate Buffered Saline Tablets (Dulbecco A) diluted in dH<sub>2</sub>O.

### **Permeabilisation buffer for immunohistochemistry**

20mM HEPES, 300mM Sucrose, 50mM Sodium chloride, 3mM Magnesium chloride, 0.5% Triton X-100 and Sodium azide.

### **Saponin buffer for immunohistochemistry**

0.5% BSA (Bovine Serum Albumin), 0.1% Saponin and Sodium azide.

### **DGVB<sup>++</sup> buffer**

2.5 mM Sodium barbital, 71 mM NaCl, 0.15 mM CaCl<sub>2</sub>, 0.5 mM MgCl<sub>2</sub>, 2.5% w/v Glucose and 0.1% w/v Gelatin.

### **EGTA Buffer**

2.5 mM Sodium barbital, 71 mM NaCl, 7 mM MgCl<sub>2</sub>, 10 mM EGTA, 2.5% w/v Glucose and 0.1% w/v Gelatin.

### **Live cell imaging medium**

140 mM NaCl, 2.5 mM KCl, 1.8 mM CaCl<sub>2</sub>, 1.0 mM MgCl<sub>2</sub> and 20mM HEPES (pH 7.4).

### **E3 medium (zebrafish embryos)**

5.0mM NaCl, 0.17 mM KCl, 0.33 mM CaCl and 0.33 mM MgSO<sub>4</sub>.

### **Mowiol Mounting Solution**

4.3mM Mowiol 4-88 (Sigma Aldrich), 0.2M Tris (pH 8.5) and 0.02% Sodium azide.

#### **SDS acrylamide gel (separating layer)**

12% acrylamide mix (37:1), 0.375M Tris (pH = 8.8), 0.1% SDS, 0.1% ammonium persulfate, 0.001% TEMED and dH<sub>2</sub>O.

#### **SDS acrylamide gel (stacking layer)**

3.75% acrylamide mix (37:1), 0.125M Tris (pH=8.8), 0.1% SDS, 0.1% ammonium persulfate, 0.1% TEMED and dH<sub>2</sub>O.

#### **SDS loading buffer**

50mM Tris (pH=6.8), 100mM dithiothreitol, 2% SDS, 0.1% bromophenol blue and 10% glycerol.

#### **Running buffer**

25mM Tris (pH=8.3), 192mM Glycine and 0.1% SDS.

#### **Transfer buffer**

25mM Tris (pH=8.3), 192mM Glycine and 20% w/v methanol.

#### **Enhanced Chemiluminescence Solution**

0.1M Tris, pH=8.8 (solution A), 90mM Coumaric acid (solution A), 250mM Luminol (solution A), 0.1M Tris, pH=8.8 (solution B) and 30% hydrogen peroxide (solution B).

## **2.2 Cell Culture**

The cells studied in this thesis are RAW 264.7 cells. RAW 264.7 is a mouse monocytic/macrophage cell line derived from the tumour of a male mouse intraperitoneal injected with Abselon Leukaemia Virus (A-MuLV). RAW cells are established models of macrophages are of particular interest in this thesis due to their ability to perform phagocytosis and pinocytosis. RAW cells are phenotypically and functionally stable, and it is a well characterised cell line with regards to macrophage-

mediated immune, metabolic and phagocytic functions (Taciak *et al.*, 2018). RAW cells were grown in cell culture flasks in a humidified incubator of 5% CO<sub>2</sub> at 37°C. RAW cells were cultured in RPMI 1640 medium (Biosera) and were passaged by scraping off adhered cells using a cell scraper once the cells were 70 - 80% confluent. RPMI cell culture media contained 1% stable glutamine (2mM), 10% FCS (Foetal Calf Serum) and 1% Pen Strep (Penicillin 100 U/ml and Streptomycin 100µg/ml, antibiotics). Experiments were performed with the cell line for up to 30 passages, since the efficacy is likely to decrease beyond that point.

### **2.3 Preparation of cells**

The cells were passaged when they were about 80% confluent and counted using a haemocytometer. Once counted, approximately 30,000 cells per well (60,000 cells/ml) were seeded in 24-well tissue culture plates and each well contained a 13mm coverslip for immunofluorescence staining. The cells were allowed to adhere and grow for 24 hours before the addition of IONPs. Prior to the addition of IONPs, the cell medium was changed to serum-free medium (FCS absent) containing 1% Pen Strep. Serum-free medium was used in order to eliminate serum proteins in the cell culture medium as a variable in the study of the uptake of IONPs by the cells.

### **2.4 Preparation and Addition of Nanoparticles**

From a stock concentration of 25 mg/ml, the IONPs were diluted appropriately to obtain a final concentration of 10 µg/ml. Studies have shown that using lower IONP (size range 15-30nm) concentrations (25-200 µg/ml) maintained >95% cell viability for prolonged exposure times when compared to high IONP concentrations (300-500 µg/ml) (Naqvi *et al.*, 2010). The study by Naqvi *et al.* concluded that using a low

optimum concentration of IONPs avoids ROS-induced cell injury and death as the damage caused to cells is both time- and concentration-dependent. For all *in vitro* experiments in this thesis, a concentration of 10 µg/ml was used after testing for the optimal concentration where cell viability is maintained after 24 hours of IONP exposure and where IONPs are clearly visible under the microscope. Additionally, due to long-term IONP supply shortages from the manufacturer at the time when experiments were performed, the amount of IONPs available had to be carefully managed. The IONPs used in this thesis are commercially available, consisting of a magnetite core, which is first covered by a lipophilic fluorescence dye, followed by a second layer enveloping the particle with a hydrophilic polysaccharide matrix (starch) (Manufacturer: Chemicell) (Figure 2.1). In addition to low toxicity, spherical magnetite NPs provide a high surface area for adsorption and for surface modifications using molecules or drugs for targeted delivery (Natarajan *et al.*, 2019). Furthermore, due to their magnetic properties, they can be controlled and separated using an external magnetic field. In this thesis, IONPs with a 100nm diameter were used for all experiments. For intracellular drug delivery, the favourable particle size for IONPs is between 10nm – 100nm as these provide the longest blood circulation times (Turrina, Berensmeier and Schwaminger, 2021). To confirm the 100nm size of the particles stated by the manufacturer and for further characterisation of IONPs, TEM (transmission electron microscopy) and DLS (dynamic light scattering) techniques can be used.

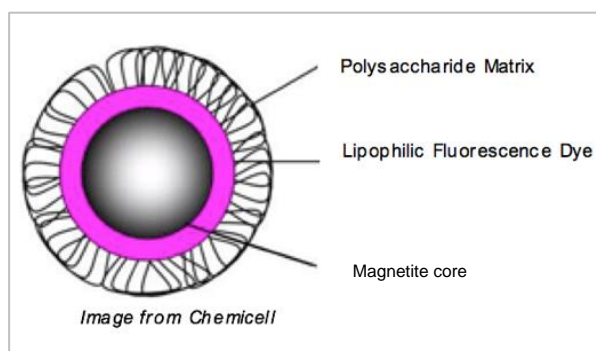


Figure 2.1. **Structure of iron oxide nanoparticles.** This image shows the composition of the nanoparticle, with a magnetite core, a layer of lipophilic fluorescence dye and a second layer of a polysaccharide matrix. Image taken manufacturer website (Chemicell)

Surface coatings on particles increase their biocompatibility and stability in bioenvironments, allowing for better targeted delivery and increased therapeutic efficacy. Additionally, due to strong magnetic attractions between particles, iron oxide particles with no surface coatings have an increased tendency of forming aggregates, resulting in large clusters, which are then cleared from the body by phagocytic cells (Xia *et al.*, 2012). Furthermore, high concentrations of local Fe ions from Fe dissolution poses additional toxicity concerns for organisms, which can be avoided by the use of surface coatings (Ali *et al.*, 2016). Due to their non-toxic nature, polysaccharides are often used as surface coatings to prevent the formation of particle aggregates as well as increasing particle stability and providing a high sorption capacity, making them favourable for targeted drug delivery (Stolyar *et al.*, 2021).

To help in understanding the uptake and intracellular fate of IONPs, 'naked' and serum deposited IONPs were added to the cells to compare uptake patterns. For the serum protein coating, IONPs were diluted in complete serum (no addition of other buffers) and the 'naked' IONPs were diluted in PBS only (Phosphate-Buffered Saline). The samples were briefly vortexed and incubated for 1 hour at 37°C on a shaker. After 1

hour, the IONPs were washed three times with PBS to remove any excess proteins or ions from the solution using the following steps: Sterile PBS was added to both Eppendorf tubes in a 1:1 ratio of the volume present in the Eppendorf tube. The Eppendorf tubes were briefly vortexed and then centrifuged at 13,000 rcf for 3 minutes using a microcentrifuge (Fisher Scientific AccuSpin Micro R Centrifuge). The tubes were then placed on a magnetic rack for about one minute before carefully removing the supernatant, without disturbing the pelleted IONPs. The first step is repeated, keeping the volume of PBS added consistent. The tubes were briefly vortexed and centrifuged for 3 minutes, then placing them again on a magnetic rack for a minute. The supernatant is carefully removed and the same amount of PBS is added once more to both tubes. Both tubes were vortexed and then ultrasonicated in a sonicator water bath (Transonic T460, Camlab) for 15-20 minutes to disperse the IONPs evenly throughout the PBS solution. After the first few experiments, the sonication method was changed to using an ultrasonic sonicator probe (MSE Soniprep 150 Sonicator, amplitude = 26) for better dispersion of IONPs in the solution.

Once the IONPs were washed and sonicated, they were added to the 24-well plate containing the cells and a magnet (Neodymium magnets) was placed underneath the wells to pull the IONPs to the bottom of the wells. The magnet was used to eliminate the NPs settling time as an influencing factor when studying uptake and percentage uptake as the IONPs take about 11 – 16 hours to naturally reach the bottom of the plate where the cells are growing (Figure 3.4).

The main time points studied were 1 hour, 2 hours, 4 hours and 24 hours after the addition of IONPs. After 1 hour, the medium in the wells was removed and the wells were washed twice with PBS. The coverslips, with the cells adhered onto them, were transferred to a fresh 24-well plate to be fixed. The cells were fixed for 10 minutes at



room temperature using 4% PFA (paraformaldehyde) in PBS. To make 4% PFA, paraformaldehyde (TAAB Laboratories) was dissolved in PBS by heating the mixture to 70°C, the pH was then adjusted to 7 using NaOH, following which the mixture was filtered and aliquoted.

After fixing, the cells were washed three times with PBS and stored at 4°C ready for immunofluorescence staining. The same process was repeated to fix the cells at the remaining time points. The cells were then stained on the same day or within the next five days.

## **2.5 Immunofluorescence Staining**

Indirect immunofluorescence was used to detect the antigens of interest. Cell membranes were permeabilised using permeabilisation buffer with Triton X-100 for 5 minutes on ice. However, Triton X-100 is a non-selective detergent, which can also extract proteins along with the lipids (Jamur and Oliver, 2010). Alternatively, other buffers such as saponin buffer can be used at room temperature throughout the staining protocol as saponin is a selective buffer which interacts with membrane cholesterol forming temporary reversible holes in the membrane (Medepalli *et al.*, 2013). If Triton X-100 is used as a permeabilising agent, the buffer used for the rest of the protocol is 5% BSA in PBS or 5% FCS in PBS. If saponin is being used as a permeabilisation agent, the permeabilisation step can be omitted, thus starting directly with the blocking step. The 24-well plate containing the fixed coverslips were blocked with a blocking solution comprising of 5% BSA in PBS (if Triton X-100 was used) or saponin buffer, depending on the antibody used. Blocking of the coverslips prevents any non-specific binding of the antibodies. After blocking, the coverslips were transferred to an incubation chamber at room temperature which contained moist

pieces of tissue paper on either side to prevent the coverslips from drying out (see figure below).

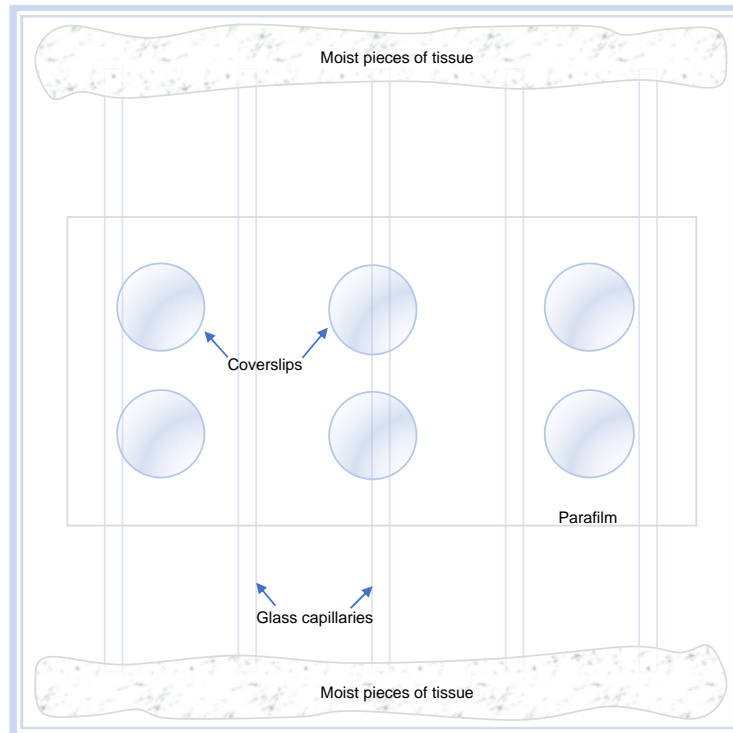


Figure 2.2. **Incubation chamber set up.** The above shows an illustration of the incubation chamber set up during immunofluorescence staining. Coverslips were placed on a piece of parafilm before adding the antibody mastermix. Moist pieces of tissue paper were placed at both ends and a lid was placed on top of the chamber to prevent drying out of coverslips.

The primary antibodies used were diluted accordingly in the buffer used. The mastermix was then pipetted onto each coverslip (30  $\mu$ l per coverslip) and left to incubate at room temperature in the incubation chamber for 30 minutes.

After the primary antibody incubation, the coverslips were transferred back into their respective wells to be washed in the buffer for 30 minutes.

The mastermix for the secondary antibodies was prepared similar to the primary antibodies. The coverslips were transferred again into the incubation chamber to be incubated with the secondary antibodies for 30 minutes. The incubation for the

secondary antibodies was carried out at room temperature in the dark to avoid any fluorophore bleaching due to the fluorescently labelled antibodies being light sensitive.

The coverslips were transferred back into the wells to be washed; the washes were also carried out in the dark for 30 minutes. The buffer was changed at regular time intervals for clearer images under the microscope. After the last wash, the coverslips were ready to be mounted onto slides. A drop of Vectashield Mounting Medium (Vector Laboratories) was added onto each coverslip before carefully placing a cover glass onto the coverslips. The slides were imaged using a Leica DM4000 Fluorescence microscope (LAS software) and Nikon Eclipse TE2000-S Confocal microscope (EZ-C1 software).

Antibody	Dilution	Stains	Primary/ Secondary	Host	Company
<b>Alexa-Fluor488 or AlexaFluor350- conjugated Wheat Germ Agglutinin (WGA)</b>	1:250	Plasma membrane	Lectin	-	Invitrogen
<b>Anti-Rab7</b>	1:200	Late endosomes	Primary	Mouse	Abcam
<b>Anti-Rab5</b>	1:200	Early endosomes	Primary	Rabbit	Abcam
<b>Anti- SOD2/MnSOD</b>	1:200	Mitochondria	Primary	Rabbit	Abcam
<b>Anti-Syntaxin 6</b>	1:200	Golgi apparatus	Primary	Mouse	BD Transduction Labs
<b>Anti-Caveolin-1</b>	1:100	Caveoli	Primary	Mouse	BD Transduction Labs
<b>Anti-ERp72</b>	1:100	Endoplasmic reticulum	Primary	Rabbit	Cell Signalling Technology
<b>Anti-Rab9</b>	1:100	Late endosomes	Primary	Rabbit	Abcam
<b>Hoechst 33342</b>	1:10000	Nucleic acid	-	-	Invitrogen
<b>Alexa Fluor 488 anti-mouse (Ex: 500nm, Em: 519nm)</b>	1:100	-	Secondary	Goat	ThermoFisher Scientific
<b>Alexa Fluor 546 anti-mouse (Ex: 561nm, Em: 573nm)</b>	1:100	-	Secondary	Goat	ThermoFisher Scientific
<b>Alexa Fluor 488 anti-rabbit</b>	1:100	-	Secondary	Goat	ThermoFisher Scientific
<b>Alexa Fluor 546 anti-rabbit</b>	1:100	-	Secondary	Goat	ThermoFisher Scientific

Figure 2.3. **Table of antibodies used in immunofluorescence staining.** This table shows all antibodies used in this thesis, along with dilution factors and manufacturers. Ex=excitation, EM=emission.

## 2.5.1 Colocalisation quantification

Following organelle staining as described above, the images obtained from microscopy were analysed using the open source software Fiji ImageJ (<https://imagej.net/Fiji>) and quantified by manual counting. An example of colocalisation quantification between human serum deposited IONPs and caveolae is shown in the table below. Quantification for 1 hour time point is given as an example below, all time points were analysed in the same way. The table includes data from two experimental repeats. All colocalisation quantifications in chapter 3 were carried out in this exact manner.

	Total number of cells in image (A)	Number of cells containing IONPs (B)	% of cells containing IONPs (C)	Number of cells with colocalisation (D)	% of cells with colocalisation (E)
17.02.17 - 1h - 002	19	7	36.84	0	0
17.02.17 - 1h - 005	10	3	30.00	0	0
17.02.17 - 1h - 007	16	5	31.25	0	0
17.02.17 - 1h - 009	13	5	98.46	0	0
17.02.17 - 1h - 011	22	7	31.82	0	0
13.03.17 - 1h - 002	9	6	66.67	0	0
13.03.17 - 1h - ph002	7	3	42.86	0	0
13.03.17 - 1h - 004	11	4	36.36	1	9.09
13.03.17 - 1h - 006	8	4	50.00	0	0
13.03.17 - 1h - 008	11	6	54.55	1	9.09
13.03.17 - 1h - 010	4	2	50.00	0	0

Figure 2.4. **Table layout for organelle quantification.** This table shows how colocalisation was quantified following organelle staining in chapter 3. The table shows data for the 1 hour time point of two independent experiments. First, the total number of cells in each image was counted. The number of cells which have internalised IONPs are then counted. The number of cells with colocalisation between IONPs and caveolae was also counted. To determine % of cells containing IONPs:  $B/A \times 100$ . To calculate % of cells with colocalisation:  $D/A \times 100$ . All graphs were plotted as an average percentage of each time point. Graphs were plotted using GraphPad Prism.

For all colocalisation quantification purposes, multiple images were taken per slide so that the quantification was carried out using at least 5 different fields of view per experiment for each time point. Experiments were carried out at least twice and average percentage colocalisation values were used to plot the graphs, using standard deviation as error bars. Colocalisation was visually identified as an overlay of both colours (red for IONPs and green for protein/organelle of interest) through the microscope lens of the Leica DM4000 microscope. Confocal microscopy was also used to take z-stack images of samples to confirm colocalisation, where strong colocalisation was seen using the Leica DM4000 microscope. Alternatively, Fiji ImageJ could be used to measure fluorescence or pixel intensity to quantify colocalisation from composite images, however, background noise and cross-staining need to be taken into account when using this method to avoid false positive results.

## **2.6 Veronal buffers**

Two veronal buffers, DGVB<sup>++</sup> and EGTA buffer, were used during IONP preparation in order to compare IONP uptake pattern in the cell line when the classical pathway was triggered *versus* the alternative pathway of the innate immune system. With the use of DGVB<sup>++</sup> buffer, we aim to measure deposition of serum components associated with the classical pathway. Even though the buffer is able to activate all three pathways (classical, alternative and lectin pathways), the classical pathway can be activated with a lower serum concentration compared to the other two pathways (Moreno-Indias *et al.*, 2012a). DGVB<sup>++</sup> buffer contains both Mg<sup>2+</sup> and Ca<sup>2+</sup> ions which are essential to activate the classical pathway because this pathway contains a calcium-dependent step. On the other hand, the EGTA buffer does not contain Ca<sup>2+</sup> ions and hence only the alternative pathway can be activated, thus only components of the alternative

pathway will be deposited on the IONPs through the use of this buffer. During IONP preparations for serum-coating, both buffers were diluted in a 1:1 ratio with the serum used. The steps for deposition were the same as described in section 2.4. Details of the buffer compositions can be found in section 2.1 (materials).

## **2.7 LysoTracker**

Approximately 60,000 cells/ml were seeded in a 24-well plate set up with 13mm coverslips and the IONPs were prepared and added to the cells as described previously. The IONPs were left to incubate with the cells at 37°C for 24 hours before adding green LysoTracker (Cell Signalling Technology, #8783) to separate wells in the plate. LysoTracker is a cell permeable dye which stains acidic compartments (lysosomes) in live cells. The concentration of lysotracker used per well was 100nM. Following addition, LysoTracker was left to incubate with the cells at 37°C for 15 minutes, after which the cells were washed three times using warm PBS. The cells were then mounted onto slides using imaging medium (section 2.1, materials), without fixing. The live cells were imaged immediately under the Leica microscope.

## **2.8 Dextran: a marker for fluid phase endocytosis**

Dextrans are polysaccharides and are made of chains of varying lengths and one of their many uses is as a fluid-phase marker. Dextrans have high water solubility and behave as Newtonian fluids (Xu *et al.*, 2009).

Cells were seeded as described in section 2.3 in a 24-well tissue culture plate, 24 hours prior to adding the IONPs and dextran. The IONPs were prepared as described previously and the FITC labelled dextran ( $M_r = 20,000, 40,000$  (Sigma) and 70,000 (Invitrogen)) was prepared to a concentration of 100mg/ml in PBS. The dextran was

further diluted to obtain a final concentration of 100 $\mu$ g/ml in each well. The dextran was added to the wells at the same time as the addition of IONPs. After incubation at 37°C, cells were washed with PBS and fixed at time points 1 hour, 2 hours, 4 hours and 24 hours using 4% PFA. Once fixed, the cells were stained with Hoechst 33342 to reveal DNA and the nucleus and imaged under the Leica fluorescence microscope and Nikon confocal microscope.

## **2.9 Western Blotting**

Western blot experiments were carried out to measure the level of C3 protein adsorption to the IONPs after 1 hour incubation with human serum vs. overnight incubation with the aim of increasing time efficiency for zebrafish embryo microinjections. IONPs were incubated with human serum as described in 2.4, following which they were run on an SDS gel as described below. After incubation with the sera and washing with PBS, IONPs were pelleted and resuspended in SDS sample buffer. Before loading on the SDS gel, samples were boiled on a heat block for 5 minutes and centrifuged for 3 minutes at 13,000 RPM using a microcentrifuge. The samples were then loaded onto a 12% SDS acrylamide gel (section 2.1, materials), along with 5 $\mu$ l of a protein marker, 'colour plus' (New England BioLabs). The gel was run on a mini-PROTEAN electrophoresis tank (BioRad) for 1 hour at constant current (25mA). Once the proteins had run to the bottom of the gel after approximately 1 hour, the membrane 'sandwich' for protein transfer onto a nitrocellulose membrane was prepared as illustrated in the figure below.



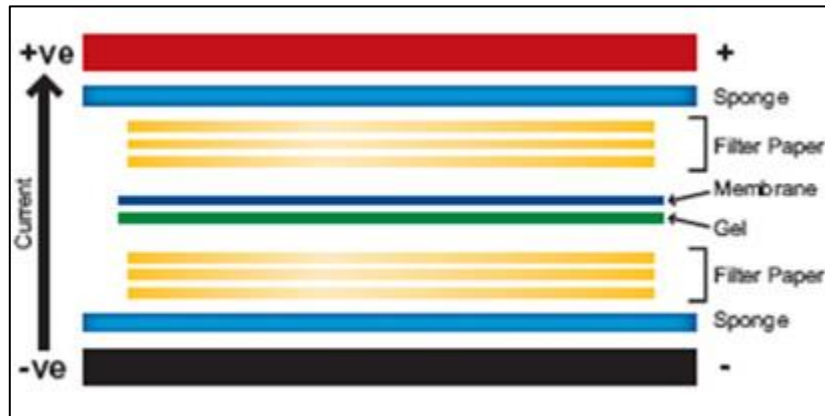


Figure 2.7. **Order of assembled membrane 'sandwich'**. After the SDS acrylamide gel was dismantled following the run, the membrane 'sandwich' was prepared as shown above. The sponges, filter papers and nitrocellulose membrane were pre-soaked in 1X transfer buffer prior to assembly. *Image from: abcam.*

The assembled membrane 'sandwich', an ice pack and a magnetic stirrer were added to the tank along with 1X transfer buffer. The transfer was run for 1 hour at constant voltage (100V). Since the transfer was run at a very high current, the ice pack and magnetic stirrer were added to avoid any overheating.

After the transfer, 5% ponceau-S in acetic acid (Sigma Life Sciences) was added to the nitrocellulose membrane in a petri dish for 3 minutes to check for the presence of protein bands on the membrane. Once the protein bands were visible, the ponceau-S was washed off with deionised water followed by PBS containing 0.1% Tween 20 (PBS-Tween) (two 5 minute washes).

After ponceau-S staining, the nitrocellulose membrane was blocked for 1 hour at room temperature with 5% milk powder in PBS-Tween on an orbital shaker. The nitrocellulose membrane was then washed twice with PBS-Tween (5 minute each) and the primary antibody was prepared according to its dilution in 5% milk and was then added onto the nitrocellulose membrane overnight at 4°C on an orbital shaker.

Following overnight incubation, the membrane was washed at room temperature with PBS-Tween (two 5 minute washes) and kept in PBS-Tween until it was developed. ECL (enhanced chemiluminescence) solutions were prepared and incubated with the nitrocellulose membrane for one minute at room temperature immediately before developing the membrane onto a film in a dark room.

## 2.10 Quantitative RT PCR

Quantitative RT PCR (qPCR) was used to measure mRNA expression levels of cytokines in response to IONP exposure. The cells were first grown in T75 flasks to 80-90% confluency and then starved in serum-free medium for 2 hours prior to the addition of IONPs. IONPs were prepared as described in section 2.4, complete media was removed from the flask, cells washed with PBS before addition of serum-free media and IONPs were then added to the flasks containing the cells for 2 hours. Following the 2 hour incubation with IONPs at 37°C, the cells were washed and scraped off the flasks for counting. A maximum of  $1 \times 10^7$  cells (counted using a haemocytometer) were harvested and spun down into a pellet. The supernatant was carefully removed and total RNA was extracted from the pelleted cells using the Qiagen RNeasy Mini Kit (#74104). RNA extraction was carried out as per the protocol provided in the kit.

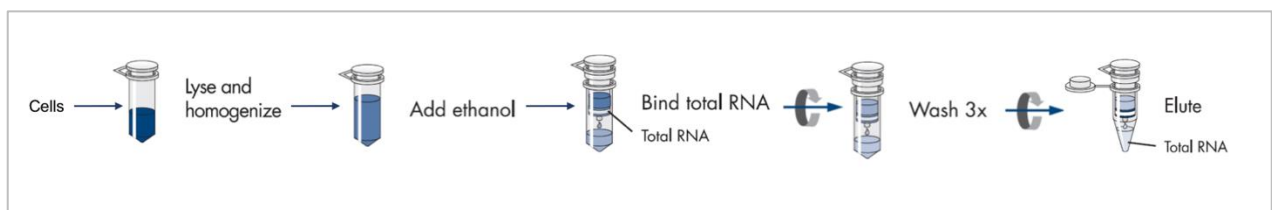


Figure 2.8. **Schematic representation of total RNA extraction protocol (Qiagen).** Pelleted cells were lysed and homogenised followed by the addition of ethanol to precipitate nucleic acids. After a series of washes and spins, the total RNA was eluted using RNase free water. *Images obtained and adapted from: Qiagen.*

Total RNA extracted was kept on ice at all times and the OD (optical density) was measured at absorbance wavelength 260/280 using a NanoDrop (2000/2000c spectrophotometer, ThermoFisher Scientific) to assess the purity of RNA. The RNA was aliquoted and stored at -80°C.

To convert the extracted RNA to cDNA, reverse transcriptase was performed using the High-Capacity RNA-to-cDNA™ Kit (ThermoFisher Scientific). Reactions were prepared in Eppendorf PCR tubes as per the manufacturer's instructions (up to 2µg of total RNA was used per 20µl reaction). Thermocycler (TETRAD2 Peltier Thermal Cycler, BioRad) settings were as follows: 37°C for 60 minutes, 95°C for 5 minutes and 4°C hold (as per protocol in the kit). cDNA was stored at -20°C until needed.

The cDNA was then used as a template for amplification by qPCR. On the day of qPCR, a mastermix was first prepared containing SYBR green PCR mastermix, forward primer, reverse primer and RNase free water. From the mastermix prepared, 9µl was pipetted into each well of a 96 well microplate. At the end, 1µl of cDNA was added to the respective wells. Negative control wells contained 1µl of RNase free water instead of cDNA. Each well contained the following:

<b>SYBR Green Mastermix (PowerUp SYBT green mastermix, Life Technologies Ltd)</b>	<b>5µl</b>
<b>Forward primer</b>	0.5µl
<b>Reverse primer</b>	0.5µl
<b>H<sub>2</sub>O (RNase Free)</b>	3µl
<b>cDNA</b>	1µl
<b>Total per well</b>	<b>10µl</b>

Figure 2.9. **Contents of each well in a 96 well microplate.** All relevant wells contained the above, with the exception of negative controls which contain 1µl of RNase free water instead of cDNA. Plates and all reagents were kept on ice at all times.

The table below lists all the primer sequences used in this thesis for qPCR reactions.

<b>Targets</b>	<b>Forward primer (5' to 3')</b>	<b>Reverse primer (5' to 3')</b>
<b>TNF-<math>\alpha</math></b>	CTGTAGCCCACGTCGTAGC	TTGAGATCCATGCCGTTG
<b>IL-1<math>\beta</math></b>	TGTAATGAAAGACGGCACACC	TCTTCTTTGGGTATTGCTTGG
<b>IFN-<math>\alpha</math></b>	GGACTIONTTGGATTCCCAGCAGGAGAAG	GCTGCATCAGACAGCCTTGCAGGTC
<b>IFN-<math>\beta</math></b>	AACCTCACCTACAGGGCGGACTTCA	TCCCACGTCAATCTTTCCTCTTGCTTT
<b>IL-6</b>	GAGGATACTACTCCCAACAGACC	AAGTGCATCATCGTTGTTTCATACA
<b>IL-8</b>	CAAGGCTGGTCCATGCTCC	TGCTATCACTTCCTTTCTGTTGC
<b>TGF-<math>\beta</math>1</b>	CAAGGGCTACCATGCCAACT	GTACTIONTGTGTCCAGGCTCCAA
<b>IL-10</b>	ATTTGAATTCCCTGGGTGAGAAG	CACAGGGGAGAAATCGATGACA
<b>NF-K<math>\beta</math>1</b>	GAAATTCTGATCCAGACAAAAAC	ATCACTIONTCAATGGCCTCTGTGTAG
<b>NLRP3</b>	AGAAGAGACCACGGCAGAAG	CCTTGGACCAGGTTTCAGTGT
<b>IL-12 p40</b>	CAGAAGCTAACCATCTCCTGGTTTG	TCCGGAGTAATTTGGTGCTTCACAC
<b>18S rRNA</b>	GTAACCCGTTGAACCCCAT	CCATCCAATCGGTAGTAGCG

Figure 2.10. **Primer sequences used in qPCR reactions.** Primers were purchased in powder form from ThermoFisher. Primers were diluted in RNase free water to a stock solution of 100 $\mu$ M and were further diluted to a working stock of 10 $\mu$ M. Primers were stored at -20°C and thawed on ice before use.

The loaded 96 well microplate is then run on a QuantStudio 7 Flex Real-Time PCR machine for DNA amplification. The run settings were set as recommended by the SYBR green mastermix manufacturer and were as follows: Initial denaturation: 95°C for 5 minutes. PCR cycle: Denaturation: 95°C for 10 seconds, Annealing and extension: 60°C for 30 seconds. Repeat: PCR cycles were repeated 40 times.

Using the QuantStudio 7 manufacturer's software, the amplification curve results were converted to excel files containing the CT values for each gene of each well. The CT value refers to that particular value where the fluorescence signal crosses the threshold line on the amplification curve. The data was then analysed using the  $2^{-\Delta\Delta CT}$

method (Rao *et al.*, 2013) to reveal fold change in gene expression, normalised against the CT values of the housekeeping gene (18s rRNA). Graphs of fold change in gene expression and  $\log_{10}$  of relative expression was plotted (chapter 4) using GraphPad Prism.

## **2.11 RNA Sequencing and Transcriptome analysis**

Cells were cultured, IONPs were prepared and incubated with cells in the same way as in the previous section, 2.11. Following incubation with IONPs, cells were counted and pelleted. Total RNA was extracted from the pelleted cells using the Qiagen RNeasy Mini Kit and the enclosed protocol was followed for RNA extraction in the same way as previously mentioned (2.11). The OD of the extracted total RNA was measured at absorbance wavelength 260/280 using the NanoDrop and the RNA was aliquoted and stored at  $-80^{\circ}\text{C}$  until samples were sent for RNA sequencing. RNA sequencing and standard RNA sequencing analysis, as described later, was performed by a company called Genewiz using the Illumina NovaSeq platform. Illumina sequencing uses short reads but allows for rapid, accurate and cost effective analyses.

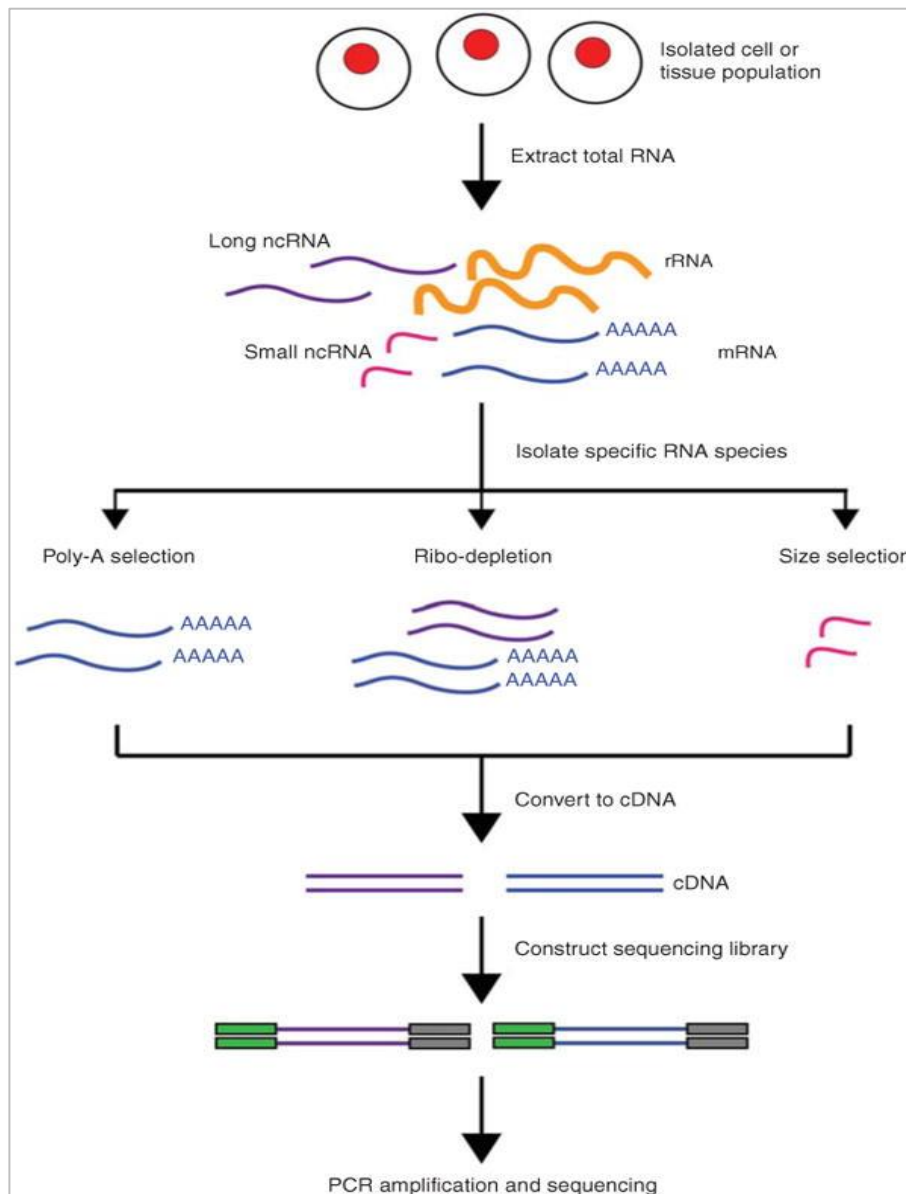


Figure 2.11. **Overview of RNA sequencing.** From total RNA extracted from a biological sample, desired RNA molecules are isolated. This can be done by three different methods as seen in the figure. In this case, poly-A-selection was used to select for RNA species, which enriches for mRNA species. The isolated RNA species is then converted to cDNA which is ready for sequencing following PCR amplification. *Reference and image from: Kukurba and Montgomery, 2015.*

On completion of sequencing, the data files are generated in an FASTQ-format, which contains the reads generated from the sequencing platform. The raw data obtained can carry errors, thus the data must be quality checked to filter out possible errors, indicated by low quality scores in the FASTQ files and data trimming was performed to remove low quality bases. Before carrying out differential gene expression analysis,

the reads obtained from RNA sequencing should be aligned to the reference genome, following which mapped reads are assembled into transcripts. Hit counts were then generated to assign the reads to specific genes or exons. Differential gene expression analysis was performed using DeSeq2 platform to compare gene hit counts and identify differentially expressed genes, which were narrowed down to significant differentially expressed genes by using a cut-off p-value of 0.05. To generate p-values and  $\log_2$  fold changes, the Wald test was used. Genes with a p-value < 0.05 and absolute  $\log_2$  fold change > 1 were called as differentially expressed genes (DEGs). Gene ontology analysis was carried out to cluster significant DEGs by their gene ontology and the enrichment of gene ontology terms was tested using Fisher exact test (GeneSCF v1.1-p2). Raw FASTQ files, data quality control, trimming, mapping, differential gene expression and gene ontology analyses were performed by Genewiz.



Figure 2.12. **Bioinformatics analysis workflow.** This workflow summarises the steps and analyses carried out by Genewiz, from quality report, FASTQ files, data QC, trimming & mapping, analysis hit counts for differential gene expression to gene ontology analysis. *Image from: Genewiz.*

From significant differentially expressed genes, gene ontology enrichment analysis was further carried out to identify genes relating to the pathways of immune processes. This was done using Uniprot, which is an online database that is updated regularly (<https://www.uniprot.org/>).

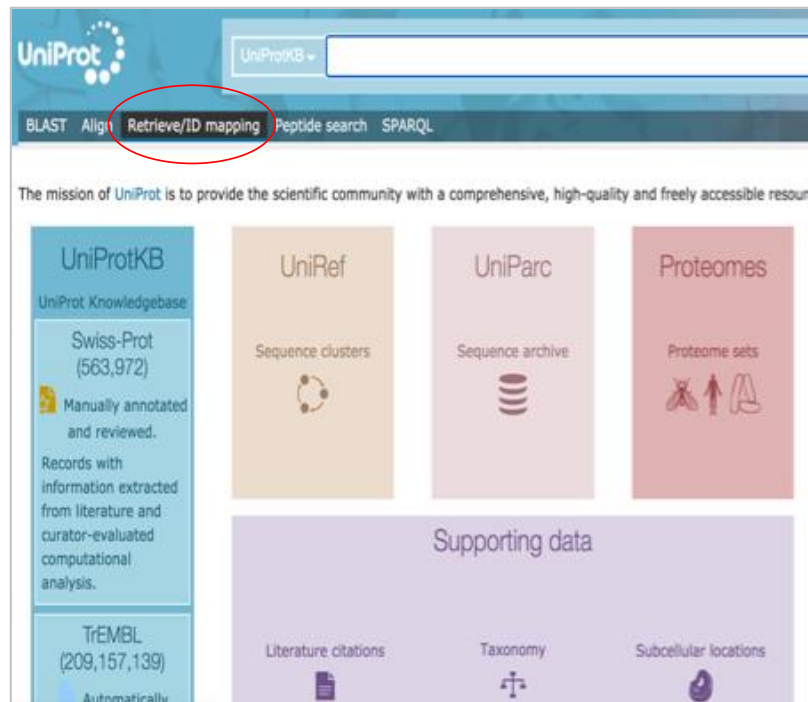


Figure 2.13. **Gene enrichment ontology analysis.** Significant DEGs were used to identify genes relating to specific pathways by using the retrieve/ID mapping tool from Uniprot (circled in red).

The gene names were entered onto the retrieve/ID mapping tool, the organism reference was set to *Mus Musculus* and the mapped results were generated and narrowed down as shown in the figure below.



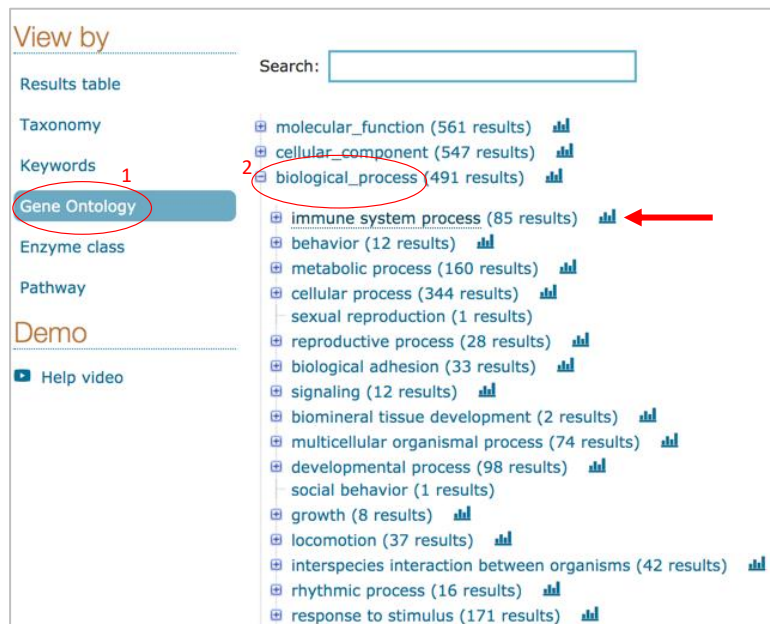


Figure 2.14. **Gene enrichment ontology analysis.** Once the mapping results was generated, the results were viewed by gene ontology pathways and 'immune system process' pathway was identified under biological processes. The results were then exported from UniProt in a microsoft excel sheet.

Once the list of gene names related to immune system processes were identified through UniProt, they were retrieved from our list of previously identified significant DEGs ( $p$ -value  $<0.05$ ). The genes with the most significance relating to immune system processes were selected and discussed in chapter 4, along with specific genes involved in innate immune responses in particular. Graphs showing upregulation and downregulation of discussed genes in chapter 4 were plotted using GraphPad Prism and heatmaps were generated using the MeV software.

## [2.12 Microinjections in zebrafish \(\*Danio rerio\*\) embryos](#)

### [2.12.1 Zebrafish breeding and husbandry](#)

Healthy adult male and female zebrafish (Wild-type, AB strain) are separated by using a tank with a removable divider in the late afternoon the day before the eggs are to be collected. Zebrafish are photoperiodic and will start breeding the next day at dawn.

They are kept in a carefully monitored room with a 14 hour light to 10 hour dark cycle and the water temperature is kept around 28°C (pH 6.2-7.5). In the morning, the divider is removed from the tank to allow spawning to begin. Once spawning has stopped, the eggs are collected into petri dishes and kept in E3 medium thereafter. The E3 medium was made as a 50X stock (section 2.1) and diluted to 1X solution when needed. A small amount of methylene blue can be added to the 1X solution as fungicide. The media should be stored at 4°C and 1X E3 solution should be warmed to 28°C before use on eggs or embryos. Once the eggs are collected, they are sorted under the microscope and any unfertilised or malformed eggs are removed. The healthy eggs are kept in a 28°C incubator until they are ready to be injected.

### [2.12.2 Nanoparticle preparations for zebrafish embryos microinjections](#)

The IONPs were incubated, washed and sonicated in the same manner as described in section 2.4 with the only difference being the concentration of IONPs used. The serum-deposited IONPs were coated with human serum proteins while the 'naked' IONPs were incubated in PBS only. Following some preliminary experiments, the best concentrations to be used where there is good IONP visibility whilst being non-lethal (>90% survival rate) to the embryos were 500µg/ml and 1000µg/ml (5µl was loaded into the needle and a final volume of 2nl was injected into the duct of Cuvier in each embryo at 2dpf, as described further later). 2-3µl of phenol red solution (Life Technologies) was added to each Eppendorf tube before the solution was loaded in the needles (described in section 2.9.3). Phenol red is used for ease of visibility during microinjections to confirm that the site of injection in the embryos is as accurate as possible every time.

### 2.12.3 Needle Preparation

The needles were made from glass capillaries using the P-97 Flaming/Brown™ Micropipette Puller (Sutter Instrument Company). The settings on the machine were adjusted as required (Heat-358, Pull-60, Velocity-80, Time-200). If the needles have a long shank, they are more likely to break during microinjections whereas if the needles have a short shank, they are more likely to damage the embryos despite being more sturdy.

Once the needles are made, they need to be prepared for injection. Using an extra-long pipette tip, the needle is carefully filled with the solution to be injected. The needle is then secured in a micromanipulator and the injection pressure is adjusted on the attached pneumatic pump to prevent any medium from flowing back into the needle. A very small bit of the needle tip is broken off to allow the solution to flow out of the needle and this is done by placing the tip in a small petri dish containing mineral oil (Sigma). A calibration micrometer slide is placed under the petri dish and using the highest magnification on a dissecting microscope (RS PRO Stereo Microscope), the tip of the needle is carefully broken off using clean tweezers. The size of the solution dot flowing out of the needle with each press of the injection foot pedal should be corresponding to the 0.15mm dot on the calibration slide, which translates to a volume of 2nl. If the droplet is slightly off the correct size, the injection pressure can be slightly adjusted to change the volume ejected from the needle. Once calibrated, the needle is ready for microinjections in embryos.

### 2.12.4 Zebrafish embryo microinjections (nanoparticles)

The zebrafish embryos were injected at 2 days post fertilisation (dpf) because they were developed enough to successfully locate the site of injection but not too

developed where they have a lot of pigment cells on their skin which would make the skin too tough to penetrate with the needle as well as making the site of injection harder to locate. The IONPs were injected in the duct of Cuvier (figure 2.4) which serves as a vein leading into the heart's sinus venosus and also collects all venous blood (Pontes *et al.*, 2017).

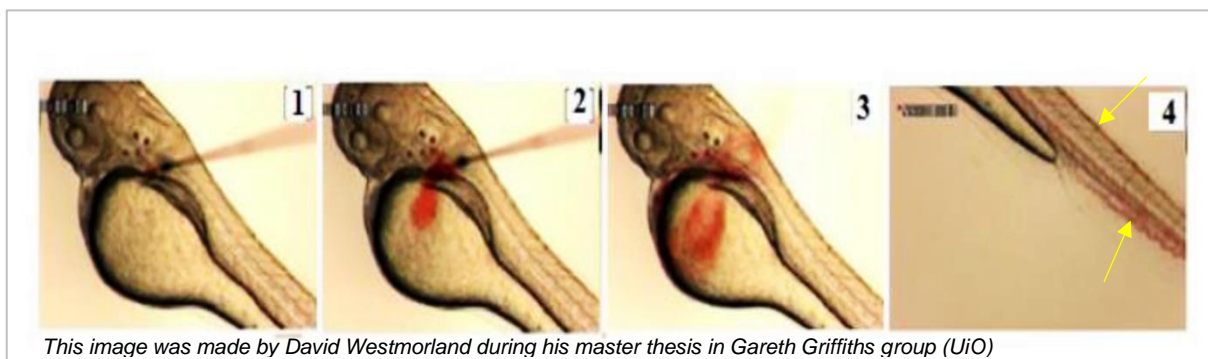


Figure 2.5. **Microinjections in the duct of Cuvier.** This series of images shows zebrafish embryo microinjections in the duct of Cuvier, which delivers the sample injected into the systemic circulation. Phenol red can be seen distributed in the circulation following injection in the last image.

Before microinjections, if they are not naturally hatched already, the embryos have to be carefully dechorionated using tweezers. Only healthy-looking embryos were chosen and placed on an agarose mould and 200µg/ml buffered tricaine methanesulfonate (MS222, Sigma Aldrich) was added dropwise to the agarose mould until the embryos were sedated. The embryos were left in MS222 for no longer than 45 minutes whilst the microinjections took place. Once sedated, the embryos were arranged and positioned to lie on their right side so that the duct of Cuvier is more accessible. The embryos are then injected and immediately placed back into E3 medium to reverse the anaesthesia. Once injected, the zebrafish embryos were monitored for any malformation or unusual swimming behaviours and imaged up until 5dpf.

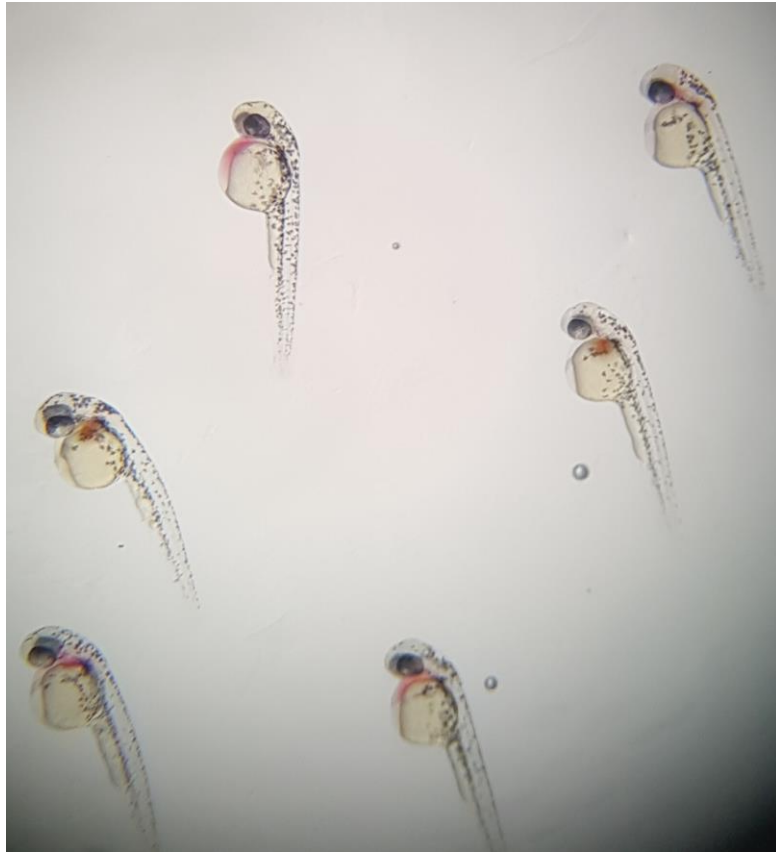


Figure 2.6. **2dpf embryo straight after IONP microinjection.** The above images show sedated embryos immediately after IONPs were injected into the duct of Cuvier. Phenol red can be seen to monitor immediate systemic delivery of injected IONPs.

### 2.12.5 Zebrafish embryo microinjections (dextran)

Dextran (Fluorescein isothiocyanate-dextran, MW = 2,000,000, Manufacturer: Sigma Aldrich) was injected in zebrafish embryos with the aim that macrophages in the embryos will phagocytose the dextran and when IONPs are injected two days later, we would be able to study the biodistribution of IONPs in relation to macrophages. The dextran was prepared at a stock concentration of 25mg/ml and diluted 1:2 to a final concentration of 12.5mg/ml in sterile PBS. 2-3 $\mu$ l of phenol red was added for ease of visualisation during microinjections. A final dextran volume of 2nl was injected in each embryo since volumes of 2-3nl were found to be optimal for yolk sac and blastomere microinjections (England and Adams, 2011). Dextran was injected

separately into two sites; one is injecting directly into the yolk sac at the 1-cell stage and the second is injecting into a peripheral blastomere at the 16 cell stage on the day of fertilisation. The needle preparation and calibration were done in the exact same way as mentioned before but at 0dpf the embryos did not need any sedation. They were placed in agarose gels that were prepared using microinjection moulds (World Precision Instruments). The width and design of the moulds are the ideal size for zebrafish embryos and allow them to align and stay in place during microinjections. Once injected, the embryos were transferred back into E3 medium and placed in a 28°C incubator, ready to be injected with IONPs at 2dpf.

#### 2.12.6 Zebrafish embryo fixing and imaging

For live imaging of the embryos, the embryos were sedated using MS222 and mounted onto slides (single depression concave microscope slides) using 3% methylcellulose (Sigma Aldrich) in E3 to keep the embryos in place. The embryos were imaged on the Leica Microscope (DMI8) using the LAS software. Following imaging, the embryos were placed back into E3 medium to dissolve the methylcellulose and reverse the anaesthesia. The selected embryos were then transferred to a 24-well plate and fixed with 4% PFA overnight for further imaging.

Once fixed, the embryos were stained using Hoechst 33342 (1:10,000 dilution) overnight at 4°C to stain the nucleic acid in cells for ease of visualisation under the microscopes. The fixed embryos were imaged on the Leica DM4000 Microscope to locate the distribution of IONPs at a lower magnification (X20) and these identified areas were imaged at a higher magnification using confocal microscopy. The embryos

were mounted on slides using 3% methylcellulose, similar to live imaging of the embryos.

The embryos were also imaged using the Nikon Eclipse TE2000-S Confocal Microscope, which takes images in a z-stack from top to bottom of the specimen. The best way found to successfully mount and image the zebrafish embryo through confocal microscopy was the use of Mowiol Mounting Solution (see section 2.1, materials) as the mounting medium. Mowiol is a liquid when mounted and solidifies after several hours at room temperature. Before oil immersion lenses are to be used, the Mowiol mounting medium should be allowed to harden in the dark overnight or at 37°C for about 20 minutes.

#### 2.12.7 Ethical Implications of using zebrafish embryos

Since all research carried out in zebrafish embryos were performed for no longer than 5 days post fertilisation, according to current legislations, no project license was required. Zebrafish embryos are considered to be protected animals after 5 days post fertilisation, following which a project license and personal license are required to carry out any further research under regulated procedures. The place of work at Brunel University London holds an establishment license, under which all zebrafish breeding and husbandry were performed. Furthermore, I hold a personal license (PIL), which helped with understanding all legislation and ethics associated with animal research.

#### 2.13. Statistical Analyses

All graphs presented in this thesis were designed using Prism (GraphPad Software Inc.). Heatmaps for the bioinformatics analyses were designed using MeV software.

Variability in all data was determined by calculating the standard deviation (using Microsoft Excel), denoted by error bars on graphs. ANOVA tests with a post-Tukey or Sinak test (as recommended by Prism based on the data sets being analysed) were carried out to determine significance when comparing multiple data sets. Results were deemed significant with a p-value  $<0.05$ . All statistical tests were performed using GraphPad Prism.



---

**3. Intracellular Localisation of Iron Oxide  
Nanoparticles in Mouse Macrophages**

---

### 3.1 Introduction

It is widely known that NPs have the ability to encapsulate and transport therapeutic components to be delivered to targeted cells. Intricately orchestrated by their nano-size, controlled drug delivery properties, surface charge and stability, NPs can cross biological barriers, such as cell membranes, and enter target cells to carry out their designed function. In spite of their desirable therapeutic purposes, NPs can also negatively affect the cells and cause unwanted adverse effects. A fundamental aspect of determining their end effect is to study the pathways that NPs use to enter cells and where they localise intracellularly. To achieve maximum therapeutic efficiency, the safe entry of drug delivery carriers into the targeted cells is of significant importance and coupled with their intracellular fate and localisation, will subsequently impact their cytotoxicity (Foroozandeh and Aziz, 2018).

The intracellular uptake routes of NPs will heavily depend on their size and surface charge, which can be engineered to suit the intended therapeutic function. These physical and chemical properties play a role in determining whether the NPs will be endocytosed via pinocytosis or phagocytosis (described in section 1.7). For example: a study used endocytic pathway inhibitors to show that 1 $\mu$ m particles were found to be endocytosed by phagocytosis and macropinocytosis whereas smaller NPs of 40nm were endocytosed by phagocytosis and macropinocytosis as well as clathrin-mediated endocytic pathways in mouse macrophages (Kuhn *et al.*, 2014). Another study also showed through the use of endocytic pathway inhibitors that 359nm modified chitosan NPs were endocytosed by more than one mechanism simultaneously in HeLa cells, suggesting that uptake mechanisms vary in different cell lines and that surface modification can also play a major role in the endocytic pathway (Nam *et al.*, 2009). Furthermore, a study showed that identical gold NPs (10nm) had different uptake

mechanisms in healthy cells compared to cancer cells, further suggesting that different cell types behave differently when exposed to NPs (Saha *et al.*, 2013). As described in chapter 1.9, once internalised, NPs are subject to intracellular vesicle trafficking from early to late endosomes before being very likely degraded in the lysosomes. The figure below gives an overview of intracellular trafficking pathways and the Rab GTPases that are involved in the intracellular trafficking of cargo molecules/particles, some of which will be encountered later in this chapter. Rab GTPases are a subfamily of Ras-like GTPases (Shi, Shi and Xu, 2017) and play important roles in the intracellular trafficking of vesicles from the moment they bud off the donor membrane as seen below.

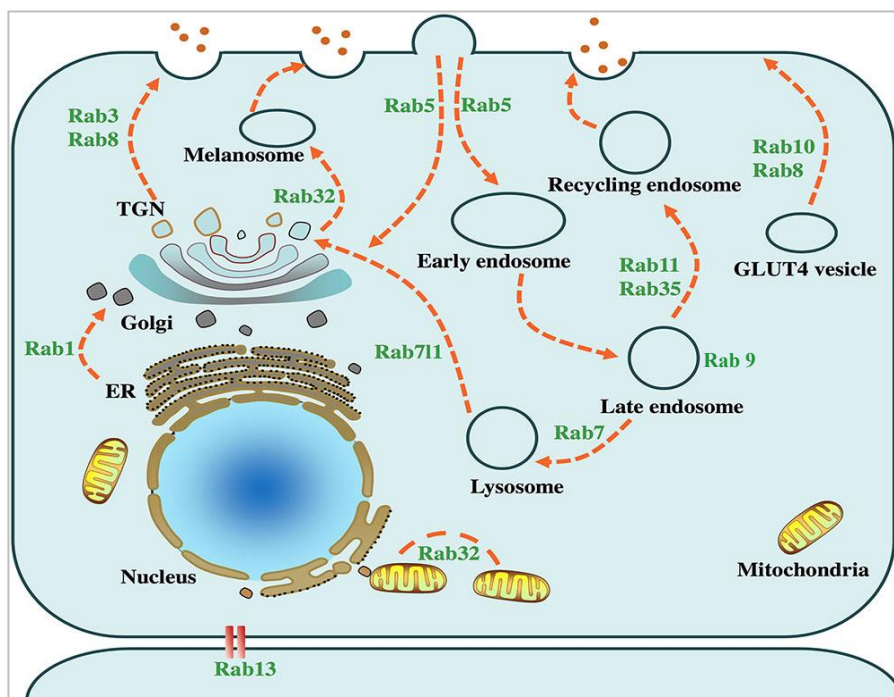


Figure 3.1. **Overview of intracellular vesicle trafficking and related Rab GTPases.** The above image shows intracellular trafficking pathways of internalised particles. For example, Rab5 is important in the formation of early endosomes at the plasma membrane. Early endosomes mature to become late endosomes, which can carry cargo to lysosomes for degradation or fuse with lysosomes (mediated by Rab7) to form endolysosomes. Orange broken arrows show the Rab proteins that facilitate that particular transport/trafficking pathway. ER: Endoplasmic reticulum, TGN: trans-Golgi network, GLUT4: glucose transporter type 4. *Image from: Shi, Shi, & Xu, 2017.*

This thesis chapter studies the intracellular localisation of iron oxide nanoparticles (IONPs) through organelle staining following the incubation of IONPs with mouse macrophages. The image below highlights the organelles studied.

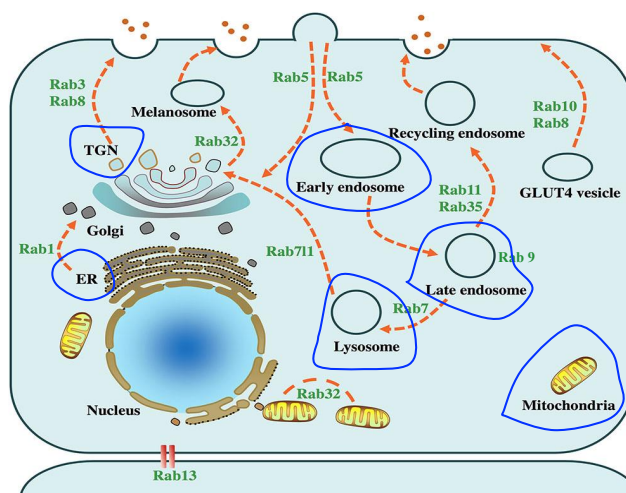


Figure 3.2. **Overview of organelles studied in this chapter.** The organelles stained through immunofluorescence and studied through microscopy are circled in blue. These include the early endosomes, late endosomes, lysosomes, mitochondria, trans-Golgi network and the endoplasmic reticulum. This pathway was chosen to be studied because this is the expected intracellular trafficking route of most NPs. *Image from: Shi, Shi, & Xu. 2017.*

We also investigated the differences in cellular uptake when the IONPs were deposited with serum proteins compared to ‘naked’/unmodified IONPs. This is because IONPs intended for therapeutic uses will encounter serum proteins in the bloodstream, especially when administered intravenously. Blood plasma contains high levels of proteins, red blood cells, white blood cells and platelets in suspension. Serum is the fluid that remains after clots from whole blood are removed. Serum/plasma is a protein-rich solution with a protein concentration of approximately 60-80 mg/ml, where 50-60% of proteins are albumins and the remaining 40% are globulins (of which 10-20% are IgG) (Leeman *et al.*, 2018). The interaction of IONPs and serum proteins *in vivo* can lead to the formation of a ‘protein corona’ on the IONP surface, which can

alter its fate and decrease therapeutic efficiency by promoting its recognition by phagocytes (Oh *et al.*, 2018). It has been reported that the deposition of serum proteins on NPs can activate the complement pathway, particularly via the alternative pathway (Moghimi and Simberg, 2017). In this study, we also investigate the differences seen in the cellular uptake of IONPs when the classical and alternative pathways of the complement system is favoured over another through the use of specific veronal buffers. Finally, fluorescent dextrans were used as markers of endocytosis. Different sized dextrans are commonly used to study endocytic pathways of various molecules, for example 10kDa dextrans are preferred to study fluid-phase endocytosis, including macropinocytosis and micropinocytosis whereas 70kDa dextrans are used mainly for studying macropinocytosis (Li *et al.*, 2015). Li *et al.* (2015) investigated the effect of different sized dextrans on endocytic pathways in HeLa cells and macrophage-like cells, and concluded that dextran 70 is a better probe to study macropinocytosis whereas smaller dextrans such as dextran 10 are better for the study of general fluid-phase endocytic pathways. Current literature shows that multiple studies have used fluorescent dextran as a marker of fluid-phase endocytosis, including a study by Iversen *et al.* (2012) who used dextran to investigate the uptake route of conjugated quantum dot NPs (approximately 30nm in diameter) and found that they are internalised by a macropinocytosis-like mechanism in HeLa cells (Iversen *et al.*, 2012). Thus, through the use of different-sized dextrans, we aim to investigate the uptake pathways of starch coated IONPs (100nm diameter).

## Aim & Hypothesis

The aim of this chapter is to investigate the intracellular uptake, trafficking and endocytic pathways of IONPs in mouse macrophages, following the formation of a protein corona. We hypothesize that IONPs with a protein corona will behave differently, especially uptake patterns, when compared to IONPs with no protein corona over a 24 hour time course. Furthermore, we hypothesize that different protein corona formulations will affect the uptake, endocytosis and intracellular fate of IONPs.

### 3.2 Results Using Human Serum

Mouse macrophages were incubated with human-serum deposited IONPs and ‘naked’ IONPs. To study the difference in uptake and their intracellular localisation, cellular organelles were labelled with fluorescent antibodies and the co-localisation with IONPs was observed with fluorescence microscopy. The table below summarises the results (Table 3.1).

<b>Organelle Stained</b>	<b>Colocalisation</b>
<b>Early endosome</b>	No
<b>Late endosome</b>	Little to none
<b>Mitochondria</b>	No
<b>Golgi apparatus</b>	No
<b>Caveolae</b>	Little to none
<b>Endoplasmic reticulum</b>	No
<b>Lysosome</b>	Yes

Table 3.1. ***Organelles stained in this part of the chapter.*** The table lists all organelles in murine RAW264.7 macrophages that were stained following incubation with IONPs. IONPs were first incubated with human serum proteins before being added to the cells. The cells were fixed with 4% PFA at time points 1h, 2h, 4h and 24h. After fixing, immunofluorescence staining was carried out and the cells were imaged with a Leica DM4000 microscope using LAS software. Lysosome staining was done in live cells using Alexa488 LysoTracker and imaged using the same equipment.

Three dextran sizes (molecular weights 20,000, 40,000 and 70,000) were used as endocytic markers and co-localisation was seen with all dextrans, with the strongest co-localisation seen with dextran 70,000.

### 3.2.1 Nanoparticle uptake over a 24h time course (serum-deposited)

To have an initial understanding of the uptake pattern of IONPs at varying time points, the surface of fluorescently labelled starch coated IONPs (568nm excitation (red fluorescence)) was deposited with complete human serum and incubated with mouse macrophages (RAW264.7). The cells were cultured on glass cover slips overnight and fixed 15 minutes, 30 minutes, 1 hour, 2 hours, 4 hours and 24 hours after exposure to IONPs. After fixation, the plasma membrane was stained using FITC labelled Wheat Germ Agglutinin (WGA), a lectin which specifically binds to N-acetyl-D-glucosamine and Sialic acid residues and Hoechst 33342 was used to label DNA and stain the nucleus. The IONPs show red fluorescence (Figure 3.3).

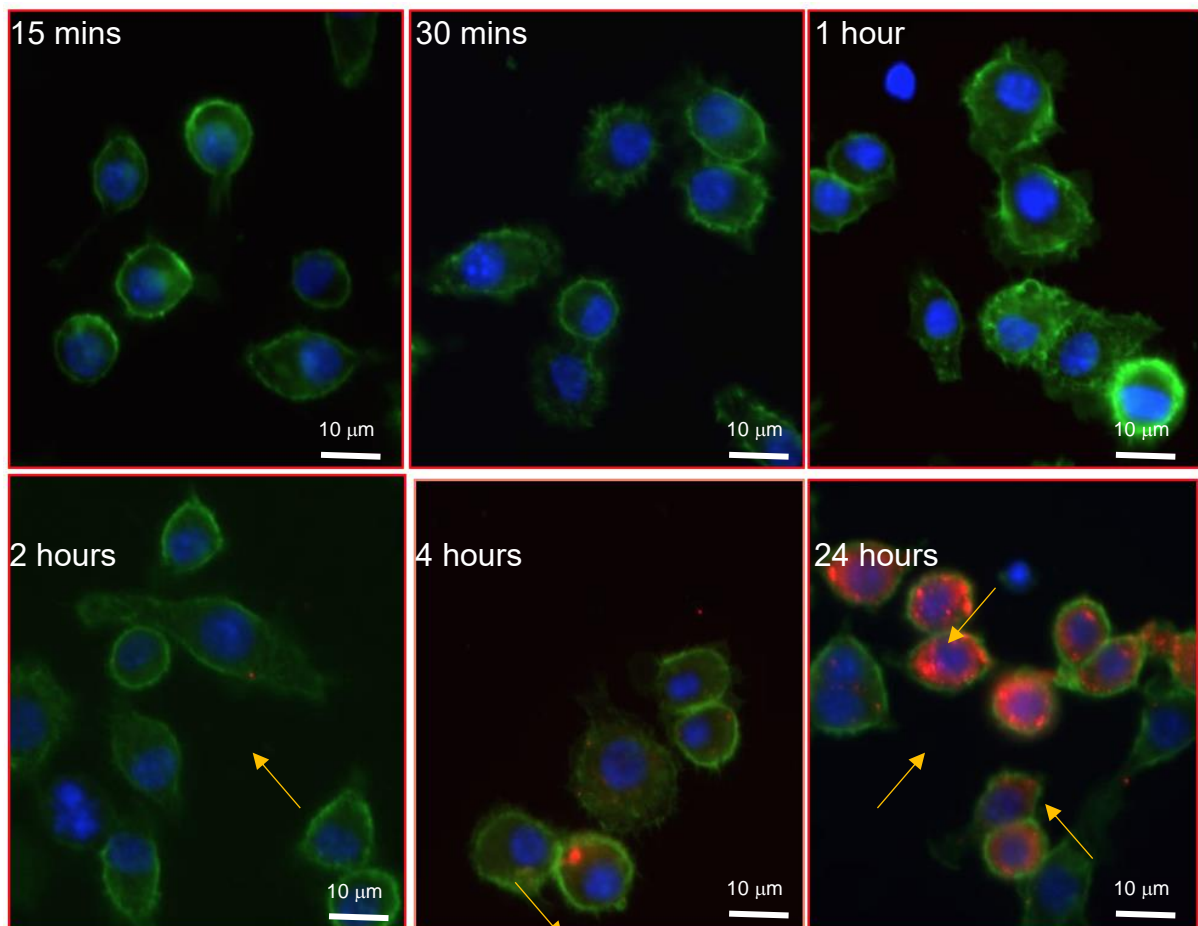


Figure 3.3. ***Uptake of serum deposited IONPs in RAW 264.7 cells over a 24h time course.*** The images show RAW 264.7 cells incubated with the fluorescently labelled IONPs for the indicated time points before fixation with 4% PFA and staining with FITC labelled WGA lectin to label the plasma membrane (green). Hoechst 33342 was used to label DNA (blue) and IONPs can be seen as red clusters (arrows). Cells were imaged on Leica DM4000 microscope using LAS software. Scale bar = 10 $\mu$ m.



Figure 3.3 demonstrates uptake in murine RAW 264.7 cells following incubation with human serum deposited IONPs. The results show some IONP uptake after 2 hours and 4 hours, however, after 24 hours, the cells appear to be almost saturated with IONPs. The earlier uptake seen varied between experiments where more IONP uptake was seen at 2 hours and 4 hours compared to the above results.

This was narrowed down to these possibilities:

1. Since the RAW cells used for the experiments had been in cell culture for over 10 weeks and thus had gone through at least 20 passages, the phenotype and functional stability of the cells might have been affected. For subsequent experiments, the cells were not used if they had gone through more than 15 passages in order not to influence data reliability.
2. The human serum used in this experiment had undergone several freeze-thaw cycles, which could have led protein instability/activity.
3. The nanoparticle settling time has to be taken into account, which was about 11-16 hours. During the initial experiments (results in section 3.2.1 and 3.2.2), no magnet was used to help the IONPs settle immediately to the bottom of the wells after addition. From section 3.2.3 onwards, a strong magnet was held against the the bottom of the 24-well plate for IONPs to immediately settle in close proximity to the cells and more IONP uptake was seen at 2 and 4 hours thereafter.

### 3.2.2 Nanoparticle Uptake – Serum-deposited vs ‘Naked’

Once the uptake pattern of serum-deposited IONPs at specific time points was established, the uptake of serum deposited fluorescently (488nm) labelled IONPs was compared to the uptake of ‘naked’ IONPs at the same time points. The plasma membrane was stained using fluorescently labelled WGA lectin and Hoechst 33342 was used to label DNA and stain the nucleus.

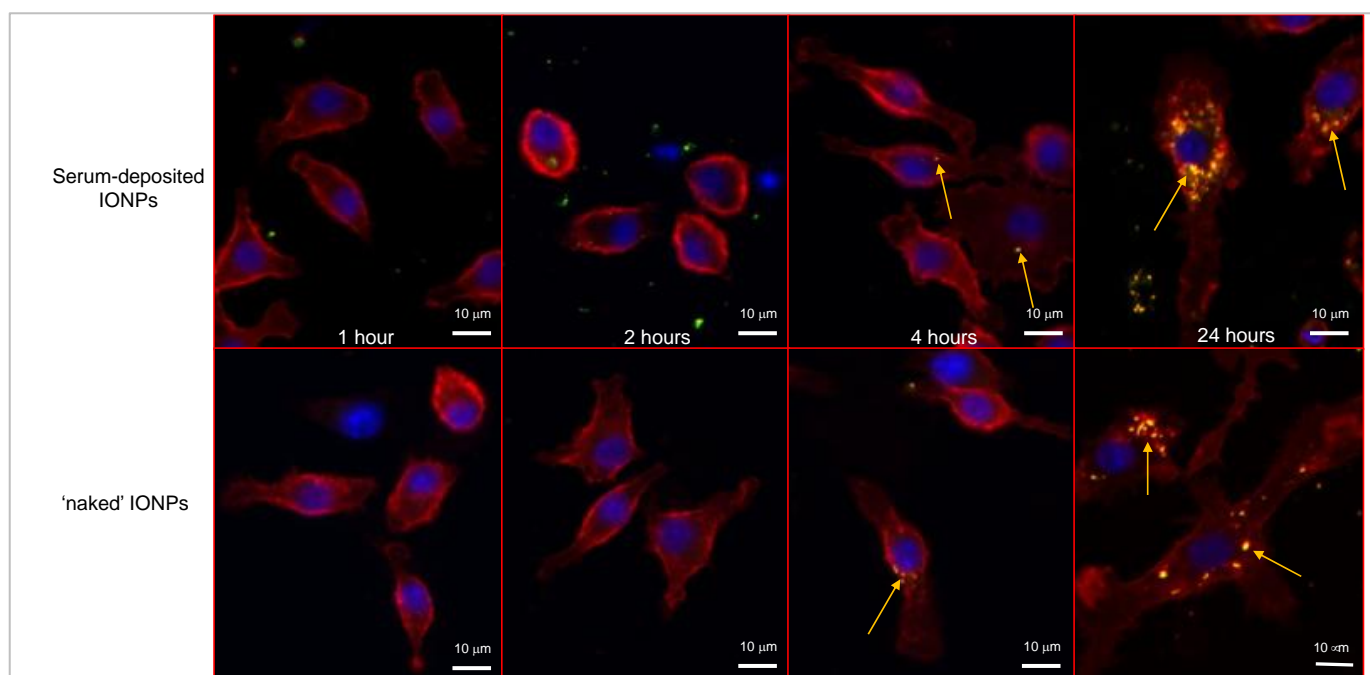


Figure 3.5. **Uptake of serum-deposited IONPs vs. ‘naked’ IONPs.** The images show uptake patterns in murine RAW264.7 macrophages seen at 1h, 2h, 4h and 24h comparing serum-deposited IONPs and ‘naked’ IONPs. The plasma membrane was stained with TRITC labelled WGA (red), Hoechst 33342 was used to stain the nucleus (blue) and IONPs can be seen in green (arrows), which appear yellow inside the cells due to the red WGA staining on the cell surface. At 24 hours, more serum-deposited IONPs were seen in the macrophages compared to ‘naked’ IONPs. Cells were incubated with IONPs, fixed at the indicated time points and stained. Cells were imaged on Leica DM4000 microscope using LAS software.

The above images (Figure 3.5) show the uptake of serum deposited IONPs in RAW cells after 1 hour, 2 hours, 4 hours and 24 hours. Similar to the previous results, the same uptake pattern is seen, with most uptake seen after 24 hours. The noticeable difference is that at 24 hours, ‘naked’ IONPs show less uptake compared to serum-deposited IONPs.

Since IONPs were incubated with starved (serum-free medium) RAW cells, this suggests that human serum derived proteins, which are absent from samples with the 'naked' IONPs, have a key role in mediating the uptake of IONPs and very likely act as opsonins to favour endocytosis. Furthermore, after 24 hours cells incubated with 'naked' IONPs show a change in cell morphology, indicating signs of stress, even though in both cases (serum-deposited and 'naked'), the cells were serum-starved. However, similar to the previous experiment described in 3.2.1, the settling time of the IONPs has to be taken into consideration as no magnet was used to enhance interaction between cells and IONPs.

As part of preliminary studies, IONP settling time was determined by adding serum-deposited and 'naked' IONPs to live cells in a petri dish. The settling was followed through live cell imaging on a Nikon inverted microscope with a heated stage using NIS-Elements software. The results below indicate that serum deposited IONPs settle to the bottom of the dish slightly faster than 'naked' IONPs. For all future experiments, strong magnets were used to help the IONPs settle immediately to the bottom of the dish, straight after their addition to the cells.

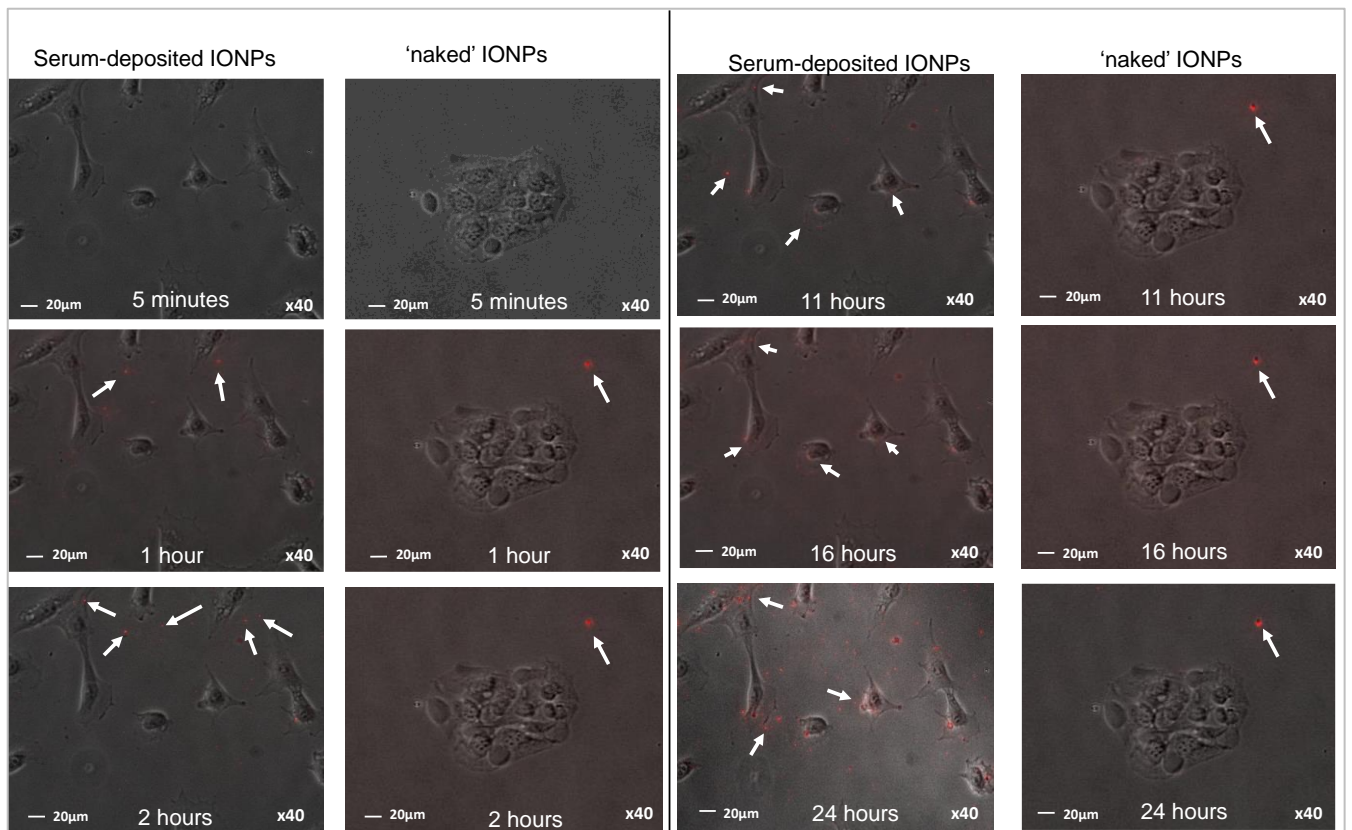


Figure 3.4. **Investigating IONPs settling time over a 24-hour time period.** IONPs were added to RAW cells in a petri dish, immediately followed by live cell imaging. The images show a faster settling time for serum-deposited IONPs compared to 'naked' IONPs. From 11 hours onwards, the cells seem to have internalised the IONPs. Thus, to avoid discrepancies regarding IONPs settling time in relation to uptake patterns, strong magnets were used during experiments to immediately pull IONPs to the bottom of the dish. The cells were imaged live using an inverted Nikon Eclipse TE2000-S Confocal Microscope (NIS-Elements software) with a heated stage.

### 3.2.3 Early Endosome Staining

Early endosomes are the first 'sorting stations' for internalised particles. Rab 5 belongs to the Rab superfamily of small GTPases and plays a key role in controlling many endocytic processes including invagination at the plasma membrane, signalling and endosomal fusion (Stone et al., 2007). Activated Rab 5 recruits its effectors at the plasma membrane and is an important regulator of vesicular trafficking during early endocytosis (Zerial and McBride, 2001). During the early endocytic pathway, Rab 5 mediates clathrin-coated vesicle transport from the plasma membrane to early endosomes and also mediates early endosome fusion (Zerial and McBride, 2001).

The images below show Rab 5 antibody staining, used as an early endosomal marker, in green, to visualise early endosomal compartments.

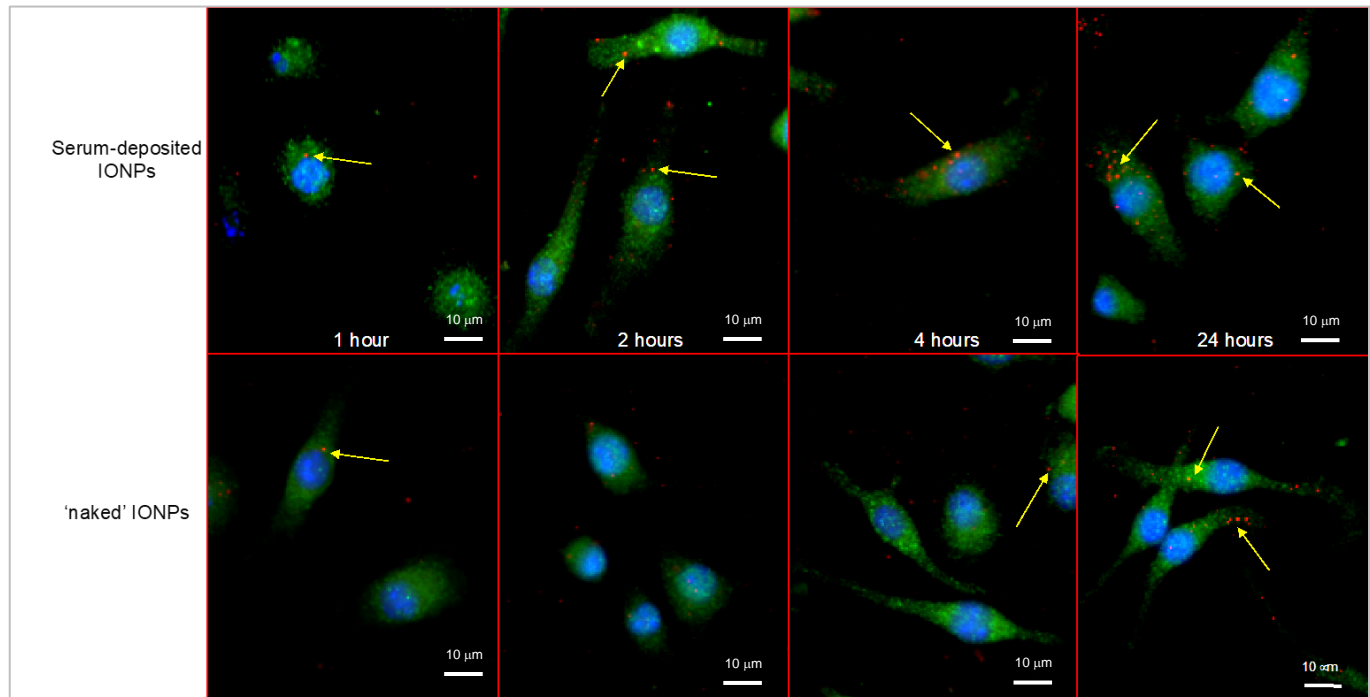


Figure 3.5. **Early endosome staining.** The images show early endosome staining in murine RAW 264.7 macrophages following addition of serum-deposited IONPs and 'naked' IONPs. IONPs were coated with serum for 1 hour at 37°C on a shaker, following which they were washed in PBS and sonicated before being added to the cells. The IONPs were left to incubate with the cells at 37°C and fixed using 4% PFA at specific time points, followed by immunofluorescence staining. Anti-Rab5 antibodies were used as early endosome marker (green), Hoechst 33342 was used to label the nucleus (blue). Uptake of IONPs (red) inside macrophages can be seen at early time points. No colocalisation between IONPs and Rab5 is seen. Two independent experiments were carried out and representative images are displayed. Cells were imaged on a Leica DM4000 microscope using LAS software.

Since it was observed during initial experiments that there was no IONP uptake at time points 15 and 30 minutes, the two first time points were omitted henceforth. The time points at which cells were fixed were 1 hour, 2 hours, 4 hours and 24 hours following the addition of IONPs. Prior to IONP incubation with cells, the IONPs were sonicated using a sonication probe rather than an ultrasonic water bath to avoid 'clusters' seen in earlier experiments and to achieve a better dispersion of IONPs. The results show some uptake as early as 1 hour, incrementally increasing until 24 hours (Figure 3.5) but no colocalisation with early endosomes (Rab 5) was observed. These results

suggest that either IONPs are not present in early endosomes at these specific time points or that their concentration in these organelles is too low for detection.

The results show consistency in the uptake pattern of serum-deposited and 'naked' IONPs, where lower uptake is seen with 'naked' IONPs.

### 3.2.4 Late Endosome Staining

Rab 7, like Rab 5, is also a member of the Rab superfamily of small GTPases. Rab 7 associates with the effector protein RIPL to regulate membrane trafficking from early to late endosomes and lysosomes (Jordens *et al.*, 2001). Rab 7 also contributes to the regulation of growth factor receptor endocytic trafficking and degradation as well as in the maturation of phagosomes (Ceresa and Bahr, 2006).

In figure 3.6 below, anti-Rab7 antibodies were used as late endosomal marker, Hoechst 33342 was used to label DNA.

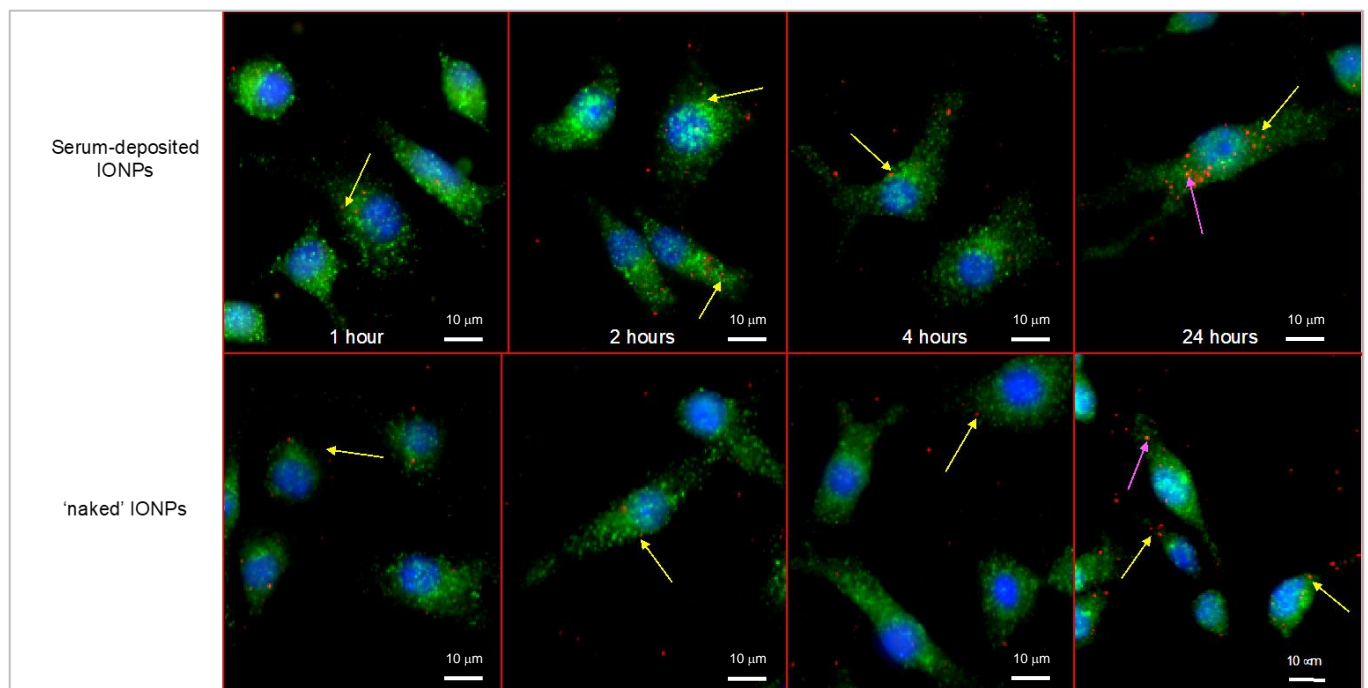


Figure 3.6. **Late endosome staining.** The images show late endosome staining in murine RAW 264.7 macrophages following addition of serum-deposited IONPs and 'naked' IONPs. IONPs were coated with serum for 1 hour at 37°C on a shaker, following which they were washed in PBS and sonicated before being added to the cells. The IONPs were left to incubate with the cells at 37°C and fixed using 4% PFA at specific time points, followed by immunofluorescence staining. Anti-Rab7 antibodies were used as late endosome marker (green), the nucleus was labelled with Hoechst 33342 (blue). Uptake of IONPs (red, yellow arrows) inside macrophages can be seen at early time points. Results show little colocalisation between IONPs and Rab7 (purple arrows). Two independent experiments were carried out and representative images are displayed. Cells were imaged on a Leica DM4000 microscope using LAS software.

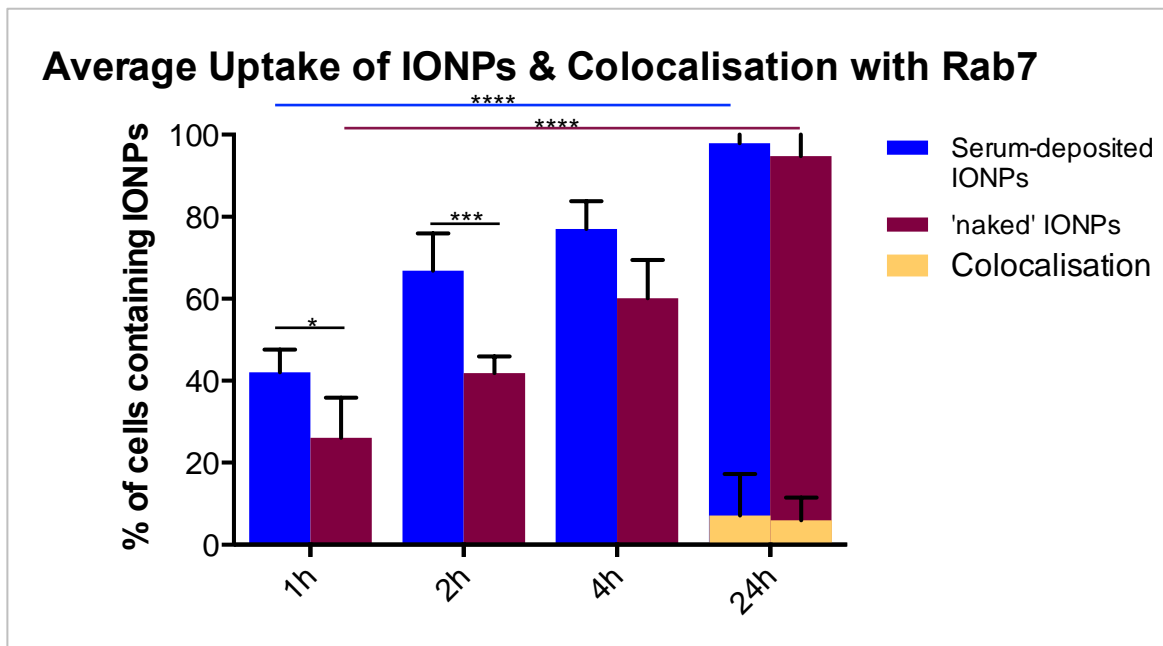


Figure 3.7. **Late endosome staining quantification.** The graph shows the average uptake of serum deposited and 'naked' IONPs in RAW264.7 macrophages. Average uptake was determined by calculating the % of cells that contained IONPs. Some colocalisation was seen at 24 hours in both IONPs conditions. Colocalisation was calculated from the number of cells where colocalisation was seen out of total number of cells. Error bars represent standard deviation. See chapter 2 (methods) for in depth detail of how the analysis was done. Two independent experiments were carried out and the graph was plotted using GraphPad Prism. A two-way ANOVA test was performed using GraphPad Prism. Statistical significance was found between the two 1h samples and the two 2h samples, as shown. Statistical significance was also found for uptake between all samples, except for 2h vs 4h (serum-deposited IONPs) and 1h vs 2h ('naked' IONPs). Some of the highest significance is shown on the graph. No statistical significance was found for colocalisation of IONPs. Black lines compare uptake for each time point.

From the above results (figure 3.7), no statistically significant colocalisation between IONPs and late endosomes (Rab 7 staining) with either serum-deposited IONPs nor 'naked' IONPs was observed, suggesting that the IONPs are not present in high amounts in the late endosomes at the time points investigated. The data shows little to no evidence of IONP presence in late endosomes of murine RAW264.7 macrophages within the first 24 hours of exposure. It is thus unlikely that for the IONPs accumulate in these organelles before either recycling back to the plasma membrane or forward movement into lysosomes for degradation within the time investigated. It is possible, however, that most IONPs have already been trafficked to degradative organelles at 24 hours. These results suggest that the resident time within late

endosomes is low and that no significant accumulation occurs. However, an alternative hypothesis is that IONPs take an alternative route to be trafficked intracellularly following endocytosis.

### 3.2.5 Mitochondrial Staining

Mitochondria are important intracellular organelles with the major task of providing energy to the cells through the production of adenosine triphosphate (ATP). However, mitochondria have many other functions including mediating cell death in a cascade of events orchestrated by apoptogenic proteins (Salnikov et al., 2007). Furthermore, increased membrane permeability of the mitochondria to macromolecules is an important contributing factor to the cell's apoptotic and necrotic death (Friedman and Nunnari, 2014). Some studies have shown that NPs such as gold NPs can localise to the mitochondria and mitochondria-targeting NPs such as modified titanium dioxide NPs were successfully retained in the mitochondria (Wongrakpanich *et al.*, 2014). NPs targeting mitochondria are also studied as therapeutic agents in treatment of mitochondrial diseases (Pathak, Kolishetti and Dhar, 2015). Hence, we investigated whether IONPs had the ability to localise to mitochondria.

The images below show mitochondrial staining in murine RAW 264.7 cells using an antibody directed against mitochondrial superoxide dismutase (SOD2) and detection with an Alexa488 labelled secondary antibody.



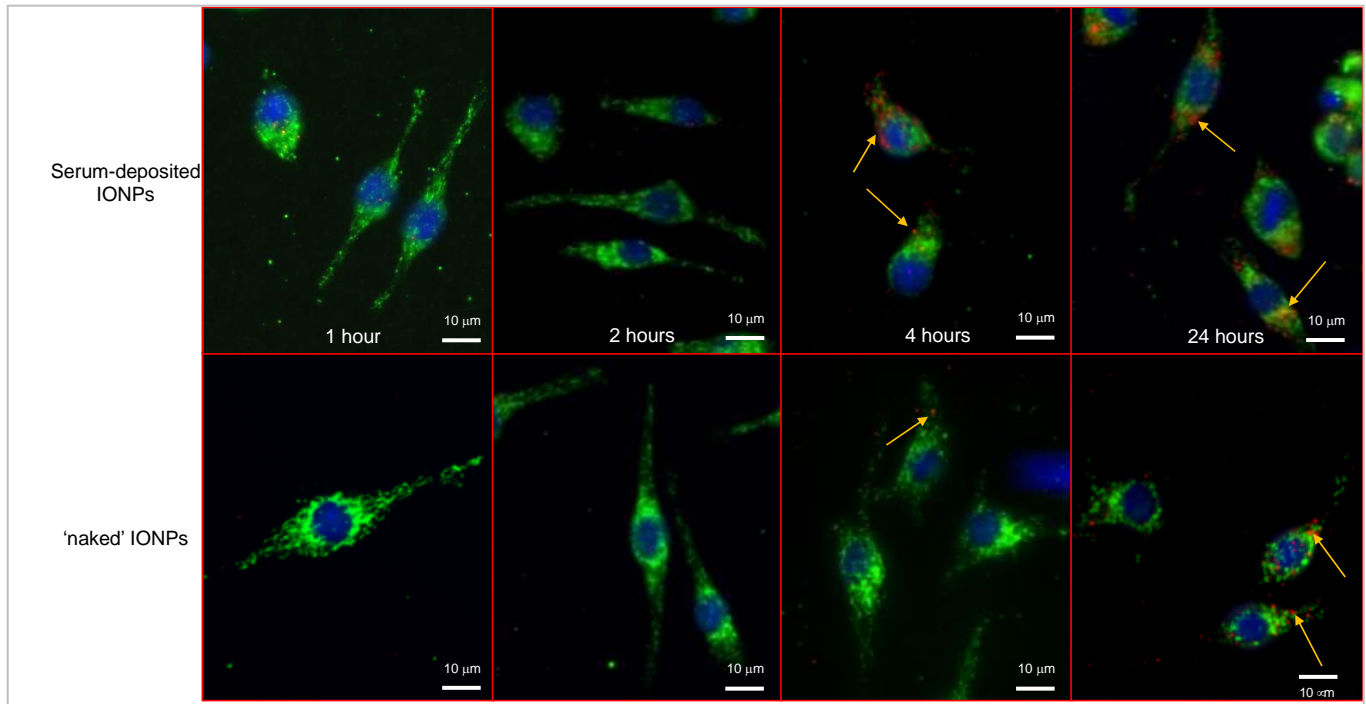


Figure 3.8. **Mitochondria staining.** The images show mitochondrial staining in murine RAW264.7 macrophages following addition of serum-deposited IONPs and 'naked' IONPs. IONPs were coated with serum for 1 hour at 37°C on a shaker, following which they were washed in PBS and sonicated before being added to the cells. The IONPs were left to incubate with the cells at 37°C and fixed using 4% PFA at specific time points, followed by immunofluorescence staining. Mitochondria were stained with an anti-SOD2 antibody (green), the nucleus was stained with Hoechst 33342 (blue). No colocalisation between IONPs (red, yellow arrows) and mitochondria was observed. Two independent experiments were carried out and representative images are displayed. Cells were imaged on a Leica DM4000 microscope using LAS software.

Following staining for early and late endosome, the next organelle investigated was mitochondria. The data and images obtained showed no colocalisation between mitochondria and serum deposited IONPs or 'naked' IONPs, suggesting the absence of IONPs in mitochondria (figure 3.8).

### 3.2.6 Golgi Staining

The Golgi apparatus is an intracellular organelle which acts as 'sorting station' for newly synthesised proteins but also receives proteins and lipids that are retrogradely transported after endocytosis (Cooper, 2000). This is an alternative pathway for cellular internalisation, avoiding the acidic and hydrolytic environment of the

lysosomes (Yameen *et al.*, 2014). In the images below (figure 3.9), the Golgi apparatus has been stained with an antibody directed against syntaxin 6 and detection with an Alexa488 labelled secondary antibody.

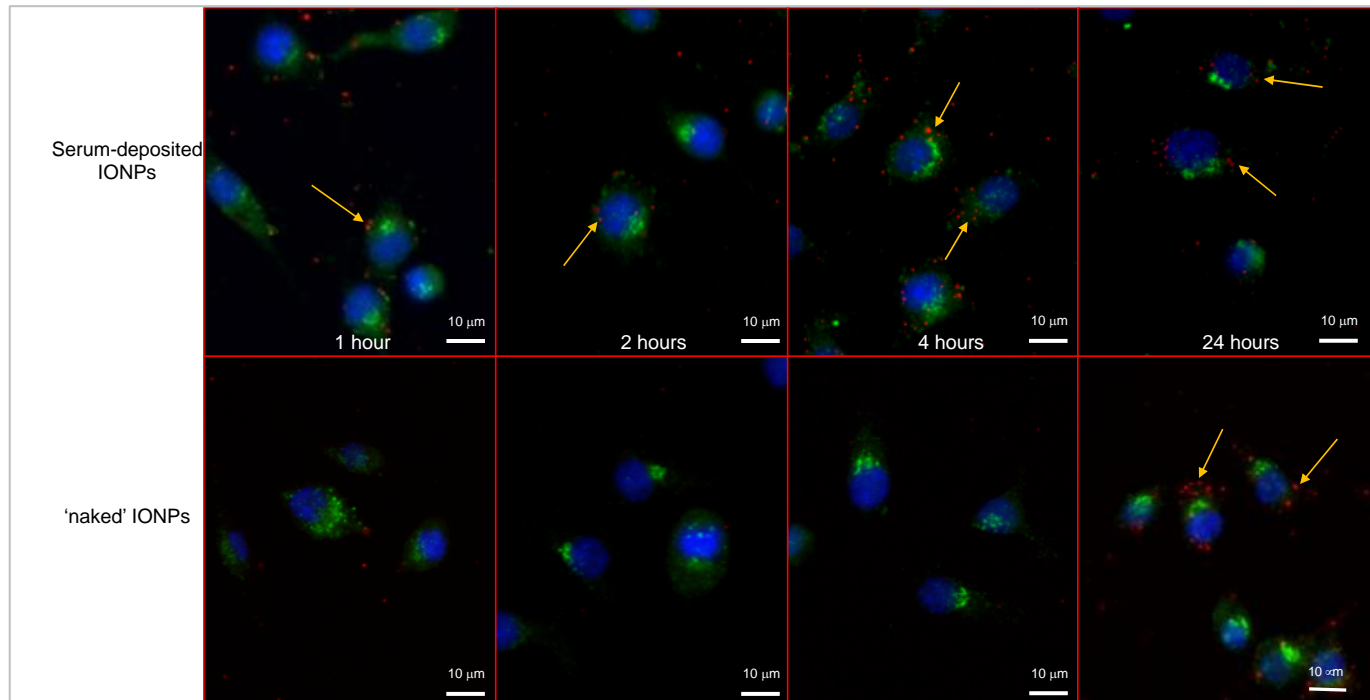


Figure 3.9. **Golgi apparatus staining.** The images show Golgi staining in murine RAW264.7 macrophages following addition of serum-deposited IONPs and 'naked' IONPs. IONPs were coated with serum for 1 hour at 37°C on a shaker, following which they were washed in PBS and sonicated before being added to the cells. The IONPs were left to incubate with the cells at 37°C and fixed using 4% PFA at specific time points, followed by immunofluorescence staining. The Golgi apparatus was stained with an anti-syntaxin 6 antibody (green), the nucleus was stained with Hoechst 33342 (blue). No colocalisation between IONPs (red, yellow arrows) and the Golgi was observed. Two independent experiments were carried out and representative images are displayed. Cells were imaged on a Leica DM4000 microscope using LAS software.

The images above (Figure 3.9) show no colocalisation between the Golgi apparatus and serum deposited NPs nor 'naked' IONPs. This indicates that IONPs were not present in the Golgi apparatus or trafficked from late endosomes to the Golgi apparatus during the first 24 hours of exposure of RAW264.7 cells to the IONPs.

### 3.2.7 Caveolae Staining

Caveolae are 60-80nm wide dips in the plasma membrane containing caveolin. These structures can bud from the cell surface and form intracellular vesicles. The function of caveolae is still not very well understood, however they are believed to mediate uptake of certain particles via receptors that cluster in caveolae (Kiss and Botos, 2009).

Caveolins make up the majority of membrane proteins of caveolae and can be detected by immunofluorescence staining. The antibody used in this case was directed against caveolin 1 and the caveolae can be seen as green punctate dots in the figure below (figure 3.10).

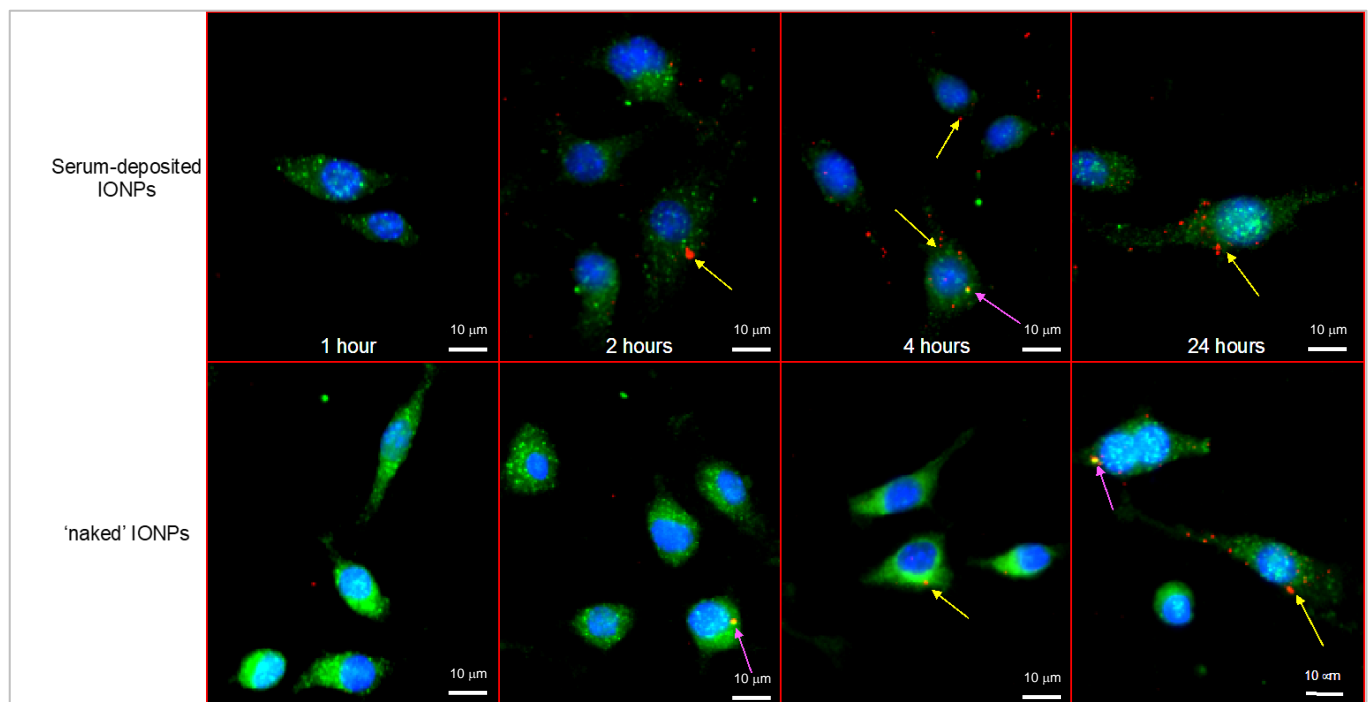


Figure 3.10. **Caveolae staining.** The images show caveolae staining in murine RAW 264.7 macrophages following addition of serum-deposited IONPs and 'naked' IONPs for the indicated times. IONPs were coated with serum for 1 hour at 37°C on a shaker, following which they were washed in PBS and sonicated before being added to the cells. The IONPs were left to incubate with the cells at 37°C and fixed using 4% PFA at specific time points, followed by immunofluorescence staining. Caveolae were stained with an anti-caveolin 1 antibody (green), the nucleus was stained with Hoechst 33342 (blue). Some colocalisation between IONPs (red, yellow arrows) and caveolae (pink arrows) was observed. Two independent experiments were carried out and representative images are displayed. Cells were imaged on a Leica DM4000 microscope using LAS software.

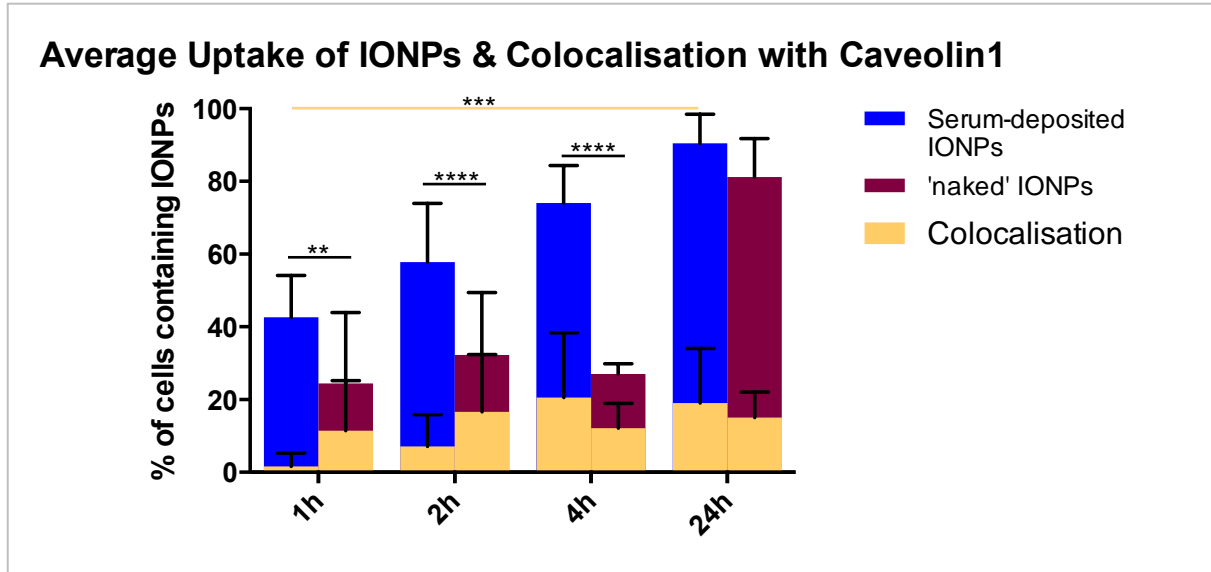


Figure 3.11. **Caveolae staining quantification.** The graph shows the average uptake of serum deposited and 'naked' IONPs. Average uptake was determined by calculating the % of cells that contained IONPs. Some colocalisation was seen at all investigated time points in both IONPs conditions. Colocalisation was calculated from the number of cells where colocalisation was seen out of total number of cells. Error bars represent standard deviation. See chapter 2 (methods) for in depth detail of how the analysis was done. Although at the earlier time points, there seem to be a higher percentage colocalisation, most colocalisation was seen in one experimental repeat whereas less colocalisation was seen in the second experimental repeat. Two independent experiments were carried out and the graph was plotted using GraphPad Prism. A two-way ANOVA test was performed using GraphPad Prism. Comparing serum-deposited vs 'naked' samples for each time point, statistical significance was found for the 1h, 2h and 4h samples only, as shown. Comparing all time points against each other per treatment condition, statistical significance was found between all samples except for: 1h vs 2h ('naked' IONPs), 1h vs 4h ('naked' IONPs) and 2h vs 4h ('naked' IONPs). Statistical significance for colocalisation is shown on the graph (yellow line). Black lines compare uptake for each time point.

The above results (figures 3.10 and 3.11) show that there seems to be some colocalisation between caveolae and IONPs. However, it should be noted that the same amount of colocalisation was not seen in all experimental repeats. Overall, the amount of colocalisation seen was not significant but it does indicate that some IONPs might have been present in the caveolae and some IONPs may have trafficked across the plasma membrane through caveolae-mediated endocytosis. Particularly, statistical significance was found for colocalisation between 1 hour and 24 hours for serum-deposited IONPs. This result may suggest that serum-deposited IONPs take longer to internalised and trafficked when compared to 'naked' IONPs. IONPs investigated here are 100nm and studies have shown that particles as large as 500nm

can be internalised through caveolae-mediated pathway of endocytosis (Rejman *et al.*, 2004). Thus, our results above may indicate differences in endocytic times when there is a protein corona present, compared to no protein corona on the IONPs. The data above is based on two experimental repeats and should be repeated to confirm our results seen, in particular the differences in endocytic times.

### 3.2.7 Endoplasmic Reticulum Staining

The endoplasmic reticulum is a key organelle, which is involved in the synthesis of proteins as well as transport of proteins and it is the largest organelle of a cell (Schwarz and Blower, 2016). Some NPs can escape lysosomal degradation through the retrograde trafficking pathway where cargo molecules in the early endosomes are trafficked to the endoplasmic reticulum and Golgi apparatus (Yameen *et al.*, 2014). Thus, it was deemed important to investigate possible localisation of IONPs in the endoplasmic reticulum. In the images below (figure 3.12), the ER was stained with an antibody directed against ERp72 and detection with an Alexa488 labelled secondary antibody.

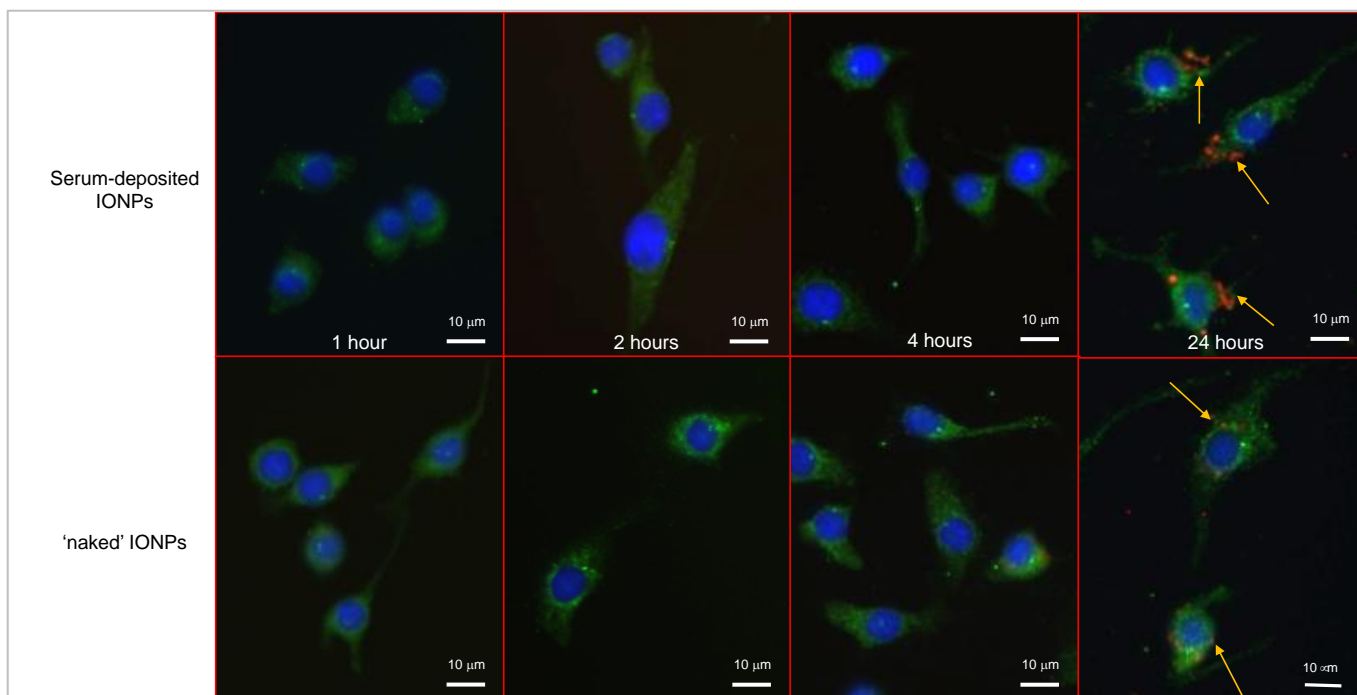


Figure 3.12. **Endoplasmic reticulum staining.** The images show endoplasmic reticulum staining in murine RAW 264.7 macrophages following addition of serum-deposited IONPs and 'naked' IONPs for the indicated times. IONPs were coated with serum for 1 hour at 37°C on a shaker, following which they were washed in PBS and sonicated before being added to the cells. The IONPs were left to incubate with the cells at 37°C and fixed using 4% PFA at specific time points, followed by immunofluorescence staining. The ER was stained with an anti ERp72 antibody (green), the nucleus was stained with Hoechst 33342 (blue). No colocalisation between IONPs (red, yellow arrows) and ER was observed. Two independent experiments were carried out and representative images are displayed. Cells were imaged on a Leica DM4000 microscope using LAS software.

The results for colocalisation between IONPs and the endoplasmic reticulum (figure 3.12) were negative, implying that IONPs are not trafficked to the ER during the first 24 hours, thus the theory of retrograde trafficking pathway of IONPs in this case is unlikely.

### 3.2.8 Dextran as marker for fluid phase endocytosis

Dextran is a hydrophilic and non-digestible carbohydrate that is commercially available in different molecular sizes (Wang et al., 2014). Fluid phase markers such as dextran can help in the study of the endocytic capacity and uptake pathways of NPs. Experiments with different sized dextrans have a key role in differentiating cellular uptake via either macro- or pinocytosis due to the cells' ability to internalise large

amounts of fluids in macropinosomes but less so in pinosomes. Fluorescently labelled dextran is one of the most convenient fluid phase markers, especially for pulse-chase experiments. Different sized dextrans can be internalised through different endocytic pathways and studies have shown that smaller dextran molecules (such as MW=10,000 Da) are more suitable to study fluid-phase endocytosis whereas larger dextran molecules (such as MW=70,000) are more suited to study macropinocytosis (Li *et al.*, 2015). Here, we investigate 3 different sizes of dextrans, MW=20,000, 40,000 and 70,000 Da.

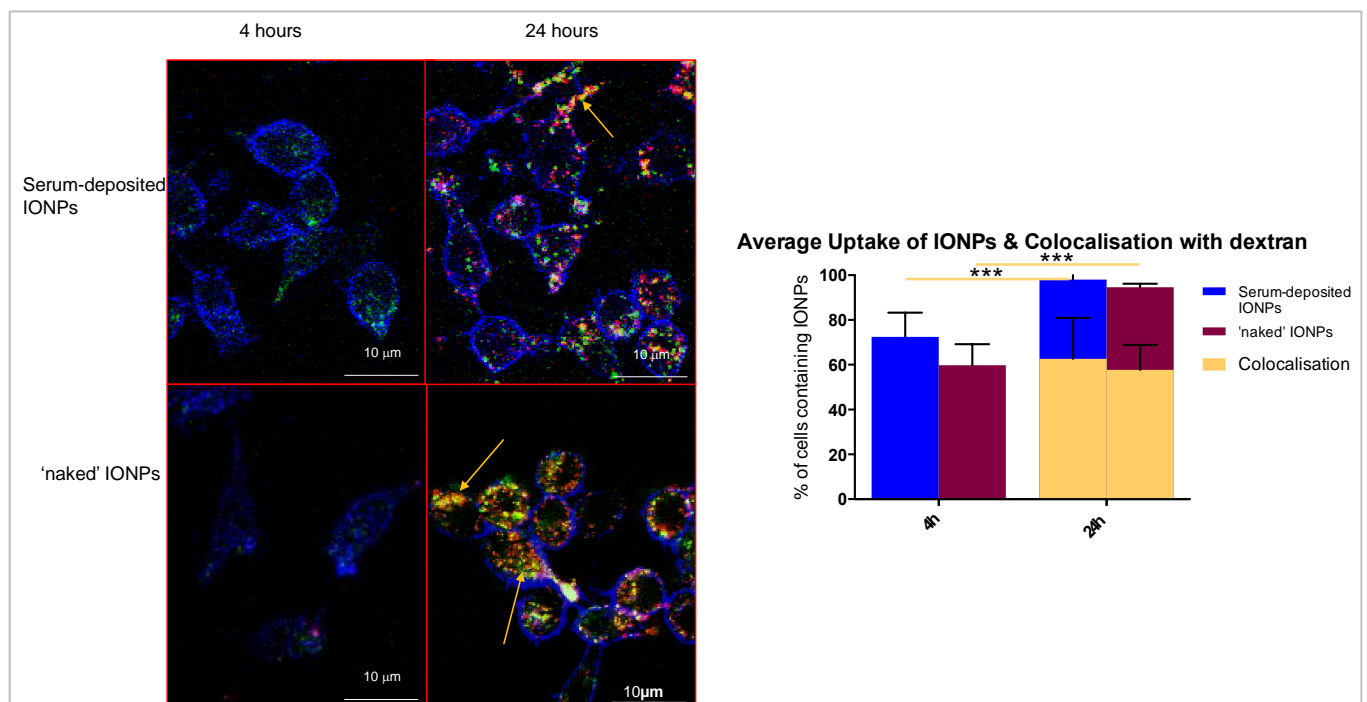


Figure 3.13. **Uptake of IONPs and FITC-labelled dextran (MW=20,000).** The images show colocalization (yellow) between IONPs (red) and dextran (green). Significant colocalisation is seen at 24 hours (arrows). IONPs were coated with serum for 1 hour at 37°C on a shaker, following which they were washed in PBS and sonicated before being added to the cells together with the dextran. The IONPs and dextran were left to incubate with the cells at 37°C and fixed using 4% PFA at specific time points, followed by immunofluorescence staining. Plasma membrane is stained with Alexafluor350 conjugated WGA (blue). The cells were imaged using the Nikon Eclipse TE2000-S Confocal Microscope (EZ-C1 software), x60 oil lens. The graph shows the corresponding quantification of colocalisation (see chapter 2 for details). Error bars represent standard deviation. A two-way ANOVA test was performed using GraphPad Prism. Comparing serum-deposited vs 'naked' samples for each time point, statistical significance was not found for uptake. Comparing both time points against each other (4h vs 24h) per treatment condition, statistical significance was found for uptake of both samples. Statistical significance was found for colocalisation, as shown on graph.

Serum-deposited and 'naked' IONPs show colocalisation with FITC-labelled dextran 20,000 after 24 hours (figure 3.13). Dextran conjugates are internalised by cells through fluid phase endocytosis, into the endosomal maturation pathway to finally accumulate in lysosomes (Fernando *et al.*, 2010). The colocalisation seen between dextran and serum deposited IONPs suggests that the IONPs have been internalised into the cells through a similar endocytic pathway.

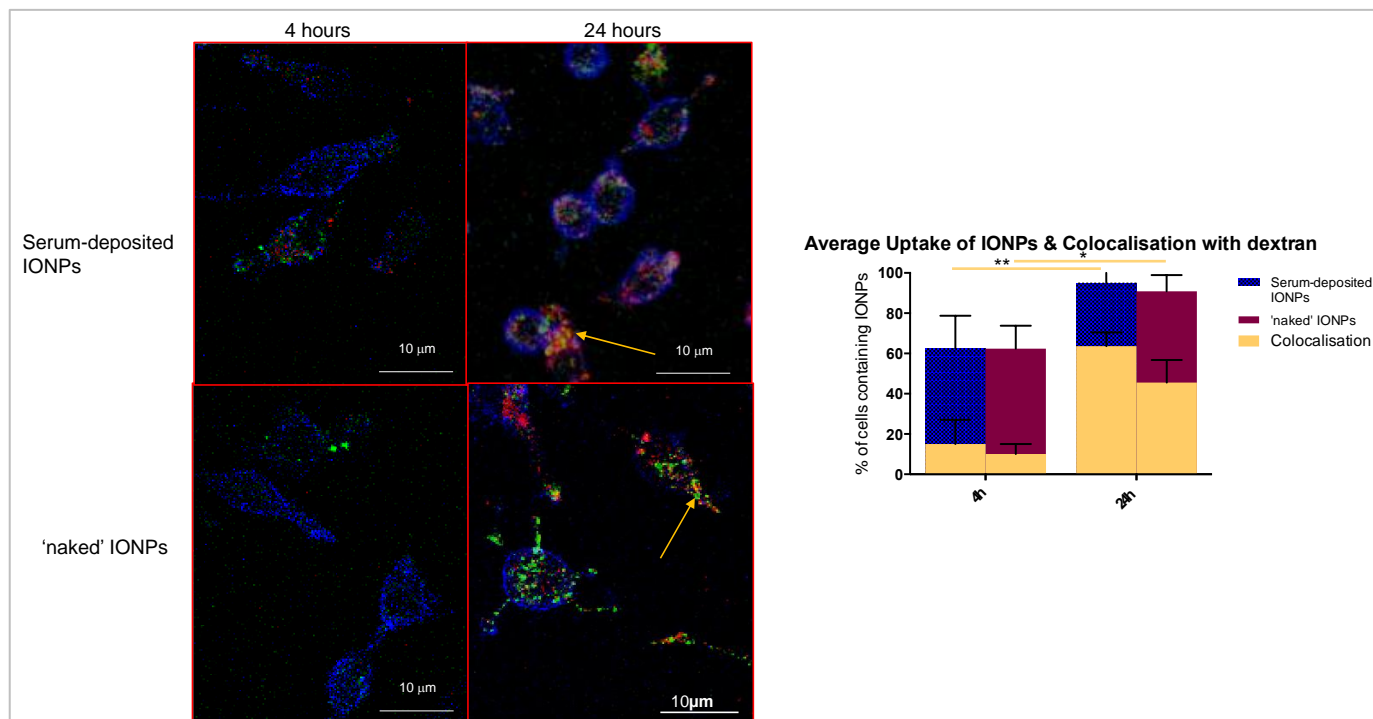


Figure 3.14. **Uptake of IONPs and FITC-labelled dextran (MW=40,000)**. The images show colocalisation between IONPs and dextran in murine RAW264.7 macrophages. IONPs were coated with serum for 1 hour at 37°C on a shaker, following which they were washed in PBS and sonicated before being added to the cells together with the dextran. The IONPs and dextran were left to incubate with the cells at 37°C and fixed using 4% PFA at specific time points, followed by immunofluorescence staining. Plasma membrane is stained with Alexafluor350 conjugated WGA (blue). The cells were imaged using the Nikon Eclipse TE2000-S Confocal Microscope (EZ-C1 software), x60 oil lens. The graph shows the corresponding quantification of colocalisation (see chapter 2 for details). Error bars represent standard deviation. A two-way ANOVA test was performed using GraphPad Prism. Comparing serum-deposited vs 'naked' samples for each time point, statistical significance was not found for uptake. Comparing both time points against each other (4h vs 24h) per treatment condition, statistical significance (\*) was found for uptake of both samples. Statistical significance was found for colocalisation, as shown on graph.

Less colocalisation is seen here (figure 3.14) compared to the dextran 20,000 (figure 3.13) which strongly indicates that dextran 40,000 is trafficked across the plasma membrane in a different manner than the lower weight dextran. Furthermore, more



colocalisation can be seen with serum-deposited IONPs which indicates that the presence of serum proteins on the IONP surface enhanced their uptake through the same mechanism as dextran 40,000 when compared to 'naked' IONPs sample. As stated before, larger dextran molecules are likely to be internalised through macropinocytosis, suggesting that serum-deposited IONPs are endocytosed in a similar manner.

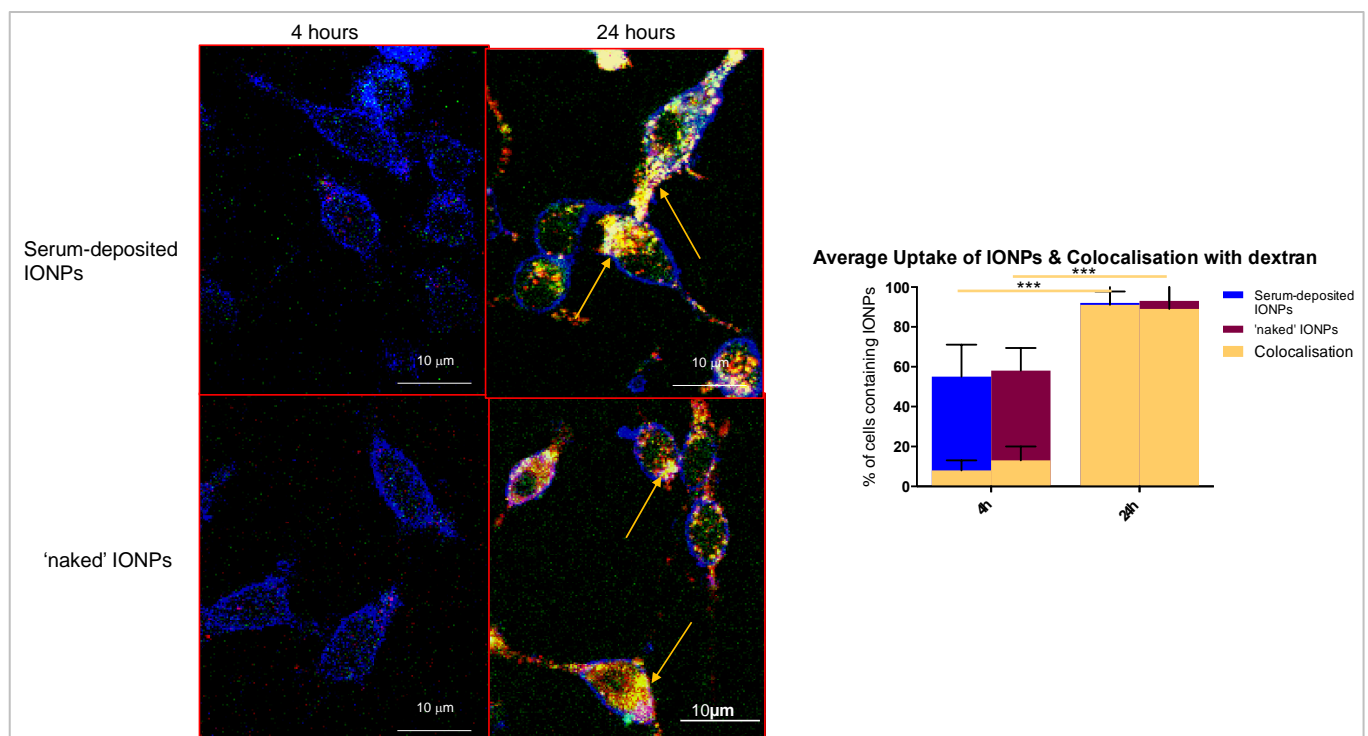


Figure 3.14. **Uptake of IONPs and FITC-labelled dextran (MW=70,000)**. The images show colocalisation between IONPs and dextran in murine RAW264.7 macrophages. Strong colocalisation is seen at 24 hours (yellow, arrows), for both IONP samples. IONPs were coated with serum for 1 hour at 37°C on a shaker, following which they were washed in PBS and sonicated before being added to the cells together with the dextran. The IONPs and dextran were left to incubate with the cells at 37°C and fixed using 4% PFA at specific time points, followed by immunofluorescence staining. Plasma membrane was stained with Alexafluor350 conjugated WGA (blue). The cells were imaged using the Nikon Eclipse TE2000-S Confocal Microscope (EZ-C1 software), x60 oil lens. The graph shows the corresponding quantification of colocalisation (see chapter 2 for details). Error bars represent standard deviation. A two-way ANOVA test was performed using GraphPad Prism. Comparing serum-deposited vs 'naked' samples for each time point, statistical significance was not found for uptake. Comparing both time points against each other (4h vs 24h) per treatment condition, statistical significance (\*) was found for uptake of both samples. Statistical significance was found for colocalisation, as shown on graph.

The result with dextran 70,000 (figure 3.14) demonstrated strong colocalisation between IONPs and dextran after 24h in murine RAW264.7 macrophages. This

provides concrete evidence that IONPs(100nm) are mainly endocytosed via macropinocytosis. With the results seen with dextran 20,000, it is possible that some IONPs are also endocytosed via fluid-phase endocytosis indicating that IONPs are taken up through a range of endocytic pathways.

### 3.1.9 LysoTracker

LysoTracker is a fluorescent dye used to visualise lysosomes. The LysoTracker dye is a small highly soluble molecule that accumulates in acidic compartments such as the lysosomes (Fogel et al., 2012). Penetration of the dye into the lysosomes is not a concern as they are taken up through diffusion and get trapped in the acidic environment of the lysosomes and endosomes.

The images below (figure 3.15) show live cell images of RAW 264.7 cells incubated with serum deposited and 'naked' IONPs for 24 hours before the addition of the LysoTracker dye for 15 minutes, which is seen in green. The cells were imaged live with a Leica DM4000 microscope after changing the media containing the LysoTracker dye.

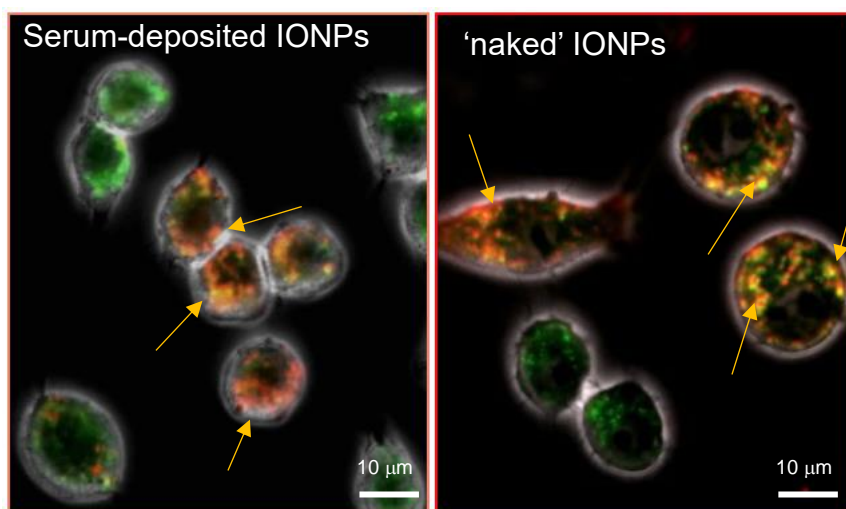


Figure 3.15. **Live cell imaging of cells incubated for 24 hours with IONPs and 15 minutes with lysotracker.** RAW cells were incubated with IONPs for 24 hours, following which the lysotracker dye was added for 15 minutes and imaged immediately. The image on the left shows serum deposited IONPs in red and the image on the right shows 'naked' IONPs in red. The lysotracker dye can be seen in green. The bright field channel on the Leica DM-4000 microscope was used to visualise cell morphology.

Strong colocalisation of IONPs with the LysoTracker dye was seen in both cases; serum deposited and 'naked' IONPs (figure 3.15). These results show that IONPs are present in an acidic organelle after 24 hours, most likely for degradation. However, trafficking of NPs to the lysosomes as a final destination can be exploited to make them a favourable drug delivery vehicle to deliver drugs specifically to lysosomes where the low pH can be employed to release their content.

### **3.3 Results Using Mouse Serum**

This section will show results of IONP uptake in the mouse macrophage cell line RAW 264.7, after preincubation with mouse serum instead of human serum (section 3.2). This was to investigate if the results seen in section 3.2 were due to activation of the murine macrophage cell line upon exposure to human serum. Furthermore, by using different veronal buffers, we aim to study the differences in complement activation via classical and alternative pathway where one is favoured over the other (see figure 3.16).

All protocols and incubations were carried out in the same way, with one exception; the mouse serum used to coat the surface of the IONPs was either diluted in DGVB<sup>++</sup> buffer to favour complement activation via the classical pathway or diluted in EGTA buffer to favour complement activation via the alternative pathway. An initial experiment comparing uptake of IONPs, using human serum and mouse serum, was carried out before organelles were stained. This was done to compare uptake using DGVB<sup>++</sup> buffer, EGTA buffer and using undiluted serum (not favouring the activation of a specific pathway of the complement system).

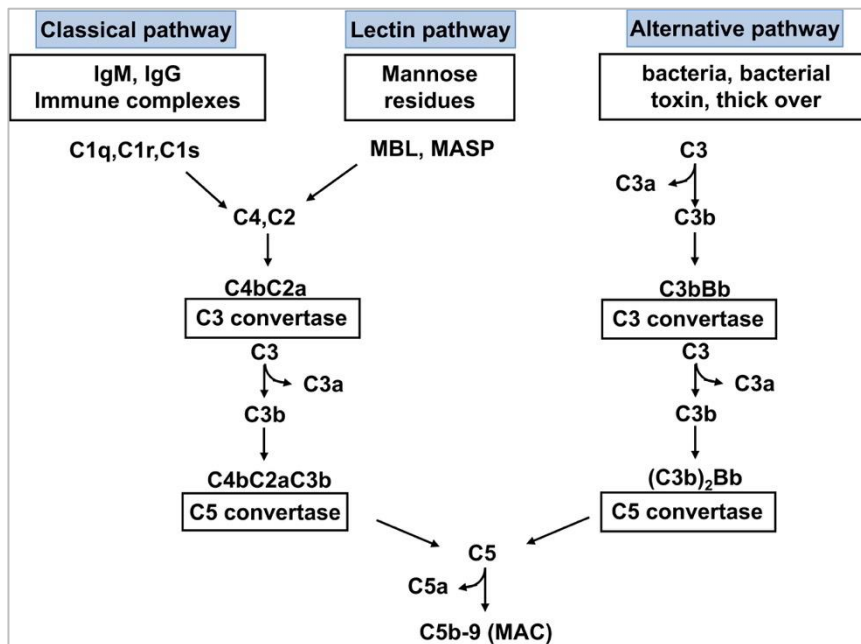


Figure 3.16. **Complement activation pathways.** The above image shows how the three pathways of complement activation are induced. Although they have different triggers, all three pathways lead to the formation of C3 complement protein. *Image from: Noris & Remuzzi, 2013.*

All experiments in section 3.3 were carried out using mouse serum, unless otherwise stated. The results from the organelle staining showed similar patterns seen with the use of human serum in 3.2, where some colocalisation was seen in late endosomes (Rab 7 and Rab 9) and a small amount of colocalisation was also observed with caveolin again. The organelle staining is summarised in the table below (table 3.2).

Organelle Stained	Colocalisation
Early endosome	No
Late endosome (Rab9)	Yes
Late endosome (Rab7)	Little to none
Mitochondria	No
Golgi apparatus	No
Caveolae	Little to none

Table 3.2. **Organelles stained in this part of the chapter.** The table lists all the organelles that were stained following incubation of murine RAW264.7 macrophages with IONPs. IONPs were first incubated with mouse serum proteins, following which they were added to the cells. The cells were fixed with 4% PFA at time points 1h, 2h, 4h and 24h. After fixation with 4% Paraformaldehyde, immunofluorescence staining was carried out and the cells were imaged under the Leica DM4000 microscope using the LAS software.

Dextran was again used as markers of endocytosis and the three sizes used are the same; MW= 20,000, 40,000 and 70,000 kDa.

### 3.3.1 Comparing uptake of IONPs with different sera

To compare the overall uptake of IONPs preincubated with either human serum or mouse serum to form the protein corona, IONPs deposited under both conditions (mouse serum and human serum) were incubated with murine RAW 264.7 cells for 2 and 24 hours and NP uptake compared. The images below (figure 3.17) show uptake at 2 hours (the time point where nanoparticle uptake was first observed) and at 24 hours (where maximum nanoparticle uptake was seen).

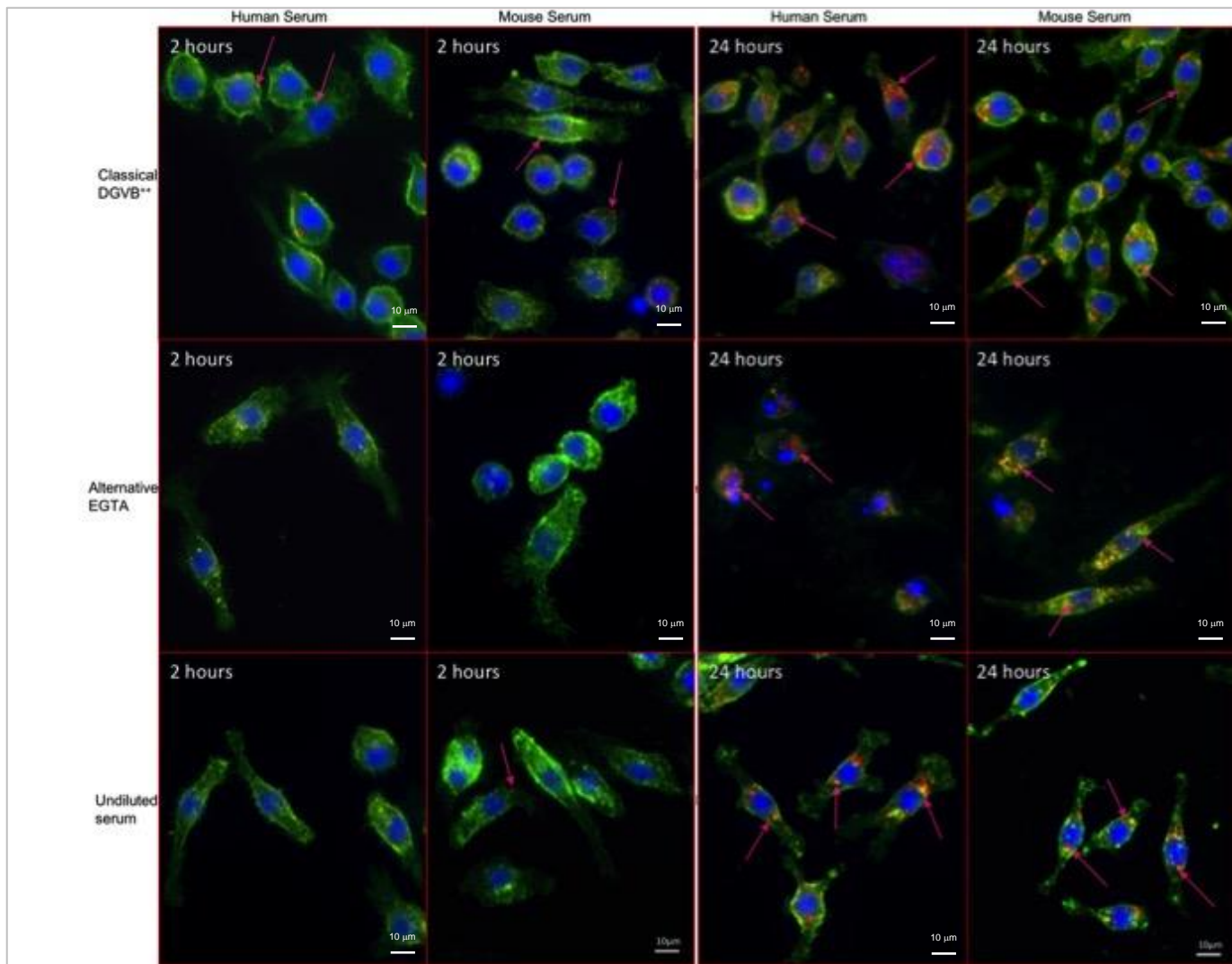


Figure 3.17. **Comparing IONP uptake preadsorbed with either human serum or mouse (serum deposited).** 'Naked' IONPs were not used here since we only want to see the difference in serum-deposition on IONPs uptake. IONPs were coated with serum for 1 hour at 37°C on a shaker, before being washed with PBS and sonicated. The IONPs were then added to the cells. The cells were fixed with 4% PFA at the respective time points, followed by immunofluorescence staining. The plasma membrane is stained with fluorescently labelled lectin WGA (green). The nucleus is stained using Hoechst 33342 (blue). Arrows show IONPs (red) inside macrophages. The cells were imaged using Leica DM-4000 microscope and the LAS software.

Similar uptake pattern can be seen with both sera, where some uptake can be seen as early as 2 hours and maximum IONP uptake is seen at 24 hours. Slightly less IONP uptake was seen with the mouse serum compared to human serum which is most likely due to the fact that human serum proteins may contain molecules that are recognised as 'foreign' by macrophages and hence are phagocytosed more readily. However, similar uptake patterns using mouse serum proteins shows that, regardless of sera used, IONPs are internalised by

macrophages. This indicated that the results seen so far using human serum are not solely a result of using human serum in a murine cell line but dependent on exposure to IONPs.

### 3.3.2 Nanoparticle Uptake – Classical vs Alternative pathway

The complement system can be activated via three different pathways: classical pathway, alternative pathway and mannose binding lectin pathway. An overview of the complement activation pathways is given at the beginning of this section (figure 3.16) and is explained in detail in chapter 1.5. The activation of classical and alternative pathways can be favoured *in vitro* through the use of different veronal buffers. Complement activation can be induced via the classical pathway using veronal buffer DGVB<sup>++</sup>, containing calcium and magnesium ions which are required for C1q complex formation and C2-C4 interactions, respectively (Okroj et al., 2012). Similarly, complement can be activated via the alternative pathway using veronal buffer with EGTA as a calcium chelating agent and magnesium ions only. The alternative pathway is the only one that can proceed in the absence of calcium ion since its activation does not involve a calcium-dependent step, unlike the other two pathways (Okroj et al., 2012). Undiluted serum (not diluted in DGVB<sup>++</sup> or EGTA) was also used as comparison for the experiments in section 3.2 (using human serum).

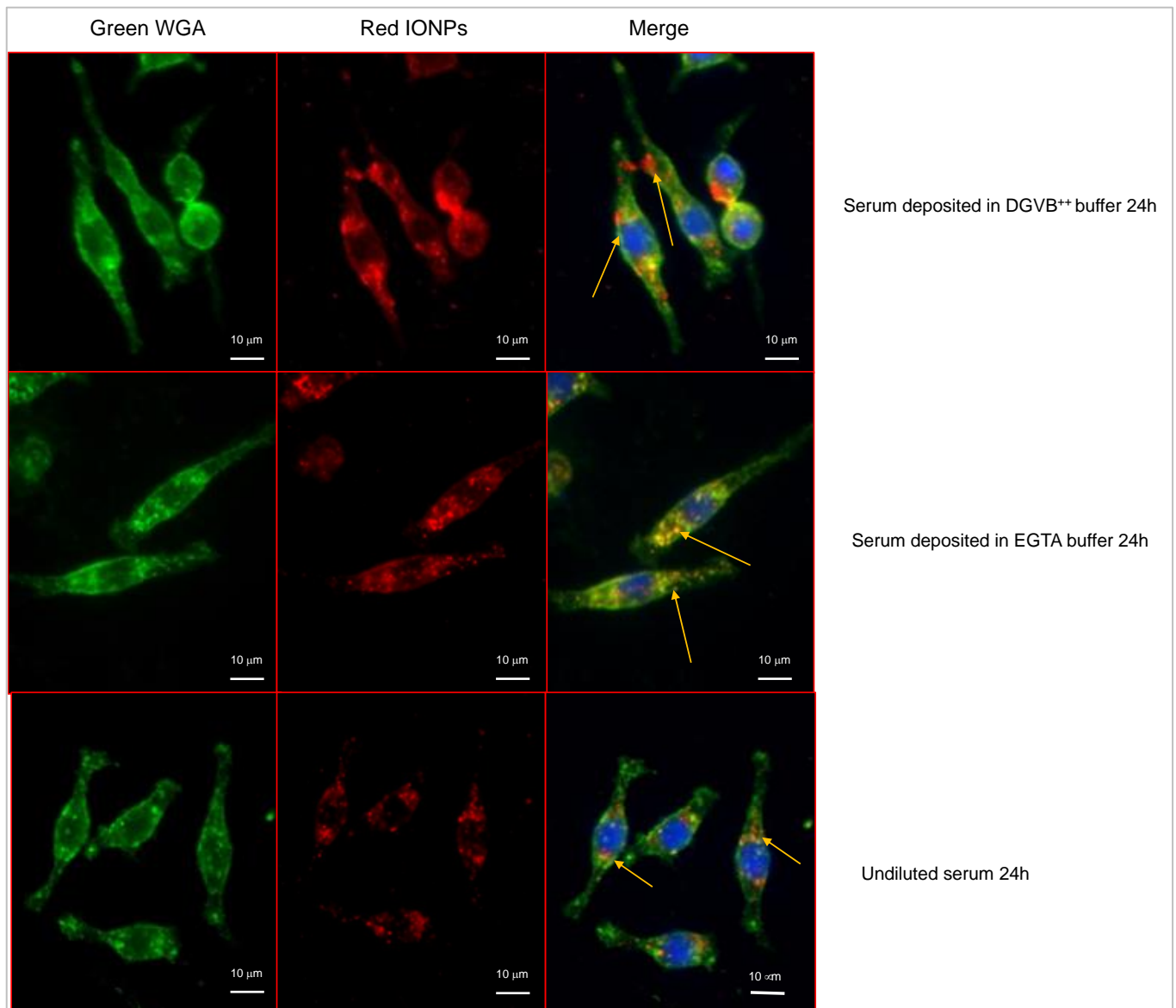


Figure 3.18. ***Uptake of serum-deposited IONPs diluted in DGVB<sup>++</sup>, EGTA buffer and undiluted serum in murine RAW264.7 macrophages.*** IONPs (red) were incubated in mouse serum diluted in DGVB<sup>++</sup> buffer, EGTA buffer as well as undiluted serum (i.e. no buffer added). The pictures show uptake of IONPs after 24 hours. IONPs were coated with serum for 1 hour at 37°C on a shaker, before being washed with PBS and sonicated. The IONPs were then added to the cells. Cells were fixed with 4% PFA and stained with fluorescently labelled lectin WGA (green) to reveal the plasma membrane and Hoechst 33342 (blue) to reveal the nucleus. Arrows show IONPs inside macrophages. The cells were imaged using Leica DM-4000 microscope and the LAS software.

The above results (figure 3.18) show the uptake of serum-deposited IONPs that were incubated in the appropriate buffer to favour the activation of classical pathway or alternative pathway. At 24 hours, the overall percentage uptake seen with the use of EGTA buffer is lower than that seen with the use of DGVB<sup>++</sup>. The least amount of uptake was seen in the undiluted serum sample, which indicates that the presence of



proteins adsorbed onto the IONPs in veronal buffers enhance uptake of IONPs by macrophages. The highest amount of uptake is seen with serum diluted in DGVB<sup>++</sup> buffer.

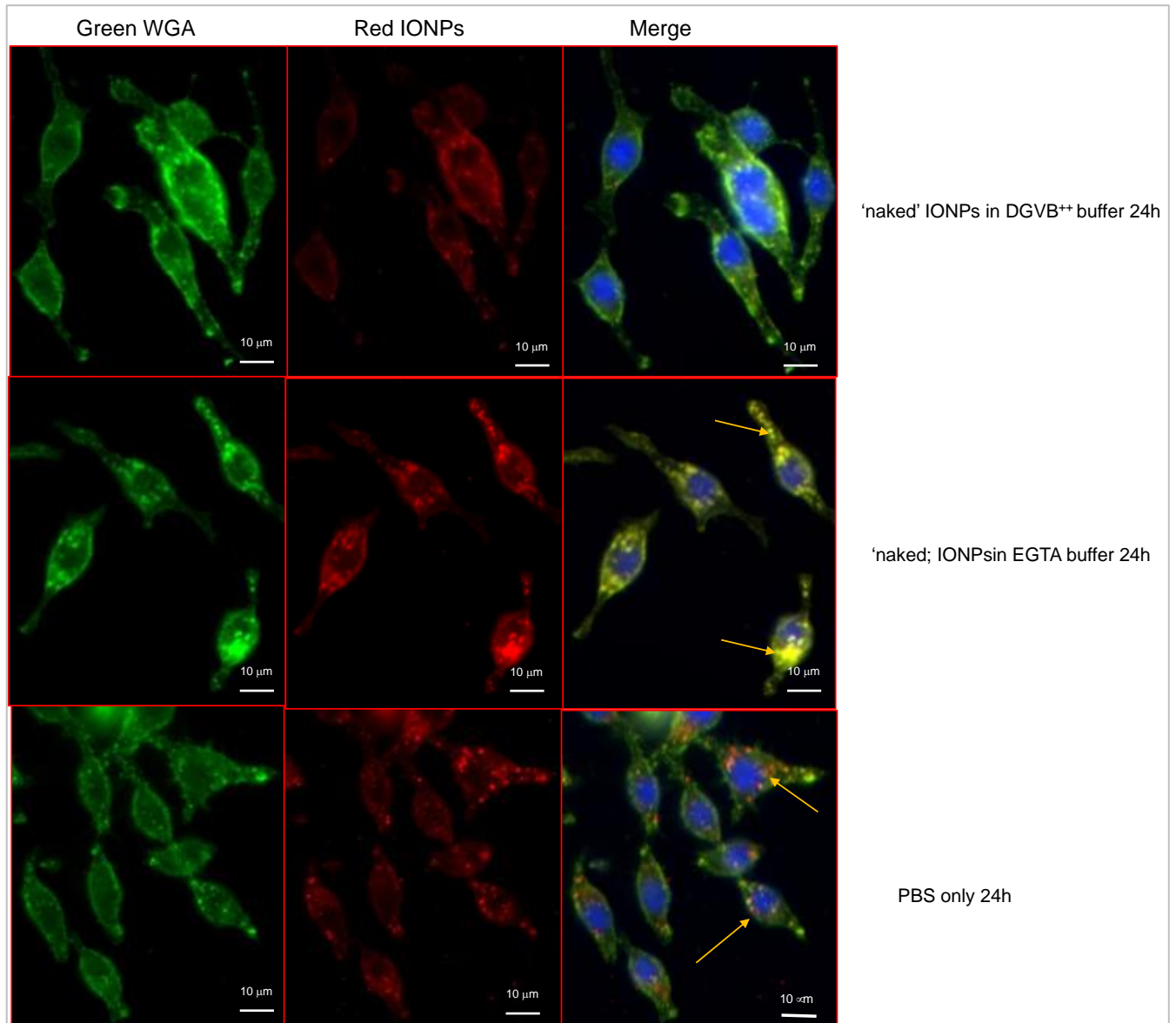


Figure 3.19. **Uptake of 'naked' IONPs diluted in DGVB<sup>++</sup> and EGTA buffer in murine RAW264.7 macrophages.** 'naked' IONPs (red) were incubated in DGVB<sup>++</sup> buffer, EGTA buffer as well as PBS. The pictures show uptake of IONPs after 24 hours. IONPs were coated with serum for 1 hour at 37°C on a shaker, before being washed with PBS and sonicated. The IONPs were then added to the cells. Cells were fixed with 4% PFA and stained with fluorescently labelled lectin WGA (green) to reveal the plasma membrane and Hoechst 33342 (blue) to reveal the nucleus. Arrows show IONPs inside macrophages. The cells were imaged using Leica DM-4000 microscope and the LAS software.

'naked' IONPs incubated in DGVB<sup>++</sup> buffer had a reduced uptake compared to serum-deposited (figure 3.18), suggesting that the presence of serum protein in DGVB<sup>++</sup> buffer has a suppressive effect on the uptake of IONPs.

### 3.3.3 Early endosome staining (Rab 5)

Rab 5 was used as an early endosome marker and the localisation of IONPs was studied in relation to early endosomes. The effect of DGVB<sup>++</sup> and EGTA buffers was investigated to determine whether the proteins adsorbed on the IONPs in the different buffers affect the trafficking of IONPs.

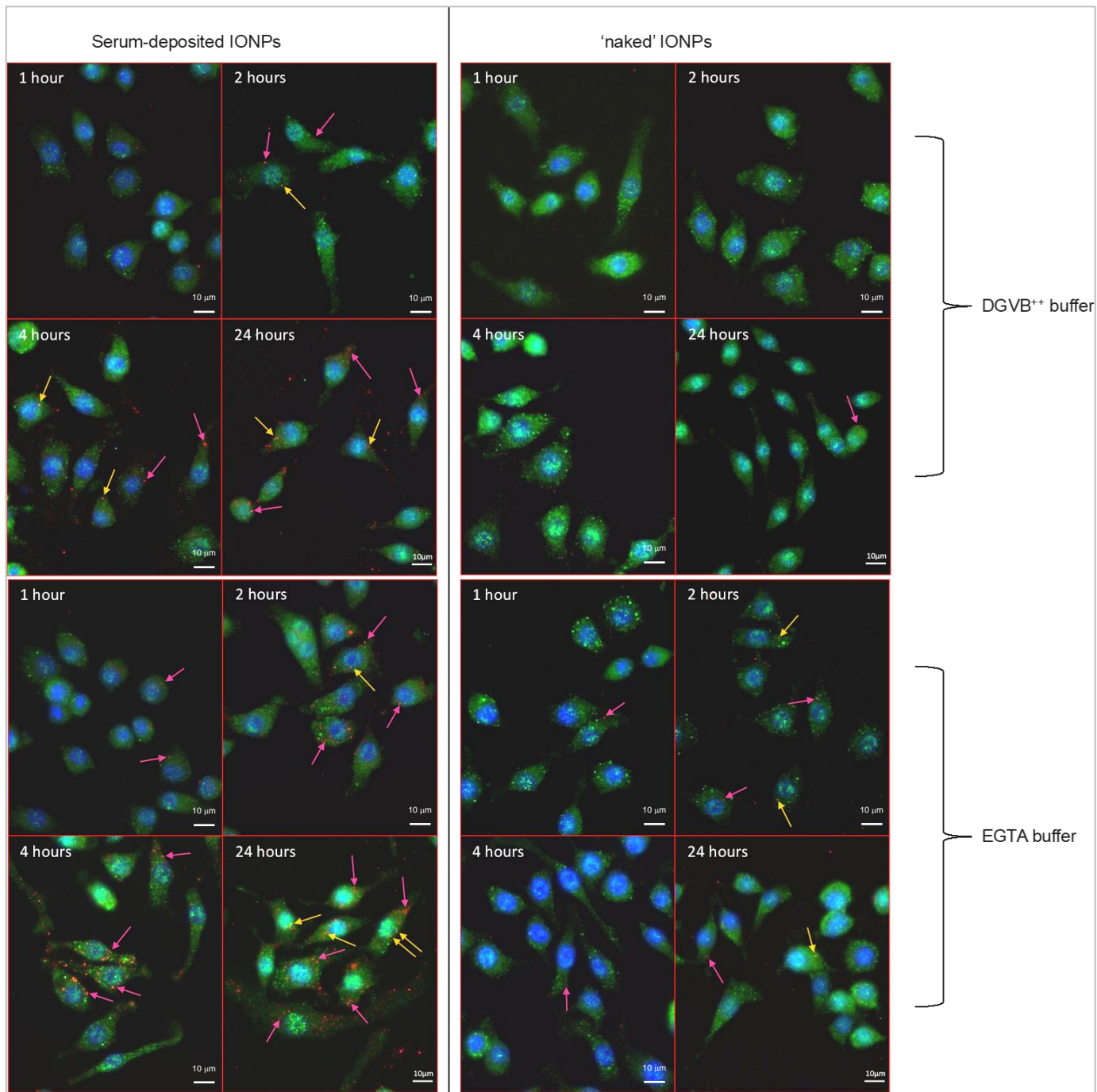


Figure 3.20. **Early endosome staining.** Serum-deposited and 'naked' IONPs (red) were prepared as before (serum deposited IONPs with mouse serum + buffer and 'naked' IONPs were incubated in the buffer only). The pictures show uptake of IONPs at 1h, 2h, 4h and 24 hours in murine RAW264.7 macrophages. IONPs were coated with serum for 1 hour at 37°C on a shaker, before being washed with PBS and sonicated. The IONPs were then added to the cells. The cells were fixed with 4% PFA followed by immunofluorescence staining. An anti-Rab5 antibody and a fluorescently labelled secondary antibody was used to stain early endosomes (green). DNA was labelled with Hoechst 33342 to stain the nucleus (blue). Pink arrows show IONPs inside macrophages and yellow arrows show colocalisation between IONPs and Rab 5. The cells were imaged using Leica DM-4000 microscope and the LAS software.

The images above (figure 3.20) show some colocalisation between early endosomes and IONPs denoted by yellow arrows. Some colocalization can be seen at earlier time points when the macrophages are likely to start internalising IONPs (figure 3.20).

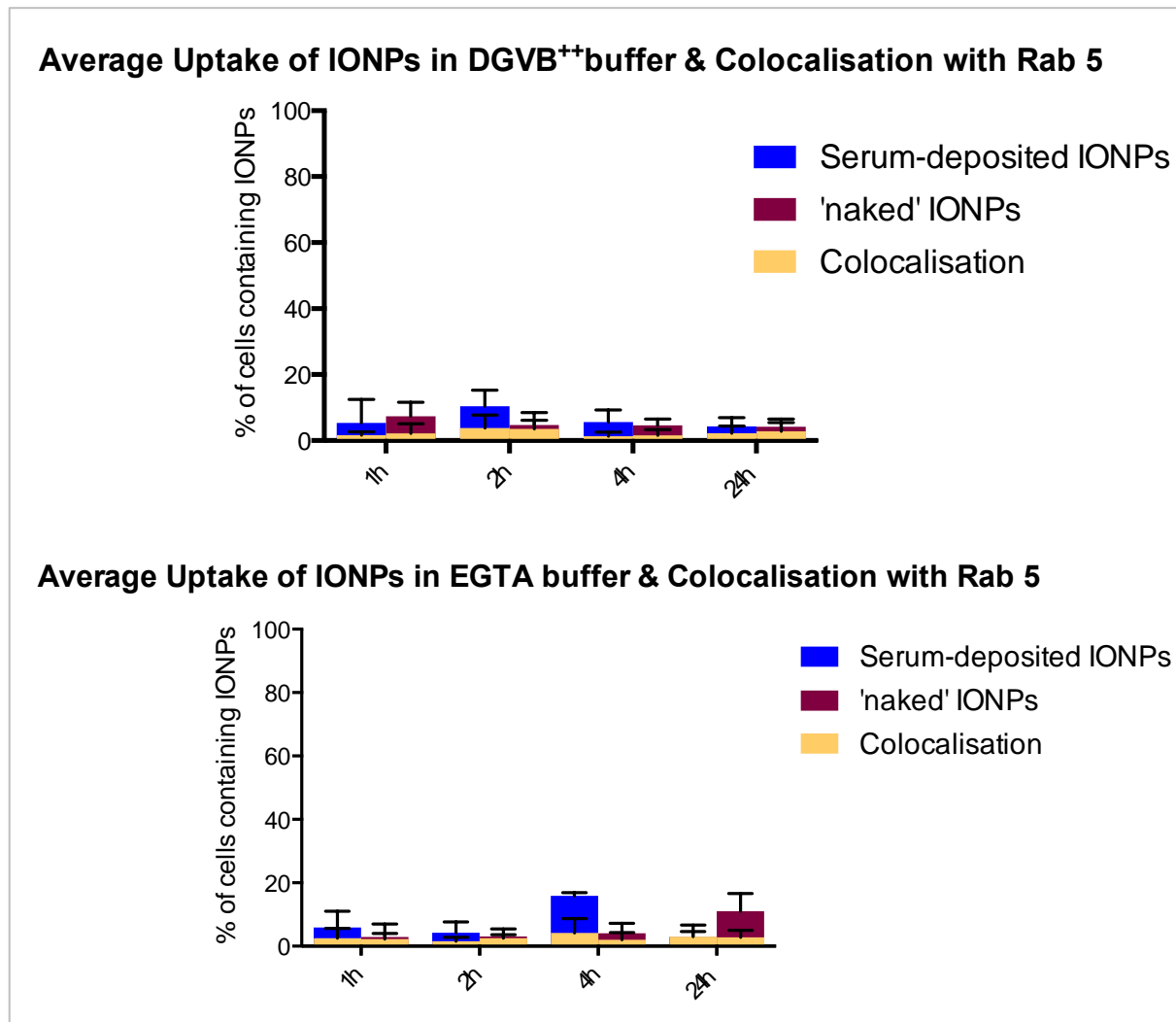


Figure 3.21. **Early endosome staining quantification.** The graph shows the average uptake of mouse serum deposited and 'naked' IONPs. Average uptake was determined by calculating the % of cells that contained IONPs. Some colocalisation was seen at all investigated time points in both conditions. Colocalisation was calculated from the number of cells where colocalisation was seen out of total number of cells. Error bars represent standard deviation. See chapter 2 (methods) for in depth detail of how the analysis was done. Two independent experiments were carried out and graphs were plotted using GraphPad Prism 6. A two-way ANOVA test was carried out using GraphPad Prism to determine statistical significance and the results were found to be not significant.

The results from early endosomal staining show that some IONPs may be present in early endosomes at most time points (figure 3.20 and 3.21). Although the percentage

of cells containing IONP is low, in some of the conditions, almost half of the cells displayed colocalisation between early endosomes and IONPs. The colocalisation observed was not strong colocalisation (figure 3.21) and the quantification for the colocalisation was not statistically significant. Hence, although the images show that there may be some early endosomal trafficking of IONPs, it is not possible to make a positive colocalisation deduction.

#### 3.3.4 Late endosome staining (Rab 7)

As mentioned previously, Rab 7 regulates membrane trafficking from early to late endosomes as well as lysosomes. Here, we use Rab 7 as a late endosomal marker to investigate whether the use of veronal buffers (DGVB<sup>++</sup> and EGTA) has a different effect in the trafficking of IONPs.

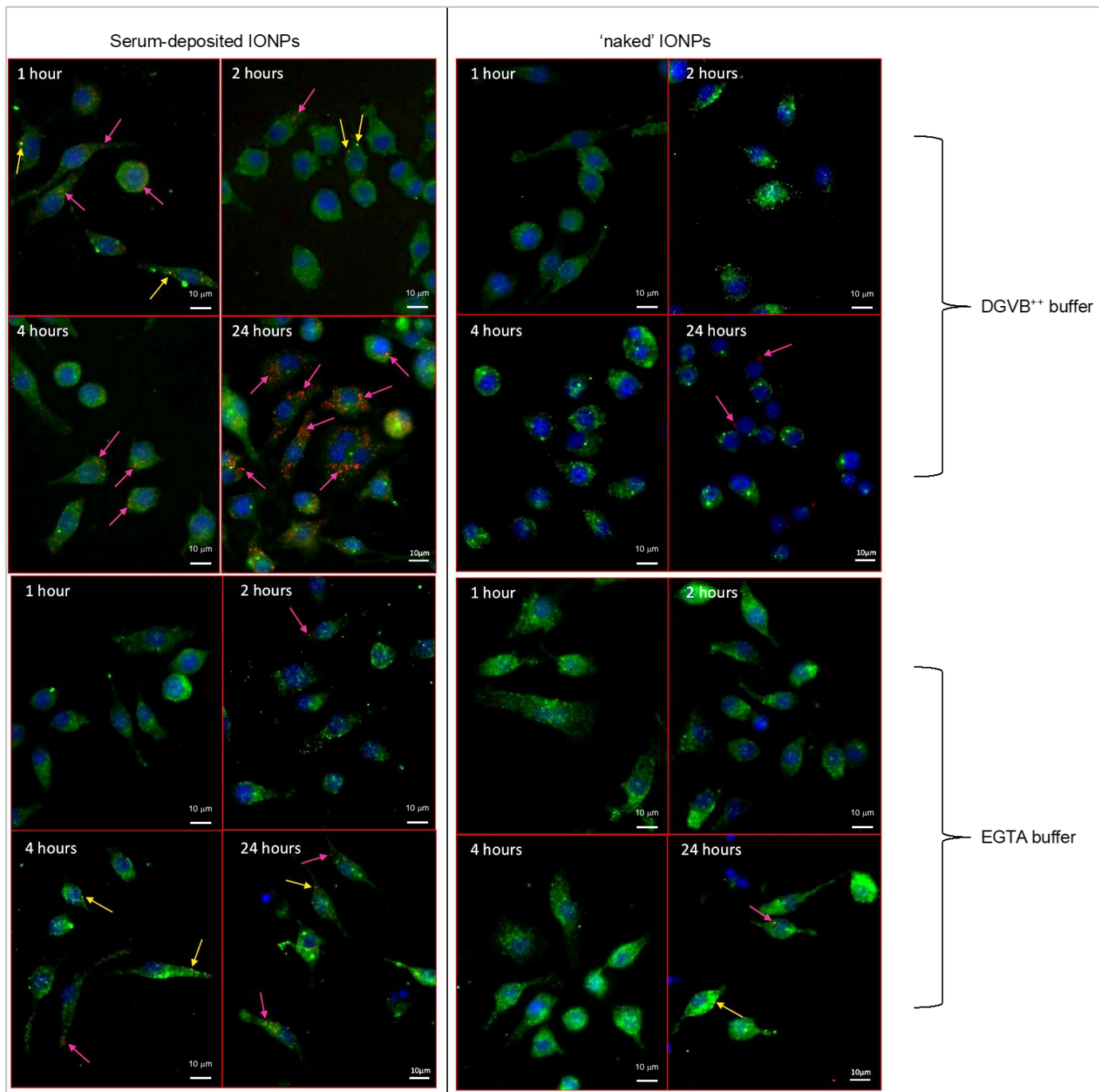
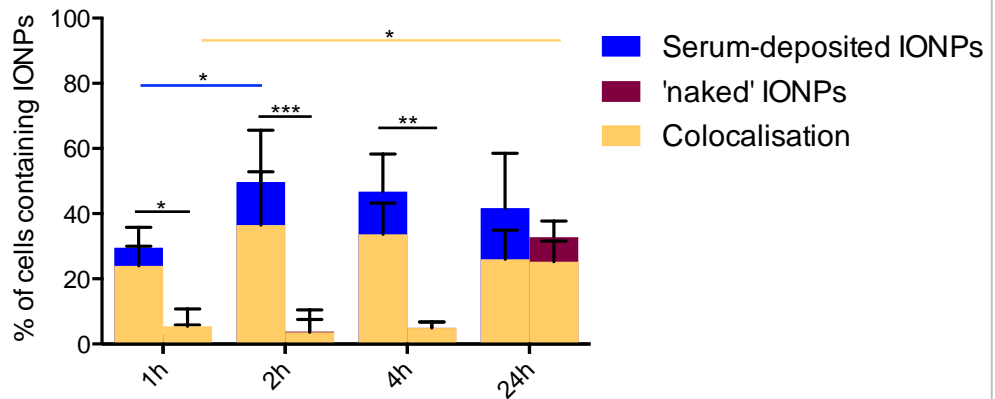


Figure 3.22. **Late endosome staining.** Serum-deposited and 'naked' IONPs (red) were prepared as before (serum deposited IONPs with mouse serum + buffer and 'naked' IONPs were incubated with the buffer only). The pictures show uptake of IONPs at 1h, 2h, 4h and 24 hours in murine RAW264.7 macrophages. IONPs were coated with serum for 1 hour at 37°C on a shaker, before being washed with PBS and sonicated. The IONPs were then added to the cells. The cells were fixed with 4% PFA followed by immunofluorescence staining. Late endosomes were labelled with an anti- Rab 7 antibody and a fluorescently labelled secondary antibody (green). The nucleus was labelled with Hoechst 33342 (blue). Pink arrows show IONPs inside macrophages and yellow arrows show colocalisation between IONPs and Rab 7. The cells were imaged using Leica DM-4000 microscope and the LAS software.

### Average Uptake of IONPs in DGVB<sup>++</sup> buffer & Colocalisation with Rab 7



### Average Uptake of IONPs in EGTA buffer & Colocalisation with Rab 7

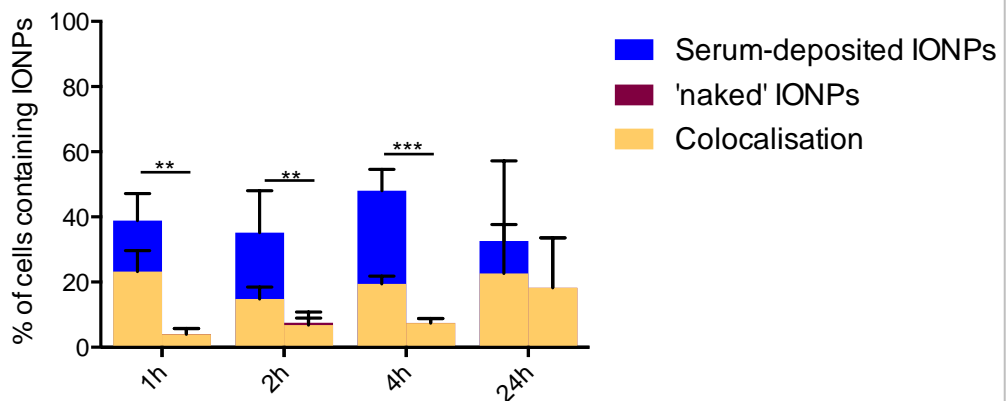


Figure 3.23. **Late endosome staining quantification.** The graph shows the average uptake of serum deposited and 'naked' IONPs. Average uptake was determined by calculating the % of cells that contained IONPs. Some colocalisation was seen at all investigated time points and all conditions. Colocalisation was calculated from the number of cells where colocalisation was seen out of total number of cells. Error bars represent standard deviation. See chapter 2 (methods) for in depth detail of how the analysis was done. Two independent experiments were carried out and graphs were plotted using GraphPad Prism 6. A two-way ANOVA test was carried out using GraphPad Prism to determine statistical significance, some of which are shown on the graph (Black lines compare uptake for each time point).

The results of the late endosome staining (Rab 7) (figure 3.22-3.23) show colocalisation between late endosomes and IONPs. However, the microscopy data does not show strong colocalisation between Rab 7 and IONPs, instead there are one or two sparsely areas spread out in each cell. The above graph shows how many cells had colocalisation out of all the cells that have internalized IONPs. This could either mean that not all internalized IONPs were present in late endosomes at the time

points, or it is also possible that there is insufficient accumulation of IONPs in these organelles even at 24 hours. Furthermore, as mentioned in the discussion later, the resolution of the microscope used may not allow the visualization of individual IONPs. Hence, there is also a probability that individual IONPs were present in the cells and organelles, which could not be seen.

### 3.3.5 Late endosomes (Rab 9)

From the results seen with the late endosomal marker Rab 7 (figures 3.22 and 3.23), limited colocalisation between IONPs and late endosomes was determined. To confirm the results another late endosome marker Rab 9 was used. Rab 9 is a member of the Ras superfamily of GTPases and is also bound to the membranes of late endosomes, similar to Rab 7 (Kucera, Bakke and Progidia, 2016). However, the main difference between the two is that Rab 7 mediates late endosomal maturation into lysosomes whereas Rab 9 mainly mediates the recycling pathway from late endosomes (Kucera, Bakke and Progidia, 2016).



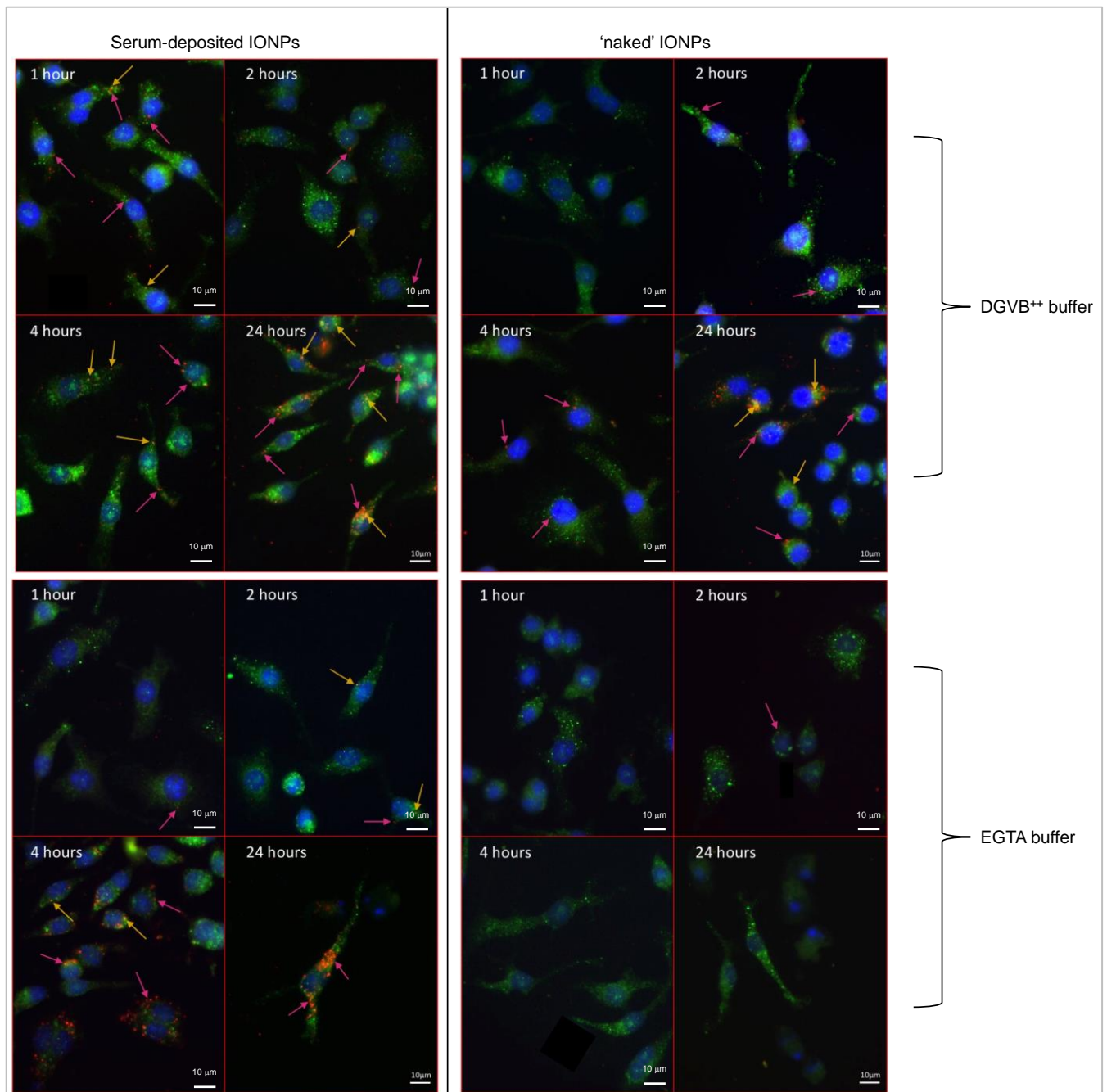
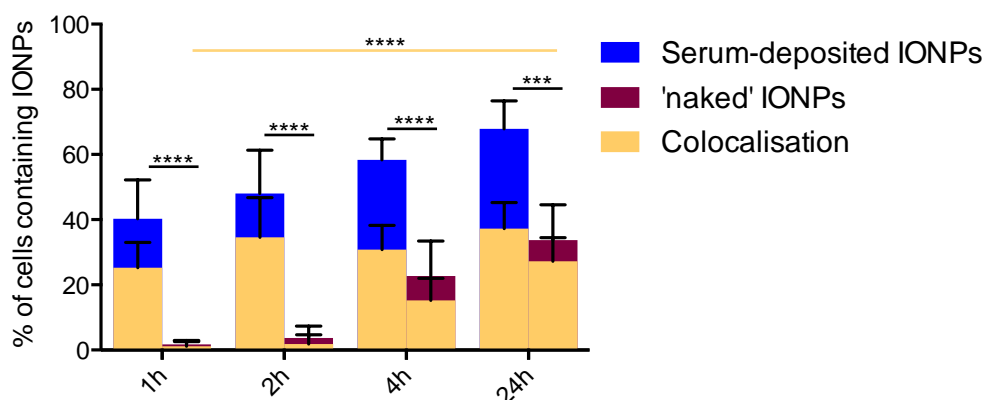


Figure 3.24. **Late endosome staining.** Serum-deposited and 'naked' IONPs (red) were prepared as before (serum deposited IONPs with mouse serum + buffer and 'naked' IONPs were incubated with the buffer only). The pictures show uptake of IONPs at 1h, 2h, 4h and 24 hours in murine RAW264.7 macrophages. IONPs were coated with serum for 1 hour at 37°C on a shaker, before being washed with PBS and sonicated. The IONPs were then added to the cells. The cells were fixed with 4% PFA followed by immunofluorescence staining. Late endosomes were labelled with an anti- Rab 9 antibody and a fluorescently labelled secondary antibody (green). The nucleus was labelled with Hoechst 33342 (blue). Pink arrows show IONPs inside macrophages and yellow arrows show colocalisation between IONPs and Rab 7. The cells were imaged using Leica DM-4000 microscope and the LAS software.

### Average Uptake of IONPs in DGVB<sup>++</sup> buffer & Colocalisation with Rab 9



### Average Uptake of IONPs in EGTA buffer & Colocalisation with Rab 9

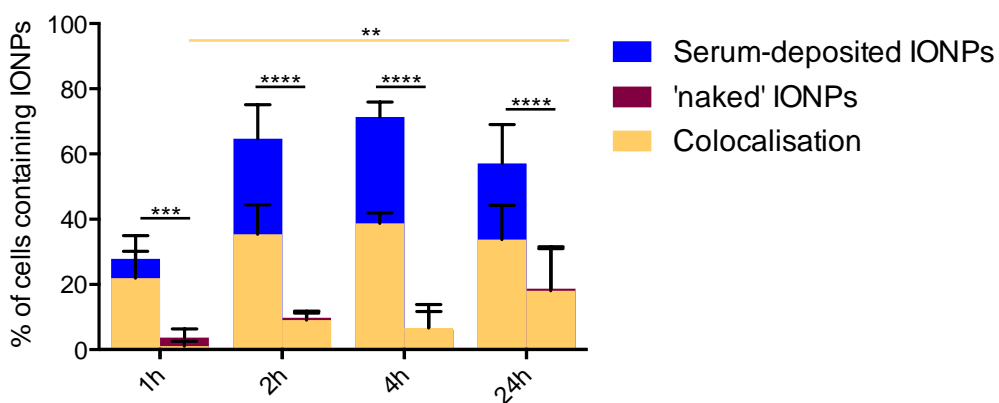


Figure 3.25. **Late endosome staining quantification.** The graph shows the average uptake of serum deposited and 'naked' IONPs. Average uptake was determined by calculating the % of cells that contained IONPs. Some colocalisation was seen at all investigated time points and conditions. Colocalisation was calculated from the number of cells where colocalisation was seen out of total number of cells. Colocalisation was seen in most samples, especially serum-deposited IONPs. Error bars represent standard deviation. See chapter 2 (methods) for in depth detail of how the analysis was done. Two independent experiments were carried out and graphs were plotted using GraphPad Prism 6. A two-way ANOVA test was carried out using GraphPad Prism to determine statistical significance, some of which are shown on the graph above (Black lines compare uptake for each time point).

The data obtained with Rab 9 staining (figures 3.24 and 3.25) support the hypothesis that IONPs reach late endosomes, especially serum-deposited IONPs. Theoretically, due to the function of Rab 9, it is possible that these IONPs are recycled, however further studies have to be done to identify if other Rab proteins involved in recycling also colocalise with IONPs. The likely end results of this IONP localisation is that IONPs are either trafficked to lysosomes or will be recycled to the plasma membrane.

To distinguish between these possibilities pulse chase experiments need to be undertaken.

### 3.3.6 Mitochondrial Staining (SOD2)

To study if IONPs localise differently in the mitochondria when mouse serum proteins are adsorbed on their surface in the presence of the different veronal buffers, mitochondria were stained and colocalization with IONPs investigated. No colocalisation was found, similar to the results obtained with human serum (section 3.2.5), indicating that IONPs are not present in the mitochondria during the time points studied.

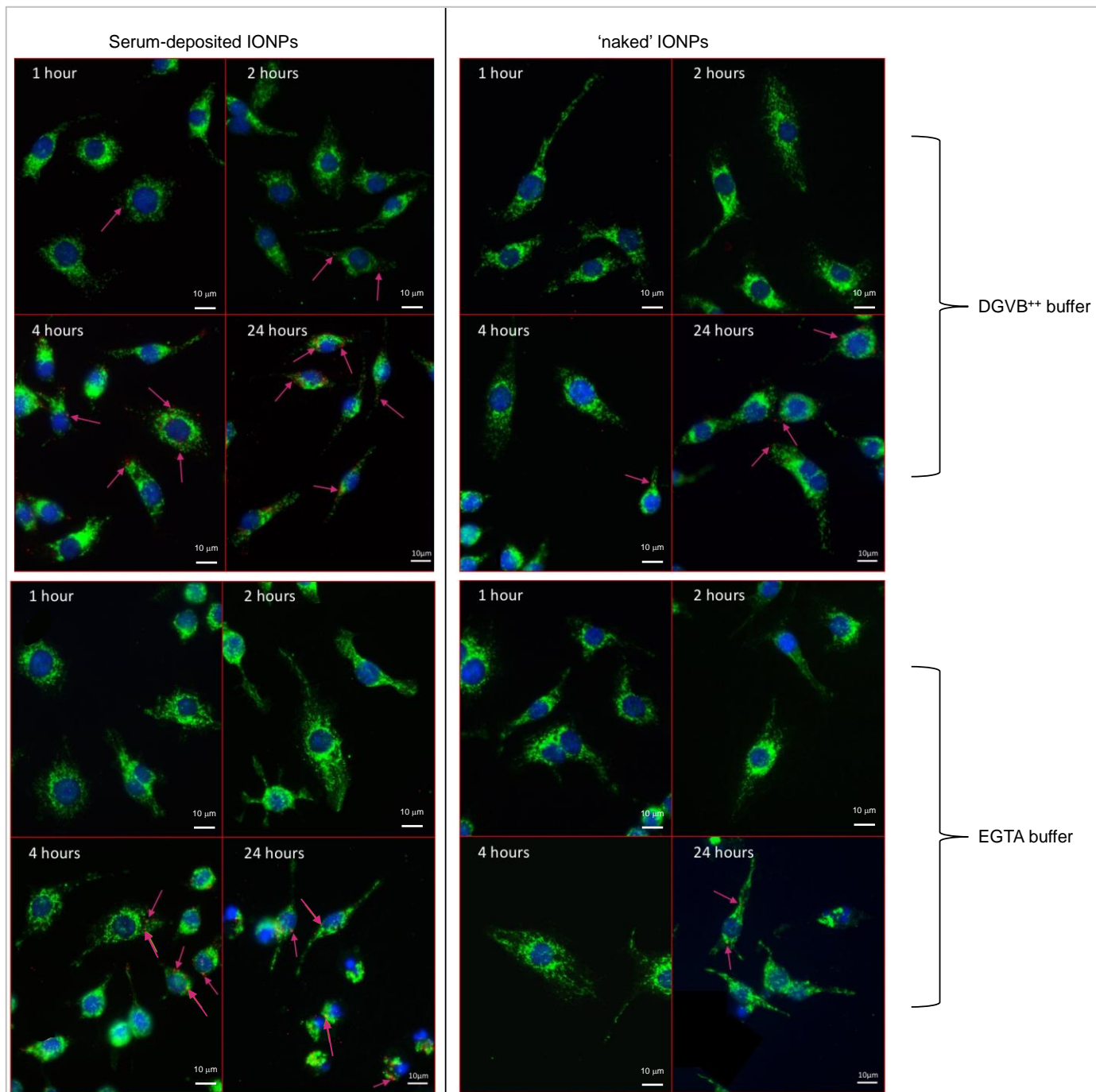


Figure 3.26. **Mitochondrial staining.** Serum-deposited and 'naked' IONPs (red) were prepared as before (serum deposited IONPs with mouse serum + buffer and 'naked' IONPs were incubated with the buffer only). The pictures show uptake of IONPs at 1h, 2h, 4h and 24 hours in murine RAW264.7 macrophages. IONPs were coated with serum for 1 hour at 37°C on a shaker, before being washed with PBS and sonicated. The IONPs were then added to the cells. The cells were fixed with 4% PFA followed by immunofluorescence staining. Mitochondria were labelled with an anti- SOD2 antibody and a fluorescently labelled secondary antibody (green). The nucleus was labelled with Hoechst 33342 (blue). Pink arrows show IONPs inside macrophages, no colocalisation with mitochondria is seen. The cells were imaged using Leica DM-4000 microscope and the LAS software.

### 3.3.7 Golgi apparatus staining (Syntaxin 6)

To check for presence of IONPs in the Golgi apparatus, the Golgi apparatus was stained using anti-syntaxin-6 antibodies. The results (figure 3.27) show limited colocalisation between the Golgi and serum deposited IONPs, independent of the buffers used. However, only two cells showed colocalisation with IONPs and these observations could not be verified in further experiments suggesting that IONPs are not transported to the Golgi network.

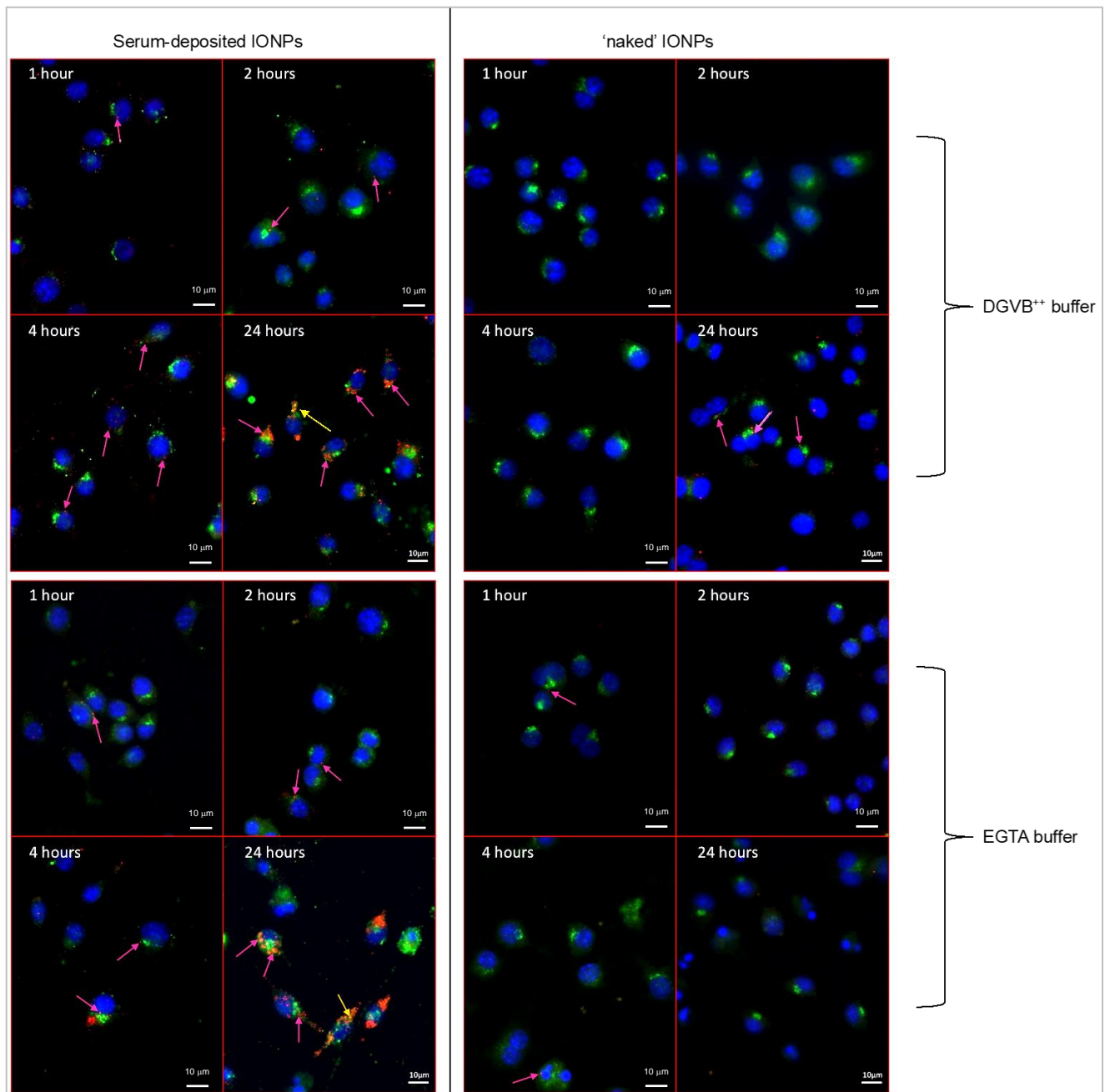


Figure 3.26. **Golgi apparatus staining.** Serum-deposited and 'naked' IONPs (red) were prepared as before (serum deposited IONPs with mouse serum + buffer and 'naked' IONPs were incubated with the buffer only). The pictures show uptake of IONPs at 1h, 2h, 4h and 24 hours in murine RAW264.7 macrophages. IONPs were coated with serum for 1 hour at 37°C on a shaker, before being washed with PBS and sonicated. The IONPs were then added to the cells. The cells were fixed with 4% PFA followed by immunofluorescence staining. Golgi apparatus were labelled with an anti-syntaxin 6 antibody and a fluorescently labelled secondary antibody (green). The nucleus was labelled with Hoechst 33342 (blue). Pink arrows show IONPs inside macrophages, limited colocalization between IONPs and Golgi is seen (yellow arrows). The cells were imaged using Leica DM-4000 microscope and the LAS software.

### 3.3.8 Caveolae staining (Caveolin 1)

Caveolae, as described previously (section 3.2.7), play an important role at the plasma membrane in receptor-mediated endocytosis. To investigate differences in possible uptake mechanisms when using IONPs deposited with serum proteins in presence of the two different veronal buffers (DGVB<sup>++</sup> and EGTA buffers), caveolin-1 antibody was used to stain caveolae and localisation of IONPs was studied through microscopy.

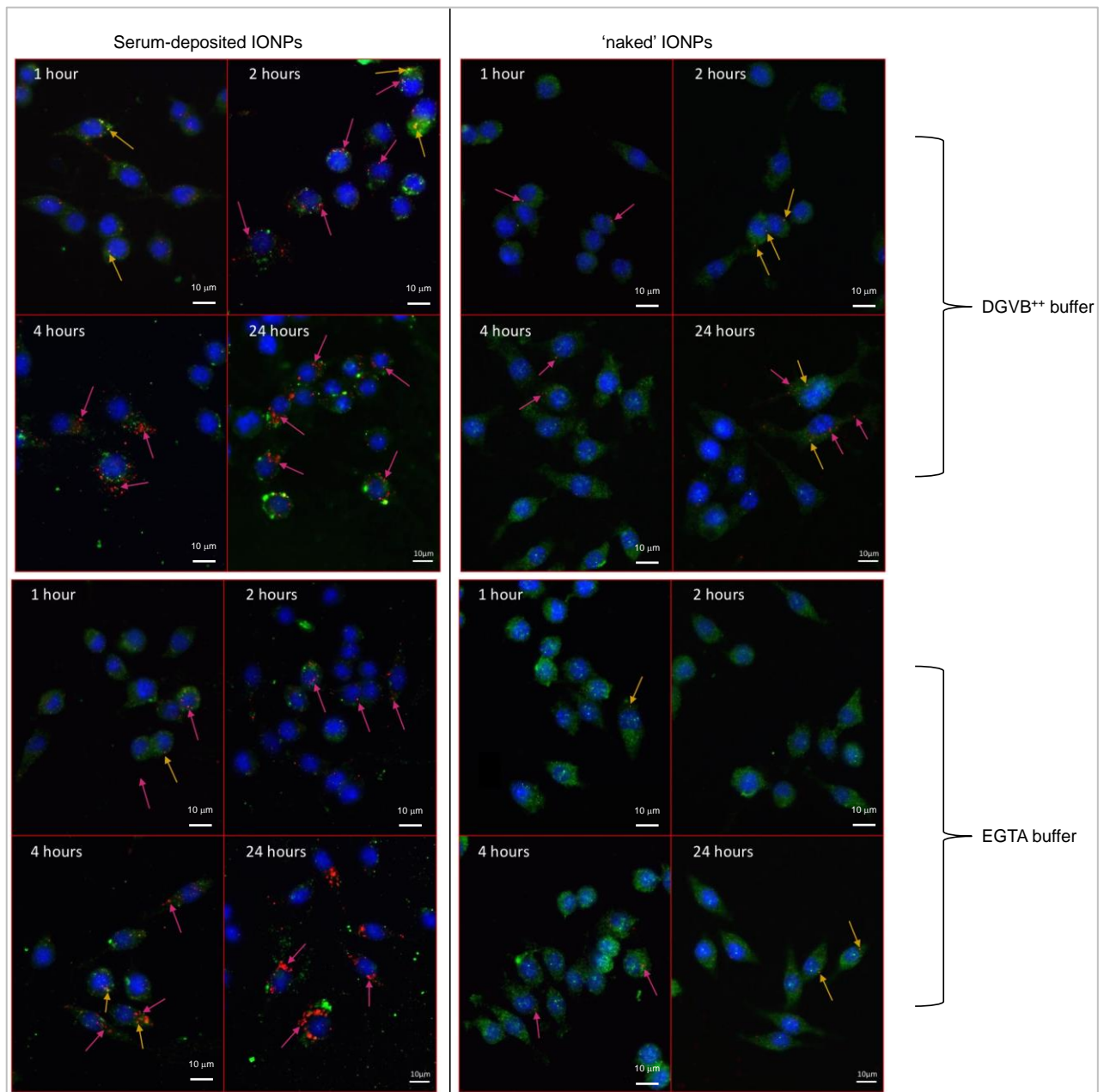
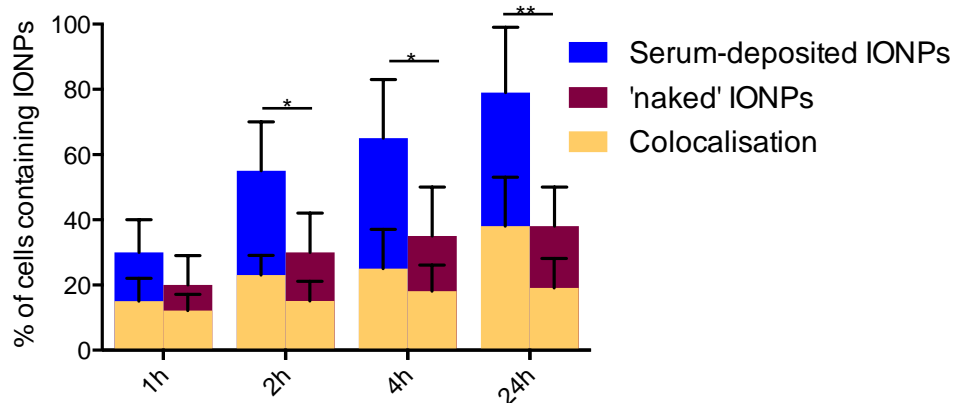


Figure 3.27. **Caveolae staining.** Serum-deposited and 'naked' IONPs (red) were prepared (serum deposited IONPs with mouse serum + buffer and 'naked' IONPs with buffer only). IONPs were coated with serum for 1 hour at 37°C on a shaker, before being washed with PBS and sonicated. The IONPs were then added to the cells. The cells were fixed with 4% PFA followed by immunofluorescence staining. Caveolae were labelled with an anti-caveolin 1 antibody and a fluorescently labelled secondary antibody (green). The nucleus was labelled with Hoechst 33342 (blue). Pink arrows show IONPs inside macrophages, limited colocalisation with caveolae is seen (yellow arrows). The cells were imaged using Leica DM-4000 microscope and the LAS software.

### Average Uptake of IONPs in DGVB<sup>++</sup>buffer & Colocalisation with Caveolin-1



### Average Uptake of IONPs in EGTA buffer & Colocalisation with Caveolin-1

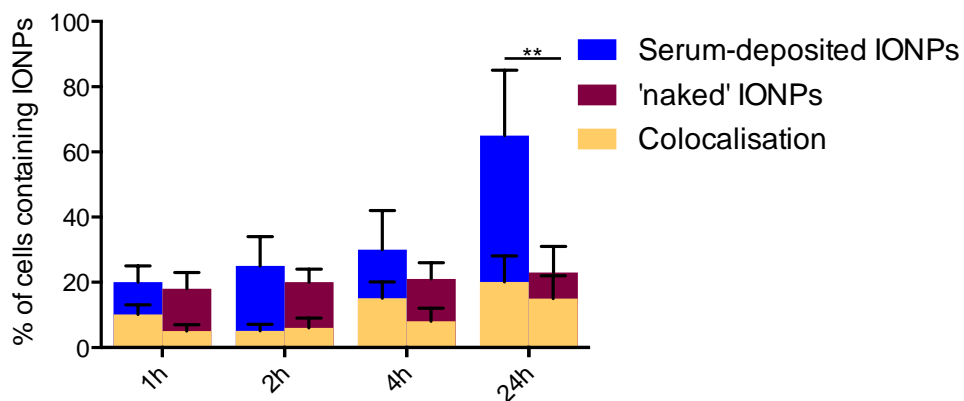


Figure 3.28. **Caveolae staining quantification.** The graph shows the average uptake of serum deposited and 'naked' IONPs. Average uptake was determined by calculating the % of cells that contained IONPs. Some colocalisation was seen at all investigated time points and conditions. Colocalisation was calculated from the number of cells where colocalisation was seen out of total number of cells. Colocalisation was seen in all samples however is not significant for a positive colocalisation result. Error bars represent standard deviation. See chapter 2 (methods) for in depth detail of how the analysis was done. Two independent experiments were carried out and graphs were plotted using GraphPad Prism. A two-way ANOVA test was carried out using GraphPad Prism to determine statistical significance, which are shown on the graph above (Black lines compare uptake for each time point). No statistically significant colocalisation was calculated when comparing time points.

Some colocalisation was observed between caveolae and IONPs in approximately half of the total number of cells that had taken up IONPs. This suggests that caveolae-mediated endocytosis may be one of the pathways through which IONPs are internalised. Furthermore, 'naked' IONPs also colocalised with caveolae, suggesting that the 'protein corona' deposited on the surface of the IONPs is not the only factor in determining caveolin-mediated endocytosis.



### 3.3.9 Dextran as a marker for fluid phase endocytosis

To further pursue elucidating the endocytic pathways of IONPs, three molecular weight dextrans were used as markers of endocytosis (MW=20,000, 40,000 and 70,000 Da). Contrary to the results obtained with IONPs deposited with human serum proteins (section 3.2.8), little colocalisation was found using mouse serum deposited IONPs. The main factor was that less IONP uptake was observed with the mouse serum deposited IONPs. Smaller dextran molecules such as dextran 20,000 Da are likely to be endocytosed through fluid-phase endocytosis, including micropinocytosis and macropinocytosis. The results presented in this section are based on one experimental repeat and should be repeated to confirm our findings and perform statistical analysis.

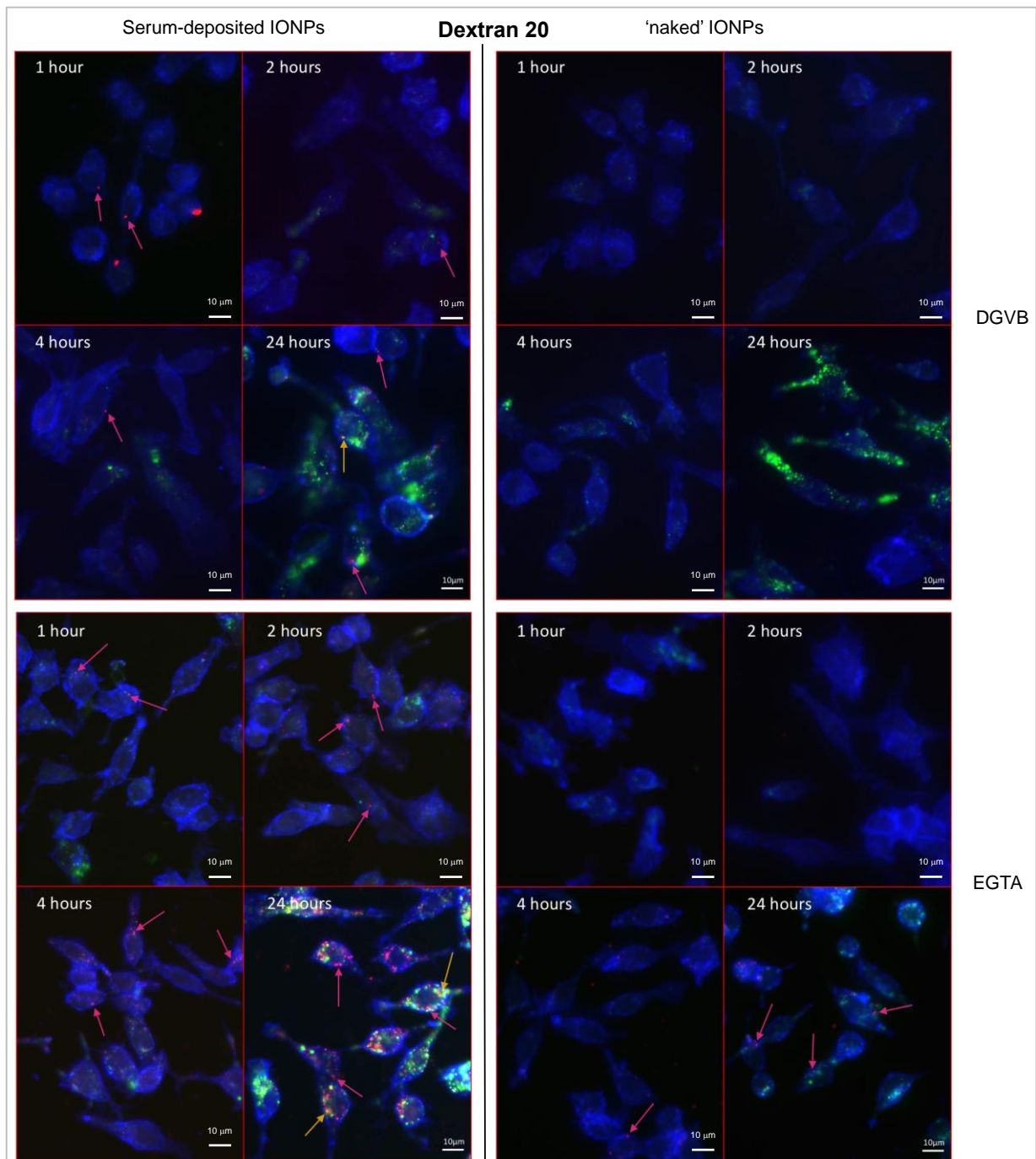


Figure 3.29. **Dextran 20,000 as an endocytic marker.** Serum-deposited and 'naked' IONPs (red) were prepared as before (serum deposited IONPs with mouse serum + buffer and 'naked' IONPs were incubated with the buffer only). The pictures show uptake of IONPs at 1h, 2h, 4h and 24 hours in murine RAW264.7 macrophages. IONPs were coated with serum for 1 hour at 37°C on a shaker, before being washed with PBS and sonicated. The IONPs were then added to the cells together with the dextran. The cells were fixed with 4% PFA at specific time points, followed by immunofluorescence staining. FITC dextran 20,000 (green) and plasma membrane stained with Alexafluor350 conjugated WGA (blue). Pink arrows show IONPs inside macrophages. Yellow arrows show colocalisation. The cells were imaged using Leica DM-4000 microscope and the LAS software.

The results with dextran 20,000 (figure 3.29) show that there is little colocalisation between IONPs and dextran except for mouse serum-deposited IONPs in EGTA buffer at 24 hours. This is strikingly different to the data obtained with human serum protein coatings on the IONPs (section 3.2.8). This could be due to the fact that there is less IONP uptake overall or it could also mean that certain proteins are absent in mouse serum which are present in human serum that play a role in stimulating fluid-phase endocytosis or vice versa. The next dextran molecule investigated was dextran 40,000.

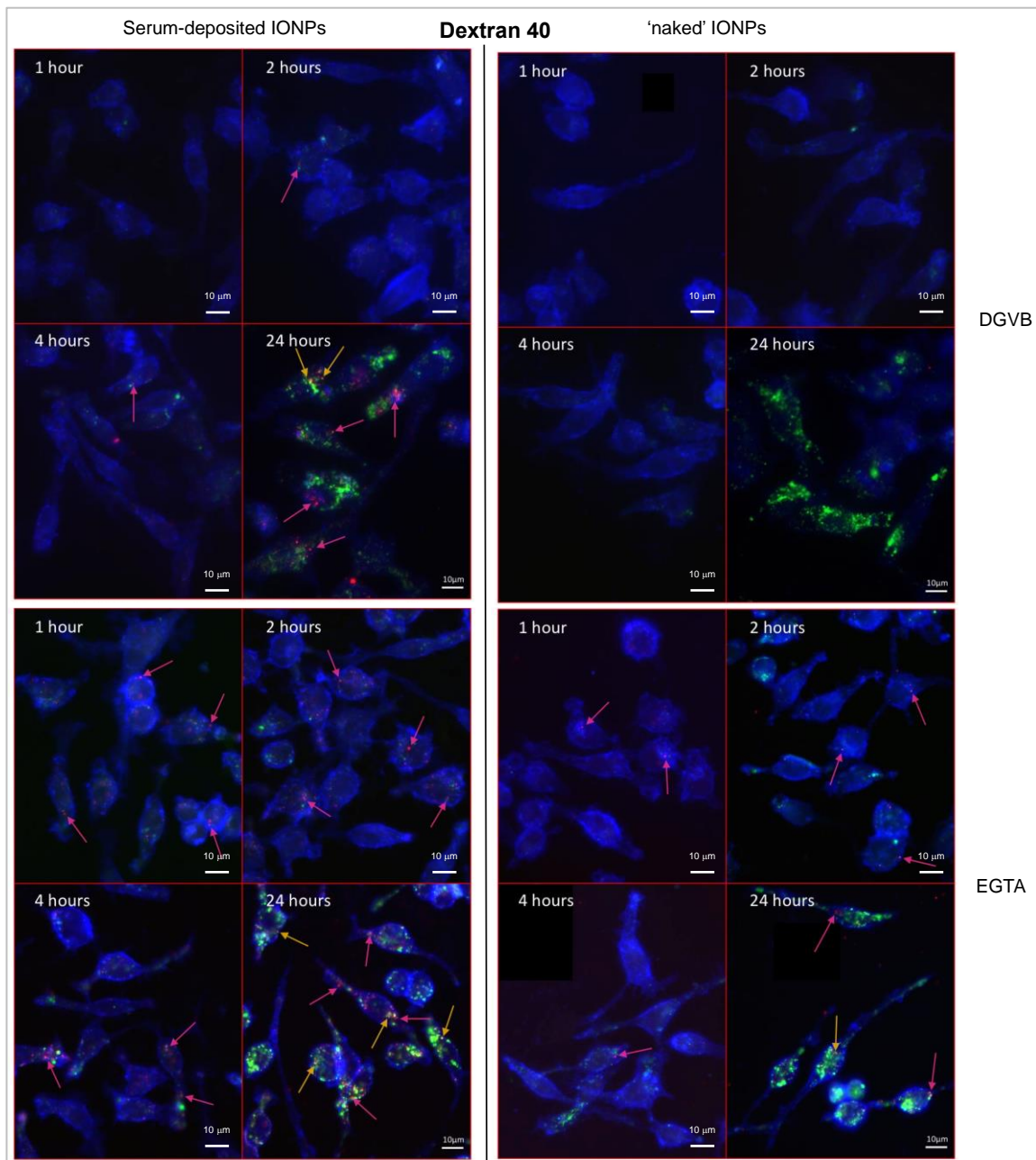


Figure 3.30. **Dextran 40,000 as an endocytic marker.** Serum-deposited and 'naked' IONPs (red) were prepared as before (serum deposited IONPs with mouse serum + buffer and 'naked' IONPs were incubated with the buffer only). The pictures show uptake of IONPs at 1h, 2h, 4h and 24 hours in murine RAW264.7 macrophages. IONPs were coated with serum for 1 hour at 37°C on a shaker, before being washed with PBS and sonicated. The IONPs were then added to the cells together with the dextran. The cells were fixed with 4% PFA at specific time points, followed by immunofluorescence staining. FITC dextran 40,000 (green) and the plasma membrane stained with Alexafluor350 conjugated WGA (blue). Pink arrows show IONPs inside macrophages. Some colocalisation can be seen as shown by yellow arrows. The cells were imaged using Leica DM-4000 microscope and the LAS software.

The results (figure 3.30) show little colocalisation between IONPs and dextran 40,000 suggesting that IONPs do not follow the same intracellular uptake mechanisms as

these dextran molecules. Similar to the previous experiment (figure 3.29), IONP uptake was not high which could also be an explanation for the lack of colocalisation seen. The last dextran investigated had a molecular weight of 70,000.

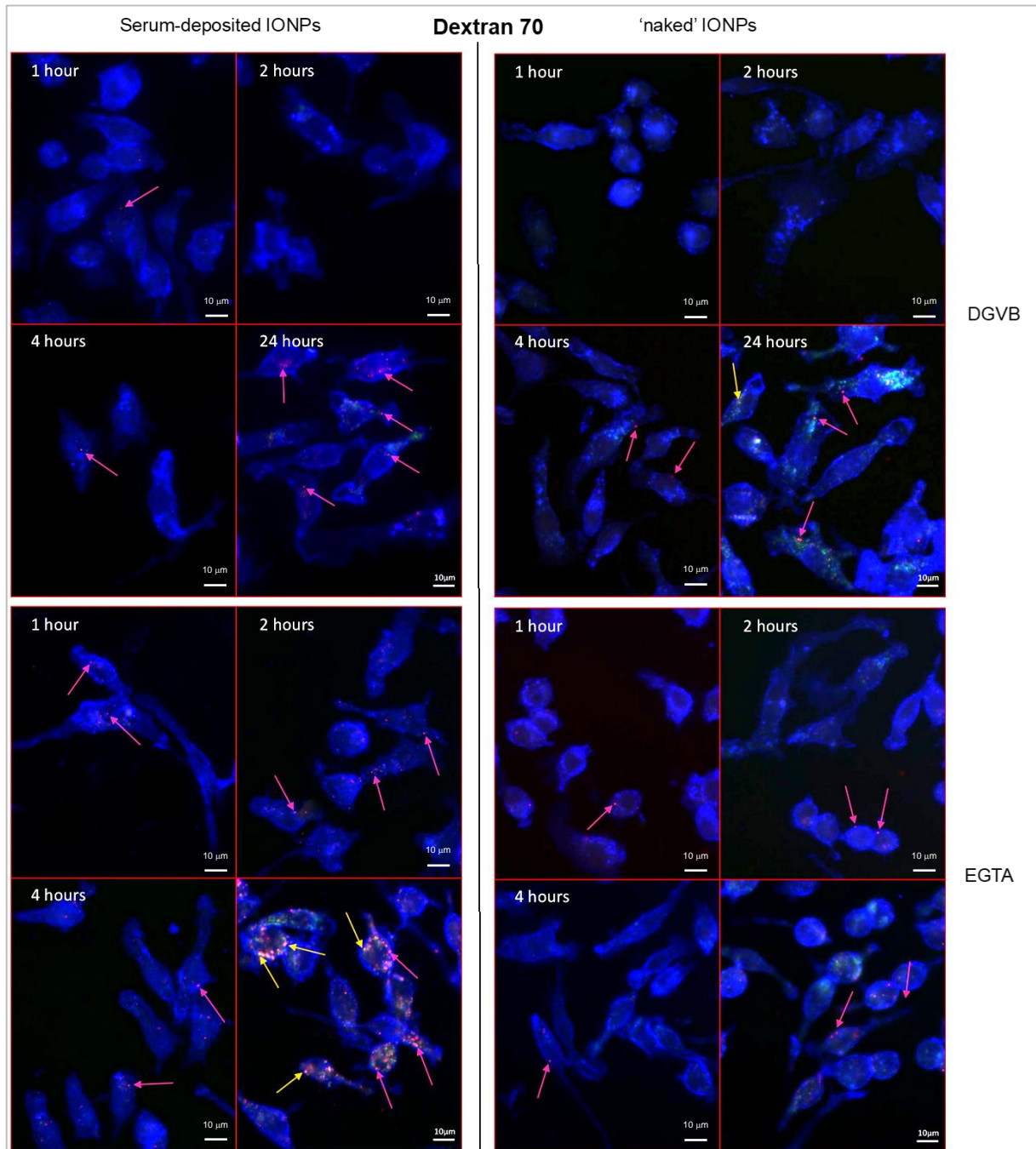


Figure 3.31. **Dextran 70,000 as an endocytic marker.** Serum-deposited and 'naked' IONPs (red) were prepared as before (serum deposited IONPs with mouse serum + buffer and 'naked' IONPs were incubated with the buffer only). The pictures show uptake of IONPs at 1h, 2h, 4h and 24 hours in murine RAW264.7 macrophages. IONPs were coated with serum for 1 hour at 37°C on a shaker, before being washed with PBS and sonicated. The IONPs were then added to the cells together with the dextran. The cells were fixed with 4% PFA at specific time points, followed by immunofluorescence staining. FITC dextran 70,000 (green) and the plasma membrane stained with Alexafluor350 conjugated WGA (blue). Pink arrows show IONPs inside macrophages. Some colocalisation can be seen as shown by yellow arrows. The cells were imaged using Leica DM-4000 microscope and the LAS software.

The results (figure 3.31) show some colocalisation with mainly the serum-deposited IONPs in EGTA buffer, which further supports the argument that mouse serum proteins adsorbed in the presence of EGTA buffer can play a role in determining the endocytic pathway of IONPs since this colocalisation is not seen in 'naked' IONPs in EGTA buffer.

### 3.4 Discussion

The aim of this study was to investigate the intracellular fate of IONPs in murine macrophages. This was done through organelle staining and microscopy. Different sized dextrans were also used as markers of endocytosis to help in the understanding uptake mechanisms of IONPs. Overall, the data produced strongly suggests that IONPs accumulate in the late endosomes and lysosomes. IONPs showed no significant colocalisation with early endosomes, mitochondria, Trans-Golgi network and the endoplasmic reticulum. Due to the low percentage of colocalisation between IONPs and these organelles observed during screening with conventional microscopy, colocalisation was not confirmed using the Nikon Eclipse Confocal microscope but images using the Leica DM4000 microscope were analysed. Some colocalisation was seen between IONPs and late endosomal protein Rab 9 and strong colocalisation was seen with LysoTracker; a pH sensitive dye used to visualise cellular compartments with low pH. This provides strong evidence that the IONPs are localised in an acidic compartment of the cell, 24 hours after IONP exposure, most likely lysosomes due to the limited colocalisation observed with the late endosomes (Rab 7 staining). Other studies have shown similar intracellular trafficking patterns. For example: a study investigated the intracellular trafficking of different sized polystyrene NPs (Sandin *et al.*, 2012). The study found that small NPs (40nm) are trafficked through Rab5 and are quickly transferred to late endosomes (Rab9) before finally localising to lysosomes (using Rab7 as a marker). They also showed that larger sized NPs (100nm) are also trafficked through the same endosomes but at a slower rate than the smaller NPs. This could explain why our results showed maximum uptake and colocalisation in late endosomes/lysosomes at 24 hours after exposure as the diameter of the IONPs used in our studies is 100nm and hence, they are likely to be trafficked at a slower rate due

to their size. Although the presence of IONPs in recycling endosomes were not studied in this chapter, some studies have shown that very few NPs are able to access the recycling endosomes (Sandin *et al.*, 2012), thus decreasing the likelihood that the IONPs may be recycled back to the plasma membrane. There is also the possibility that some of the IONPs escaped the endolysosomal system and were located in clusters in the cytoplasm. If IONPs escape endosomes prior to fusion with lysosomes, these IONPs can bypass lysosomal degradation (Behzadi *et al.*, 2017). To investigate whether IONPs remain free in the cytoplasm, cytoplasmic markers could be used to investigate possible colocalisation.

To investigate the pathway the IONPs take to enter macrophages, an anti-caveolin 1 antibody was used to localise caveolae. Some colocalisation was seen with IONPs and caveolae, which indicates that these IONPs are being taken up through caveolae mediated endocytosis. One reason why more IONPs colocalisation was not seen within the caveolae could be the size of the IONPs (100nm). Although caveolae are small invaginations with a diameter of about 60-80 nm, they are able to internalise molecules of a bigger size, although not as efficiently (Wang *et al.*, 2009). For example, a study showed that smaller NPs of size 20-40 nm were endocytosed 5-10 times more than larger NP sizes of 100nm (Wang *et al.*, 2009). Thus, the size of the IONPs used in our experiments could be the reason why stronger colocalisation with caveolae was not seen.

Using dextran molecules as fluid-phase endocytosis markers has helped understanding the endocytic pathway of the IONPs. Different molecular weights of dextran were used to distinguish the different endocytic pathways as they will be endocytosed via distinctive pathways. Lower molecular weight dextrans are endocytosed via classical pinocytosis pathways whereas higher molecular weight



dextran are endocytosed via constitutive macropinocytosis (Li *et al.*, 2015). Colocalisation of IONPs with different sized dextran molecules was observed indicating that macropinocytosis is likely to be the major endocytic pathway of IONP uptake in murine macrophages. This was especially observed with human serum deposited IONPs. Although it is not possible to know how many IONPs were internalised and colocalised with dextran, the uptake and colocalisation of IONPs can be measured using the intracellular area covered as a measuring parameter and quantifying the fluorescence intensity on ImageJ. Other studies have used different methods of quantifying colocalisation by using Imaris software (Bitplane), where colocalisation within a manually masked region of the cell can be measured (Sandin *et al.*, 2012). Nevertheless, some of our results show strong and clear colocalisation between IONPs and dextran based on 2 experimental repeats and this finding could be further studied and exploited for the targeting of tumour cells. This is of particular interest as certain types of tumour cells are known to have increased macropinocytic activity, thus NPs entering cells through macropinocytosis could be favourable drug delivery in these cells (Desai, Hunter and Kapustin, 2019).

Mouse serum was also used to determine the differential effects seen with the use of human serum in a murine cell line. Similar to the results obtained with human serum, little to no colocalisation was seen with the early endosomes, mitochondria and the Trans-Golgi network. However, with late endosomal marker Rab 7, differences were seen in colocalisation between the human serum and mouse serum samples. This could indicate the possibility of different trafficking pathways of IONPs due to different protein corona compositions of IONPs. More colocalisation was seen with the late endosomal marker Rab 9 than other organelles, with the overall percentage of

colocalisation being about 40% for serum-deposited IONPs. This shows that the presence of a different protein corona can influence the intracellular trafficking of IONPs as higher colocalisation percentages are seen between IONPs and late endosomes when using mouse serum as the protein coating compared to using human serum as the protein coating.

To distinguish between the different pathways of complement activation, different veronal buffers, DGVB<sup>++</sup> and DGVB-EGTA, were used to favour adsorption of complement components of the classical and alternative pathway respectively. Through the use of DGVB<sup>++</sup> buffer, we have aimed to adsorb proteins associated with the classical pathway of the complement system. Although DGVB<sup>++</sup> buffer is able to activate all three pathways of the complement system, proteins of the classical pathway would be more prevalent since they can be activated at lower serum concentrations compared to the others (Moreno-Indias *et al.*, 2012). DGVB<sup>++</sup> buffer contains both calcium and magnesium ions, both of which are required for C2-C4 interaction, leading to the formation of C1q complex, an important molecule of the innate immune response (Okroj *et al.*, 2012). With the use of EGTA buffer, we aimed to adsorb proteins of the alternative pathway because it is the only pathway that can be activated without calcium. The results in figures 3.18 and 3.19 show differences between the uptake pattern when the classical pathway associated proteins had been adsorbed compared to those associated with the alternative pathway. More uptake of IONPs was seen with the classical pathway than the alternative pathway. This difference in uptake between the two different buffers is most likely due to the different proteins adsorbed to the IONPs and may suggest that the presence of EGTA buffer can lead to reduced uptake of IONPs, which can be exploited to avoid unwanted clearance of IONPs *in vivo* by the mononuclear phagocytic system (MPS). It is well-

known that different protein corona compositions can play a major role in influencing the uptake of NPs. With *in vivo* applications of NPs, the formation of a protein corona can determine the stability, protein interactions, biodistribution, toxicity and clearance from the body by the MPS (Rampado *et al.*, 2020). Thus, it is important to understand which protein corona formulations satisfy the most criteria to offer the best therapeutic efficacy. Taking this forward, the protein corona when different buffers are used in the coating can be analysed by using electrophoresis methods and relating the results to the uptake patterns seen in our experiments.

Different molecular weight dextran molecules were also used to study the endocytic pathway of IONPs incubated with mouse serum. These preliminary results differ from the results seen with human serum. Less dextran molecules were endocytosed at the earlier time points (1 hour, 2 hours and 4 hours) and high levels of endocytosed dextran are only seen after 24 hours, especially in the EGTA buffer sample. These results again strongly suggest that the IONPs favour macropinocytosis as an endocytic route and additionally, the difference in buffers incubated with the IONPs may also influence their uptake as different uptake patterns are seen with the two different buffers. It is important to also note that protein corona is a dynamic structure that is subject to changes over time and this may affect the uptake and intracellular fate of IONPs. Since this data was produced by one experimental repeat, it needs to be repeated to validate our results. A study investigating the uptake and endocytosis of different sized silver NPs showed that the uptake of larger sizes AgNPs (50nm and 100nm) was reduced when 5-(N-ethyl-N-isopropyl) amiloride was used as a macropinocytosis inhibitor, suggesting that macropinocytosis is one of the preferred uptake pathways for larger sized NPs (Wu *et al.*, 2019). This correlates to the results found in this chapter where macropinocytosis was shown as the likely route for IONP

(100nm) endocytosis. The results can be further confirmed by using other methods to study endocytic pathways such as the use of specific endocytic inhibitors (Dejonghe *et al.*, 2019). Endocytic routes taken by IONPs is by using surface-enhanced Raman spectroscopy in combination with endocytic inhibitors, as carried out by a recent study where the endocytosis of gold NPs was investigated using this method (Yılmaz and Culha, 2021). As another future avenue, molecular techniques such as RNA interference (RNAi) and small interfering RNA (siRNA) can be used to investigate and assess the role of key proteins involved in the different endocytic pathways of IONPs. The data produced so far helps our understanding of the intracellular trafficking and intracellular fate of larger sized IONPs in murine macrophages. Through organelle staining, we have shown strong evidence of IONPs localising in the endolysosomal system. This can be particularly exploited in the development of nanotherapeutics targeting low pH organelles. For instance, abnormal function of the lysosome has been linked to multiple neurodegenerative diseases and autoimmune diseases (Ma *et al.*, 2016) and the accumulation of IONPs in lysosomes could be an interesting strategy for lysosomal-targeted nanotherapeutics. Furthermore, our data suggests that one of the main routes of endocytosis is through macropinocytosis, which, as mentioned earlier, can also be exploited to develop strategic targeting of certain tumour cells which show increased macropinocytic activity due to growth factor activation. In addition, the data presented in this chapter can be further explored and taken forward to investigate strategies that can be developed in order to avoid unwanted clearance of IONPs by phagocytes, especially with further studies on protein corona formulations.

Some limitations were present in this study which need to be considered when planning future work. For example, the resolution of the microscope used (Leica

DM4000) may not be very effective for the visualisation of individual IONPs but rather are more easily seen when IONPs are present in small clusters. Hence, for visualisation of individual IONPs, higher magnifications can be used (such as TEM). Furthermore, the use of a sonication probe can affect the integrity of the protein corona formed on the IONPs, which can influence their uptake. To assess changes which may occur following sonication, the IONP coating and protein corona can be analysed by using electrophoresis techniques (Lundqvist *et al.*, 2008). Lastly, serum starvation of cells can downregulate certain endocytic pathways such as clathrin-independent endocytosis (Rennick *et al.*, 2021) and although this endocytic pathway was not of particular interest in this chapter, since all experiments were performed in serum-free media, it is important to acknowledge that serum starvation can play a role in mediating endocytosis. All experiments were carried out at least twice and those experiments with two experimental repeats should be carried out again to confirm our results, however, we believe our current findings so far have built a good foundation for future studies of the intracellular trafficking and fate of IONPs in macrophages.

---

## **4. Immunotoxicity of Iron Oxide Nanoparticles**

---

## 4.1 Introduction

As engineered NPs are becoming more important in the drug delivery world, their toxicity remains a concern. Inevitably, NPs administered via the bloodstream will be in direct contact with cells of the innate immune system such as macrophages with the increased likelihood of triggering an immune response against the NPs. NPs with different surface compositions and properties will interact with the immune system in different ways, resulting in a downregulated or upregulated immune response (Elsabahy and Wooley, 2013). To understand the immune response against IONPs, selected cytokines were used as biomarkers of inflammation. Cytokine responses can translate to pathology through fever, muscle pain, headache, nausea and vomiting, amongst others (Elsabahy and Wooley, 2013). Several authors have shown the ability of a number of metal oxides to be able to trigger cytokine production (Borgognoni *et al.*, 2018). One study investigated cytokine secretion by human macrophages following exposure to TiO<sub>2</sub> NPs (approximate size of 100-120nm). The study found that cytokine secretion is concentration dependent where at high NP concentrations, IL-1 $\beta$ , IL-6 and IL-10 were secreted whereas at lower NP concentrations, only IL-6 secretion was found (CF *et al.*, 2015). This secretion of IL-6 may contribute to the development of autoimmune diseases as well as the secretion of acute phase proteins (CF *et al.*, 2015). Furthermore, other studies have investigated the inflammatory ability of TiO<sub>2</sub> through the activation of the NLRP3 inflammasome in human macrophages, leading to the secretion of IL-1 $\beta$  and IL-1 $\alpha$  (Yazdi *et al.*, 2010). NPs Hence, studying cytokine expression levels is considered a key step in determining immunotoxicity during the development of nanotherapeutics, as well as other biotherapeutics.

Pro-inflammatory cytokines, such as TNF- $\alpha$ , IL-6, IL-1 $\beta$  are released upon immune response stimulation and through a series of events, lead to the activation and infiltration of immune cells and cytokines, an important process of the host's defence against invading pathogens (Ray, 2016). As much as pro-inflammatory cytokines are important, their overexpression can lead to the development of diseases and tumorigenesis. Hence, the release of anti-inflammatory cytokines, such as IL-10, IL-13 and IL-4, is an important protective mechanism against the adverse effects of pro-inflammatory cytokines by inhibiting or suppressing their activity resulting in a suppressed immune response (Chatterjee *et al.*, 2014). The delicate balance of pro-inflammatory and anti-inflammatory cytokine secretion is thus key to an effective immune response.

Quantitative Real-Time PCR was used to detect and measure the expression levels of selected pro-inflammatory and anti-inflammatory cytokines in response to incubation with IONPs in mouse macrophages. The cytokines initially investigated were TNF- $\alpha$ , IL-1 $\beta$ , IFN- $\alpha$ , IFN- $\beta$ , TGF- $\beta$ 1, IL-6, IL-8, IL-10, NF- $\kappa$ B1, IL-12p40 and NLRP3, which are discussed later. Transcriptome sequencing (RNA-sequencing) was also carried out to identify differentially expressed genes at the mRNA expression level. RNA-sequencing is a highly accurate and precise method of quantifying gene expression as well as effective comparisons between experiments. Amongst other advantages, RNA-sequencing also allows for specific signalling pathways that are upregulated or downregulated to be identified. For example, through transcriptome profiling, a study recently identified over 4,000 genes that were differentially expressed in response to nanoparticle treatment for 48 hours (Carrow *et al.*, 2018). The same study showed that specific signalling pathways such as MAPK (mitogen-activated protein kinase) and stress-responsive pathways were upregulated. Through RNA-



sequencing, we aim to identify differentially expressed genes and upregulated pathways relating to immune responses in order to better understand and evaluate IONPs-induced toxicity. If IONPs alter gene regulation in any way, this could lead to cell death or the development of abnormal cells, which in turn can lead to the development of autoimmune diseases, hypersensitivity reactions or the formation of tumours. This chapter aims at studying the immunotoxicity of IONPs in mouse macrophages, which is a crucial part in establishing their biosafety as drug delivery vehicles. We hypothesize that an enhanced immune response will occur with the exposure of 'naked' IONPs, compared to serum-deposited IONPs and different IONP treatments will elicit different responses.

## 4.2 Results

### 4.2.1 Using cytokines as biomarkers of inflammation following uptake of IONPs by macrophages

To study if IONPs trigger a pro-inflammatory or anti-inflammatory immune response, cytokine expression levels were measured by qPCR. The previous chapter focused on the intracellular fate of IONPs following phagocytosis by macrophages and the earliest intracellular uptake was seen at 2 hours after the addition of IONPs. Hence, cytokine expression levels were measured following a 2 hour incubation period with IONPs to understand the initial immune response by macrophages. We also wanted to see the difference in innate immune activity when the IONP surface was deposited with different sera; human serum and mouse serum as well as differences between the activation of classical and alternative pathways by using the same veronal buffers used previously (DGVB<sup>++</sup> and EGTA buffers). The different conditions used are listed in the table below.

Serum	Veronal Buffer	Aim
<b>1) IONPs incubated in mouse serum</b>	DGVB <sup>++</sup>	To favour classical pathway activation in the presence of mouse serum proteins
<b>2) IONPs incubated in mouse serum</b>	EGTA	To favour alternative pathway activation in the presence of mouse serum proteins
<b>3) IONPs incubated in human serum</b>	DGVB <sup>++</sup>	To favour classical pathway activation in the presence of human serum proteins
<b>4) IONPs incubated in human serum</b>	EGTA	To favour alternative pathway activation in the presence of human serum proteins
<b>5) 'naked' IONPs</b>	DGVB <sup>++</sup>	To favour classical pathway activation in the absence of serum proteins
<b>6) 'naked' IONPs</b>	EGTA	To favour alternative pathway activation in the absence of serum proteins

Table 4.1. **IONPs incubations in different sera and buffers.** The IONPs were incubated under the conditions listed in this table. The IONPs were incubated for 1 hour with the serum + buffer. IONPs were then washed with PBS before adding to serum-starved cells for 2 hours, following which the RNA was extracted.

Reverse transcriptase was carried out on the extracted RNA to produce cDNA (described in section 2.10), which served as a template for the gene expression studies using qPCR. The amplification results were analysed using the  $2^{-\Delta\Delta CT}$  method (see section 2.10 for details) and the fold change in gene expression results were plotted on a graph, based on two independent experimental repeats.

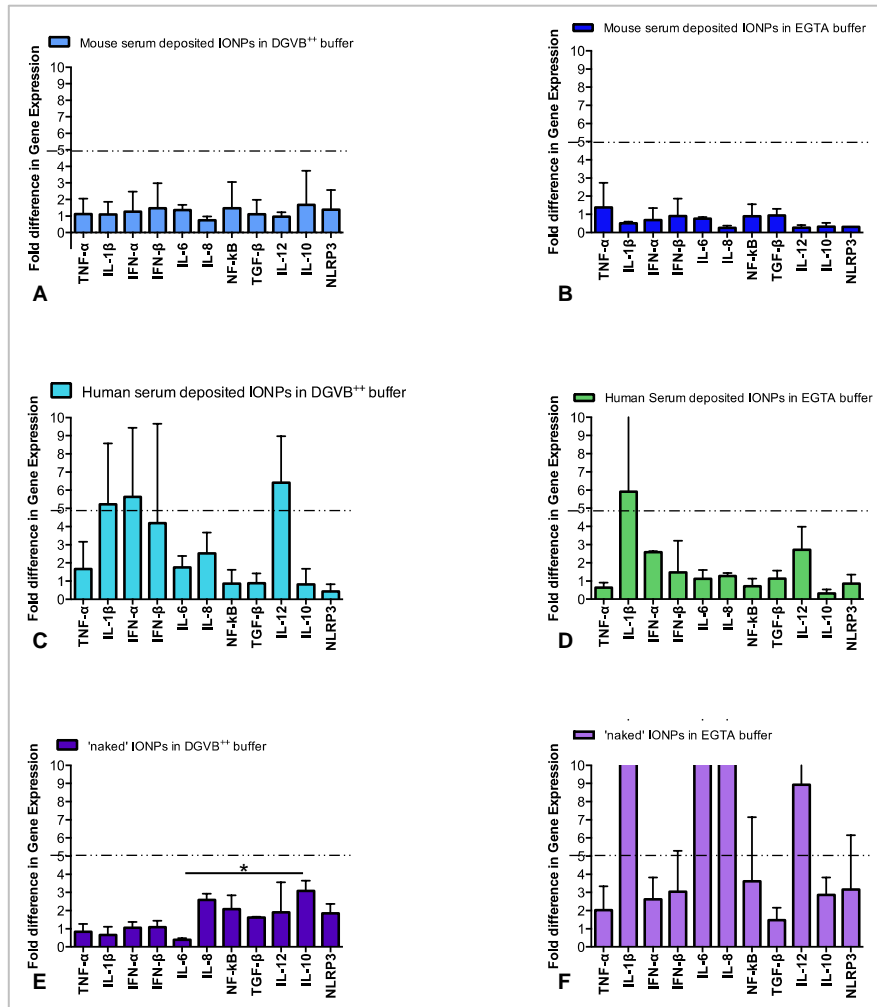


**Figure 4.2. Fold difference in gene expression for selected cytokines after exposure of serum starved mouse macrophages to IONPs for two hours.** The graphs show the fold change/difference in gene expression for each cytokine investigated after exposure of mouse macrophages for 2 hours with IONPs pre-incubated with human or mouse sera in DGVB<sup>++</sup> or DGVB-EGTA buffers. Cells with without IONP addition were used as control to normalise the data. The housekeeping gene used was 18s rRNA. Error bars show standard deviation. qPCR data of 2 independent experiments was analysed with the  $2^{-\Delta\Delta CT}$  method. A one-way ANOVA test was carried out on GraphPad Prism to determine statistical significance. Due to large error bars, statistical significance was only obtained between IL-6 and IL-10 in the 'naked' IONP in DGVB<sup>++</sup> buffer. Dotted lines were added as a minimum threshold to show where significant fold differences may occur. Graphs were cut off at 10 X fold change.

The graph (figure 4.2) shows that in both mouse serum deposited IONP samples (A & B), transcriptional expression of all investigated cytokines was minimally changed when normalised to the housekeeping gene. In both human serum deposited IONP samples (figure 4.2 C & D), expression of some cytokines was elevated, with IL-1 $\beta$  on

average being overexpressed 5 fold. IL-1 $\beta$  is a potent pro-inflammatory cytokine mainly secreted by immune cells such as monocytes and macrophages in response to the detection of PAMPs (pathogen associated molecular patterns) (Lopez-Castejon and Brough, 2011). While it is an important cytokine in the host's defence mechanism, overexpression of IL-1 $\beta$  can induce apoptotic events and its upregulation in cancer cells can promote tumour growth (Tu *et al.*, 2008).

Comparing the two 'naked' IONP samples (figure 4.2 E & F), the EGTA sample showed higher expression (by at least 9 fold) for 4 out of 11 cytokines compared to the DGVB<sup>++</sup> sample. These cytokines included IL-1 $\beta$ , IL-6, IL-8 and IL-12p40. Along with IL-1 $\beta$ , IL-8 and IL-12p40 are pro-inflammatory cytokines and some studies have shown that IL-12 can play a role in the production and release of IL-8 (Ethuin *et al.*, 2001). This seems to correlate with the expression levels of IL-12 and IL-8 seen in the above figure 4.2. IL-6 is a pleiotropic cytokine, which can act as both pro-inflammatory and anti-inflammatory cytokine, and is usually secreted during infections or cell damage (Velazquez-Salinas *et al.*, 2019).

The difference seen between the two 'naked' IONPs samples (figure 4.2 E & F) could indicate that the DGVB<sup>++</sup> buffer containing Ca<sup>2+</sup> and Mg<sup>2+</sup> ions triggers a lower inflammatory response than EGTA buffer, which lacks Ca<sup>2+</sup> ions. However, presence of mouse serum proteins (B) greatly reduces the inflammatory immune response, indicating that the deposition of serum proteins modulates the inflammatory cell response. The data also indicates that different serum protein compositions on the IONPs has different effect on inflammatory responses, as demonstrated by the differences in human serum and mouse serum samples (figure 4.2 A,B,C,D).

NLRP3 expression was also increased by at least 2 fold in both 'naked' IONPs samples (figure 4.2 E & F), with the higher increase seen in 'naked' IONPs in EGTA buffer (Note: this data is based on two separate experiments done in triplicates. Due to error bar size, the experiment should be repeated to confirm these findings. However, during RNA-sequencing, NLRP3 was differentially expressed but expression was not significantly altered, which corresponds to the findings seen here.

NLRP3 is a protein that upon stimulation, forms and activates the NLRP3 inflammasome, which plays an important role in innate immunity (Zahid *et al.*, 2019). NLRP3 inflammasome activation mediates the release of pro-inflammatory cytokines such as IL-1 $\beta$ , and as described previously, pro-inflammatory cytokines are key players in response to infections and tissue damage (Kelley *et al.*, 2019). Furthermore, aberrant NLRP3 inflammasome activation has been associated with a number of diseases including diabetes, inflammatory bowel disease (IBD), certain cardiovascular diseases and cancers (Zahid *et al.*, 2019).

To compare overall upregulated and downregulated cytokine expression, a log<sub>10</sub> graph of fold difference in gene expression was plotted and is shown in figure 4.3 below.

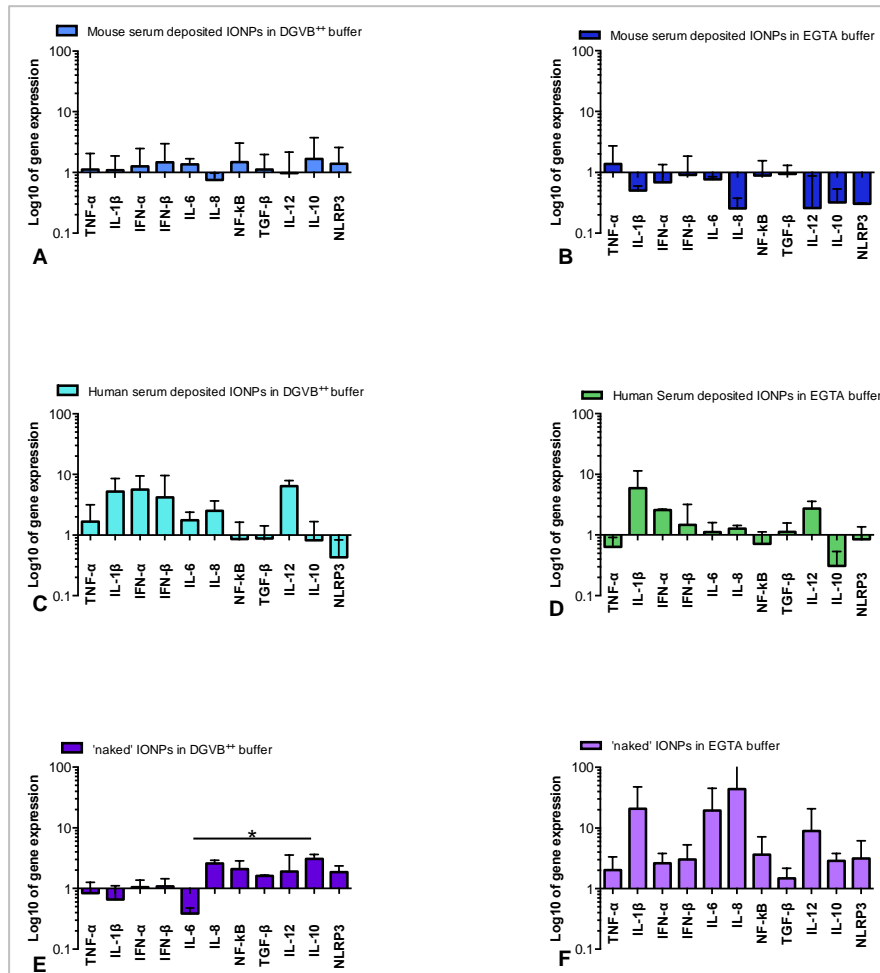


Figure 4.3. **Log<sub>10</sub> values of fold differences for selected cytokines after exposure of serum starved mouse macrophages to IONPs for two hours..** The graph shows the log<sub>10</sub> values of fold change/difference in gene expression for each cytokine investigated after exposure of mouse macrophages for 2 hours with IONPs pre-incubated with human or mouse sera in DGVB++ or DGVB EGTA buffers. Values greater than 1 show an upregulation in cytokine expression whereas values less than 1 show a downregulation in cytokine expression. Cells with and without NP addition were used as control to normalise the data. The housekeeping gene used was 18s rRNA. Error bars show standard deviation. qPCR data of 2 independent experiments was analysed with the  $2^{-\Delta\Delta CT}$  method. A one-way ANOVA test was carried out using the log<sub>10</sub> values on GraphPad Prism to determine statistical significance. Due to large error bars, statistical significance was only obtained between IL-6 and IL-10 in the 'naked' IONP in DGVB++ buffer.

The above graph (figure 4.3) shows an overview and comparison of upregulated cytokines and downregulated cytokines for each of the different experimental conditions. The 'naked' IONP samples incubated in EGTA buffer showed the highest upregulation of cytokine expression compared to the other samples, including 'naked' IONPs in DGVB<sup>++</sup> buffer. This suggests that 'naked' IONPs in the presence of EGTA buffer is more likely to trigger an inflammation reaction since some of the pro-inflammatory cytokines such as IL-1 $\beta$ , IL-6, TNF- $\alpha$  and IL-12p40 are marginally upregulated. However, IONPs incubated in the presence of mouse serum proteins diluted in EGTA buffer showed a low inflammatory response suggesting that triggering the activation of the alternative pathway in the presence of mouse serum proteins does not generate as high of an inflammatory response. Both mouse serum deposited IONPs showed the lowest inflammatory response whereas IONPs deposited with human serum triggered an inflammatory response with the upregulation of potent pro-inflammatory markers such as IL-1 $\beta$ .

Overall, IONPs deposited with mouse serum proteins, irrespective of the buffer used to deposit proteins, do not seem to trigger an enhanced immune response, with the lowest seen in the EGTA buffer sample (figure 4.3B). In fact, in the serum-deposited IONPs in EGTA buffer sample (figure 4.3B), most of the pro-inflammatory cytokines are downregulated with the exception of TNF- $\alpha$ . In the absence of serum proteins however, 'naked' IONPs in EGTA buffer (figure 4.3F) elicited the highest immune response, with the upregulation of all pro-inflammatory cytokines investigated. In the IONPs deposited in human serum proteins samples (figure 4.3C & D), there is an elevation in pro-inflammatory cytokine expression and a downregulation for the anti-inflammatory cytokine IL-10. This could be due to the fact that some components of



human serum proteins may have been recognised as foreign by the mouse macrophages.

### 5.2.2 Investigating the toxicity of IONPs using transcriptome and gene expression analysis

To study the effects of IONPs exposure on gene expression in macrophages, cells were incubated for 2 hours with IONPs under different conditions, after which RNA was extracted from the cells and sequenced (Company: Genewiz) using Illumina RNA sequencing (poly(A) tail).

The RNA samples sequenced are as follows:

- Mouse serum deposited IONPs in DGVB<sup>++</sup> buffer
- Mouse serum deposited IONPs in EGTA buffer
- 'naked' IONPs in DGVB<sup>++</sup> buffer
- 'naked' IONPs in EGTA buffer
- No exposure to IONPs (control)

Following library preparation and sequencing, all samples were compared against each other and all genes showing significant differential expression (DEGs) were identified. Once a list of DEGs was obtained, gene ontology enrichment analysis was carried out using UniProt to filter and extract genes that are involved in immune system processes. The method of this analysis is explained in more detail in chapter 2.12.

#### Mouse serum deposited IONPs

The two mouse serum deposited samples (DGVB<sup>++</sup> and EGTA buffers) were compared against each other. The graph (figure 4.4) below shows the results from Gene Ontology analysis which denotes specific pathways where the significant DEGs

identified are involved in. Gene Ontology terms are organised as a hierarchy of annotated pathways/terms that help visualise and interpret the data at different levels.

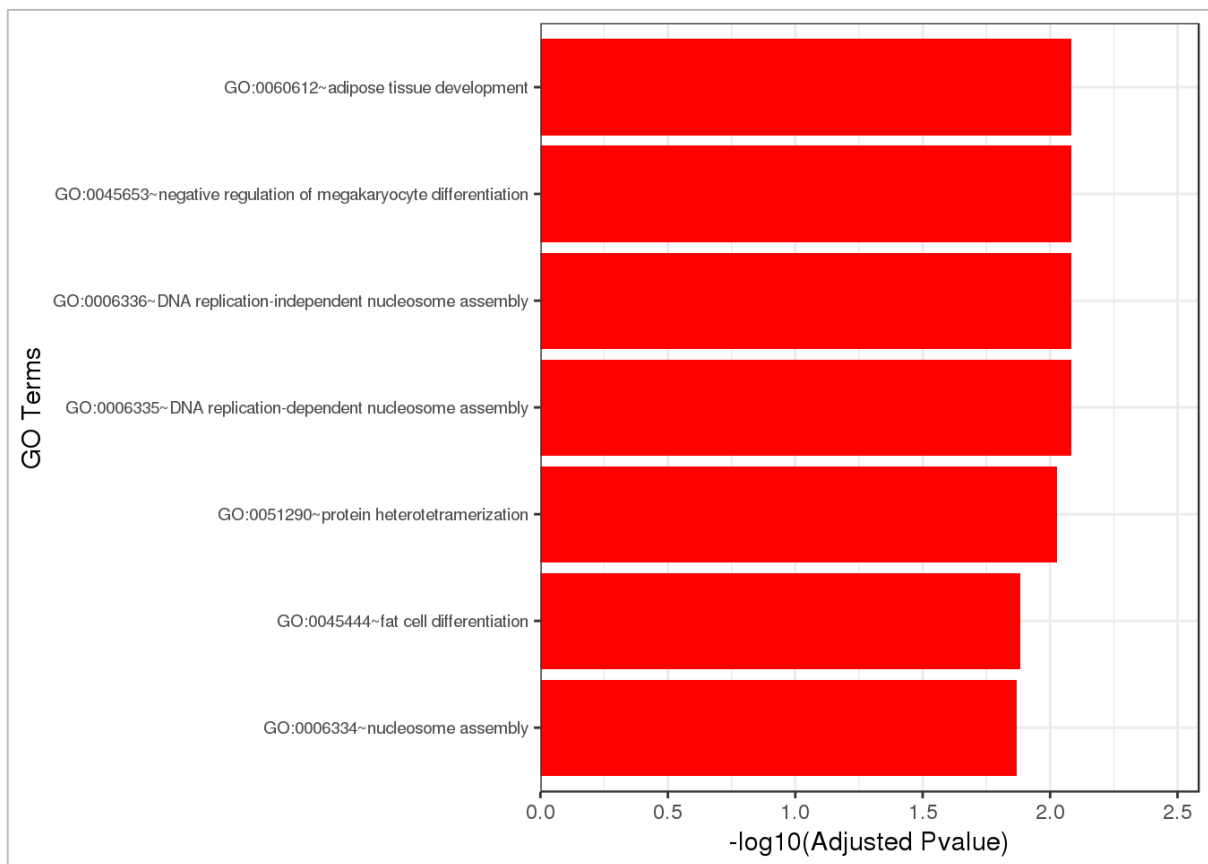


Figure 4.4. **Gene Ontology Analysis Overview.** Differentially expressed genes were clustered by their gene ontology and the enrichment of gene ontology terms was tested using Fisher exact test (GeneSCFv1.1-p2). The above figure shows gene ontology terms that are significantly enriched with an adjusted p-value ( $P < 0.05$ ) in the differentially expressed gene sets. Since only 2 DEGs were significant in this case, not many GO terms were identified. The pathways shown above are pathways where the significant DEGs are involved in.

The gene ontology analysis showed few pathways where the significant DEGs were involved; this was because in this comparison, only two significant DEGs were identified.

The two samples showed very little DEGs overall suggesting that mouse serum proteins reduce a transcriptional response in mouse macrophages independent of complement pathway activation. The volcano plot below (figure 4.5) shows an overview of DEGs and significant DEGs in the two samples.

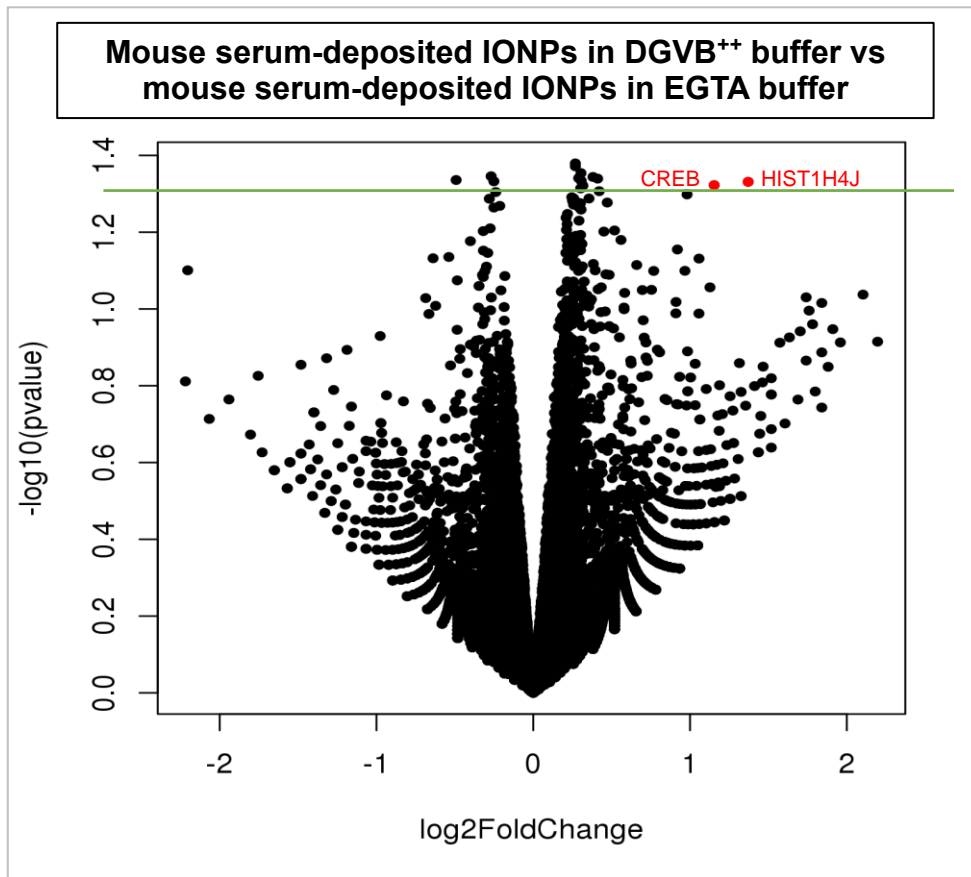


Figure 4.5. **Volcano plot showing global transcriptional change.** The graph shows all DEGs when the two mouse serum deposited IONPs samples were compared. Each data point in the scatter plot represents a gene. The left side of the graph shows downregulated genes and the right side of the graph shows upregulated genes. Of 13,136 DEGs, only two genes (denoted by red dots) were significantly upregulated ( $p$  value  $< 0.05$ ). The x-axis shows  $\log_2$  fold change of each gene and the y-axis shows the  $-\log_{10}$  of its p-value. Significant p-value was considered at  $p < 0.05$ , i.e. above 1.3 on the  $-\log_{10}$  scale, as denoted by green line on the plot.

The two samples compared had two DEGs upregulated ( $p < 0.05$ ) in the mouse serum deposited IONPs in EGTA buffer and no downregulated DEGs. The two genes identified were CREB5 and HIST1H4J - neither of which relate to immune system processes - are described below.

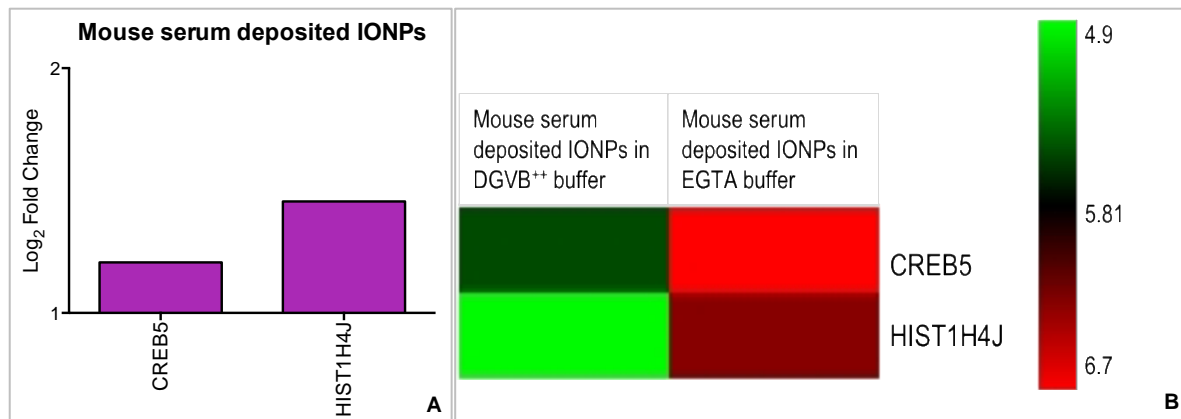


Figure 4.6. **Bar chart and heatmap showing significant DEGs.** Graph A shows the Log<sub>2</sub> fold change of expression for CREB5 and HIST1H4J. Graph B shows a heat map of the upregulation of the two significant DEGs, plotted using log<sub>2</sub> of expression values. The left column represents mouse serum deposited IONPs in DGVB<sup>++</sup> buffer and the right column represents the corresponding EGTA buffer sample. Mouse serum deposited IONPs in EGTA buffer show the most significant change for both genes.

CREB5 (cAMP responsive element binding protein 5) is a transcriptional factor and functions in cell cycle regulation, growth, proliferation and differentiation (He *et al.*, 2017). Overexpression of CREB5 by at least 2 fold has been identified in several types of cancers such as prostate cancer, ovarian cancer, colorectal cancer and hepatocellular carcinomas (Wang *et al.*, 2020, Zhang *et al.*, 2019). HIST1H4J encodes for a histone that is replication-dependent and is part of the histone H4 protein family (Tessadori *et al.*, 2020). Very little is known of the effects of HIST1H4J upregulation however, a recent study by Tessadori *et al.* (2020) showed that a variant of the HIST1H4J gene is related to the development of neurodevelopmental disorders and caused severe developmental defects in zebrafish embryos.

Gene name	Log <sub>2</sub> Fold Change
CREB5	1.15
HIST1H4J	1.37

Figure 4.7. **Table showing summary of genes discussed in this comparison.** The table lists the significant DEGs identified in this comparison and the log<sub>2</sub> fold change values.

## DGVB<sup>++</sup> buffer: Mouse serum deposited IONPs vs. 'naked' IONPs

To evaluate the effects of mouse serum proteins associated with classical pathway activation adsorbed to IONPs, mouse serum deposited IONPs in DGVB<sup>++</sup> buffer was compared against 'naked' IONPs in DGVB<sup>++</sup> buffer. The analysis showed some significant upregulated and downregulated genes, as discussed below.

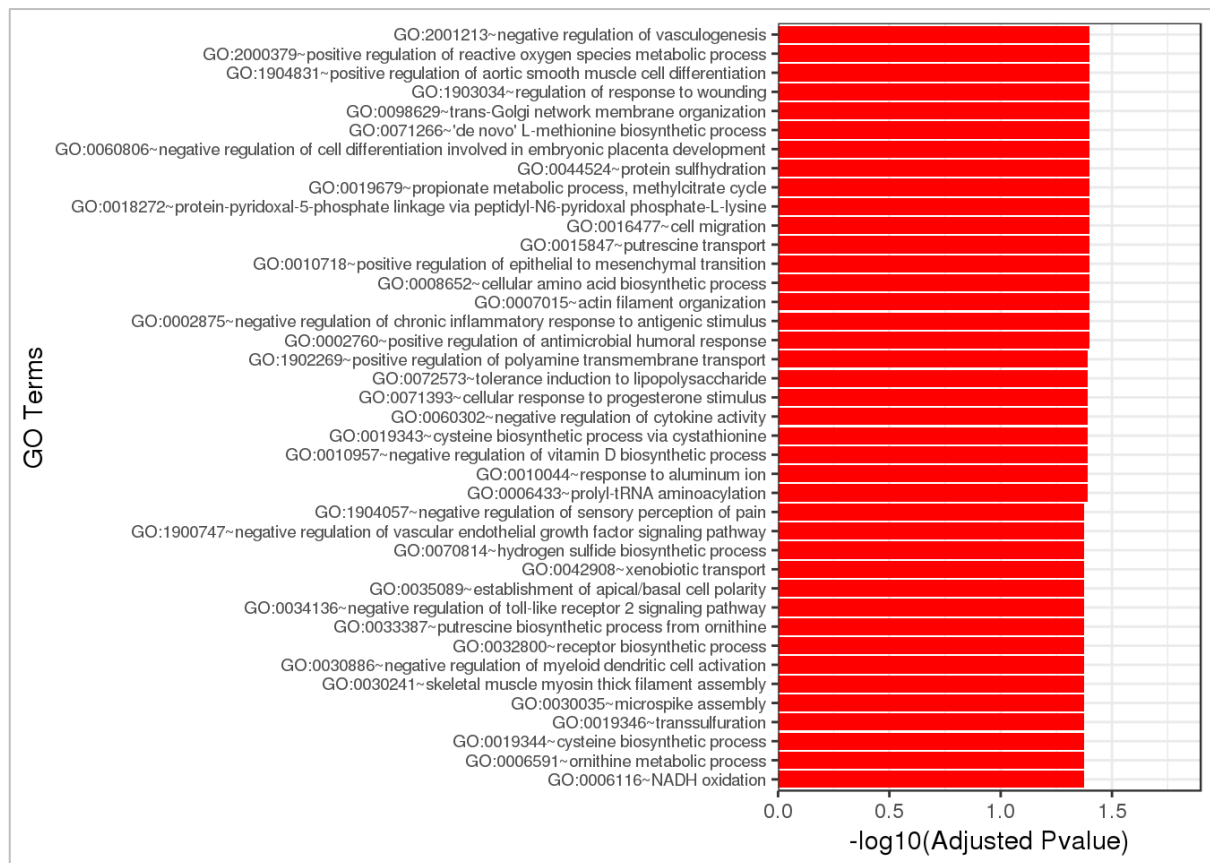


Figure 4.7. **Gene Ontology Analysis Overview.** Differentially expressed genes were clustered by their gene ontology and the enrichment of gene ontology terms was tested using Fisher exact test (GeneSCFv1.1-p2). The above figure shows gene ontology terms that are significantly enriched with an adjusted p-value ( $P < 0.05$ ) in the differentially expressed gene sets. Up to 40 GO terms are shown in the above figure.

The Gene Ontology analysis (figure 4.7) results revealed the several pathways where the significant DEGs in this comparison are involved in.

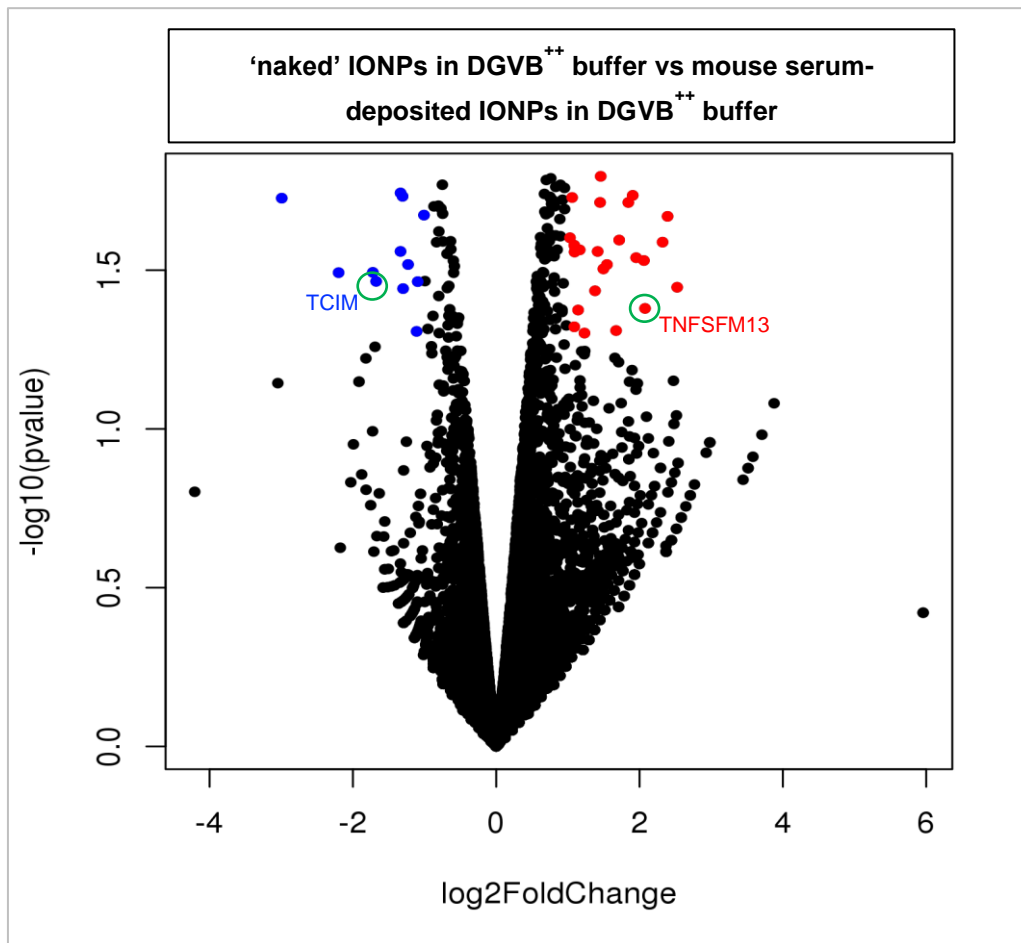


Figure 4.8. **Volcano plot showing global transcriptional change.** The graph shows all DEGs when mouse serum deposited sample was compared to the 'naked' IONPs in DGVB<sup>++</sup> buffer. Of 12,805 DEGs, 37 genes were significant (p value <0.05). The red dots on the right of the graph show genes that were significantly upregulated and the blue dots on the left show genes that were significantly downregulated. The x-axis shows log<sub>2</sub> fold change of each gene and the y-axis shows the -log<sub>10</sub> of its p-value. Significant p-value was considered at p<0.05, i.e. above 1.3 on the -log<sub>10</sub> scale. Of the genes identified relating to immune system processes discussed in the text, the most upregulated and downregulated genes are circled and labelled on the volcano plot.

Of the 37 significant DEGs, 25 genes were upregulated and 12 genes were downregulated (figure 4.8). Gene ontology enrichment analysis was carried out to identify the significant DEGs involved in immune system processes (chapter 2.11). 7 genes were found to be related to the immune system, 2 of which are downregulated and 5 are upregulated (figure 4.9).

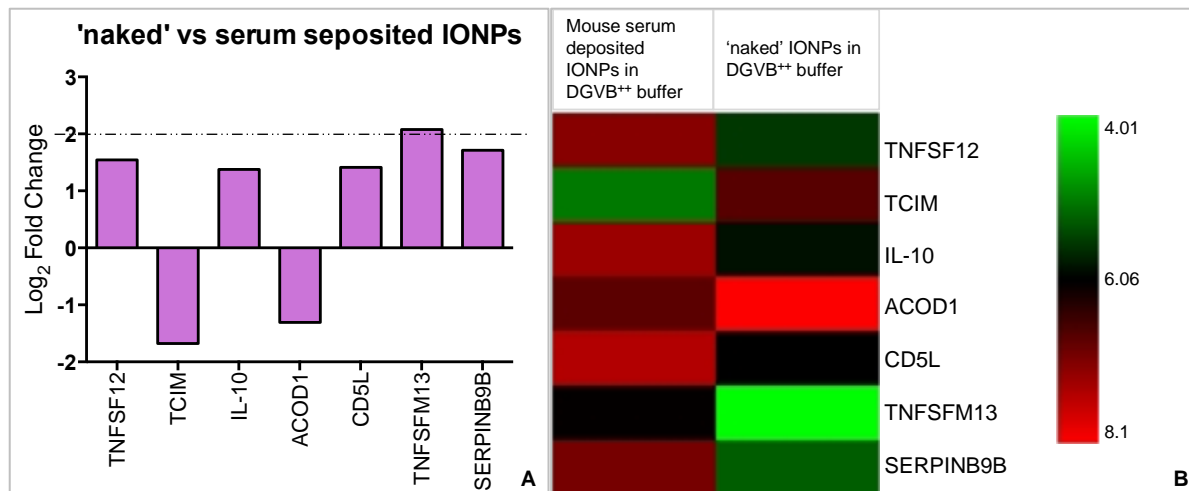


Figure 4.9. **Bar chart and heatmap showing significant DEGs.** Graph A shows the Log<sub>2</sub> fold change of expression for the significant DEGs. Graph B shows a heat map of the significant upregulated and downregulated DEGs, plotted using log<sub>2</sub> of expression values. The left column represents mouse serum deposited IONPs in DGVB<sup>++</sup> buffer sample and the right column represents the corresponding EGTA buffer sample. Mouse serum deposited IONPs in EGTA buffer show the highest number of upregulated genes. The dotted line represents the threshold value for fold change, where significant changes may occur within the cell. Heatmaps show which sample the gene was more upregulated in.

The data shows that TNFSF12, TNFSF13, IL-10, CD5L, and SERPINB9B are upregulated while TCIM and ACOD1 are downregulated in the serum deposited sample when compared to the 'naked' IONPs sample (figure 4.9).

TNFSF12 (tumour necrosis factor superfamily member 12) is one of the genes that encode for TRAIL (TNF-related apoptosis-inducing ligand) proteins, which upon activation induces caspase-8 activity, leading to receptor-induced cell death (Wan *et al.*, 2018). Hence, TNFSF12 signalling can have some pro-apoptotic effects, especially seen in tumour cell lines (Abend, Uldrick and Ziegelbauer, 2010). TNFSF12 signalling also plays a role in cell proliferation and migration, suggesting that it is involved in wound repair, angiogenesis and tumorigenesis (Abend, Uldrick and Ziegelbauer, 2010).

Another member of the same family, TNFSF13 (tumour necrosis factor superfamily member 13) has been shown to be involved in the progression of several types of cancers and may be involved in the development of tumours, as well as B cells (Qian

*et al.*, 2014). A study by Qian *et al.* (2014) found that TNFSF13 was overexpressed in some types of lung cancers, with the highest upregulation associated with adenocarcinomas. TNFSF13 overexpression was also found in colorectal adenocarcinoma fibroblasts (Petty *et al.*, 2009).

IL-10 (interleukin 10) is one of the most potent anti-inflammatory cytokines and plays an important role towards limiting the immune response upon exposure to pathogens. IL-10 prevents the production of cytokines, chemokines and costimulatory molecules, thus reducing host cell damage and autoimmune reactions (Iyer and Cheng, 2012). On the other hand, by suppressing immune system functions, IL-10 can contribute to the development of cancer as tumours have an increased chance of escaping immune surveillance (Wei, Wang and Li, 2020).

CD5L (CD5 molecule-like) is a glycoprotein, mainly secreted by macrophages, and when secreted is involved in inflammatory responses (Sanjurjo *et al.*, 2018). A study carried out by Sanjurjo *et al.* (2018) showed that CD5L is similar to IL-10 in the way that they both induce M2 macrophage polarisation. CD5L is regarded as an apoptosis inhibitor in macrophages and plays an important role in inflammation to maintain normal tissue homeostasis (Martinez *et al.*, 2014). Whilst this is an important process during inflammation, the occurrence of apoptosis is a crucial part of tumour protection and if this function is impaired, the progression of tumours is favoured (Silke and Meier, 2013).

SERPINB9B (serine protease inhibitor, clade B, member 9b) is one of the lesser studied serpin family member so far, however the serine protease inhibitor superfamily



is known to play a role in regulating immune system processes such as apoptosis, blood coagulation and complement activation (Kaiserman and Bird, 2010).

ACOD1 (Aconitate decarboxylase 1) also known as IRG1 (Immunoresponsive gene 1) is upregulated in macrophages during pro-inflammatory reactions, however its exact role and cellular mechanisms remain unexplored (Michelucci *et al.*, 2013, Wu *et al.*, 2020).

Gene name	Log <sub>2</sub> Fold Change
<b>TNFSF12</b>	1.55
<b>TCIM</b>	-1.68
<b>IL-10</b>	1.38
<b>ACOD1</b>	-1.31
<b>CD5L</b>	1.42
<b>TNFSFM13</b>	2.08
<b>SERPINB9B</b>	1.72

Figure 4.10. **Table showing summary of genes discussed in this comparison.** The table lists the significant DEGs identified in this comparison and the log<sub>2</sub> fold change values.

### [EGTA buffer: Mouse serum deposited IONPs vs. 'naked' IONPs](#)

Mouse serum deposited IONPs in EGTA buffer were compared against 'naked' IONPs in EGTA to evaluate the effect of mouse serum proteins associated with alternative pathway activation adsorbed on IONPs. The data showed hundreds of significant DEGs and gene ontology enrichment analysis was carried out to identify those relating to immune system process (figure 4.11).

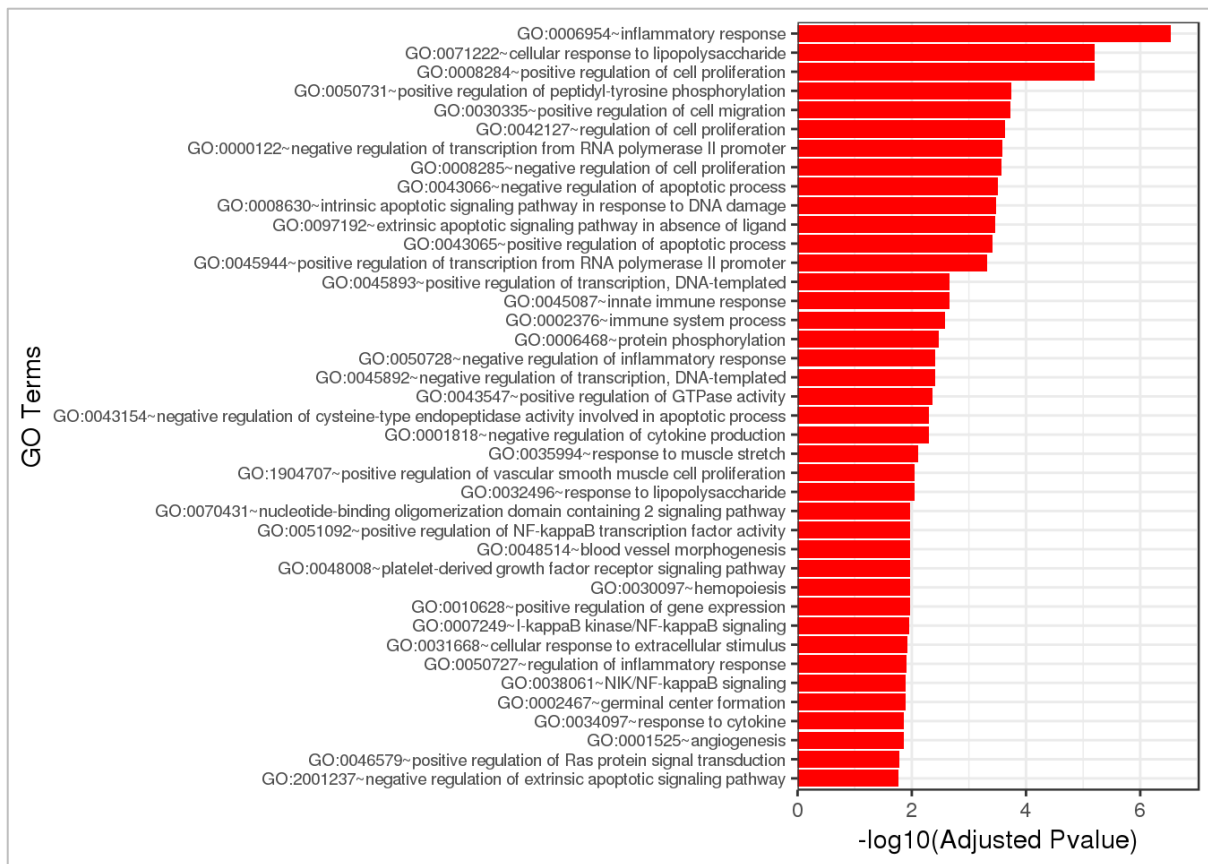


Figure 4.11. **Gene Ontology Analysis Overview.** Significantly differentially expressed genes were clustered by their gene ontology and the enrichment of gene ontology terms was tested using Fisher exact test (GeneSCFv1.1-p2). The above figure shows gene ontology terms that are significantly enriched with an adjusted p-value ( $P < 0.05$ ) in the differentially expressed gene sets. Up to 40 GO terms are shown in the above figure.

The Gene Ontology analysis results revealed several pathways where the significant DEGs in this comparison are involved in (figure 4.11). The most upregulated pathway was found to be ‘inflammatory response’, which means one of the conditions investigated here elicited a significant inflammatory response in the cells.

The graph below (figure 4.12) shows an overview of DEGs, including significantly upregulated and downregulated DEGs.

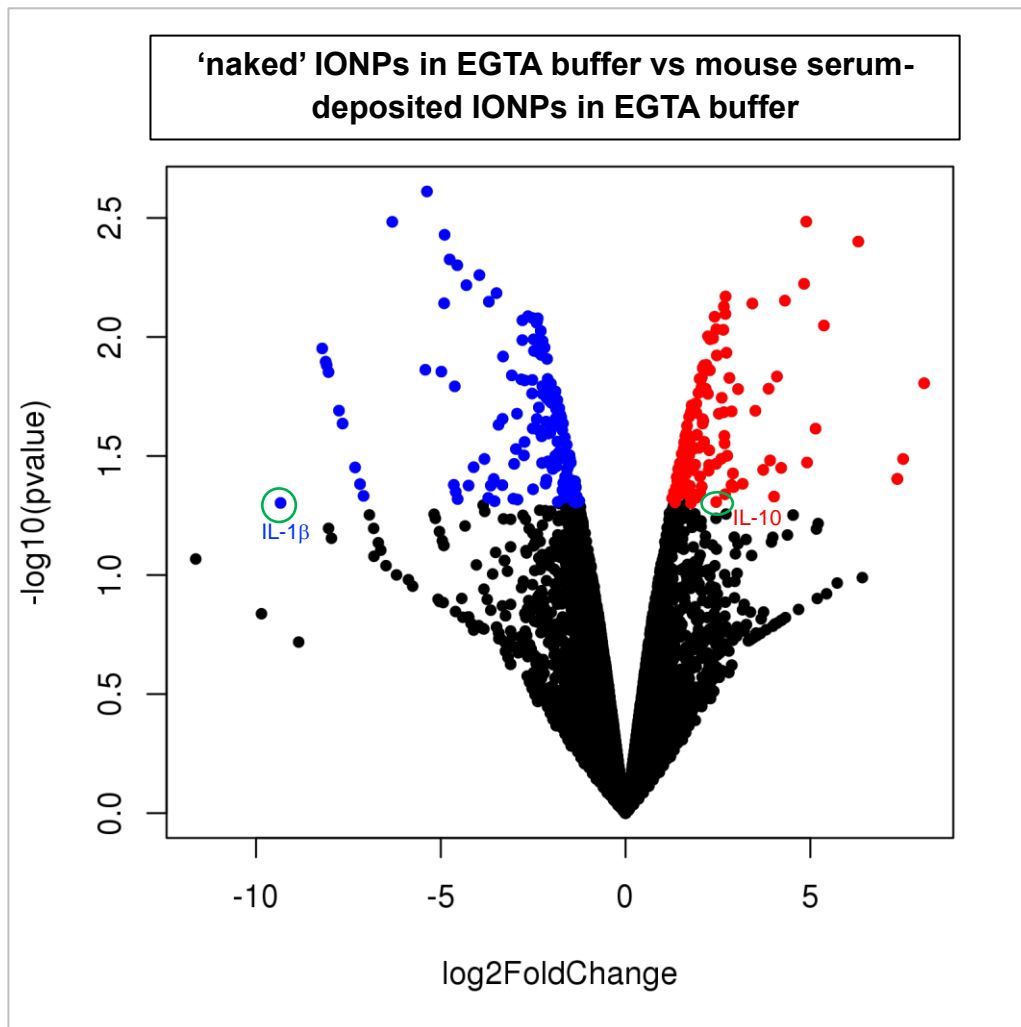


Figure 4.12. **Volcano plot showing global transcriptional change.** . The graph shows all DEGs when mouse serum deposited sample was compared to the 'naked' IONPs in EGTA buffer. Of 13,134 DEGs, 289 genes were significantly (p value <0.05) changed. The red dots on the right of the graph show genes that were significantly upregulated and the blue dots on the left show genes that were significantly downregulated. The x-axis shows log<sub>2</sub> fold change of each gene and the y-axis shows the -log<sub>10</sub> of its p-value. Significant p-value was considered at p<0.05, i.e. above 1.3 on the -log<sub>10</sub> scale. Of the selected genes relating to innate immune processes discussed in the text, the most upregulated and downregulated genes are circled and labelled on the volcano plot.

Of 289 significant DEGs, 159 genes were downregulated and 130 were upregulated (figure 4.12). Through gene ontology enrichment analysis, 75 DEGs were found to be related to immune system processes. Some of the genes which are related to cytokine

expression and inflammation reactions were selected and are discussed below (figure 4.13).

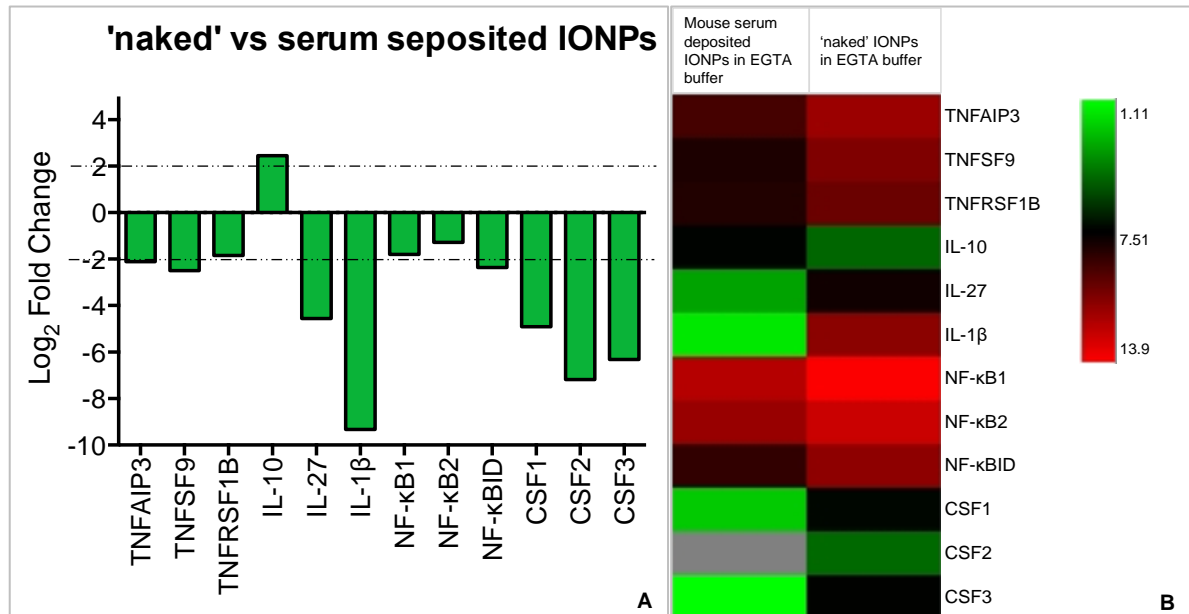


Figure 4.13. **Bar chart and heatmap showing significant DEGs.** Graph A shows the Log<sub>2</sub> fold change of expression for selected DEGs relating to immune system processes. Graph B shows a corresponding heat map of the significant upregulated and downregulated DEGs, plotted using log<sub>2</sub> of expression values. The left column represents mouse serum deposited IONPs in EGTA buffer and the right column represents 'naked' IONPs in EGTA buffer. Most of the genes were downregulated in the serum deposited sample when compared to the 'naked' IONPs sample, with the exception of IL-10 which was upregulated in the serum deposited sample. The dotted lines show the threshold value after which significant changes may occur within cells. Heatmaps show in which sample the gene was more upregulated. Grey blocks indicate no expression or low expression below the detection limit.

Most of the genes shown in graph 4.13, except IL-10, were significantly downregulated in the serum deposited IONPs in EGTA buffer when compared to 'naked' IONPs in EGTA buffer. IL-1β showed the highest change in expression levels among all significant DEGs and was downregulated 9.34 fold. As mentioned previously, IL-1β is a potent pro-inflammatory cytokine that plays a crucial role in the host's defence in response to injury and infections.

The TNFAIP3 gene codes for the protein A20, also known as tumour necrosis factor  $\alpha$ -induced protein 3 (TNFAIP3), which is an anti-inflammatory protein that closely regulates the activation of NF- $\kappa$ B during inflammation (Coornaert, Carpentier and Beyaert, 2009). The A20 protein is a negative regulator of NF- $\kappa$ B signalling and in fact a study carried out in mice showed that A20-deficient mice were unable to inhibit NF- $\kappa$ B activation, which resulted in severe inflammation (Lee *et al.*, 2000). NF- $\kappa$ B signalling is activated during inflammation reactions, which in turn regulates the expression of pro-inflammatory genes coding for cytokines and chemokines. As seen with other pro-inflammatory cytokines, overexpression of NF- $\kappa$ B can lead to autoimmune reactions (Lawrence, 2009). NF- $\kappa$ BID is a protein initially thought to be inhibiting NF- $\kappa$ B signalling, however is now reported to be able to both inhibit as well as promote NF- $\kappa$ B signalling depending on cell type (Schuster *et al.*, 2013).

TNFSF9 (tumour necrosis factor superfamily 9), also known as CD137L, is a ligand that is expressed by antigen presenting cells (APCs) and upon interaction with its receptor triggers a cell-mediated immune response, which causes pro-inflammatory cytokines to be secreted (Dharmadhikari *et al.*, 2016).

IL-27 is a cytokine secreted by APCs that has both pro-inflammatory and anti-inflammatory properties and forms part of the IL-6 and IL-12 cytokine family (Kourko *et al.*, 2019). Even though IL-27 is secreted when innate immunity is activated, it plays an important role in modulating the adaptive immune response, especially Th1 and Th2 responses (Fabbi, Carbotti and Ferrini, 2017). As pro-inflammatory cytokine, IL-27 can promote an efficient Th1 response by encouraging clonal expansion and proliferation of CD4<sup>+</sup> and CD8<sup>+</sup> T cells respectively (Fabbi, Carbotti and Ferrini, 2017).

Although these mechanisms are yet to be fully understood, as an anti-inflammatory cytokine, IL-27 inhibits the expression of an important Th2 transcription factor, thus suppressing Th2 immune responses (Villarino, Huang and Hunter, 2004, Kourko *et al.*, 2019).

CSF-1 (colony-stimulating factor 1), also known as M-CSF (macrophage CSF) is an important part of innate immunity and a growth factor which plays a key role in the proliferation, survival and differentiation of macrophages by binding to its receptor (Jones and Ricardo, 2013). CSF2 (granulocyte-macrophage colony-stimulating factor) and CSF3 (granulocyte colony-stimulating factor) are other growth factors also involved in the proliferation, differentiation and survival of immune cells, however CSF2 is for macrophages and neutrophils whereas CSF3 is only for granulocytes (He *et al.*, 2008). CSF2 and CSF3 can also promote inflammatory responses by triggering the secretion of pro-inflammatory cytokines (He *et al.*, 2008).

Gene name	Log <sub>2</sub> Fold Change
TNFAIP3	-2.11
TNFSF9	-2.49
TNFRSF1B	-1.85
IL-10	2.45
IL-27	-4.55
IL-1 $\beta$	-9.34
NF- $\kappa$ B1	-1.79
NF- $\kappa$ B2	-1.28
NF- $\kappa$ BID	-2.35
CSF1	-4.90
CSF2	-7.19
CSF3	-6.31

Figure 4.14. **Table showing summary of genes discussed in this comparison.** The table lists the significant DEGs identified in this comparison and the log<sub>2</sub> fold change values.

### 'naked' IONPS

The 'naked' IONPs in DGVB<sup>++</sup> buffer sample was compared to the 'naked' IONPs in EGTA buffer sample to look at the effects each of these pre-treatments - in the absence of serum proteins - could have on subsequent gene expression in macrophages. Hundreds of significant DEGs were identified and gene ontology enrichment analysis was performed to narrow down the genes relating to immune system processes (figure 4.15).

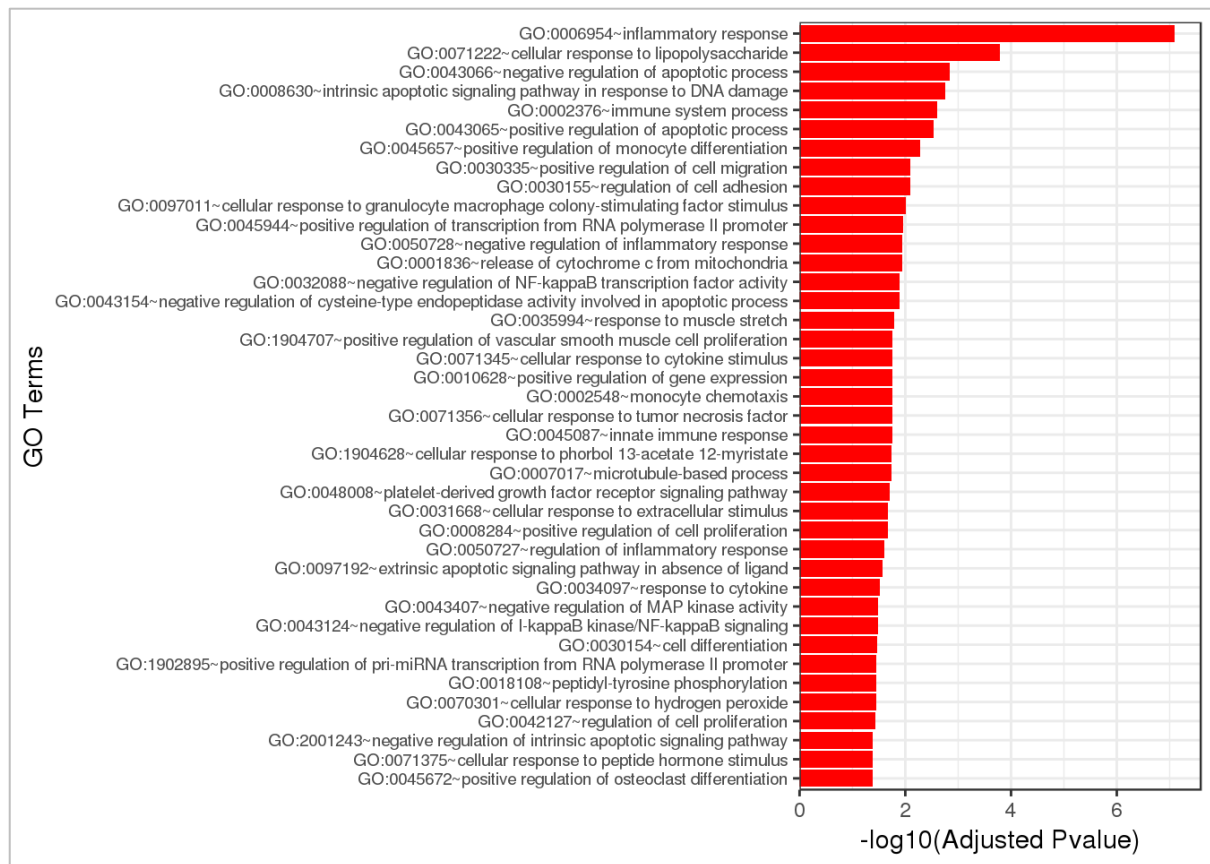


Figure 4.15. **Gene Ontology Analysis Overview.** Differentially expressed genes were clustered by their gene ontology and the enrichment of gene ontology terms was tested using Fisher exact test (GeneSCFv1.1-p2). The above figure shows gene ontology terms that are significantly enriched with an adjusted p-value ( $P < 0.05$ ) in the differentially expressed gene sets. Up to 40 GO terms are shown.

The Gene Ontology analysis results (figure 4.15) revealed a large number of pathways the significant DEGs in this comparison are involved in. The most upregulated pathway was found to be 'inflammatory response', which again means one of the conditions investigated here elicited a significant inflammatory response in the cells, the common factor being the use of EGTA buffer with 'naked' IONPs.



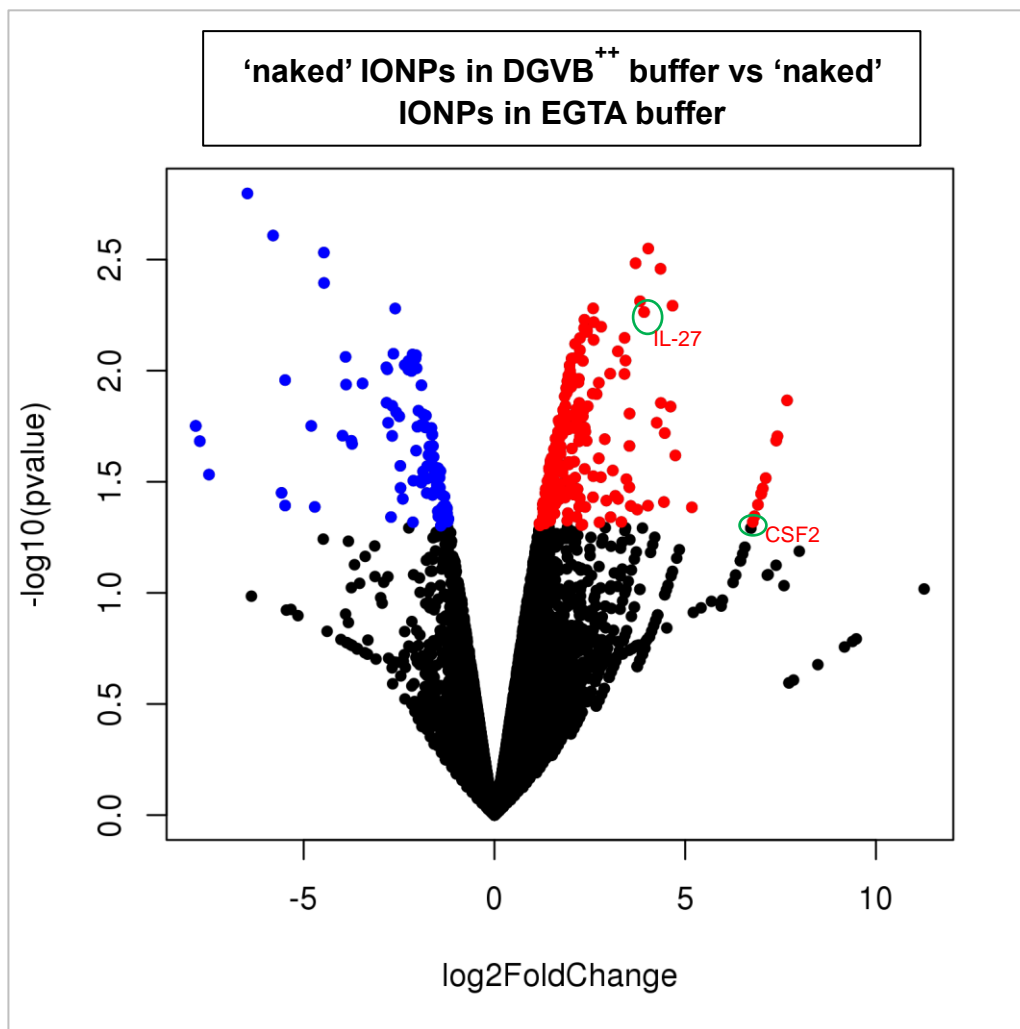


Figure 4.16. **Volcano plot showing global transcriptional change.** This graph shows all DEGs when the two 'naked' IONPs samples (DGVB<sup>++</sup> and EGTA buffer) were compared against each other. Of 12,785 DEGs, 320 genes were significant (p value <0.05). The red dots on the right of the graph show genes that were significantly upregulated and the blue dots on the left show genes that were significantly downregulated. The x-axis shows log<sub>2</sub> fold change of each gene and the y-axis shows the -log<sub>10</sub> of its p-value. Significant p-value was considered at p<0.05, i.e. above 1.3 on the -log<sub>10</sub> scale. Of the selected genes relating to innate immune processes discussed in the text, some genes are circled and labelled on the volcano plot.

From the graph (figure 4.16), it can be seen that there were more upregulated genes (220 genes) compared to downregulated genes (100 genes). Of 320 significant DEGs, 80 were identified to be related to immune system processes through GO enrichment analysis. A few genes related to the innate immune system and inflammation were selected and are discussed below.

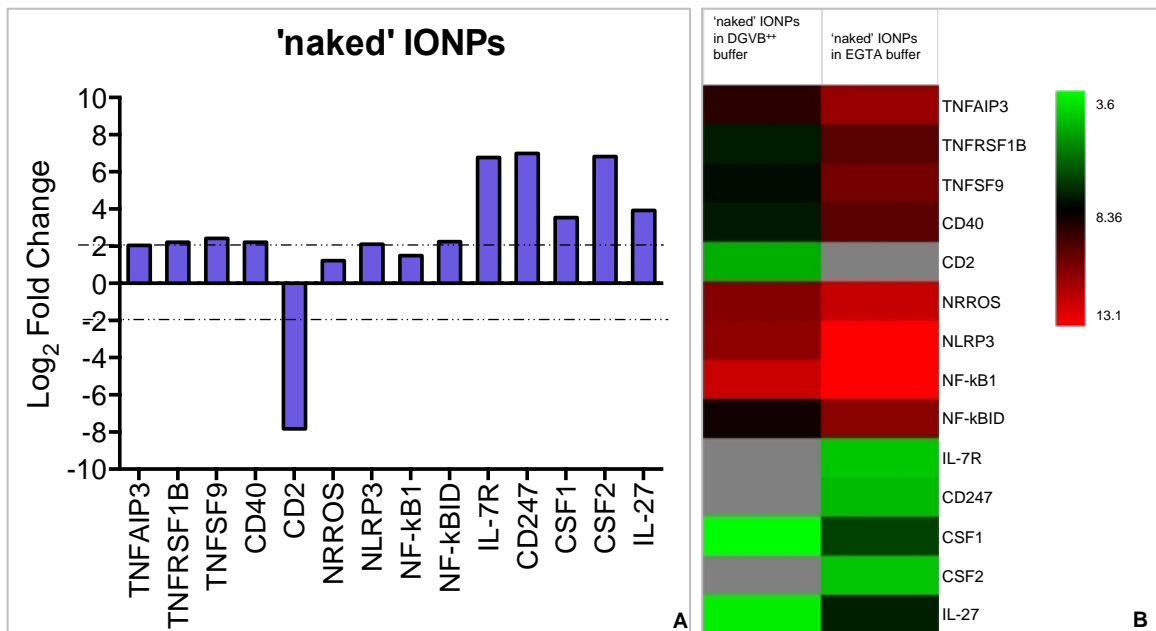


Figure 4.17. **Bar chart and heatmap showing significant DEGs.** Graph A shows the Log<sub>2</sub> fold change of expression for selected DEGs relating to immune system processes. Graph B shows a corresponding heat map of the significant upregulated and downregulated DEGs, plotted using log<sub>2</sub> of expression values. The left column represents 'naked' IONPs in DGVB<sup>++</sup> buffer and the right column represents 'naked' IONPs in EGTA buffer. The dotted lines show threshold values, following which significant changes may occur within cells. Heatmaps show in which sample the gene was more upregulated in. Grey blocks indicate no expression or expression below the detection limit.

From the above graphs (figure 4.17), it can be seen that most of the selected genes are significantly upregulated in the 'naked' IONPs in EGTA buffer when compared to 'naked' IONPs in DGVB<sup>++</sup> buffer. The downregulated gene in 'naked' IONPs in EGTA buffer sample is CD2 (T-cell surface antigen CD2). The CD2 gene codes for CD2 protein, a glycoprotein, which participates in a pathway important for T cell activation (Binder *et al.*, 2020, Altevogt, Michaelis and Kyewski, 1989).

A number of the genes upregulated in the presence of 'naked' IONPs in EGTA buffer (TNFAIP3, TNFSF9, TNFRSF1B, NLRP3, NF-κB1, NF-κBID, CSF1, CSF2, IL-27) have been described in the section above. This is an indication that a greater inflammatory response is triggered in the EGTA buffer since a few of the genes upregulated, such as TNFSF9, NLRP3, NF-κB1, CSF1 and CSF2 are activated during

and promote inflammation reactions. Upregulation of anti-inflammatory factors such as TNFAIP3, which encodes the A20 protein, a negative regulator of NF- $\kappa$ B, can also be seen, further indicating a balanced reaction between pro-inflammatory and anti-inflammatory responses.

CD40 gene encodes the protein CD40, belonging to the TNF superfamily, which is a receptor expressed on B cells and macrophages. Upon activation by its ligand (CD40L found on T cells) it is a mediator of adaptive immunity, particularly in T-cell immunity (Ara, Ahmed and Xiang, 2018). CD40 receptor engagement with its ligand can also trigger the expression of other TNF receptors and consequently can cause the activation of NF- $\kappa$ B signalling (Michel, Zirlik and Wolf, 2017).

NRROS (negative regulator of reactive oxygen species) reduces the amount of ROS (reactive oxygen species) secreted by phagocytes during inflammation reactions (Noubade *et al.*, 2014). Production of ROS by phagocytes is an important part of the host's immune response against pathogens, however unregulated production of ROS can be harmful and can lead to oxidative stress and autoimmune diseases (Di Dalmazi *et al.*, 2016). Through interactions with the latent TGF- $\beta$  complex, NRROS can also activate TGF- $\beta$ , a cytokine with both pro-inflammatory and anti-inflammatory properties (Smith *et al.*, 2020).

IL-7R (IL-7 receptor) is expressed by activated macrophages after activation of the innate immune system and its expression can also be activated by TNFs during an inflammatory reaction (Al-Mossawi *et al.*, 2019). IL-7R plays an important role in both the innate and adaptive arms of the immune system, particularly in the survival,

differentiation and development of T cells through propagating pro-inflammatory signalling of the IL-7 cytokine (Passtoors *et al.*, 2015).

CD247 forms part of the T-cell receptor complex and is important for optimal functions of T-cells during inflammation (Lundholm *et al.*, 2010). In fact, downregulation of the CD247 component of the receptor complex is known to be seen in patients with chronic inflammations caused by suppressed activity of the immune system (Eldor *et al.*, 2015).

Gene name	Log <sub>2</sub> Fold Change
TNFAIP3	2.04
TNFRSF1B	2.20
TNFSF9	2.42
CD40	2.21
CD2	-7.83
NRROS	1.23
NLRP3	2.11
NF-κB1	1.50
NF-κBID	2.24
IL-7R	6.77
CD247	6.99
CSF1	3.54
CSF2	6.82
IL-27	3.92

Figure 4.18. **Table showing summary of genes discussed in this comparison.** The table lists the significant DEGs identified in this comparison and the log<sub>2</sub> fold change values.

## Mouse serum deposited IONPs in DGVB<sup>++</sup> buffer vs. Control

To study the effects of mouse serum deposited IONPs in DGVB<sup>++</sup> buffer on gene expression, the sample was compared to a control sample where the cells were not exposed to any IONPs. This will give us a good indication of the inflammation response triggered when serum proteins associated with the classical pathway are adsorbed onto IONPs. The results for Gene Ontology analysis are shown in the graph below (figure 4.19).

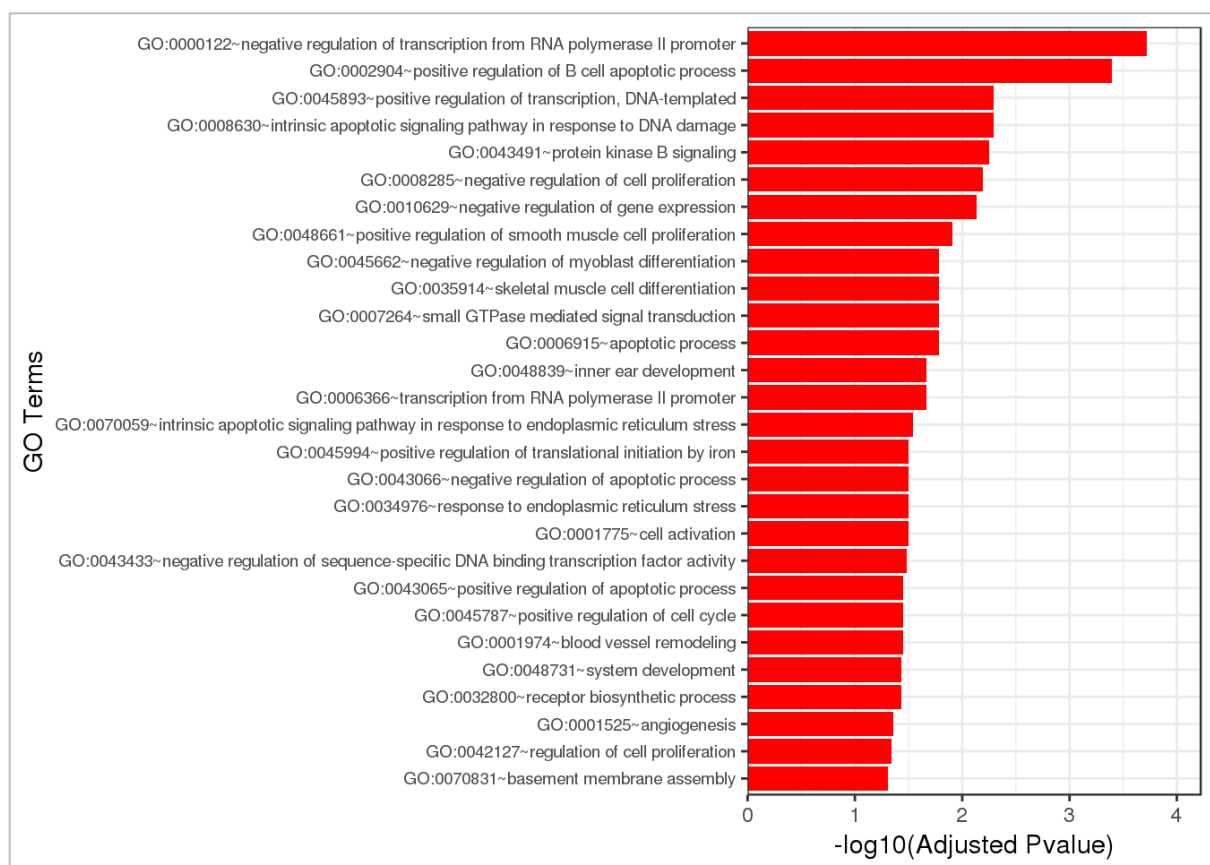


Figure 4.19. **Gene Ontology Analysis Overview.** Differentially expressed genes were clustered by their gene ontology and the enrichment of gene ontology terms was tested using Fisher exact test (GeneSCFv1.1-p2). The above figure shows gene ontology terms that are significantly enriched with an adjusted p-value ( $P < 0.05$ ) in the differentially expressed gene sets. Up to 40 GO terms are shown in the above figure.

The Gene Ontology analysis results revealed several pathways the significant DEGs in this comparison are involved in (figure 4.19).

An overview of DEGs are shown in the volcano plot below.

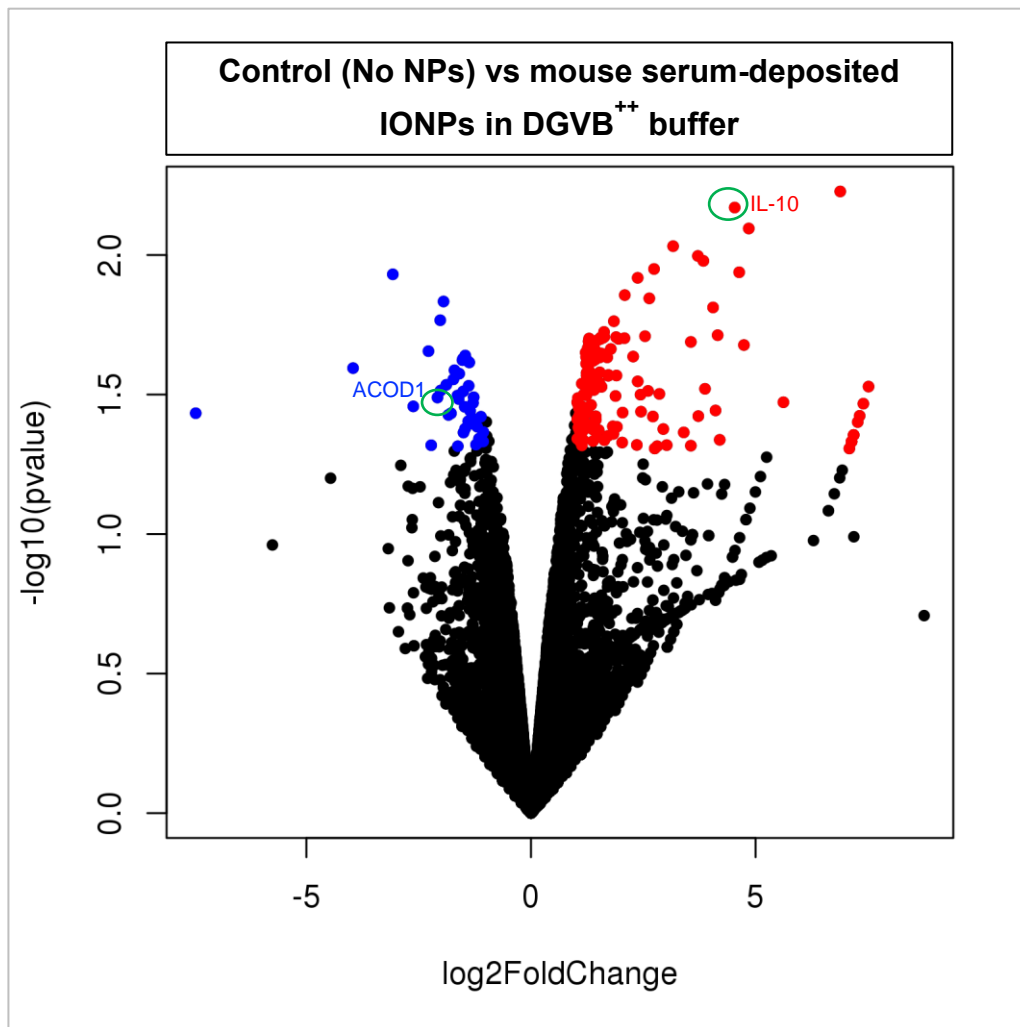


Figure 4.20. **Volcano plot showing global transcriptional change.** This graph shows all DEGs when the control (no IONPs) sample was compared against mouse serum deposited IONPs in DGVB<sup>++</sup> buffer. Of 13,119 DEGs, 188 genes were significant (p value <0.05). The red dots on the right of the graph show genes that were significantly upregulated and the blue dots on the left show genes that were significantly downregulated. The x-axis shows log<sub>2</sub> fold change of each gene and the y-axis shows the -log<sub>10</sub> of its p-value. Significant p-value was considered at p<0.05, i.e. above 1.3 on the -log<sub>10</sub> scale. Of the selected genes relating to innate immune processes discussed in the text, some genes are circled and labelled on the volcano plot.

From the volcano plot (figure 4.20), it can be clearly seen that the number of upregulated significant DEGs greatly outnumbers the number of downregulated DEGs. Of 188 significant DEGs, 43 genes were downregulated and 145 genes were upregulated. GO enrichment analysis was performed to identify genes relating to immune system processes and 32 genes were identified. Of those, genes that were

the most relevant to innate immune processes and inflammation reactions were selected and are shown in the graphs below (figure 4.21).

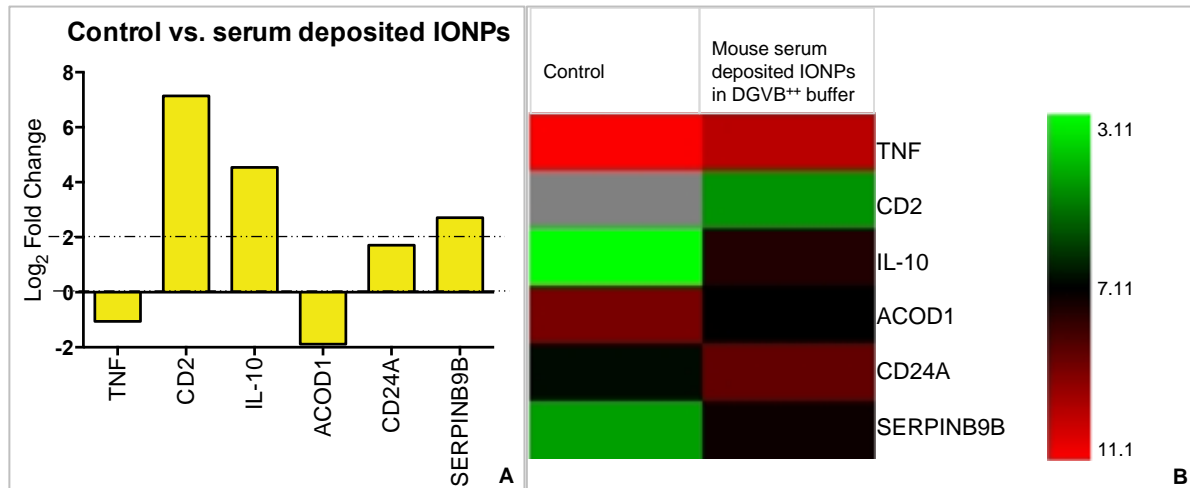


Figure 4.21. **Bar chart and heatmap showing significant DEGs.** Graph A shows the Log<sub>2</sub> fold change of expression for selected significant DEGs relating to immune system processes. Graph B shows a corresponding heat map of the significant upregulated and downregulated DEGs, plotted using log<sub>2</sub> of expression values. The left column represents the control (no IONPs) sample and the right column represents mouse serum deposited IONPs in DGVB<sup>++</sup> buffer. The dotted lines show the threshold value, following which significant changes may occur within cells. Heatmaps show in which sample the gene was more upregulated in. Grey blocks indicate no expression or expression below the detection limit.

The downregulated TNF gene seen in the graph above codes for an important pro-inflammatory cytokine (TNF- $\alpha$ ) which is crucial during an inflammatory response. ACOD1 expression, which is usually upregulated in macrophages during pro-inflammatory responses as discussed previously, is also downregulated in the mouse serum deposited sample. The two most upregulated genes are IL-10, an anti-inflammatory cytokine, and CD2 which is a T-cell surface antigen important in the activation of T cells, a key part of adaptive immunity. Of all 32 genes identified relating to immune system processes, CD2 showed the highest level of upregulation.

Gene name	Log <sub>2</sub> Fold Change
TNF	2.04
CD2	2.20
IL-10	2.42
ACOD1	2.21
CD24A	-7.83
SERPINB9B	1.23

Figure 4.22. **Table showing summary of genes discussed in this comparison.** The table lists the significant DEGs identified in this comparison and the log<sub>2</sub> fold change values.

### Mouse serum deposited IONPs in EGTA buffer vs. Control

The control sample (with no IONPs exposure) was compared to the mouse serum deposited IONPs in EGTA buffer to look at the effects of serum proteins associated with the alternative pathway adsorbed onto the IONPs. The results for Gene Ontology analysis are shown in the graph below (figure 4.23).



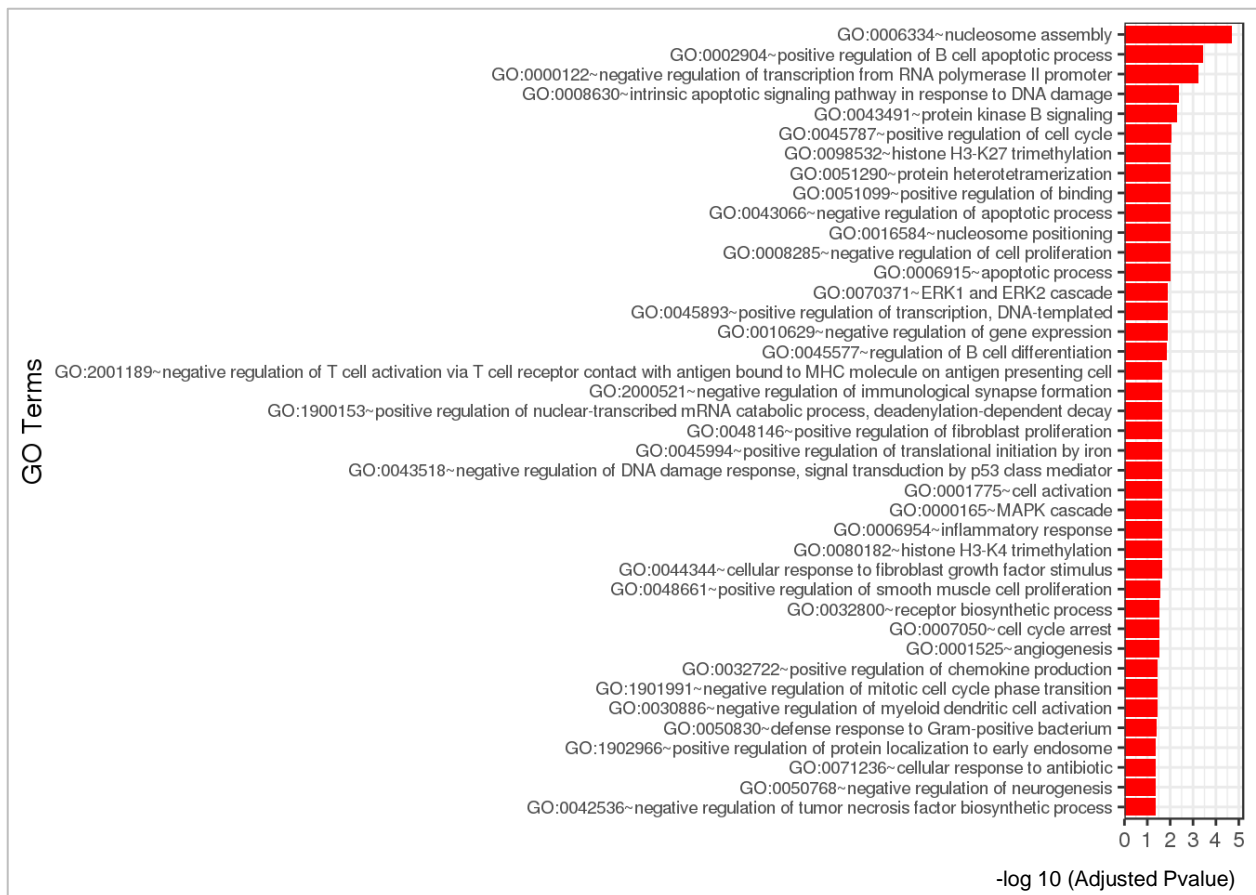


Figure 4.23. **Gene Ontology Analysis Overview.** Differentially expressed genes were clustered by their gene ontology and the enrichment of gene ontology terms was tested using Fisher exact test (GeneSCFv1.1-p2). The above figure shows gene ontology terms that are significantly enriched with an adjusted p-value ( $P < 0.05$ ) in the differentially expressed gene sets. Up to 40 GO terms are shown.

The volcano plot below shows an overview of all DEGs.

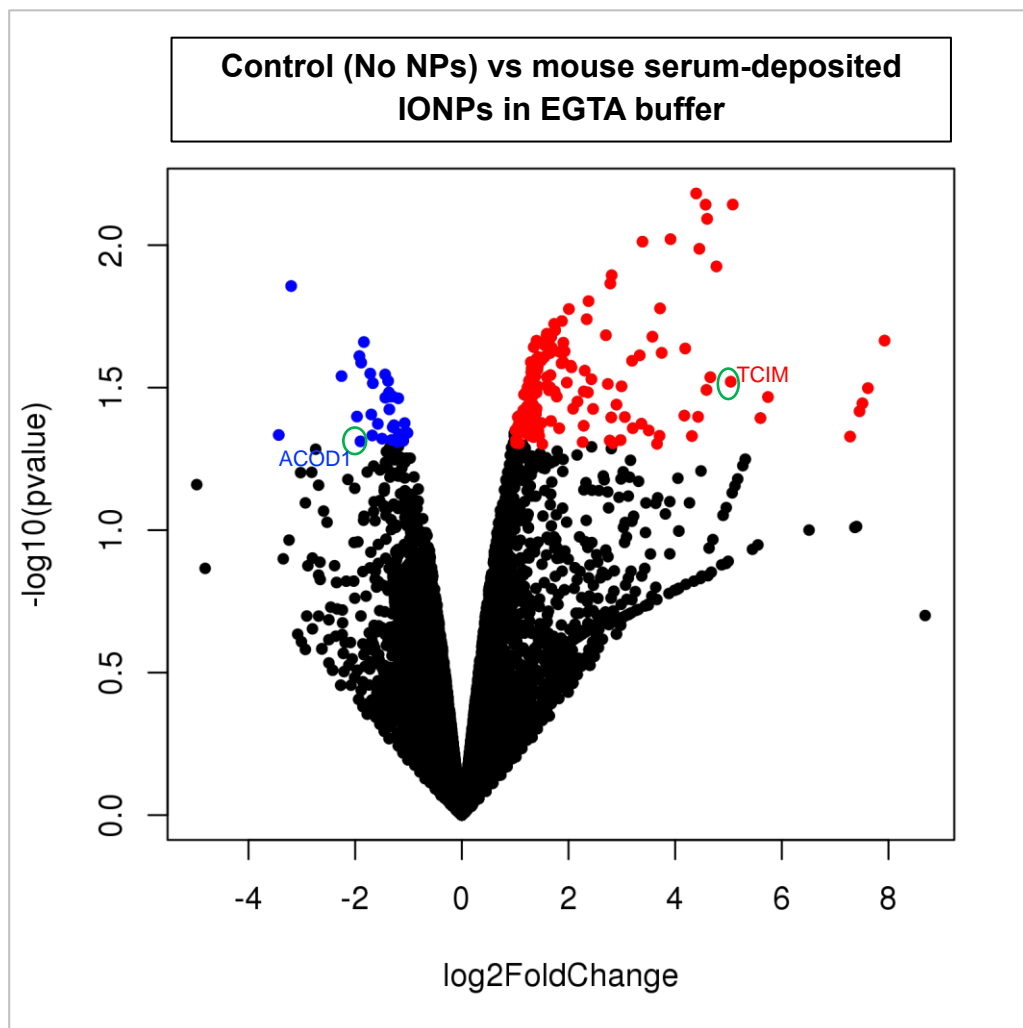


Figure 4.24. **Volcano plot showing global transcriptional change.** This graph shows all DEGs when the control (no IONPs) sample was compared against mouse serum deposited IONPs in EGTA buffer sample. Of 12,192 DEGs, 183 genes were significant ( $p$  value  $< 0.05$ ). The red dots on the right of the graph show genes that were significantly upregulated and the blue dots on the left show genes that were significantly downregulated. The x-axis shows  $\log_2$  fold change of each gene and the y-axis shows the  $-\log_{10}$  of its  $p$ -value. Significant  $p$ -value was considered at  $p < 0.05$ , i.e. above 1.3 on the  $-\log_{10}$  scale. Of the selected genes relating to innate immune processes discussed in the text, some genes are circled and labelled on the volcano plot.

The above volcano plot (figure 4.24) shows that there were many more upregulated genes than downregulated genes when the two samples were compared. Of 183 significant DEGs, 152 were upregulated whereas 31 genes were downregulated. Gene ontology enrichment analysis was carried out with the significant DEGs to

identify those that relate to immune system processes. 36 genes were identified and those that were the most relevant to innate immune response and inflammation were selected and are discussed further below (figure 4.25).

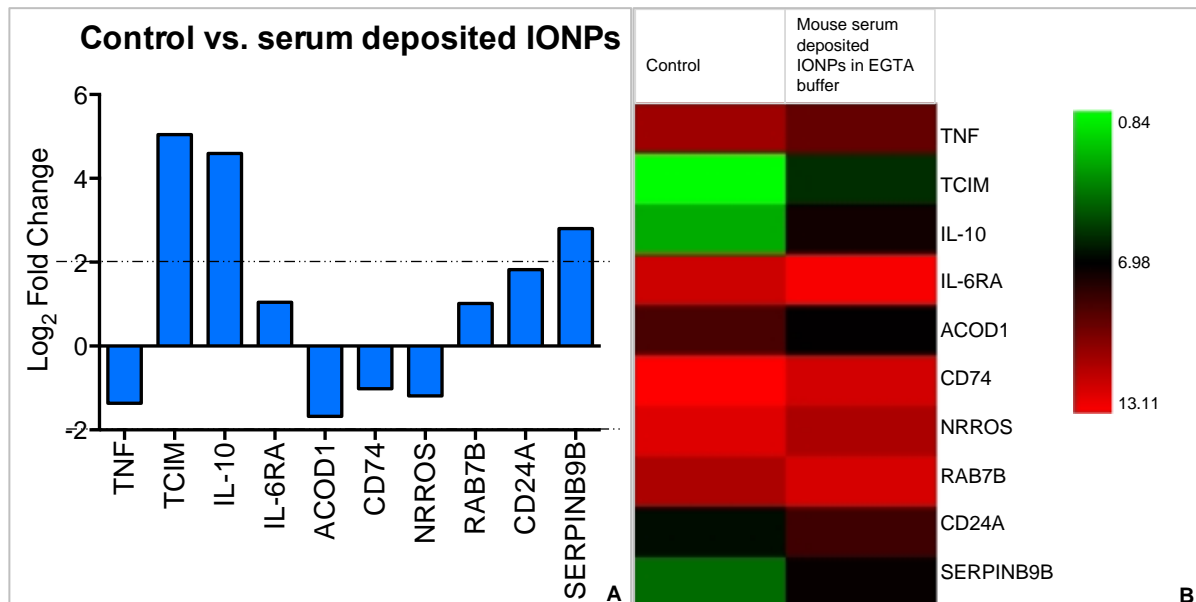


Figure 4.25. **Bar chart and heatmap showing significant DEGs.** Graph A shows the Log<sub>2</sub> fold change of expression for selected significant DEGs relating to immune system processes. Graph B shows a corresponding heat map of the significant upregulated and downregulated DEGs, plotted using log<sub>2</sub> of expression values. The left column represents the control (no IONPs) sample and the right column represents mouse serum deposited IONPs in EGTA buffer. The dotted lines show the threshold value, following which significant changes may occur within the cell. Heatmaps show which sample the gene was more upregulated in.

A few common patterns are seen with serum deposited IONPs in EGTA buffer and serum deposited IONPs in DGVB<sup>++</sup> buffer (figures 4.25 and 4.21) where pro-inflammatory related genes such as TNF and ACOD1 are downregulated and the anti-inflammatory cytokine IL-10 is upregulated. NRROS and CD74 are also downregulated in serum deposited IONPs in EGTA buffer compared to the control sample. NRROS, as described earlier, is a negative regulator of ROS production, thus regulating oxidative damage in cells. CD74 gene codes for the transmembrane protein CD74 that is important during antigen processing and presentation by chaperoning MHC class II molecules onto the surface of APCs (Schröder, 2016). Some studies

have also shown that CD74, through a series of binding and formation of complexes, is able to activate NF- $\kappa$ B signalling (Gil-Yarom *et al.*, 2017).

Amongst the upregulated genes are TCIM, IL-10, IL-6RA, RAB7B, CD24A and SERPINB9B, some of which have already been described previously. Of all 36 genes identified relating to immune system processes, TCIM (Transcriptional and Immune Response Regulator) showed the highest level of upregulation (5 fold) in the serum deposited sample compare to untreated cells. TCIM is associated with Wnt/b-catenin signalling and plays a role in the proliferation of tumour cells. Overexpression of TCIM was shown to suppress the cytotoxic function of intratumoral CD8<sup>+</sup> T cells (Tsukumo and Yasutomo, 2018; Dai *et al.*, 2017).

IL-6R $\alpha$  (IL-6 receptor  $\alpha$ -subunit) is an IL-6 receptor. IL-6 is an important cytokine which plays a role in various functions such as inflammation and immune responses. Aberrant IL-6 expression can give rise to inflammatory diseases and autoimmune diseases (Su, Lei and Zhang, 2017).

The Rab superfamily of proteins are crucial players of intracellular trafficking, as described in chapter 3. Rab7b expression is upregulated in activated monocytes following exposure to LPS (lipopolysaccharide) (Bucci, Bakke and Progida, 2010). Rab7b is part of the Rab GTPase protein family and acts in a similar manner to Rab7. It is thus important for lysosomes function as well as during the trafficking of receptors from late endosomes to the trans-Golgi network (Progida *et al.*, 2010).

Gene name	Log <sub>2</sub> Fold Change
TNF	-1.37
TCIM	5.04
IL-10	4.60
IL-6RA	1.04
ACOD1	-1.68
CD74	-1.02
NRROS	-1.19
RAB7B	1.02
CD24A	1.83
SERPINB9B	2.80

Figure 4.26. **Table showing summary of genes discussed in this comparison.** The table lists the significant DEGs identified in this comparison and the log<sub>2</sub> fold change values.

### 'naked' IONPs in DGVB<sup>++</sup> buffer vs. Control

To look at the effects of IONPs incubated in two different buffers, first the 'naked' IONPs in DGVB<sup>++</sup> buffer sample was compared to the control sample (from cells not exposed to IONPs). The results from Gene Ontology analysis are displayed in the graph below (figure 4.27).

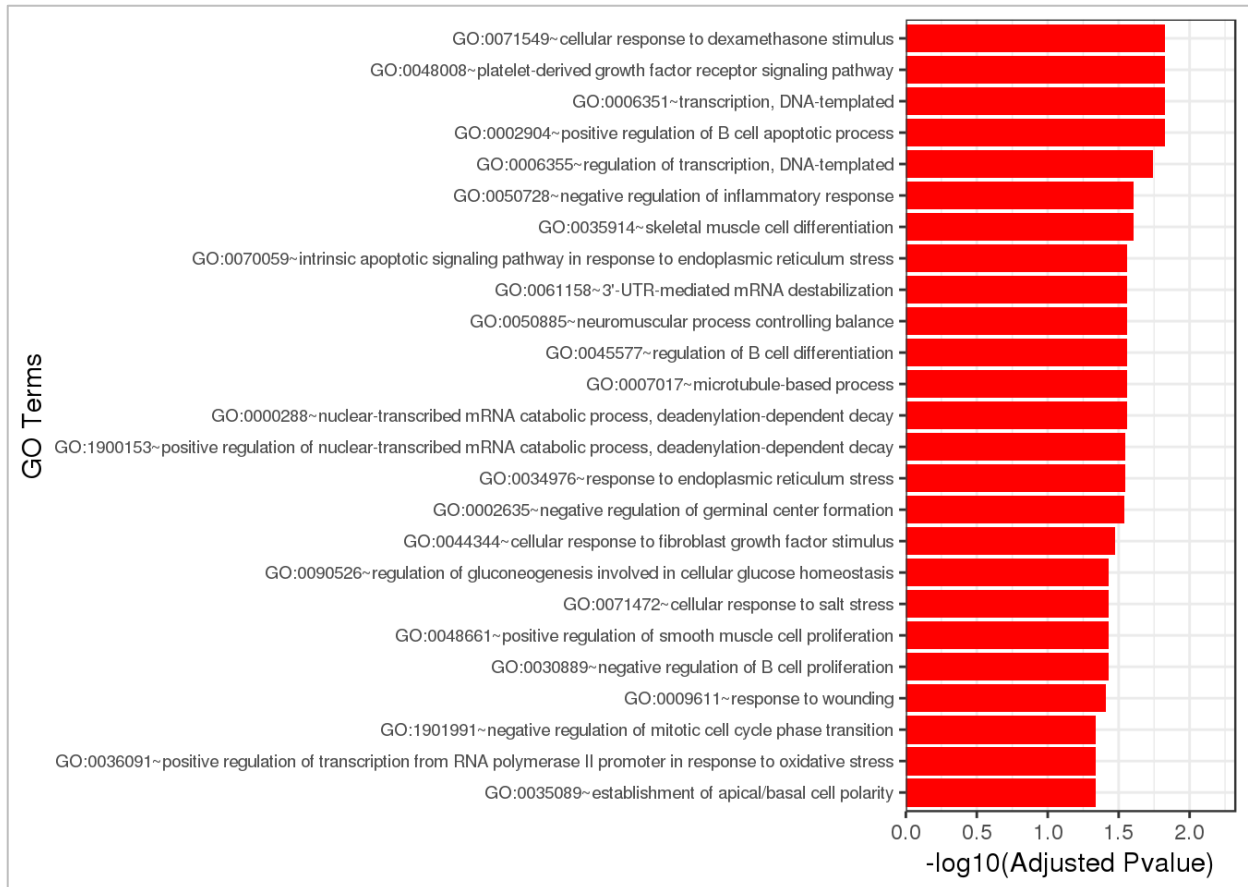


Figure 4.27. **Gene Ontology Analysis Overview.** Significantly differentially expressed genes were clustered by their gene ontology and the enrichment of gene ontology terms was tested using Fisher exact test (GeneSCFv1.1-p2). The above figure shows gene ontology terms that are significantly enriched with an adjusted p-value ( $P < 0.05$ ) in the differentially expressed gene sets. Up to 40 GO terms are shown in the above figure.

An overview of all the DEGs are represented in the volcano plot below.

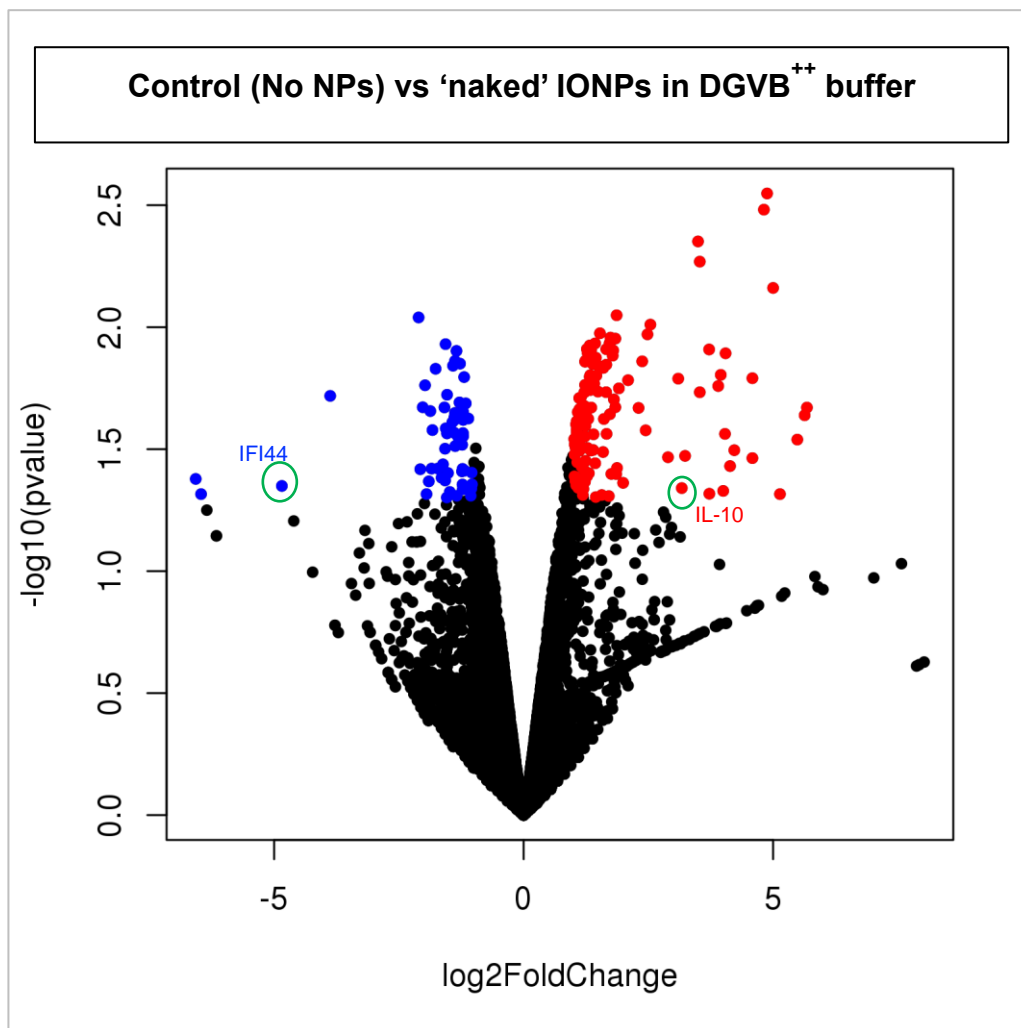


Figure 4.28. **Volcano plot showing global transcriptional change.** This graph shows all DEGs when the control (no IONPs) sample was compared against 'naked' IONPs in DGVB<sup>++</sup> buffer sample. Of 12,567 DEGs, 188 genes were significant (p value <0.05). The red dots on the right of the graph show genes that were significantly upregulated and the blue dots on the left show genes that were significantly downregulated. The x-axis shows log<sub>2</sub> fold change of each gene and the y-axis shows the -log<sub>10</sub> of its p-value. Significant p-value was considered at p<0.05, i.e. above 1.3 on the -log<sub>10</sub> scale. Of the selected genes relating to innate immune processes discussed in the text, some genes are circled and labelled on the volcano plot.

From the volcano plot (figure 4.28), it can be seen that there were more upregulated than downregulated significant DEGs when the 'naked' IONPs sample was compared to the control sample. Of 188 significant DEGs, 130 genes were upregulated and 58 genes were downregulated. Gene ontology enrichment analysis was performed to

identify the list of genes related to immune system processes and 27 genes were identified, some of which are described below (figure 4.29).

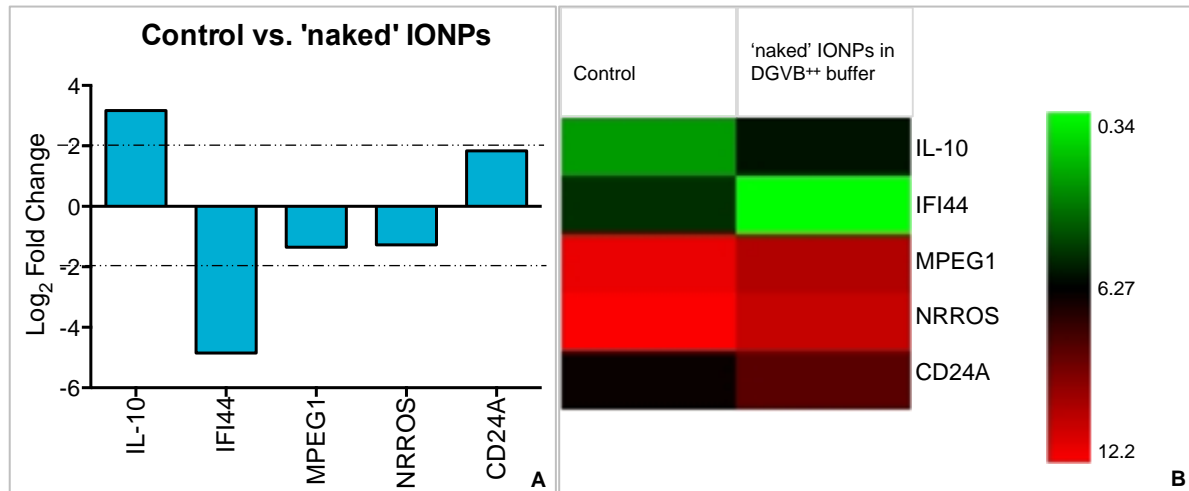


Figure 4.29. **Bar chart and heatmap showing significant DEGs.** Graph A shows the Log<sub>2</sub> fold change of expression for selected significant DEGs relating to immune system processes. Graph B shows a corresponding heat map of the significant upregulated and downregulated DEGs, plotted using log<sub>2</sub> of expression values. The dotted lines show the threshold value, following which significant changes may occur within the cell. The left column represents the control (no IONPs) sample and the right column represents 'naked' IONPs in DGVB<sup>++</sup> buffer. Heatmaps show in which sample the gene was more upregulated in.

Two upregulated genes in the graph (figure 4.29) are the anti-inflammatory cytokine IL-10 and CD24A, also known as CD24, which acts as signal transducer. CD24 suppresses the immune response during inflammatory reactions by interacting with proteins (Siglec-10) on innate immune cells, which inhibits signalling cascades leading to decreased engulfment of foreign and unwanted material by macrophages (Barkal *et al.*, 2019). Whilst this can be an effective protective mechanism against cell damage, it can be exploited by cancer cells as a way to evade immune surveillance.

Amongst the downregulated genes are IFI44, MPEG1 and NRROS, the latter of which has been described previously as a negative regulator of ROS. IFI44 (Interferon-induced protein 44) has the ability to negatively regulate IFN responses during innate



immune activation, particularly during antiviral responses, which plays an important role in protecting against host damage and autoimmune diseases (DeDiego *et al.*, 2019). MPEG1 (macrophage-expressed gene 1) encodes a protein important for macrophages to protect the host against pathogens, particularly during intracellular defence against bacteria (McCormack *et al.*, 2015). Downregulation of MPEG1 can be favourable for the growth and survival of pathogenic bacteria.

Gene name	Log <sub>2</sub> Fold Change
IL-10	3.17
IFI44	-4.85
MPEG1	-1.35
NRROS	-1.27
CD24A	1.84

Figure 4.30. **Table showing summary of genes discussed in this comparison.** The table lists the significant DEGs identified in this comparison and the log<sub>2</sub> fold change values.

### [‘naked’ IONPs in EGTA buffer vs. Control](#)

The final comparison was to look at the effects of ‘naked’ IONPs in EGTA buffer compared to the control sample (no exposure to IONPs). The results of the Gene Ontology analysis is shown below (figure 4.31).

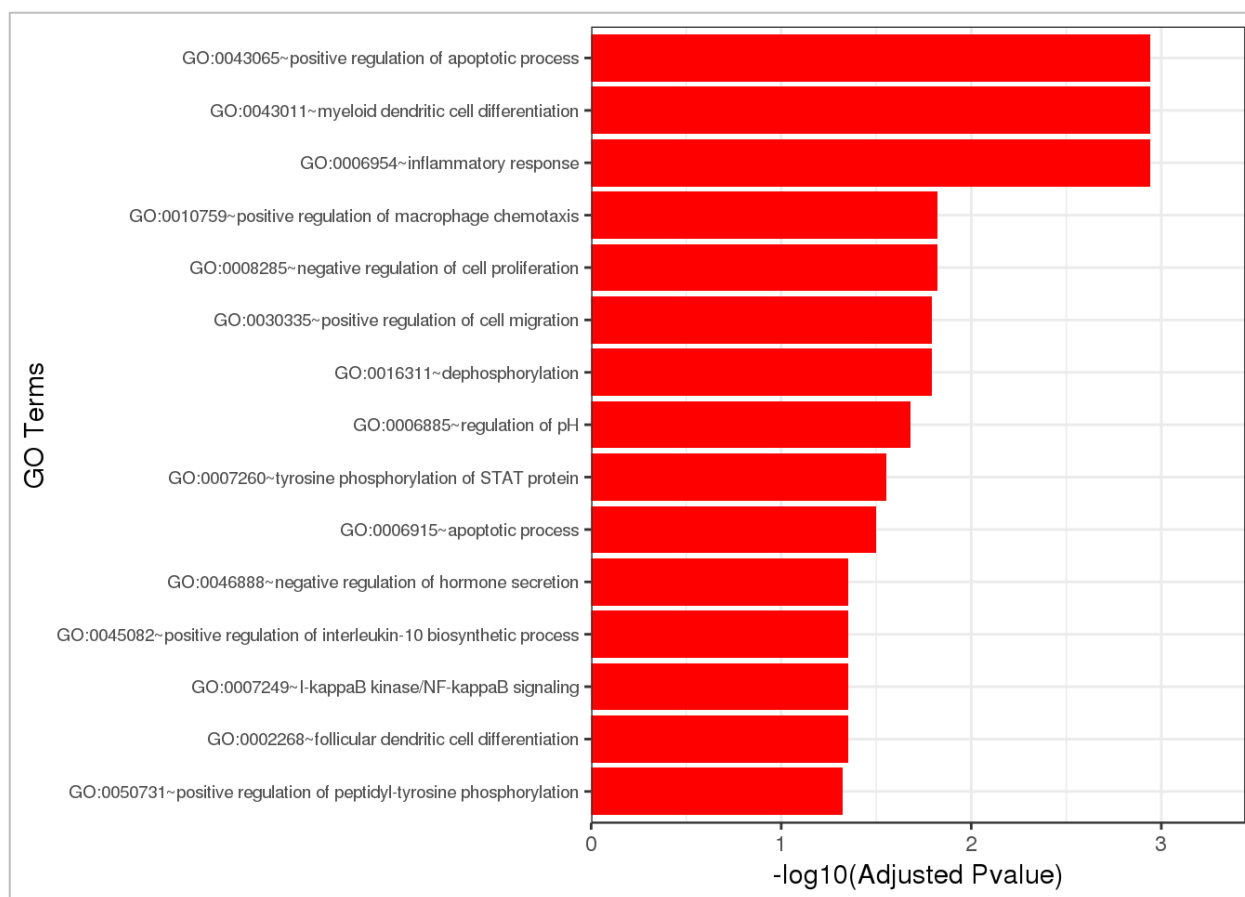


Figure 4.31. **Gene Ontology Analysis Overview.** Differentially expressed genes were clustered by their gene ontology and the enrichment of gene ontology terms was tested using Fisher exact test (GeneSCFv1.1-p2). The above figure shows gene ontology terms that are significantly enriched with an adjusted p-value ( $P < 0.05$ ) in the differentially expressed gene sets.

The Gene Ontology analysis results (figure 4.31) show ‘inflammatory responses’ as the third highest term/pathway suggesting that the presence of EGTA buffer triggers a higher inflammatory response in the mouse macrophages as this is also seen when the two ‘naked’ samples were compared (Figure 4.15). Furthermore, preliminary studies carried out by members of our lab showed that the IONPs, which have a starch coating on the surface, activated complement more via the alternative pathway than the classical pathway (figure 4.32).

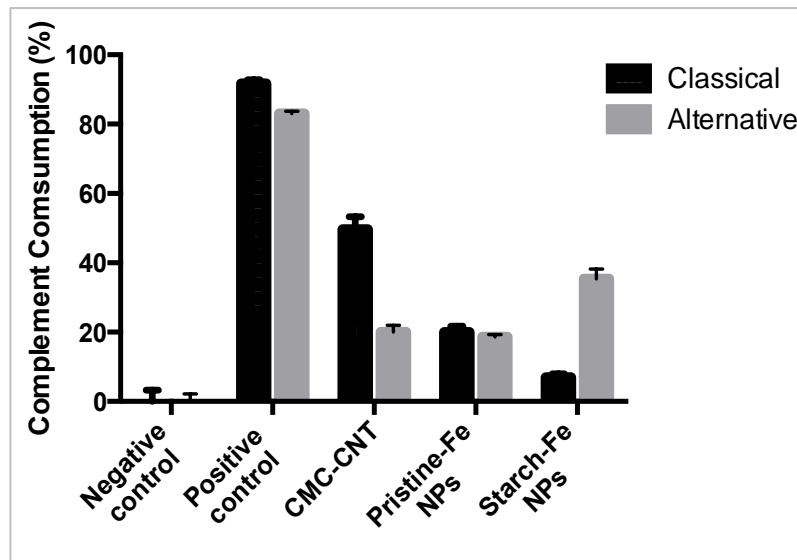


Figure 4.32. **Activation of the classical and alternative pathways with different nanoparticles.** Human serum was incubated with E cells overnight at 4°C. The serum was then separated from the E cells via centrifugation. The absorbed serum that was obtained was diluted in DGVB<sup>++</sup> buffer in the ratio of 1:1. The serum was then incubated with carbon nanotubes, iron nanoparticles (Pristine) and Zymosan for 1 hour at 37°C. The serum was spun down at maximum speed for 10 minutes and the supernatant was collected. 200µl of serum was inoculated in a 94 well plate and was serial diluted with 100µl of DVGB buffer in the other wells up to the dilution of 1:4096. Complete lysis (100%) was carried out in neat serum. The graph shows that starch coated iron oxide nanoparticles activate the alternative pathway more than the classical pathway. Experiment carried out by another lab member, Basudev Paudyal.

These results show that the IONPs studied here are potent activators of the alternative pathway of the complement system (figure 4.32).

To compare 'naked' IONPs in EGTA vs. control cells, an overview of all DEGs are represented in the volcano plot below (figure 4.33).

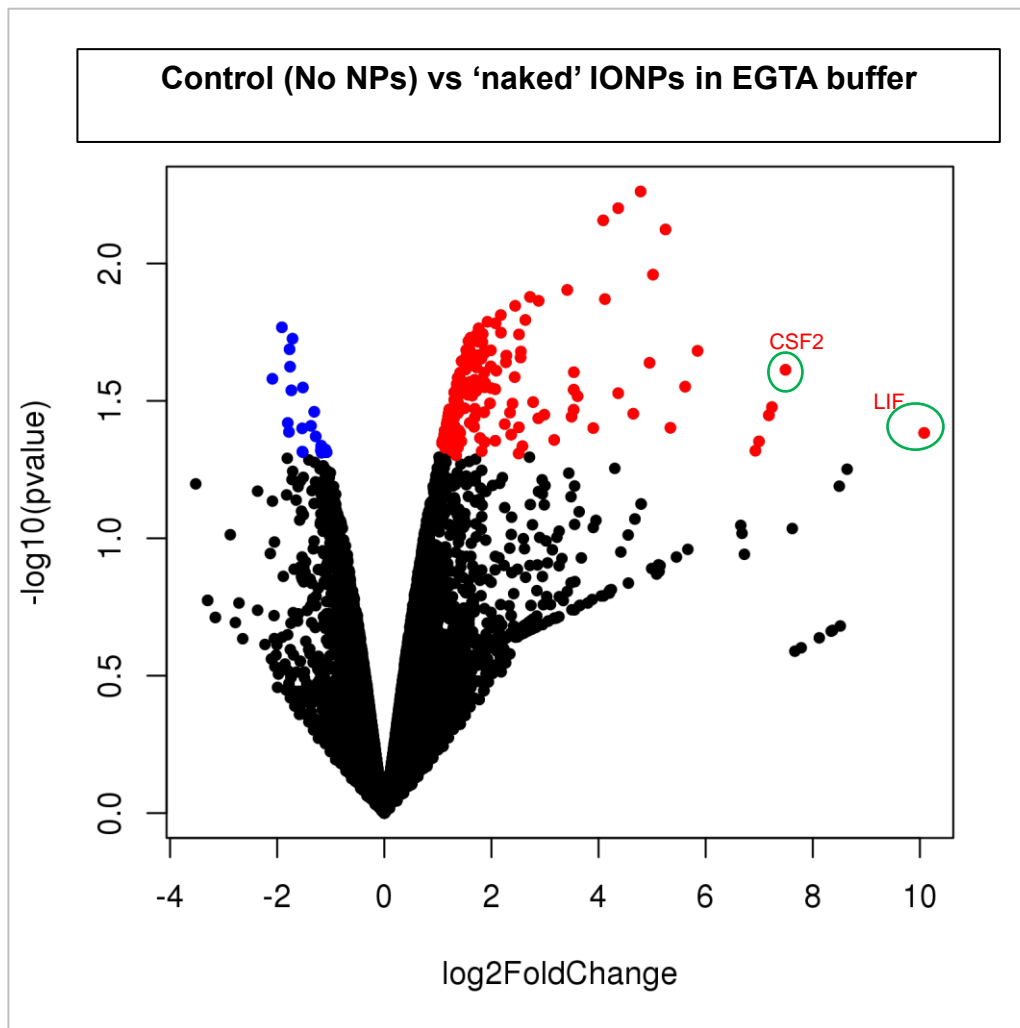


Figure 4.33. **Volcano plot showing global transcriptional change.** This graph shows all DEGs when the control (no IONPs) sample was compared against 'naked' IONPs in EGTA buffer sample. Of 13,114 DEGs, 201 genes were significant (p value <0.05). The red dots on the right of the graph show genes that were significantly upregulated and the blue dots on the left show genes that were significantly downregulated. The x-axis shows  $\log_2$  fold change of each gene and the y-axis shows the  $-\log_{10}$  of its p-value. Significant p-value was considered at  $p < 0.05$ , i.e. above 1.3 on the  $-\log_{10}$  scale. Of the selected genes relating to innate immune processes discussed in the text, some genes are circled and labelled on the volcano plot.

The volcano plot above shows that similar to some previous trends, the upregulated genes vastly outnumber the downregulated genes in the 'naked' IONPs sample compared to the control sample (figure 4.33). Of 201 significant DEGs, 21 genes were downregulated whereas 180 genes were upregulated. Gene ontology enrichment analysis was performed to identify the genes relating to immune system processes and 52 genes were identified, some of which are discussed below (figure 4.34). Of

note, the number of significant DEGs relating to immune system processes in this case is almost double compared to the 'naked' IONPs in DGVB<sup>++</sup> buffer seen in the previous section.

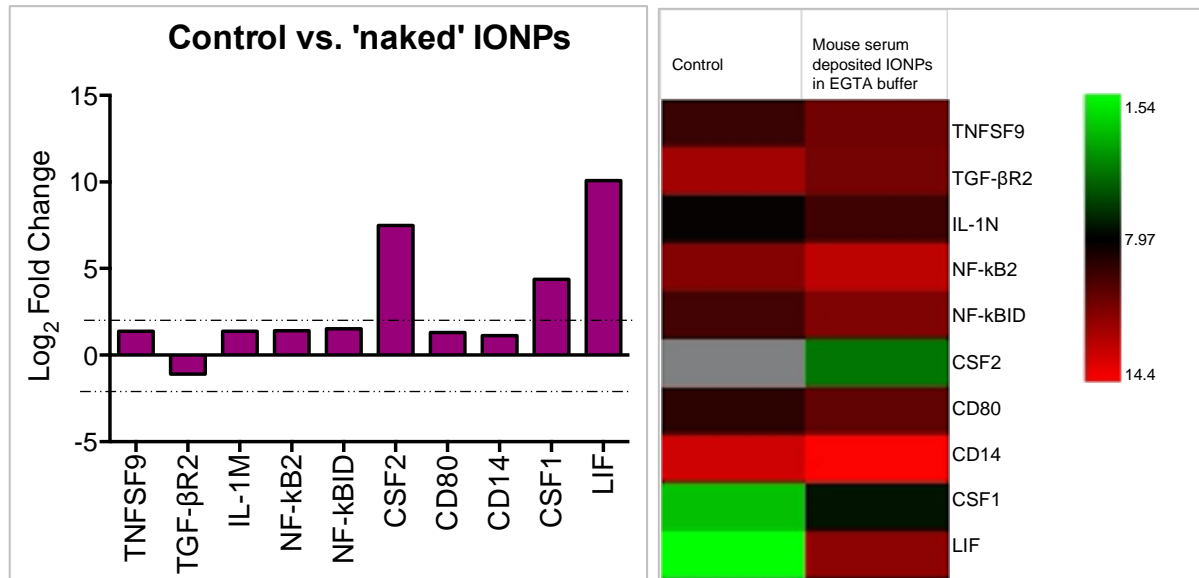


Figure 4.34. **Bar chart and heatmap showing significant DEGs.** Graph A shows the Log<sub>2</sub> fold change of expression for selected significant DEGs relating to immune system processes. Graph B shows a corresponding heat map of the significant upregulated and downregulated DEGs, plotted using log<sub>2</sub> of expression values. The dotted lines show the threshold value (2), following which significant changes may occur within the cells. The left column represents the control (no IONPs) sample and the right column represents 'naked' IONPs in EGTA buffer. Heatmaps show which sample the gene was more upregulated in. Grey blocks indicate no expression or expression below the detection limit.

Of all 52 significant DEGs relating to immune system processes, 47 genes were upregulated and 5 genes were downregulated. LIF (leukaemia inhibitory factor), a member of the IL-6 family, was the most upregulated gene of all 13,144 DEGs (figures 4.34 and 4.35). This is the only sample where significant upregulation of LIF was seen. LIF is a cytokine and, as its name suggests, plays an important role in the inhibition of leukaemia progression, however, upregulation of LIF can occur during inflammation, which can enhance the formation and progression of solid tumours by promoting metastasis (Yue, Wu and Hu, 2015). TGF-βR2 gene encodes for TGF-β receptor 2

molecule and is slightly downregulated in the 'naked' IONPs sample compared to the control sample.

Other upregulated genes include IL-1RN, CD80 and CD14. IL-1RN (interleukin 1 receptor antagonist) is an anti-inflammatory protein that counteracts the effects of the potent pro-inflammatory cytokine IL-1, including IL-1 $\beta$  (SHIIBA *et al.*, 2015). CD80 (T-lymphocyte activation antigen) is a ligand usually expressed on APCs and acts as co-stimulatory molecule in T-cell activation during adaptive immune responses (LI *et al.*, 2016). CD14 (monocyte differentiation antigen) is mainly produced by monocytes and macrophages and when stimulated, can promote the release of pro-inflammatory cytokines and chemokines by enhancing specific signalling pathways (Marcos *et al.*, 2010).

Gene name	Log <sub>2</sub> Fold Change
<b>TNFSF9</b>	1.38
<b>TGF-<math>\beta</math>R2</b>	-1.10
<b>IL-1RN</b>	1.37
<b>NF-<math>\kappa</math>B2</b>	1.42
<b>NF-<math>\kappa</math>BID</b>	1.52
<b>CSF2</b>	7.49
<b>CD80</b>	1.30
<b>CD14</b>	1.13
<b>CSF1</b>	4.37
<b>LIF</b>	10.1

Figure 4.35. **Table showing summary of genes discussed in this comparison.** The table lists the significant DEGs identified in this comparison and the log<sub>2</sub> fold change values.

### 5.3 Discussion

Nanomaterials are very promising agents in the treatment as well as diagnosis of many diseases, including cancer. However, there still are a lot of roadblocks and gaps to be filled in the existing literature when it comes to the safety of using nanomaterials for therapeutic and diagnostic purposes. Depending on their size, shape and chemical properties, NPs can trigger many toxicity issues, ranging from acute localised inflammation to systemic damage (Hannon *et al.*, 2019). Undesirable effects from the activation of the immune system by NPs include inflammation reactions, hypersensitivity and anaphylaxis (Zolnik *et al.*, 2010). Of particular note, the effects of aberrant cytokine expression can vary from mild (example: fever, nausea) to more severe and fatal effects such as organ damage (Hannon *et al.*, 2019).

Other than triggering a pro-inflammatory response, NPs can also have the opposite effect of suppressing the immune system, which is more favourable for tumour growth as cancer cells are able to evade a suppressed immune surveillance (Ilinskaya and Dobrovolskaia, 2014). Hence, studying cytokine expression levels is an excellent way to assess the type of immune response triggered by NPs. The aim of this study was to further understand the immunotoxicity of IONPs by using cytokines as biomarkers of inflammation and transcriptome profiling to study gene expression changes at the mRNA level.

From the bioinformatics results comparing the mouse serum deposited IONPs samples (figure 4.6), no significantly differentially expressed genes relating to the immune system, irrespective of the buffer used, were observed. In fact, out of more than 13,000 genes, only two were significantly differentially expressed. This indicates

that the inflammatory response triggered by both mouse serum deposited samples are quite similar, which also correlates to what was seen from the qPCR results in figures 4.2-4.3. It is important to note that the differences seen with the different treatments may relate to the differences in overall IONP uptake. The results from the previous chapter showed less IONP uptake in general when IONPs were coated with mouse serum compared to human serum. Thus, the differences seen in inflammatory responses from the qPCR results where mouse serum treatments seem to elicit a more suppressed immune response compared to human serum treatments could be linked to the differences in IONP uptake.

When the mouse serum deposited IONPs in DGVB<sup>++</sup> buffer was compared against its corresponding 'naked' IONPs sample, significant upregulation and downregulation of some genes were identified, including the upregulation of anti-inflammatory cytokine, IL-10. The other upregulated genes seen were those associated with inflammation responses.

When the mouse serum deposited IONPs sample in EGTA buffer was compared to 'naked' IONPs sample in EGTA, the only upregulated gene shown in the graph was of the anti-inflammatory cytokine IL-10. All other pro-inflammatory genes were significantly downregulated and of all 289 significantly differentially expressed genes, IL-1 $\beta$  was the most downregulated gene by almost 10-fold. Complement-dependent downregulation of IL-1 $\beta$  was also seen in a study carried out by Pondman *et al.*, (2016) investigating the interactions of carbon nanotubes and immune cells. This indicates that the mouse serum deposited IONPs in EGTA sample might have more of an immunosuppressive effect than that elicited by IONPs without the presence of mouse



serum coating. The qPCR results in figure 4.3 support this pattern where common pro-inflammatory cytokines such as IL-1 $\beta$  and NF- $\kappa$ B1 were downregulated in the serum deposited sample. In fact, through gene ontology analysis results for this comparison showed 'inflammatory response' as the pathway identified with the most significant DEGs (figure 4.15).

When the two 'naked' IONPs samples were compared against each other, most genes relating to a pro-inflammatory reaction were significantly upregulated in the 'naked' IONPs in EGTA sample compared to 'naked' IONPs in DGVB<sup>++</sup> buffer. Gene ontology analysis for this comparison also revealed 'inflammatory response' as the pathway with the most significant DEGs. This confirms our qPCR results, where 'naked' IONPs in EGTA buffer triggered a marginally higher cytokine profile. These results so far strongly suggest IONPs in the EGTA veronal buffer, in the absence of serum proteins, trigger a much higher pro-inflammatory response.

To look at the effects of each of the different IONP samples on gene expression, the samples were individually compared to a control sample, where the cells were not exposed to any IONPs or either of the veronal buffers. The first comparison included mouse serum deposited IONPs in DGVB<sup>++</sup> buffer against the control sample. The most upregulated gene relating to the immune system was CD2 which is involved in the activation of T cells in humans. Anti-inflammatory cytokine IL-10 was also upregulated, however not many genes relating to a pro-inflammatory reaction were upregulated. Furthermore, 'inflammatory response' was not a significant pathway identified following gene ontology analysis, indicating that serum-deposited IONPs in DGVB<sup>++</sup> do not have a significant effect on an inflammation response. However, 'positive

regulation of B cell apoptosis' was the second pathway with most significant DEGs identified. Apoptosis is crucial in protecting the host against diseased or damaged cells, but aberrant apoptosis signalling can play a role in autoimmune diseases, neurodegenerative diseases and cancer (Opferman, 2008).

When the serum deposited IONPs in EGTA buffer was compared to the control sample, IL-10 was again upregulated as well as TCIM (an immune response regulator). Gene ontology analysis again revealed 'positive regulation of B cell apoptotic process' as the second most common pathway amongst the significant DEGs. Inflammatory response was also another pathway identified but had less than half of the number of associated genes compared to the B cell apoptotic pathway.

The next comparison included 'naked' IONPs in DGVB<sup>++</sup> buffer against the control sample and the anti-inflammatory cytokine IL-10 was again upregulated, which also confirms the results seen with qPCR. Most genes associated with pro-inflammatory responses were downregulated and furthermore, gene ontology analysis identified 'positive regulation of B cell apoptotic process' and 'negative regulation of inflammatory response' amongst the 10 most common pathways identified.

The last comparison included 'naked' IONPs in EGTA buffer against the control sample and as expected, most genes contributing to a pro-inflammatory response were upregulated. Of 52 significant DEGs relating to the immune system, LIF, a member of the IL-6 family, was the most upregulated by almost 10-fold. As mentioned previously, upregulation of LIF can promote metastasis and hence promote the progression of solid tumours. Gene ontology analysis results revealed that 'positive

regulation of apoptotic process', 'inflammatory response' and 'positive regulation of macrophage chemotaxis' were amongst the top 5 pathways identified.

Changes in gene expression levels is an important part of studying a cell's functionality and fate. Any significant differentially expressed gene could cause changes within a cell, for example, by affecting genetic interactions or forming a different variant of a protein, which can lead to protein malfunction and cause unwanted phenotypic changes. A recent study carried out in a modified E.coli strain showed that a change in gene expression can not only influence the type of genetic interaction but also the strength of the genetic interaction (Li *et al.*, 2019). Furthermore, it is also well documented that gene networks regulate immune cell development and their function, which are crucial in the modulation of immune responses (Díaz-Muñoz and Turner, 2018). Thus, for our purpose of establishing the biosafety of IONPs as drug delivery vehicles, it was important to study and identify changes in gene expression that may occur following the exposure of IONPs.

The results presented in this chapter have significantly contributed to our understanding of the immune responses triggered by IONPs at the base level. The most common gene ontology pathways seen across most comparisons were the apoptotic pathway and inflammatory response. The bioinformatics results presented showed IL-10 as the gene that is the most consistently affected, which is also visible from the qPCR data (especially with 'naked' IONP samples) produced in this chapter. The qPCR results are based on 2 experimental repeats and should be repeated to validate the results. However, our results seen with IL-10 align with other studied from published literature. For example, a study investigating the interactions of carbon nanotubes and the immune system identified IL-10 as an important player in the

interactions between NPs and immune cells (Pondman *et al.*, 2016). Even though it is not as straightforward to pinpoint the 'safest' opsonised method for IONPs from the presented results, they are all factors identified that can be further studied and tackled to reduced unwanted inflammatory responses triggered by IONPs.

The route of administration of NPs is crucial in determining their fate and toxicity effects (Elsabahy and Wooley, 2013). In this study, we have mimicked intravenous administration by opsonisation with serum proteins, which the NPs will naturally encounter in the blood plasma. Furthermore, studies have shown that complement deposition on carbon nanotubes leads to enhanced uptake in human macrophages (Kouser *et al.*, 2018), thus the presence of serum proteins on NPs may also influence the inflammatory response. In our study, the effects of IONPs exposure was studied after a 2 hour exposure in RAW 264.7 cells, which gives a good indication of the initial immune response, however a longer IONPs exposure time could be studied to observed cytokine levels over a prolonged period of time. Some studies have shown that cytokine expression levels can increase or decrease over time (Denner *et al.*, 2013), hence it could be beneficial to study cytokine expression levels after 24 hours of IONPs exposure to see whether the inflammatory responses are further increased or suppressed over time. A recent study carried out in mice showed that gold NPs can increase the expression of IL-1 $\beta$  and IL-6 over the course of a few days in a size dependent manner; small-sized gold NPs increased cytokine expression much more than larger gold NPs (Khan *et al.*, 2019). This supports the argument that immunotoxicity of IONPs seen in our findings can heavily depend on size and other smaller IONPs may elicit different immune responses, better or worse.

This study identified a number of genetic changes relating to the immune response, some of which were not validated using qPCR. For further studies, it is recommended that the significant changes in the identified genes are confirmed using qPCR to validate the bioinformatics results. IL-10 results were particularly eye-catching and in future work, it can be exploited as an immunomodulatory molecule to manage interactions between NPs and immune cells, thus potentially avoiding unwanted clearance of NPs. It is also important to note that RNA-sequencing for this study was carried out only once due to budget restraints. The data presented in this chapter focused solely on the immunotoxicity of IONPs and identifying genes relating to cytokine expression and promoters of inflammation reactions, however the RNA-sequencing results also showed significant differences in other pathways that were not discussed here, including significant upregulation of proto-oncogenes. To fully understand the changes in gene expression and other toxicity issues in response to IONPs exposure, these other pathways should be explored as they all contribute towards establishing the immediate and long-term biosafety of IONPs.

---

**5. Zebrafish (*Danio rerio*) Embryos: A Model to**  
**Study Iron Oxide Nanoparticle Toxicity**

---

## 5.1 Introduction

Zebrafish, as an animal model in the adult stage as well as embryonic stage, is becoming increasingly popular in the field of biomedical research, especially for nanoparticle toxicology studies. For example, embryo and adult zebrafish have been used in recent years to study the pathology and treatment of tuberculosis by fluorescently labelling the mycobacterium, drug-loaded NPs and/or macrophages to visually observe the pathogenesis and treatment efficacy (Fenaroli *et al.*, 2014; van Leeuwen, van der Sar and Bitter, 2014; Torraca *et al.*, 2014). The use of embryos in particular is grabbing the attention of scientists as they are considered a very good replacement for animal experiments (Strahle *et al.*, 2012).

Along with their low maintenance costs compared to mammals, zebrafish possess unique characteristics which make them favourable for biomedical research. These include their small size, quick development, very high reproducibility, transparency of the embryo and acquiescent to genetic and chemical screens (Chakraborty *et al.*, 2016). Another fundamental advantage of using zebrafish in research is the fact that they share a striking amount (approximately 70%) of genetic identity with humans (Howe *et al.*, 2013), and several zebrafish organ systems are remarkably similar to those in humans (Seth *et al.*, 2013), thus scientific discoveries in zebrafish can be theoretically applicable to humans.

The transparency of the embryo is also a major advantage as it eases the non-intrusive visualisation of organs and biological processes *in vivo* (Seth, Stemple and Barroso, 2013). Zebrafish eggs also develop outside the mother's body and are therefore an ideal model to study non-invasive early development and developmental toxicity. The major organ systems of zebrafish are all developed and start to function

within the first 5 days after fertilisation (Howe *et al.*, 2013). Figure 5.1 shows a representation of zebrafish embryonic development up to 72h post fertilisation (hpf).

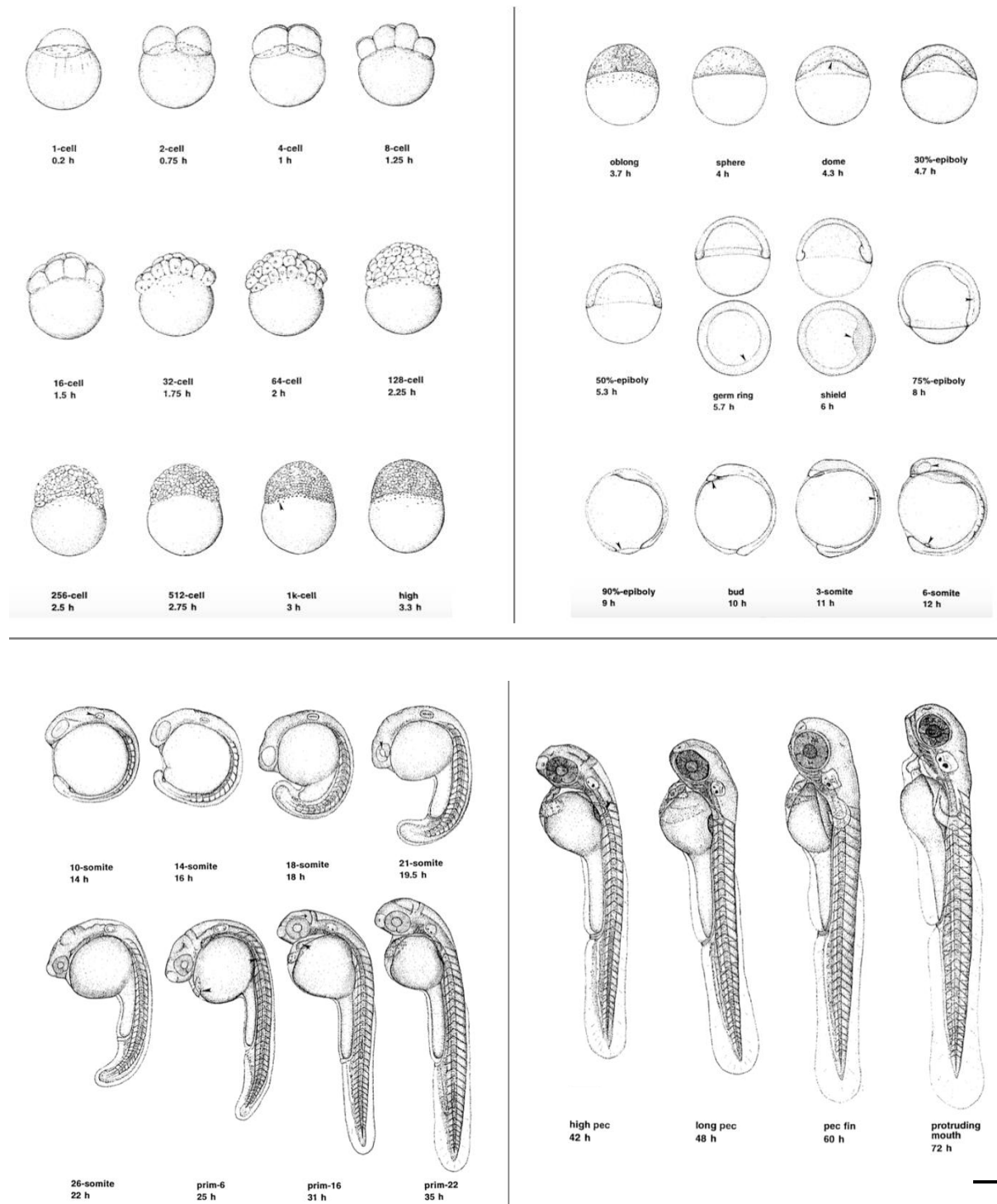


Figure 5.1. **Embryonic development of zebrafish.** The above images show the embryonic development of zebrafish from fertilisation to 3 days post fertilisation (dpf). Hatching of zebrafish embryos usually occur at 2-4 dpf and the protruding mouth stage is generally considered as the end of the embryonic stage. Thereafter, they enter the larval stage and begin to actively feed at 5dpf. In this chapter, microinjections are described that were carried out at the 1-cell stage, 16-cell stage and at the long pec stage (48 hpf). Scale bar = 250 $\mu$ m. Image from Kimmel *et al.*, 1995.



The life cycle of a zebrafish is characterised by four main stages: embryo (from fertilisation to hatching stage, which can be any time from 2-4 dpf), larva (embryo is hatched but is not at the juvenile stage yet), juvenile (development of most adult characteristics, but sexual maturity is not reached) and adult (sexual maturity reached and they can breed) (Parichy *et al.*, 2009).

Zebrafish embryos have an increasing popularity in nanoparticle research, one of the main reasons being its transparency which allows for clear visualisation of fluorescently labelled NPs, thus the biodistribution of administered NPs can be directly studied at a whole organism level. Zebrafish embryos used in the toxicity studies of Silicon dioxide (SiO<sub>2</sub>) NPs showed that the chorion of zebrafish acts as a protective barrier before hatching. Vranic *et al.* (2019) observed the morphological effects using fluorescently labelled NPs visualised through fluorescence microscopy following NP exposure (Vranic *et al.*, 2019). A different study recently carried out by Kocere *et al.* (2020) demonstrated the therapeutic capability of NPs in cancer treatment by inducing tumour formation in the embryos first through injection of melanoma cells into the embryos. Tumour formation, macrophage recruitment and accumulation of injected NPs in the tumour area were visualised and quantified through fluorescence microscopy, thus proposing zebrafish embryos as efficient animal models to study NP toxicity and its therapeutic capability in cancer (Kocere *et al.*, 2020). Furthermore, behavioural studies in zebrafish embryos investigating toxicity of copper NPs (CuNPs) showed that CuNPs exposure to the embryos resulted in several side effects, including abnormal cardiac function, inhibition of the hatching stage, developmental abnormalities and a higher mortality rate (Sun *et al.*, 2016).

Other than visualisation and behavioural studies, zebrafish embryos are great models to study toxicity at the gene expression level due to their acquiescence to genetic

screening. A gene expression study carried out in zebrafish embryos to study the toxicity of silver NPs (Ag NPs) showed that acute toxicity seen with AgNPs was due to the dispersion of Ag<sup>+</sup> ions in the media surrounding the embryos and was also size-dependent on the AgNPs (Olasagasti *et al.*, 2014). A more recent study by Qiang *et al.* also confirmed the size-dependent toxicity of AgNPs using zebrafish embryos as models and using mRNA expression levels to assess toxicity. The study compared two different sizes of AgNPs and showed that the smaller sized AgNPs (4nm) displayed slightly higher toxicity compared to the larger sized ones (10nm) (Qiang *et al.*, 2020).

In this chapter, IONPs biodistribution and toxicity of IONPs were studied in zebrafish up to 5 dpf. Microinjections of zebrafish were carried out at 0.2 hpf (hours post fertilisation) and 1.5 hpf (for dextran microinjections only) and at 48 hpf in the duct of Cuvier for IONPs microinjections (this is described in more detail in chapter 2.9). The duct of Cuvier is a wide blood circulation vessel on the yolk sac and connects the heart to the trunk vasculature (Saraceni *et al.*, 2016). The duct of Cuvier is one of the preferred sites of microinjections at 2-3 dpf for immediate systemic delivery of the injected material (Benard *et al.*, 2012). At 2 dpf, when IONPs microinjections were carried out, the embryo develops significant craniofacial features as well as major sensory organs (eyes and ears) (von Hellfeld *et al.*, 2020), making it easier to locate the duct of Cuvier. Figure 5.2. shows an overview of the normal development of zebrafish from 1 dpf to 5 dpf. The duct of Cuvier has been highlighted in the embryo picture at 2 dpf.

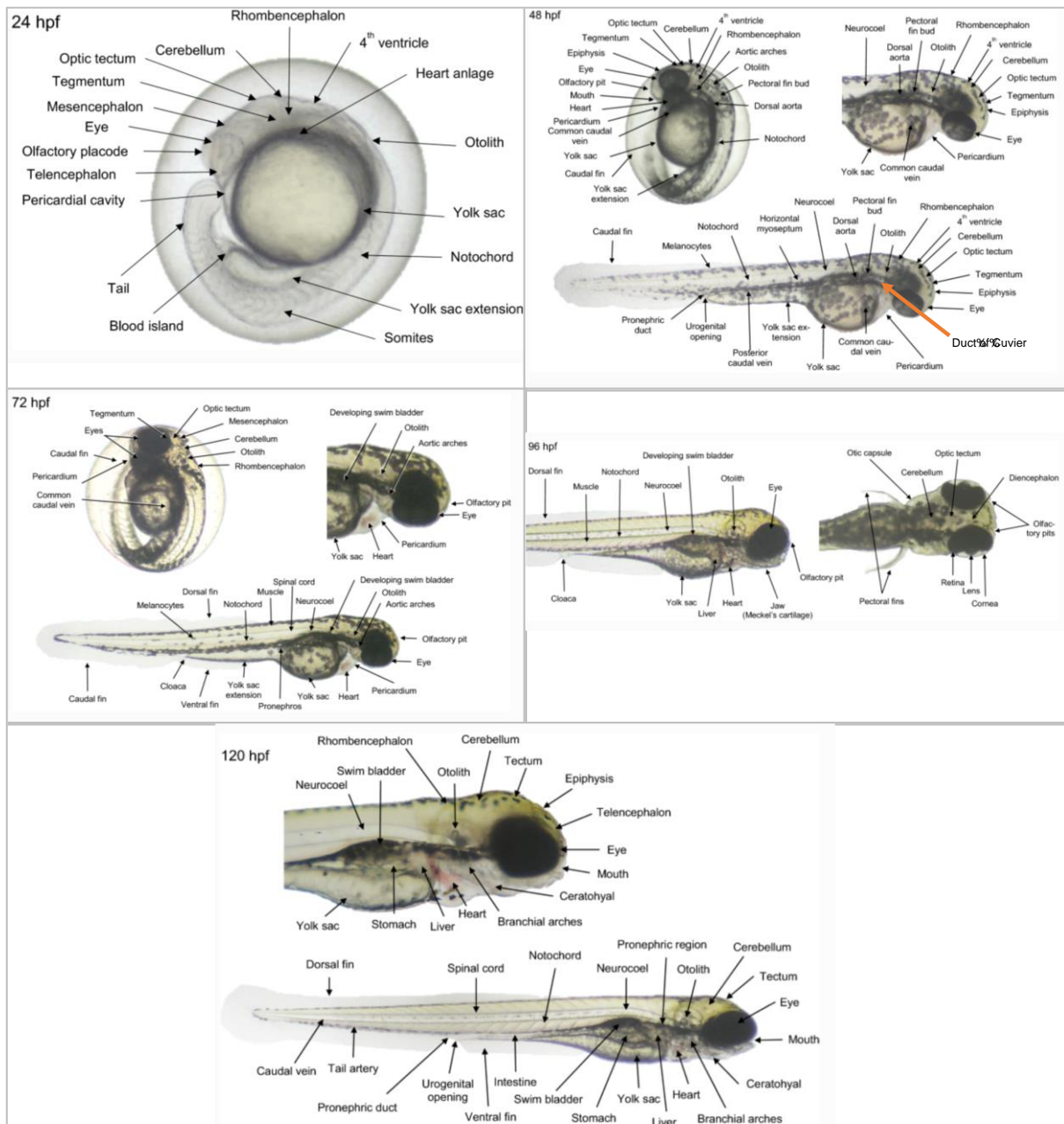


Figure 5.2. **Embryonic-larval anatomy of zebrafish.** The above images show an overview of all major structures and organs that are formed by 5dpf. From 2 dpf (48h) onwards, embryos start to develop pigment cells and hatching usually starts at this stage. Alternatively, the embryos can be safely dechorionated manually at 2dpf for microinjections of IONPs in the duct of Cuvier (orange arrow). Images acquired and adapted from *von Hellfeld et al., 2020*.

Following administration of NPs, they will be subject to excretion. The biodistribution of NPs and the amount of time they remain in the embryo depends on the surface charge of the administered particle (*Paatero et al., 2017*). A study carried out in mice showed that differently charged NPs of the same size had different residence times in

mouse models where positively charged NPs stay in the kidneys for up to 4 days before excretion whereas neutral and negatively charged NPs stayed in the spleen and liver (Balogh *et al.*, 2007). Other than surface charge, different sized NPs can also have different resident times in the body. In zebrafish embryos, the clearance of different sized NPs was shown to be mostly dependent on the MPS (Mononuclear Phagocytic System), which resulted in the NPs being trafficked to the digestive organs before elimination, mainly the liver, pancreas and gallbladder (van Pomeran *et al.*, 2019). The study also showed that the different sized NPs accumulated in these organs in different ratios, with the nanosphere accumulating the most in the liver, which is the main organ involved in clearance (Truong *et al.*, 2015).

A fundamental advantage of zebrafish embryos, particularly relevant to our studies, is the development of their immune system, where the embryos initially lack an adaptive immune system. After 1 dpf, zebrafish embryos already develop phagocytic activity against pathogens (Herbomel, Thisse and Thisse, 1999) and they rely solely on their innate immune response until their adaptive immune system develops around 3 weeks post fertilisation (Lam *et al.*, 2004). This characteristic makes zebrafish embryos and larvae an ideal way of studying the innate immune response, in the absence of B- and T-cell responses. The complement system is a crucial part of the innate immune response, as well as bridging the innate and adaptive immune responses. The zebrafish complement system bears functional and structural similarity to the mammalian complement system as per a recent study, which investigated all known homologs of the mammalian complement system in zebrafish, including C3, factor H and C1 components (Zhang and Cui, 2014). The liver is the main site of production of complement components in zebrafish, however they can also be produced in extrahepatic sites (Zhang and Cui, 2014). Macrophages in zebrafish can arise from

three known origins: the rostral blood island (RBI) produces primitive haematopoietic macrophages, the poster blood island (PBI) produces erythromyeloid precursors (EMPs) which can give rise to macrophages lineages and finally, in adult zebrafish, the ventral wall of the dorsal aorta (VDA) which can produce haematopoietic lineages including macrophages (Lin, Wen and Xu, 2019) (figure 5.3).

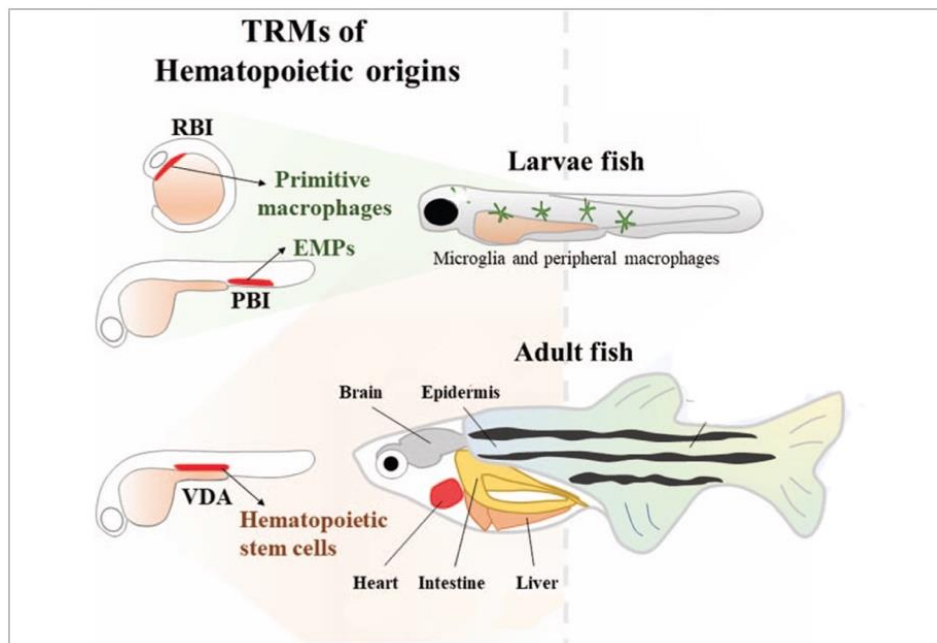


Figure 5.3. **Illustration on the known origins of tissue resident macrophages (TRMs).** The above image shows the three major origins of TRMs from the larvae to adult stage. In the embryonic stage, mostly microglia and peripheral macrophages are generated. These macrophages will eventually be replaced by macrophages produced from the ventral wall of the dorsal aorta (VDA) in adult zebrafish, which tend to accumulate in the brain, epidermis, heart, intestine and liver. Image obtained from *Lin, Wen and Xu, 2019*.

The aim of this study is to use zebrafish embryos to study IONPs toxicity within innate immunity by investigating developmental abnormalities, mortality rate and the biodistribution of IONPs following microinjections. A high molecular weight dextran was also injected with the aim of labelling macrophages in zebrafish embryos to study the distribution of IONPs in relation to macrophages.

## 5.2 Results

As part of the preliminary studies, zebrafish embryos were injected at 2 dpf with different 'naked' IONPs concentrations (5 µg/ml, 50 µg/ml, 100 µg/ml, 500 µg/ml and 1000 µg/ml) to test for lethal toxicity concentrations of injected IONPs. The IONPs were injected in the duct of Cuvier and the mortality rate and developmental defects were monitored until 5dpf. The graph below shows the survival rate of the embryos at 5 dpf (figure 5.4).

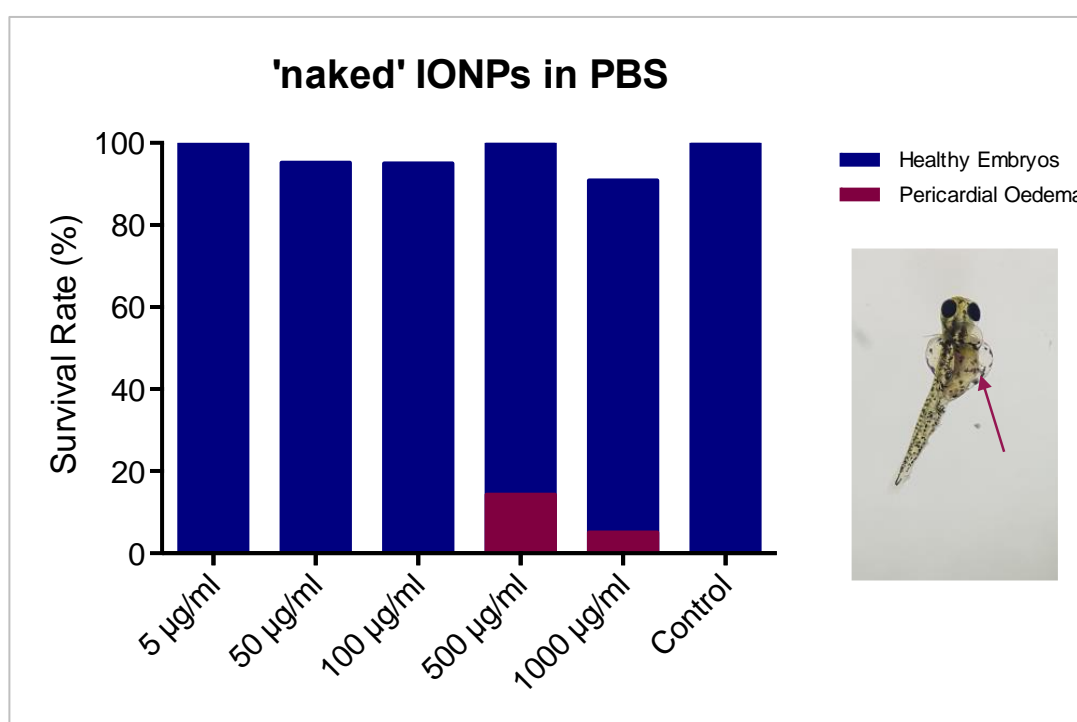


Figure 5.4. **Bar chart showing survival rates of zebrafish larvae at 5dpf.** The graph shows the survival rates of injected zebrafish embryos using different concentrations of 5 µg/ml, 50 µg/ml, 100 µg/ml, 500 µg/ml and 1000 µg/ml IONPs, with the survival percentages of 100%, 95.2%, 95%, 100% and 90.9%, respectively. The control larvae were injected with PBS only at 2dpf. 14.3% of larvae at 500 µg/ml and 5% at 1000 µg/ml displayed characteristics of pericardial oedema. Number of injected embryos were 20-22 per concentration. The image on the right shows a larvae with severe pericardial oedema.

Overall, the IONPs injected embryos showed a low mortality rate, at least 90.9% survived, however, 14.3% and 5% of zebrafish larvae injected with 500 µg/ml and 1000 µg/ml of IONPs, respectively, showed signs of cardiotoxicity through severe pericardial oedema, as shown in the above picture. These larvae in particular had a

slower heartbeat than normal and were unresponsive to any external stimulus. Pericardial oedema in zebrafish embryos is a marker of toxicity and a defective cardiovascular system can lead to an overall defective growth and severe malformations of the larvae (Chahardehi, Arsad and Lim, 2020).

'naked' IONPs microinjections were repeated, with slightly different concentrations with the aim of investigating the ideal concentrations for the visualisation of IONPs. The graph below shows the survival rates of injected embryos using 100 µg/ml, 300 µg/ml, 500 µg/ml and 1000 µg/ml of IONPs (figure 5.5).

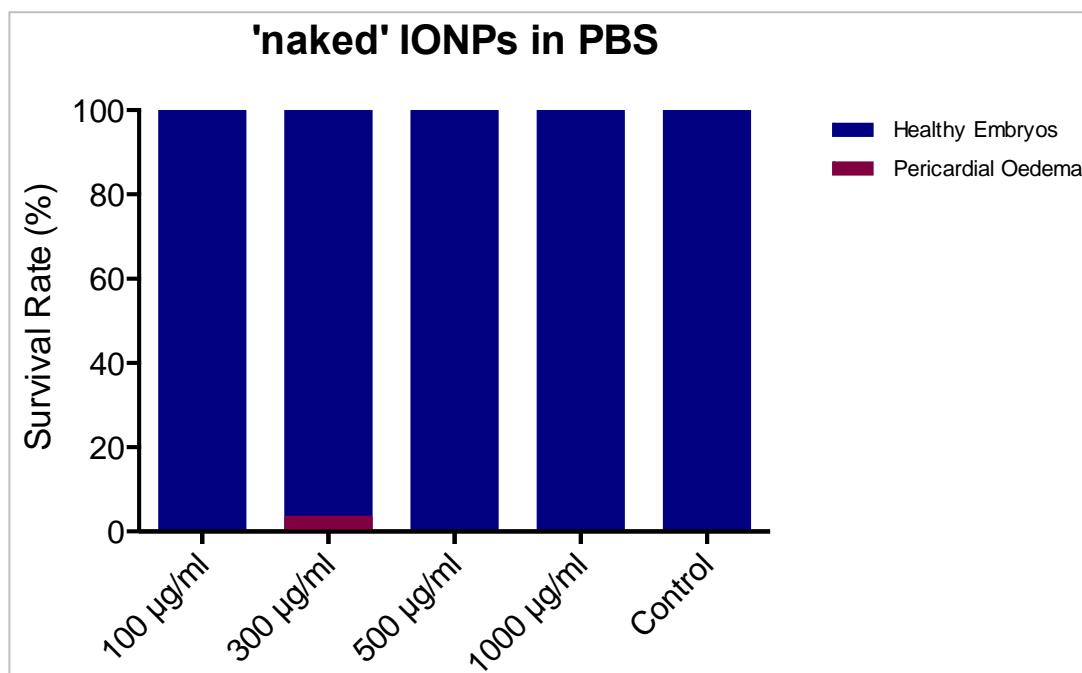


Figure 5.5. **Bar chart showing survival rates of zebrafish larvae at 5dpf.** The graph shows the survival rates of injected zebrafish embryos using different concentrations of 100 µg/ml, 300 µg/ml, 500 µg/ml and 1000 µg/ml IONPs, with the survival percentages of 100% in all conditions. The control larvae were injected with PBS only at 2dpf. 3.33% of larvae at 300 µg/ml displayed characteristics of pericardial oedema. Number of injected embryos were 25-30 per concentration.

The above graph shows a survival rate of 100% in all concentrations injected, with 3.33% of larvae showing pericardial oedema at 300 µg/ml and none at higher

concentrations, conversely to what was seen previously (figure 5.5). This could be due to human error during microinjections, some embryos being slightly more developed than others or this batch of egg lay could have been healthier in general. These larvae were then imaged to determine the concentrations at which IONPs can be visualised under the microscope (figure 5.6).

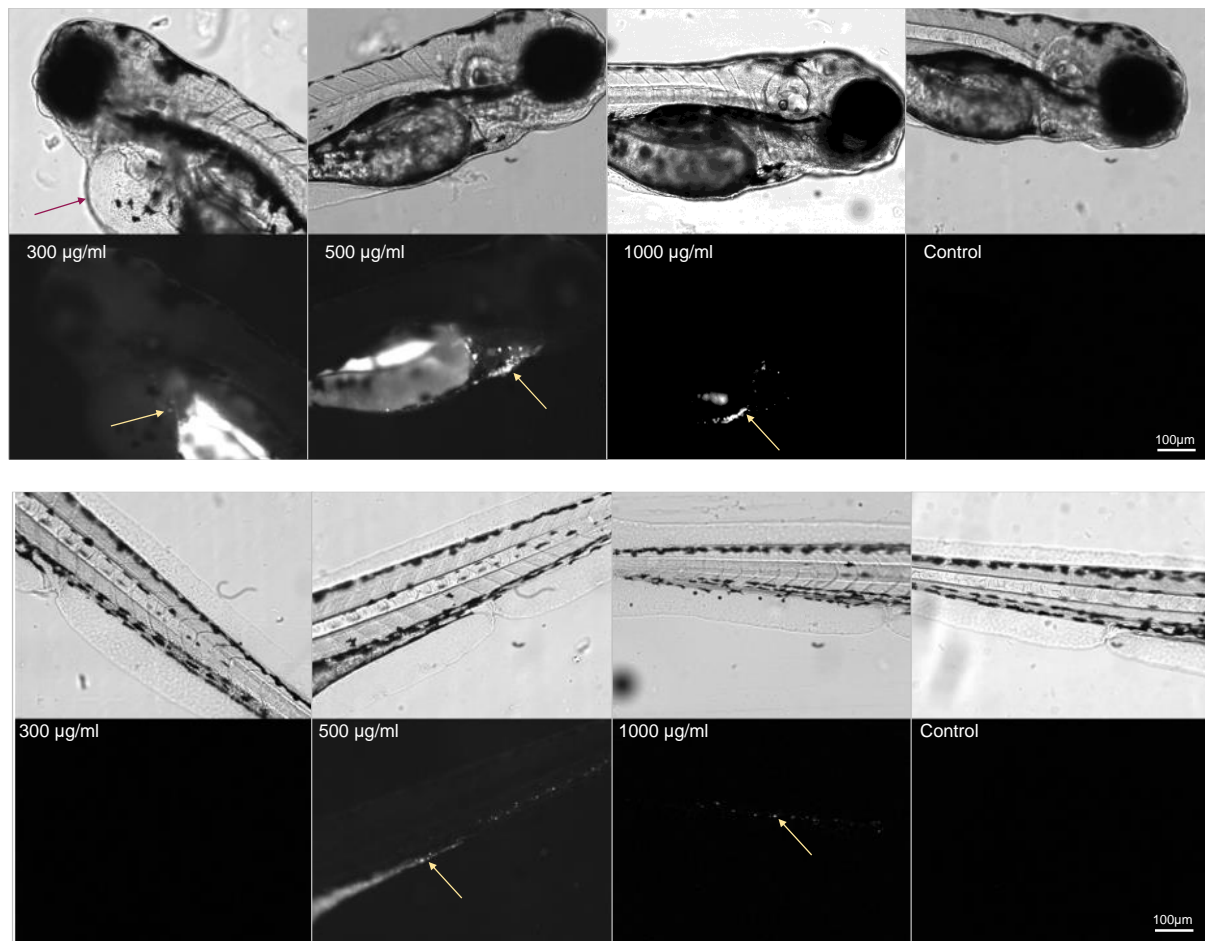


Figure 5.6. **Injected zebrafish larvae at 5 dpf.** The images above show zebrafish larvae imaged at 5 dpf using a Leica DMI8 microscope (10X objective) with brightfield and fluorescence (568nm excitation and 603nm emission). At 300 µg/ml, only a few IONPs were seen, whereas at 500 µg/ml and 1000 µg/ml a higher amount of IONPs were clearly visible in the pericardial area as well as the tail. The control larvae were injected with PBS only at 2 dpf, along with the different IONPs concentrations. An **arrow** in the top left picture points to pericardial oedema in the larvae and yellow arrows show IONPs. Brightfield images are in the first and third row showing embryo morphology and the second and fourth row showing fluorescent images in black and white. Representative image of 2 imaged embryos, 22-25 per group.



From the above images (figure 5.6), IONPs could hardly be seen at concentration 300 µg/ml, whereas at higher concentrations of 500 µg/ml and 1000 µg/ml, IONPs were clearly visible under the microscope. Thus, IONP concentrations of 500 µg/ml and 1000 µg/ml were deemed as the ideal dosage to be further studied. Since IONPs were incubated at 37°C for 1 hour in serum, washed and sonicated on the day of microinjections, the time available to carry out the microinjections was limited, hence also limiting the number of embryos injected per experiment. To maximise the time available and to increase the amount of embryos injected, overnight incubation of IONPs instead was investigated and through western blotting, the level of C3 protein adsorption to the IONPs was compared (figure 5.7).

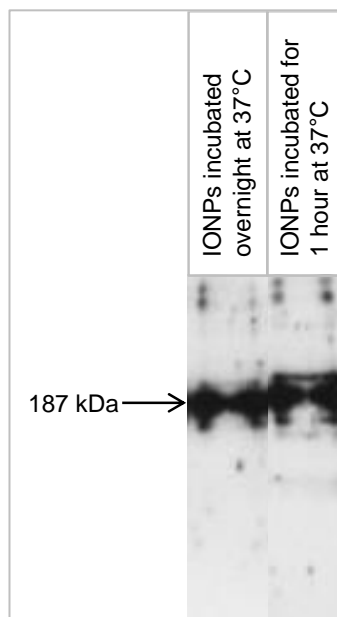


Figure 5.7. **Western blot showing levels of C3 protein.** The results show that incubating the IONPs in human serum overnight and for 1 hour results similar levels of C3 protein adsorption.

Since the levels of C3 protein adsorption were similar in IONPs incubated overnight vs. 1 hour, all subsequent IONPs microinjections were carried out using IONPs

incubated at 37°C overnight, followed by the washes and sonication on the day of injections. This allowed for greater time efficiency and more injected per condition. The next microinjections were carried out to investigate the effects of the deposition of human serum proteins on the surface of the IONPs. The graphs below show the mortality rate for serum-deposited IONPs and 'naked' IONPs (figure 5.8). Experiments for each of the following conditions were performed three times.

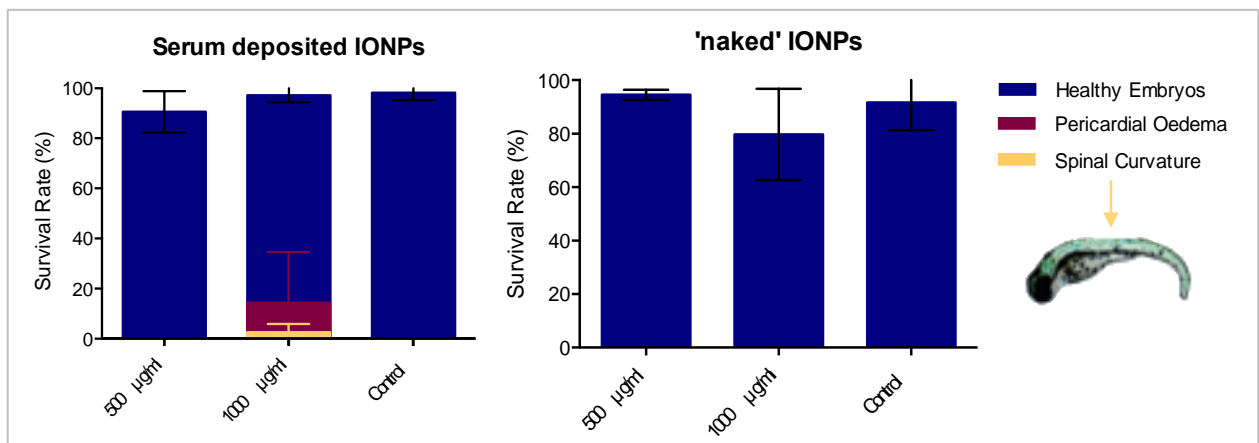


Figure 5.8. **Bar chart showing survival rates of zebrafish larvae at 5 dpf.** The graph shows the survival rates of injected zebrafish embryos using different concentrations of 500 µg/ml and 1000 µg/ml, comparing serum deposited IONPs and 'naked' IONPs. The control larvae were injected with PBS only at 2 dpf. 28.3% of larvae injected with serum-deposited IONPs at 1000 µg/ml displayed characteristics of pericardial oedema. However, all 28.3% of these larvae with pericardial oedema were observed during one of the experimental repeats. In the same experimental repeat, 4.8% of larvae developed a spinal curvature. Number of injected embryos were 20-35 per concentration. The image on the right shows spinal curvature in an embryo. Image of embryo obtained from *Buchan et al., 2014*. A one-way ANOVA test was carried out in GraphPad prism to determine statistical significance. No statistical significance was found between the different concentrations for survival rate, embryos with pericardial oedema or embryos with spinal curvature.

Injection of embryos with serum-deposited IONPs resulted in a low mortality rate, however some larvae developed pericardial oedema and spinal curvature as shown in the above graph (figure 5.8). Spinal curvature in zebrafish larvae can be an indication of idiopathic scoliosis, which has been linked to severe defects in cerebrospinal fluid flow (Grimes *et al.*, 2016). However, this was the only case of spinal curvature seen in all experiments carried out in this study.

The larvae were also imaged under the microscope at 4 dpf and 5 dpf to study the biodistribution of the injected serum-deposited IONPs (figure 5.9).

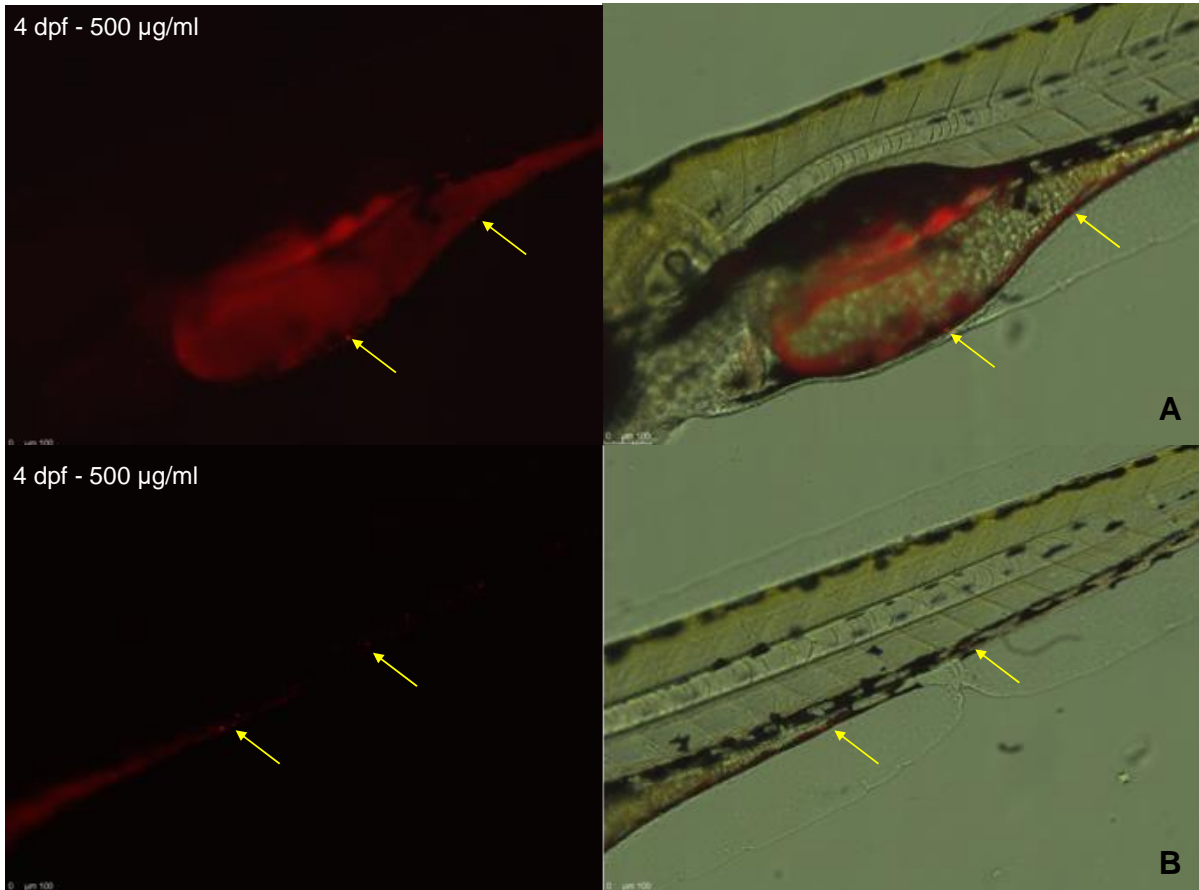


Figure 5.9. **Injected zebrafish larvae at 4dpf.** The images above show zebrafish larvae imaged at 4 dpf using the Leica DMI8 microscope (20X objective). Serum deposited IONPs injected at a concentration of 500 µg/ml were found to be distributed along the yolk sac (A) and around the intestine leading to the cloaca (B) (figure 5.2). Overlays of bright field and fluorescent images (right hand panels) show larvae morphology and IONP distribution. Fluorescence only images are on the left. Arrows indicate IONP accumulation. Diffuse red staining around the yolk sac close to the injection site is seen. Representative image of 2 imaged embryos, 24 per group.

The above images (figure 5.9) show the localisation of serum deposited IONPs at 4 dpf (2 days post microinjections, 500 µg/ml IONPs per injection). The IONPs are distributed around the bottom of the yolk sac, leading into the yolk sac extension, intestine and cloaca, where they may be excreted. The next images below show larvae injected with 1000 µg/ml of serum deposited IONPs (figure 5.10).

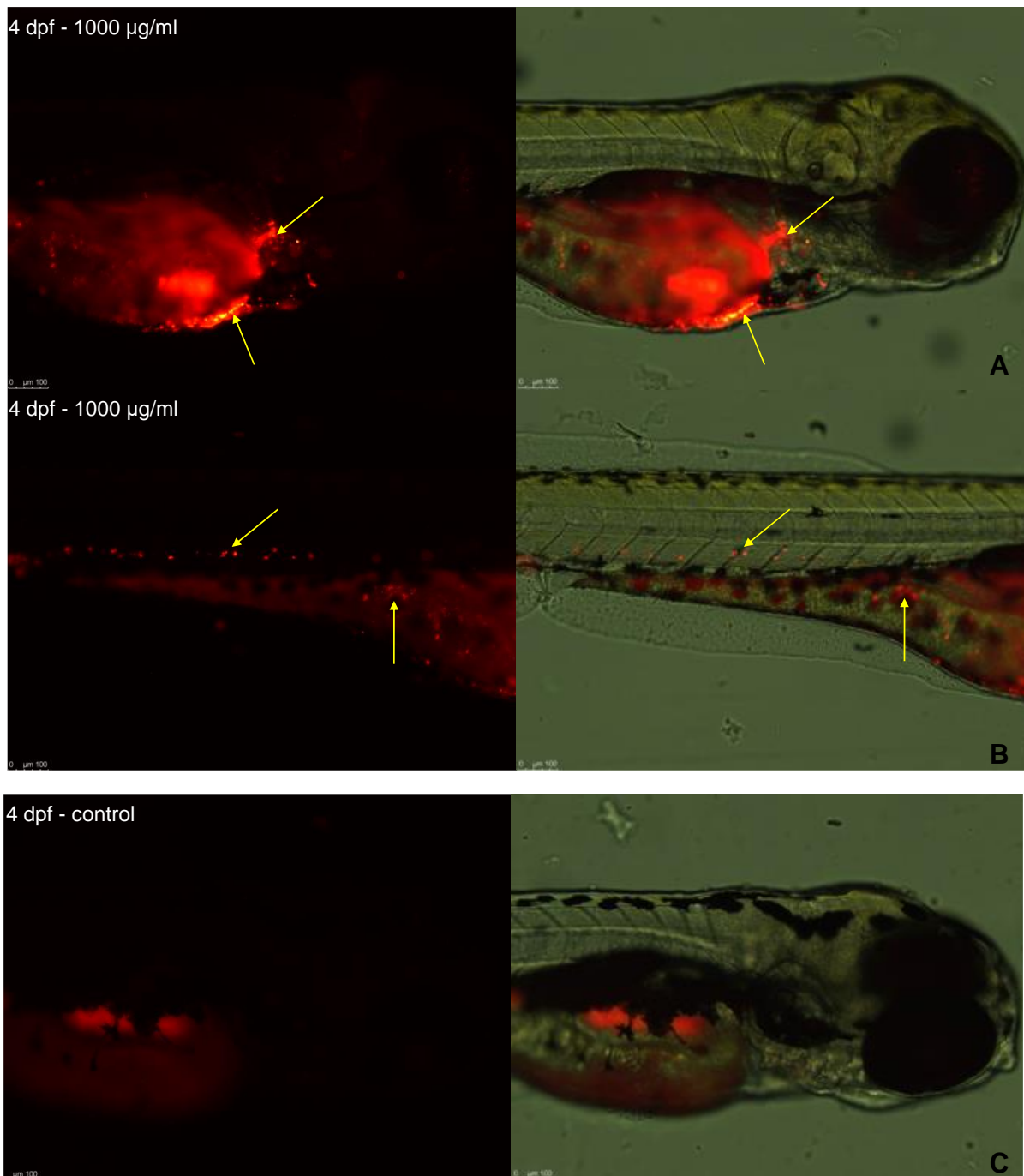


Figure 5.10. **Injected zebrafish larvae at 4 dpf.** The images above show zebrafish larvae imaged at 4 dpf using the Leica DMI8 microscope (20X objective). Serum deposited IONPs injected at a concentration of 1000 µg/ml were found to be distributed along the yolk sac, heart, liver (A) and around the intestine leading to the cloaca (B) (figure 5.2). Control larvae was injected with PBS only (C). Overlays of bright field and fluorescent images (right hand panels) show larvae morphology and IONP distribution. Fluorescence only images are on the left. Arrows indicate IONP accumulation. Diffuse red staining around the yolk sac close to the injection site is seen also in the control animals indicating autofluorescence from the yolk sac proteins. Representative image of 2 imaged embryos, 22-25 per group.

These images (figure 5.10) show that serum deposited IONPs at a higher concentration accumulate around the heart and the liver, where they may remain until excreted. IONPs were also noticed around the intestine and cloaca suggesting that they would be excreted shortly afterwards. The next images below (figure 5.11) show the same concentrations of injected serum deposited IONPs but in 5 day old larvae.

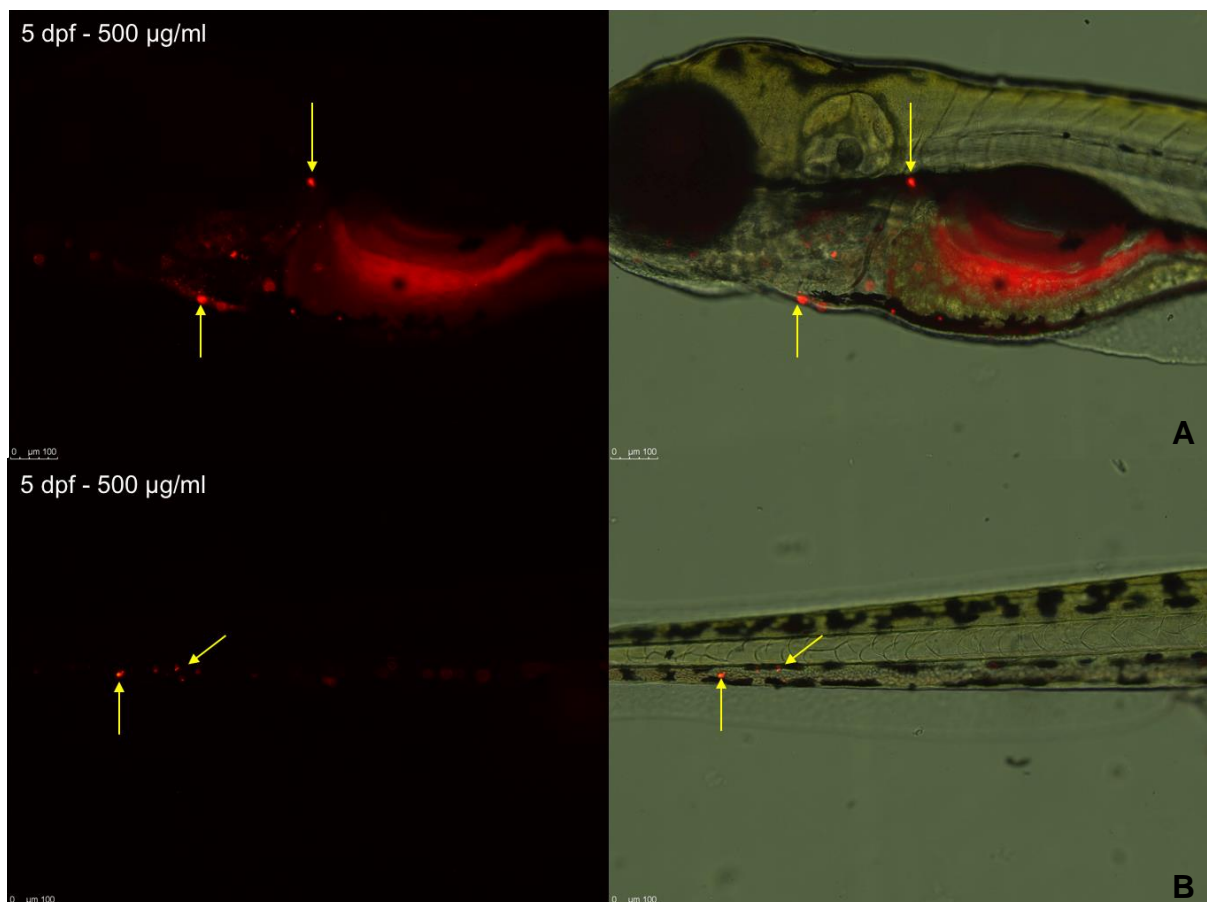


Figure 5.11. **Injected zebrafish larvae at 5dpf.** The images above show zebrafish larvae imaged at 5 dpf using the Leica DMI8 microscope (20X objective). Serum deposited IONPs injected at a concentration of 500 µg/ml were found to be distributed along the yolk sac, heart, liver (A) and in the caudal vein in the tail (B) (figure 5.2). Overlays of bright field and fluorescent images (right hand panels) show larvae morphology and IONP distribution. Fluorescence only images are on the left. Arrows indicate IONP accumulation. Diffuse red staining around the yolk sac close to the injection site is seen. Representative image of 2 imaged embryos, 25 per group.

The above images (figure 5.11) show that serum-deposited IONPs accumulate in the pericardium and liver, likely stored until they are excreted. IONPs were also seen in

the caudal vein in the tail, whose function is to return blood from the trunk and tail to the heart (Kimmel *et al.*, 1995).

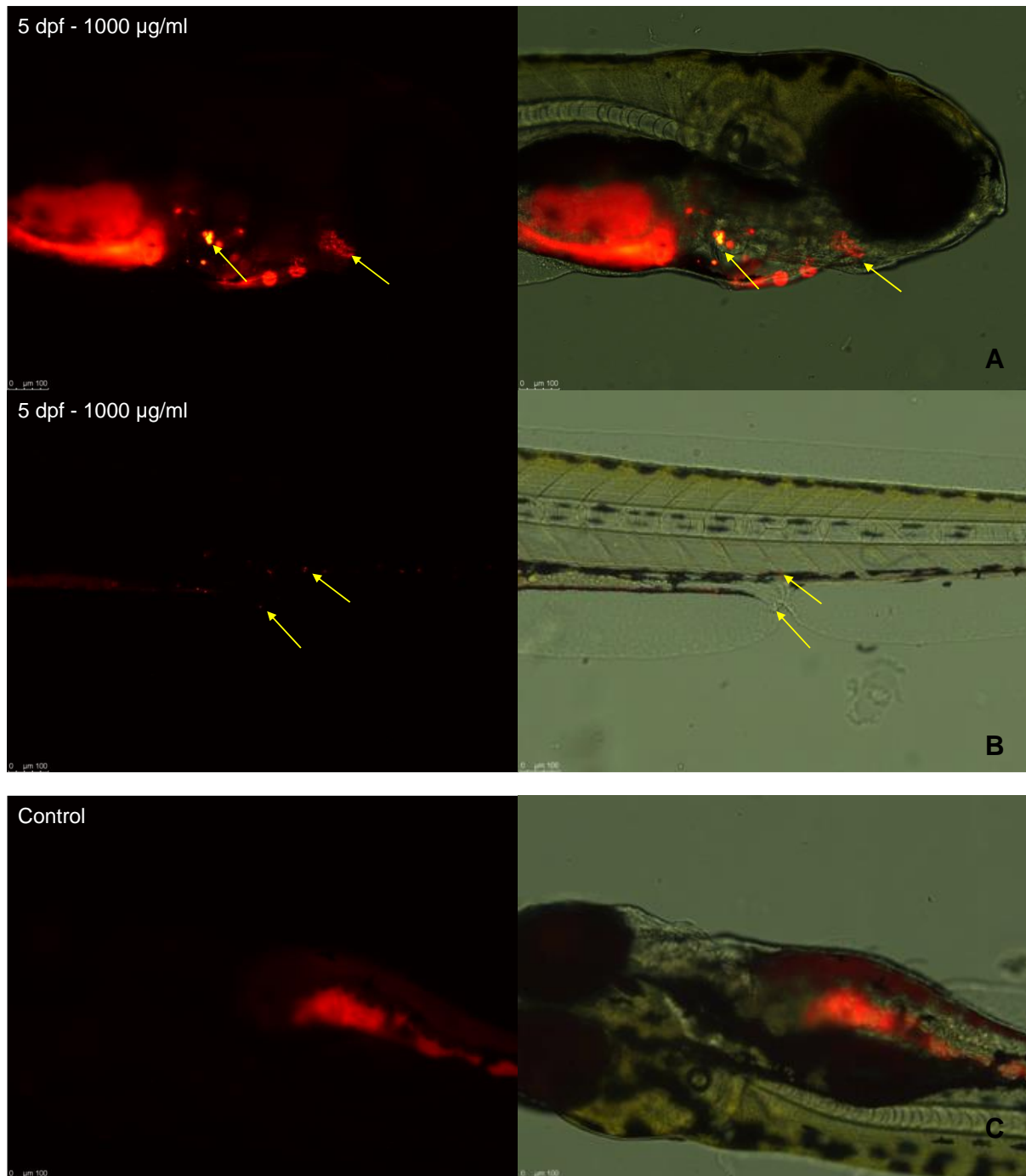


Figure 5.12. **Injected zebrafish larvae at 5dpf.** The images above show zebrafish larvae imaged at 5 dpf using the Leica DMI8 microscope (20X objective). Serum deposited IONPs injected at a concentration of 1000 µg/ml were found to be distributed along the heart, liver, some seen in the ceratohyal (below eye) (A) and in the intestine as well as the pronephric duct (B) (figure 5.2). Control larvae were injected with PBS only (C). Overlays of bright field and fluorescent images (right hand panels) show larvae morphology and IONP distribution. Fluorescence only images are on the left. Arrows indicate IONP accumulation. Diffuse red staining around the yolk sac close to the injection site is seen also in the control animals indicating autofluorescence from the yolk sac proteins. Representative image of 2 imaged embryos, 26 per group.

Other than the same pattern seen in the heart and liver, some IONPs were also seen in the ceratohyal, which is a cartilage important in the support and structure of the lower jaw (figure 5.12) (Wu, Su and Shu, 2018). If the ceratohyal cartilage develops abnormally, it leads to the development of smaller heads in the larvae which can impact their feeding behaviour (Wu, Su and Shu, 2018). Some IONPs were also seen at the pronephric duct, which is a duct of the embryonic kidney called the pronephrons (figure 5.12) (Kimmel *et al.*, 1995). This provides strong evidence of IONPs excretion at 5 dpf.

Zebrafish larvae injected with the same concentrations of 'naked' IONPs were also imaged to study the biodistribution of 'naked' IONPs at 4 dpf and 5 dpf. The images below (figure 5.13) show 4 dpf larvae injected with 'naked' IONPs at concentration 500  $\mu\text{g/ml}$ .

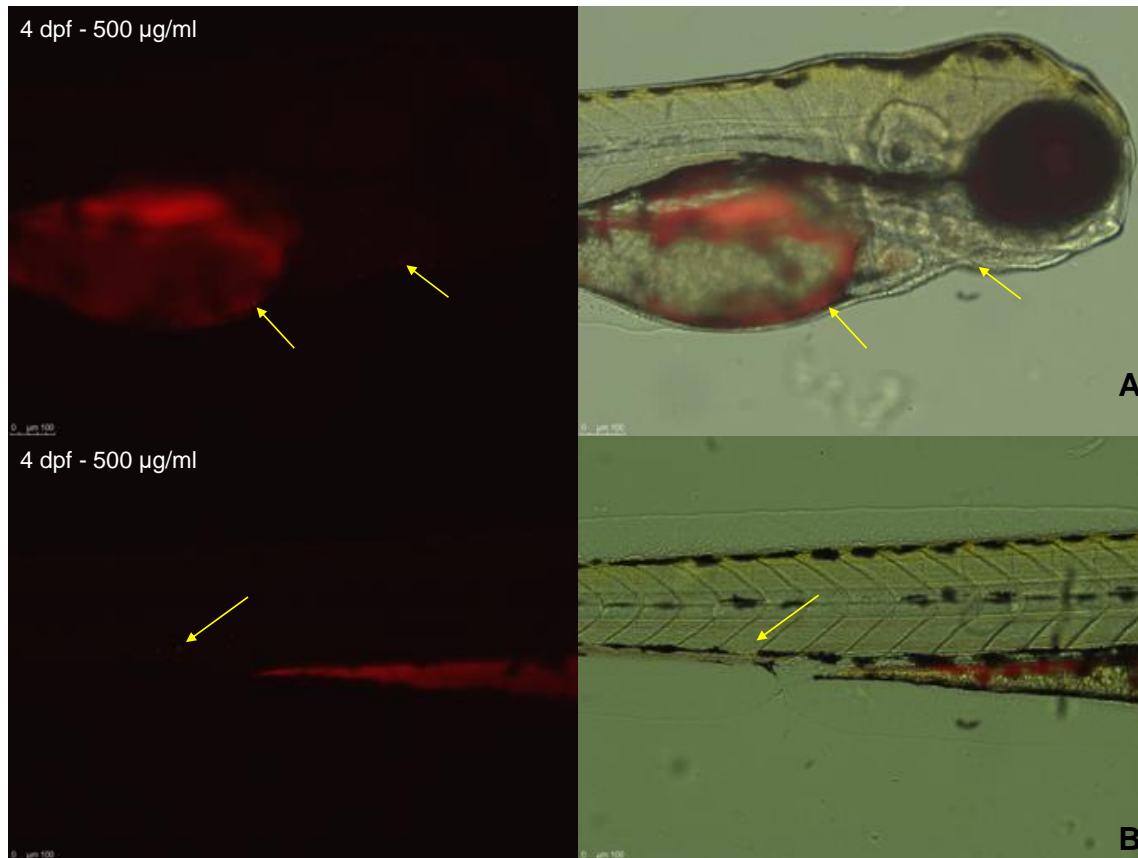


Figure 5.13. **Injected zebrafish larvae at 4 dpf.** The images above show zebrafish larvae imaged at 4 dpf using the Leica DMI8 microscope (20X objective). 'Naked' IONPs injected at a concentration of 500  $\mu\text{g/ml}$  were found to be distributed around the yolk sac and very few in the ceratohyal (below eye) (A) and near the caudal vein in the tail (B) (figure 5.2). Overlays of bright field and fluorescent images (right hand panels) show larvae morphology and IONP distribution. Fluorescence only images are on the left. Arrows indicate IONP accumulation. Diffuse red staining around the yolk sac and in the tail are also seen. Representative image of 2 imaged embryos, 28 per group.

The above images (figure 5.13) show a small amount of IONPs around the yolk sac and in the caudal vein in the tail. The images below (figure 5.14) show 'naked' IONPs distribution when 1000 µg/ml of IONPs was injected.

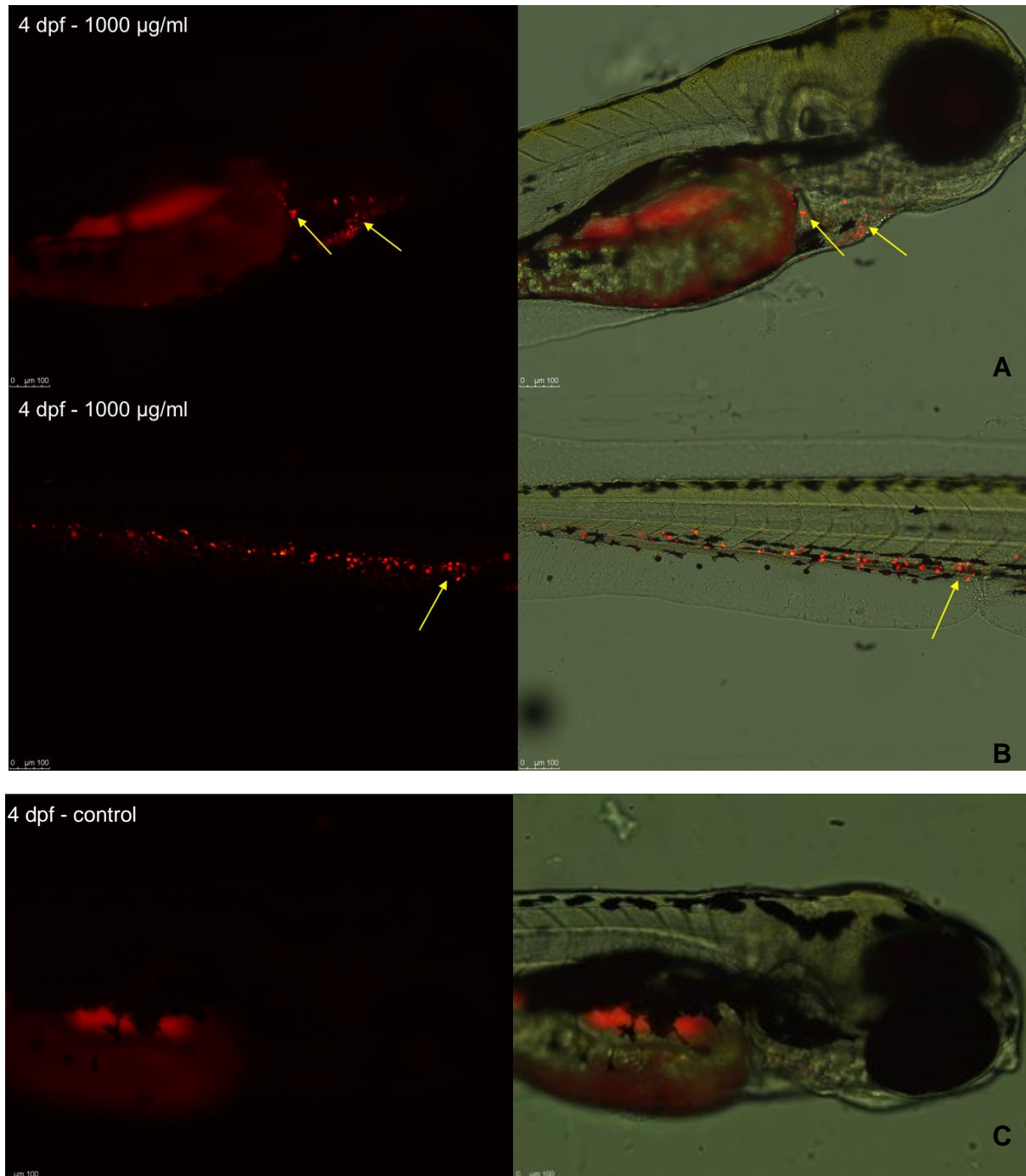


Figure 5.14. **Injected zebrafish larvae at 4 dpf.** The images above show zebrafish larvae imaged at 4 dpf using the Leica DMI8 microscope (20X objective). 'Naked' IONPs injected at a concentration of 1000 µg/ml were found to be distributed in the pericardium and liver (A) and near the caudal vein in the tail and the pronephric duct (B) (figure 5.2). Control larvae was injected with PBS only (C). Overlays of bright field and fluorescent images (right hand panels) show larvae morphology and IONP distribution. Fluorescence only images are on the left. Arrows indicate IONP accumulation. Diffuse red staining around the yolk sac close to the injection site is seen also in the control animals indicating autofluorescence from the yolk sac proteins. Representative image of 2 imaged embryos, 25 per group.



The above images (figure 5.14) show that the ‘naked’ IONPs injected at a concentration of 1000 µg/ml accumulate in the heart and liver, similar to what was seen with the serum-deposited IONPs. IONPs were also seen in the caudal vein of the tail as well as the pronephric duct, once again demonstrating strong evidence of IONP excretion. Of note, ‘naked’ IONPs are visible in the pronephric duct at 4 dpf (figure 5.14) whereas serum-deposited IONPs were first visible in the pronephric duct at 5 dpf (figure 5.12 B). This could suggest that serum-deposited IONPs have a slightly higher residence time in the larvae before being excreted. The images below show ‘naked’ IONPs localisation at 5dpf.

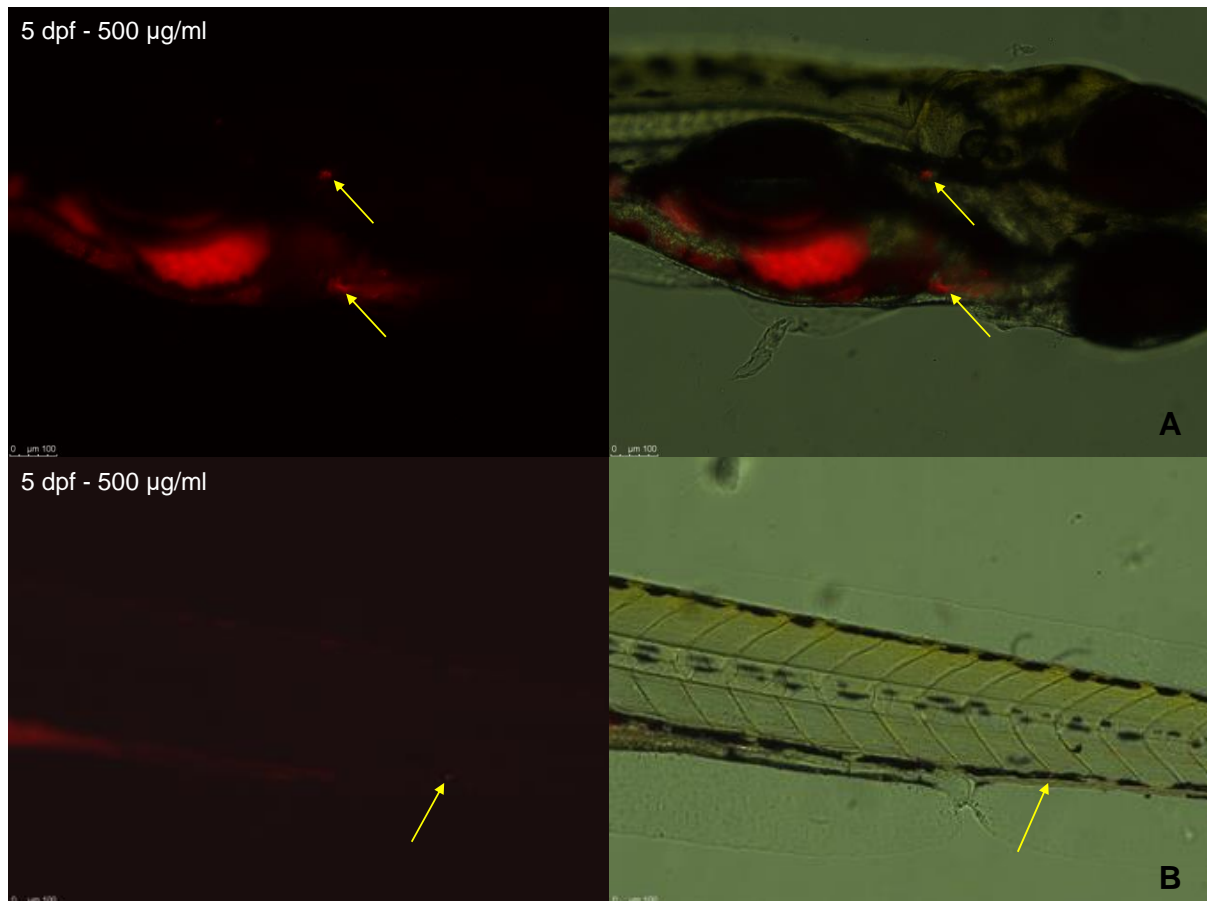


Figure 5.15. **Injected zebrafish larvae at 5dpf.** The images above show zebrafish larvae imaged at 5 dpf using the Leica DMI8 microscope (20X objective). ‘Naked’ IONPs injected at a concentration of 500 µg/ml were found to be in the liver and pericardium (A) and near the caudal vein in the tail and the pronephric duct (B) (figure 5.2). Overlays of bright field and fluorescent images (right hand panels) show larvae morphology and IONP distribution. Fluorescence only images are on the left. Arrows indicate IONP accumulation. Diffuse red staining around the yolk sac close to the injection site is also seen. Representative image of 2 imaged embryos, 25 per group.

The images above (figure 5.15) show a few IONPs localised in the liver and heart, following the same pattern seen in other conditions. A few IONPs were also seen along the tail artery, however it is not clear whether these IONPs (figure 5.15 B) are in the tail artery or embedded in the muscle of that area. The images below (figure 5.16) show the localisation of 'naked' IONPs at 5 dpf when injected at a concentration of 1000  $\mu\text{g/ml}$ .

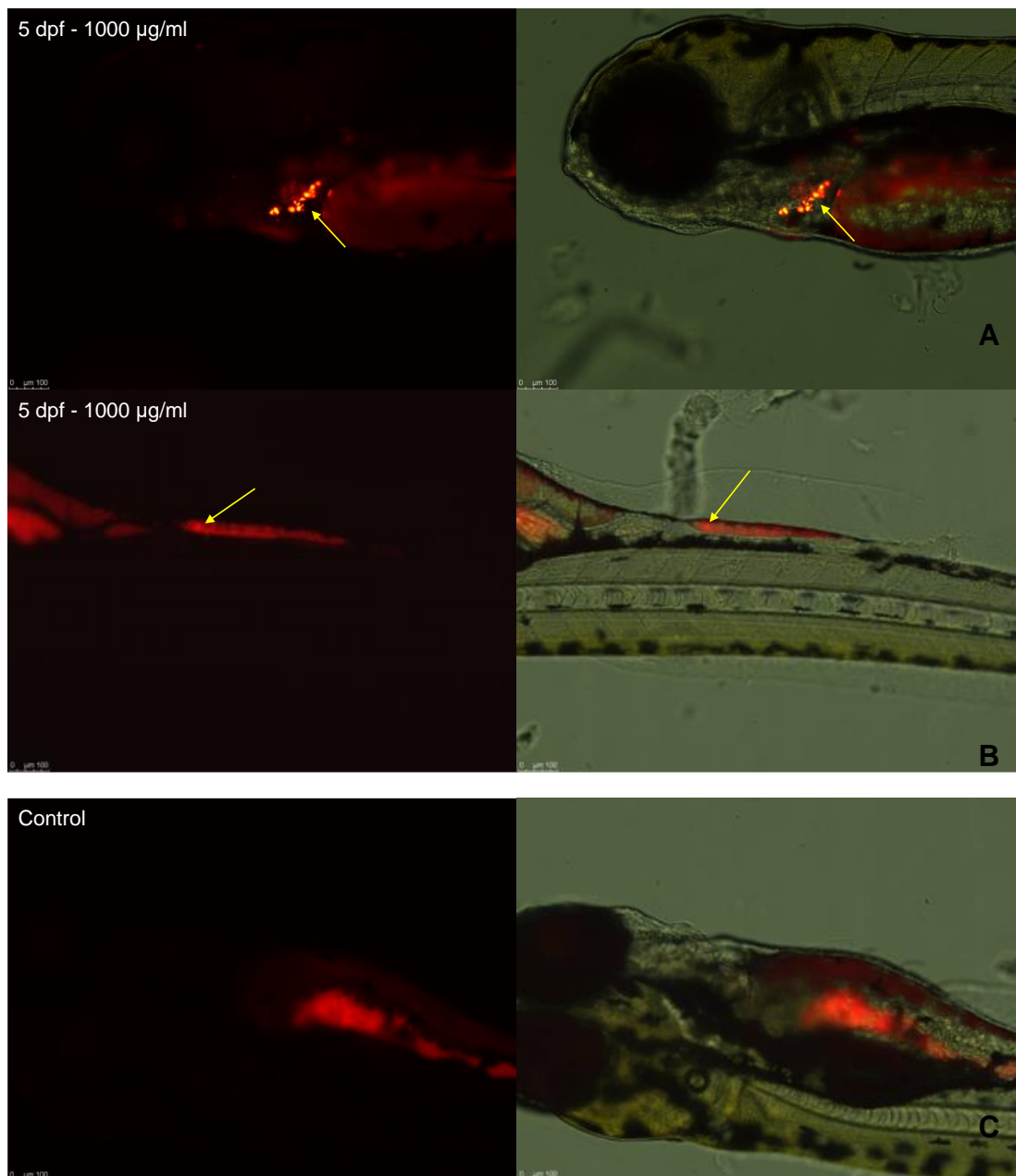


Figure 5.15. **Injected zebrafish larvae at 5 dpf.** The images above show zebrafish larvae imaged at 5 dpf using the Leica DMI8 microscope (20X objective). 'Naked' IONPs injected at a concentration of 1000  $\mu\text{g/ml}$  were found to be accumulated in the heart (A) and a few in the intestine (B) (figure 5.2). Control larvae were injected with PBS only (C). Overlays of bright field and fluorescent images (right hand panels) show larvae morphology and IONP distribution. Fluorescence only images are on the left. Arrows indicate IONP accumulation. Diffuse red staining around the yolk sac close to the injection site is seen also in the control animals indicating autofluorescence from the yolk sac proteins. Representative image of 2 imaged embryos, 23-25 per group.

The above images (figure 5.15) once again confirm the patterns previously seen where IONPs accumulate in the heart and along the excretory routes. The next question to be investigated was if macrophages are present or recruited at the sites where IONPs were seen to accumulate. With the aim of macrophage labelling, a high molecular weight dextran (MW = 2,000,000) fluorescently labelled with FITC was injected into the embryos at an early developmental stage. An earlier study showed that primitive macrophages from the ventral mesoderm can migrate to the yolk sac and to differentiate between ventral and dorsal macrophages, injection of a high molecular weight dextran into one of the blastomeres at the 16-cell stage (Herbomel, Thisse and Thisse, 1999) is a useful tool. Another study also successfully labelled macrophages using dextran in mouse models (Wang *et al.*, 2002).

In this study, to label macrophages in zebrafish embryos, two dextran injection methods were investigated; microinjection of dextran in the yolk sac at the 1-cell stage and microinjection of dextran in a blastomere at the 16-cell stage. The two injections methods were separately carried out and are discussed further below. Each experiment was carried out twice.

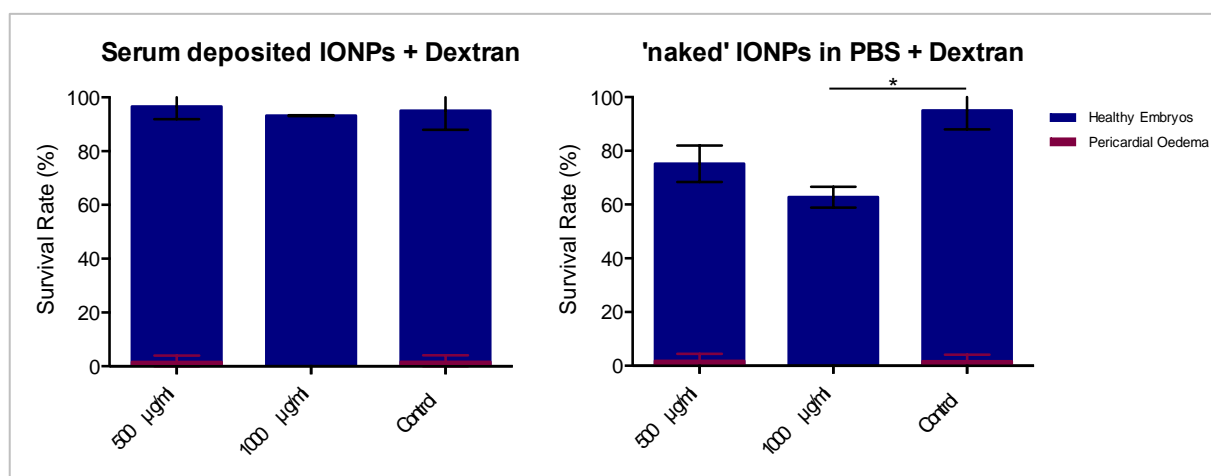


Figure 5.16. **Dextran injected in yolk sac.** The above graphs show the survival rates of zebrafish larvae at 5 dpf, following dextran microinjections at 0.2 hpf and IONPs microinjections at 2 dpf. Embryos injected with serum-deposited IONPs showed a better survival rate than those injected with 'naked' IONPs. The control larvae were injected with dextran in the yolk sac at 0.2 hpf, followed by PBS microinjections at 2 dpf. Results of two independent experiments are shown. Error bars show standard deviation. A one-way ANOVA test was carried out in GraphPad prism to determine statistical significance. Statistical significance was found between the control sample and 1000µg/ml sample for 'naked' IONPs.

The above graphs (figure 5.16) demonstrate a high survival rate in the larvae injected with dextran in the yolk sac and serum-deposited IONPs, with a low percentage of pericardial oedema seen. However, a lower survival rate was seen in the corresponding 'naked' IONPs injected larvae. This could suggest that the dextran microinjections into the yolk sac already exhibit a toxic effect on the embryos since a small percentage of control larvae, injected with only the dextran, also displayed characteristics of pericardial oedema, which was not seen in any control larvae (injected with PBS) prior to these experiments. One explanation for this could be the fact that up to 5 dpf, the embryos/larvae feed from the yolk sac, thereafter they independently feed. Thus, absorbing the dextran molecules along with their nutrients from the yolk sac could pose a certain level of toxicity, which is not translated to visible deformities, but when challenged with 'naked' IONPs (without deposition of serum proteins), may trigger a toxic effect in a dose-dependent manner. This effect is reduced by the presence of serum proteins deposited on the IONPs.

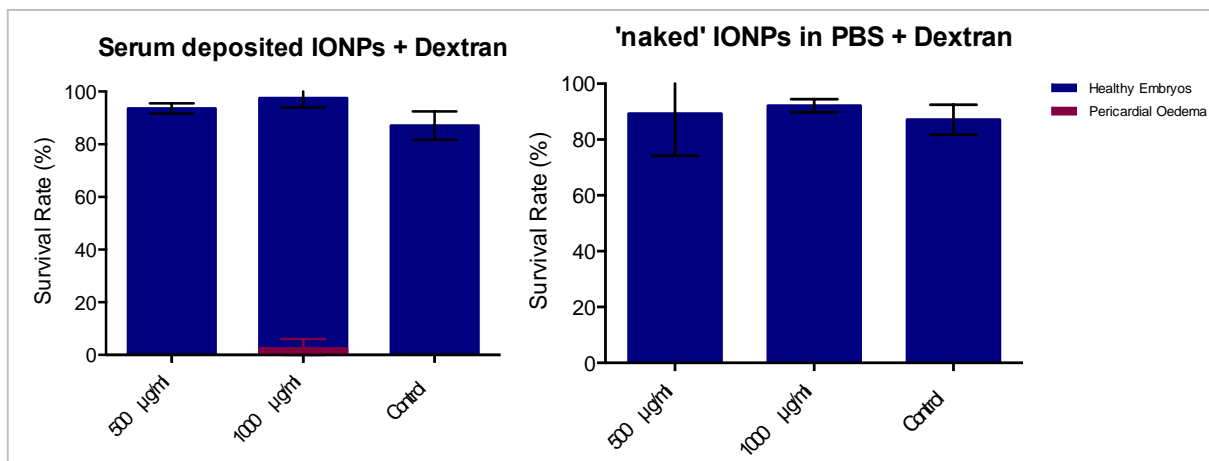


Figure 5.17. **Dextran injected in blastomeres.** The above graphs show the survival rates of zebrafish larvae at 5 dpf, following dextran microinjections at 1.5 hpf and IONPs microinjections at 2 dpf. The serum-deposited IONPs showed a similar survival rate to the 'naked' IONPs. The control larvae were injected with dextran into a blastomere at 1.5 hpf, followed by PBS microinjections at 2 dpf. Representative image of 2 imaged embryos. A one-way ANOVA test was carried out in GraphPad prism to determine statistical significance. No statistical significance was found between the different concentrations for survival rate or embryos with pericardial oedema.

The results (figure 5.17) show the survival rate of zebrafish larvae at 5 dpf following dextran microinjections in one of the blastomeres at 1.5 hpf (16-cell stage) and IONPs microinjections at 2 dpf. The serum-deposited IONPs larvae showed a similar survival rate observed in the previous results with dextran injections into the yolk sac, but a noticeable difference is observed with the 'naked' IONPs injected larvae, which showed a better survival rate than of those that had received dextran microinjections into the yolk sac. This indicates that dextran microinjections into the blastomeres are less harmful to the embryos than those into the yolk sac allowing for a better survival rate following subsequent injections at 2 dpf.

Confocal microscopy was used to obtain detailed information on IONP distribution in larvae injected with dextran and IONPs. The results (figures 5.18 - 5.25) show the same pattern of biodistribution of the IONPs as established previously, where they mostly accumulate in the pericardium, liver and excretory routes. In particular, the localisation of IONPs in relation to macrophages was studied in the images below.

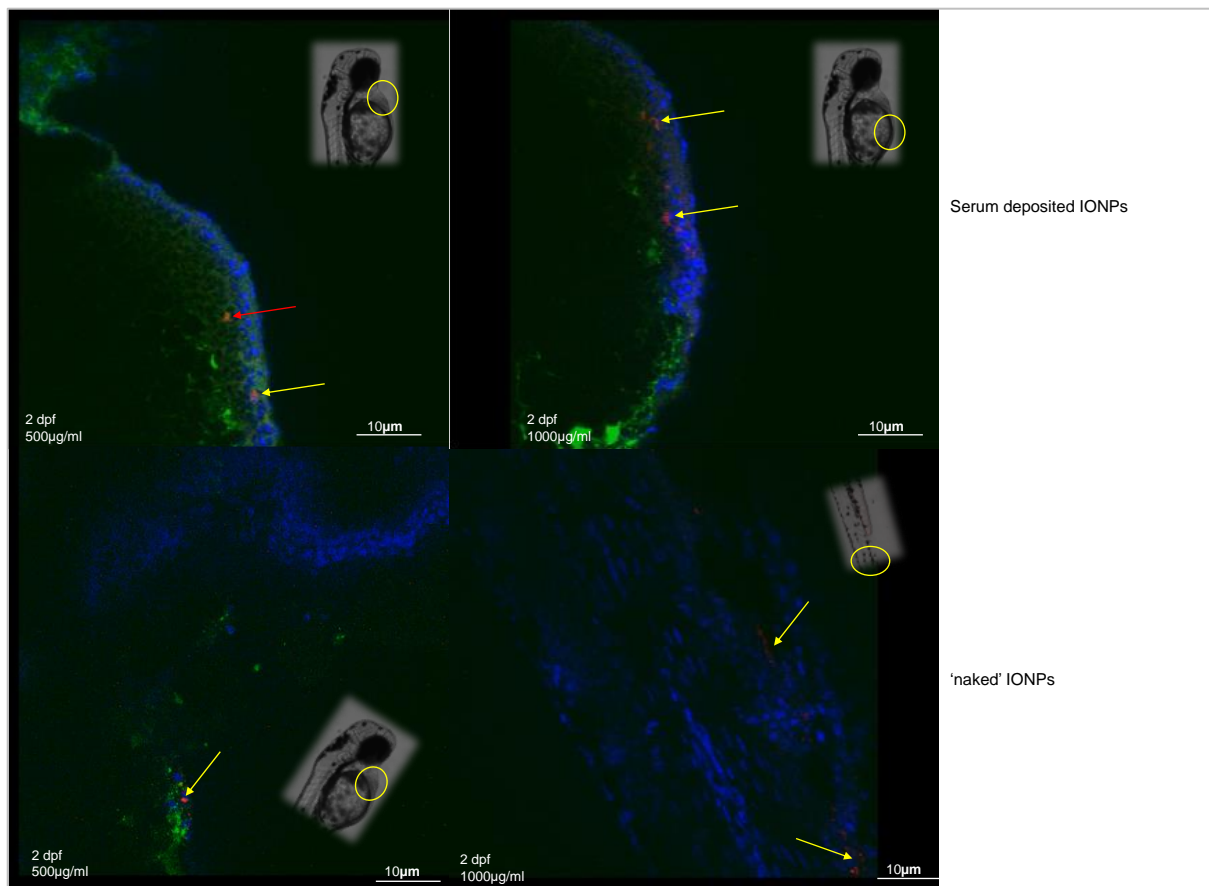


Figure 5.18. **Dextran injected in yolk sac.** The above images show the localisation of IONPs using confocal microscopy. Dextran 2,000,000 was injected into the yolk sac at the 1-cell stage followed by IONP injections (500ug/ml) (red) at 2dpf. Zebrafish embryos at 2 dpf, on the same day that IONPs microinjections were carried out, were fixed and stained with Hoechst 33342 to reveal cell nuclei (blue) before imaging with a *Nikon Eclipse TE2000-S Confocal Microscope* with a x60 oil lens. Yellow arrows point to IONPs and the red arrow shows likely colocalisation of dextran and IONPs. Images were taken at the positions indicated in the grey insets and single sections of a z-stack where IONPs were visible are displayed. Scale bar 10um. Representative image of 2 imaged embryos, 30 per group.

The above images (figure 5.18) show IONP localisation in 2 day old zebrafish embryos, on the same day of the IONPs microinjections (embryos were fixed 4 hours post injection, stained and imaged). The dextran 2,000,000 was injected at 1-cell stage (0.2 hpf) into the yolk sac. Dextran can be seen in the yolk sac and remained mostly contained within the yolk sac. Compared to 3 dpf (see images below figure 5.19), clusters of IONPs accumulation were not seen most likely because they had just been injected on the day through systemic delivery and IONPs being so small can only be seen when they accumulate in clusters.

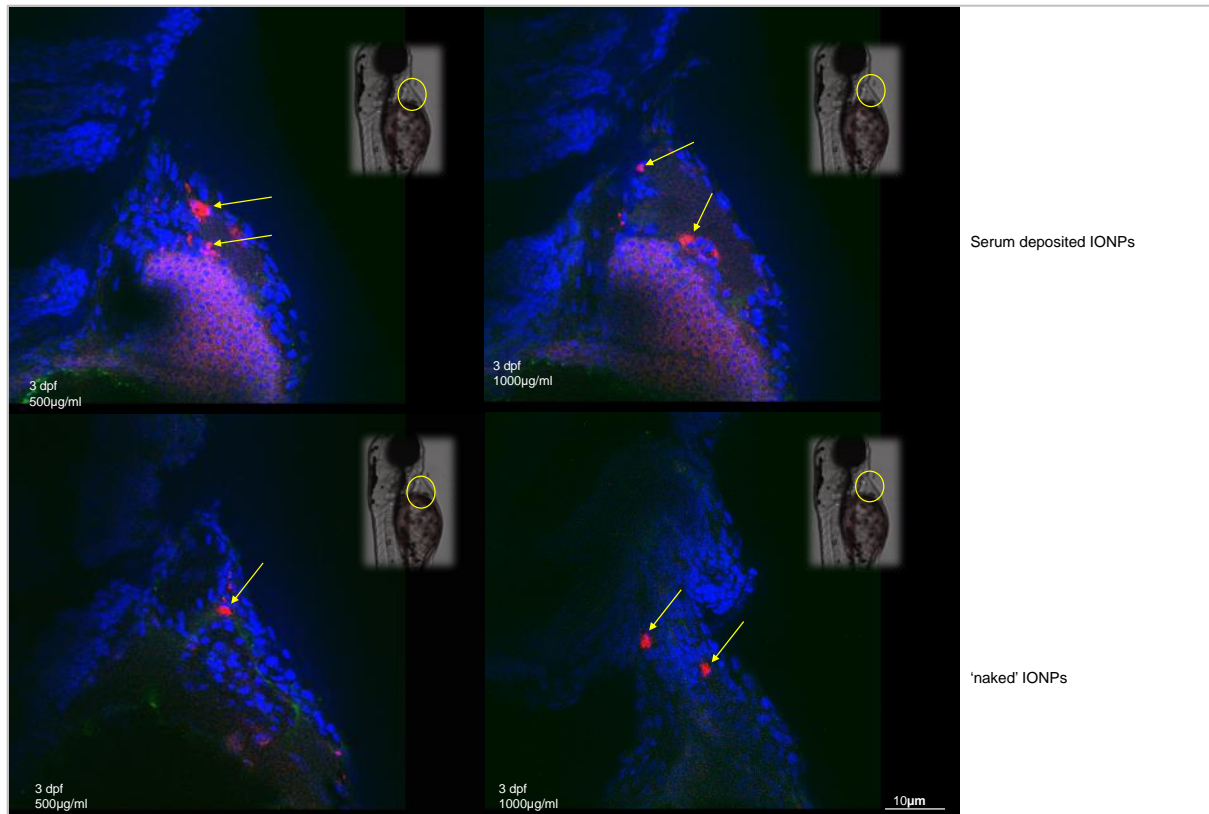


Figure 5.19. **Dextran injected in yolk sac.** The above images show the localisation of IONPs using confocal microscopy. Dextran 2,000,000 (green) was injected into the yolk sac at the 1-cell stage followed by IONPs (500ug/ml, red) injections at 2dpf. Zebrafish embryos at 3 dpf, one day after IONP microinjections were carried out, were fixed and stained with Hoechst 33342 to reveal cell nuclei (blue) before imaging with a *Nikon Eclipse TE2000-S Confocal Microscope* with a x60 oil lens. Yellow arrows point to IONP accumulations. Images were taken at the positions indicated in the grey insets and single sections of a z-stack where IONPs were visible are displayed. Scale bar 10um. Representative image of 2 imaged embryos, 28 per group.

The above images (figure 5.19) show accumulation of IONPs at 3 dpf mostly near the heart and liver. IONPs accumulate in clusters with no sign of successfully labelled macrophages outside the yolk sac as dextran was visible only within the yolk sac.

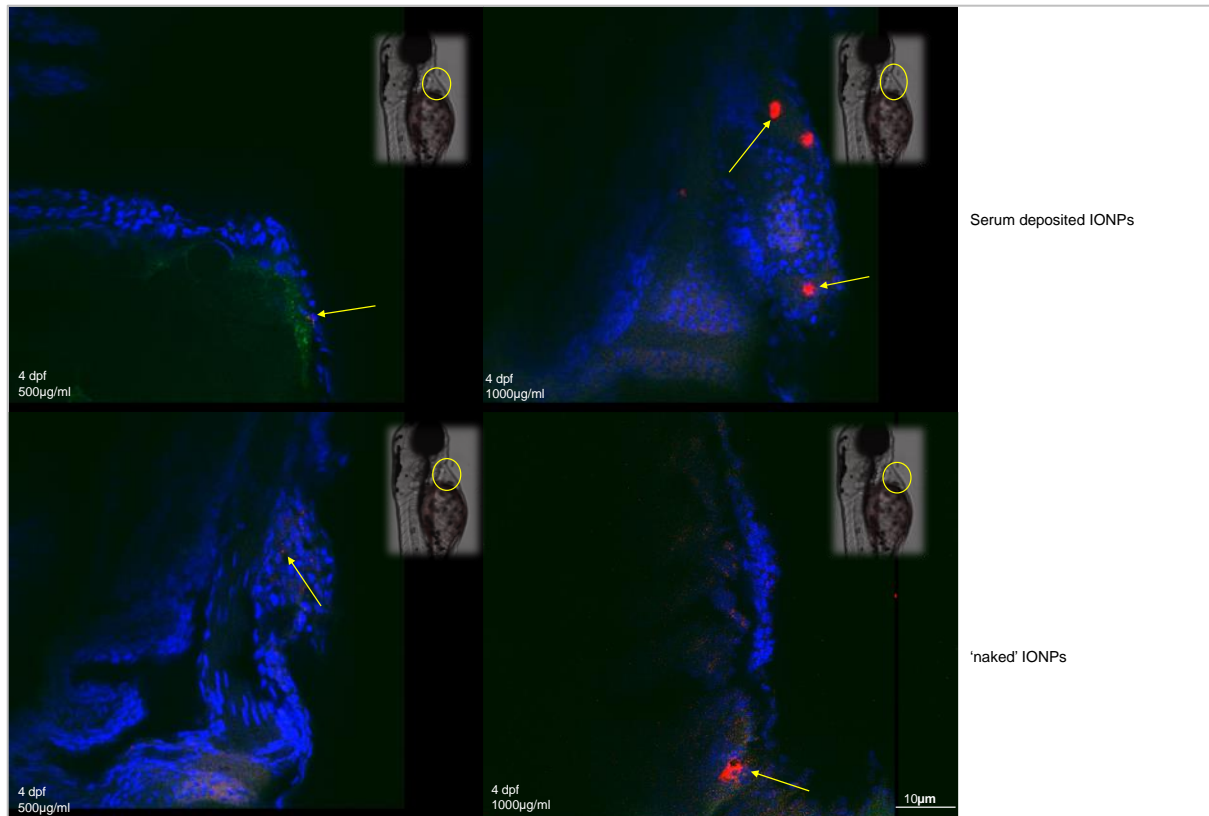


Figure 5.20. **Dextran injected in yolk sac.** The above images show the localisation of IONPs using confocal microscopy. Dextran 2,000,000 (green) was injected into the yolk sac at the 1-cell stage followed by IONPs injections (500ug/ml and 100ug/ml (red)) at 2dpf. Zebrafish embryos at 4 dpf were fixed and stained with Hoechst 33342 to reveal cell nuclei (blue) before imaging with a *Nikon Eclipse TE2000-S Confocal Microscope* with a x60 oil lens. Yellow arrows point to IONP clusters. Images were taken at the positions indicated in the grey insets and single sections of a z-stack where IONPs were visible are displayed. Scale bar 10um. Representative image of 2 imaged embryos, 27 per group.

At 4 dpf, similar IONP localisation patterns were observed in the pericardium area, for both concentrations of IONPs used independent of serum deposition. The next images below (figure 5.21) show the last time point of zebrafish larvae images, at 5 dpf.



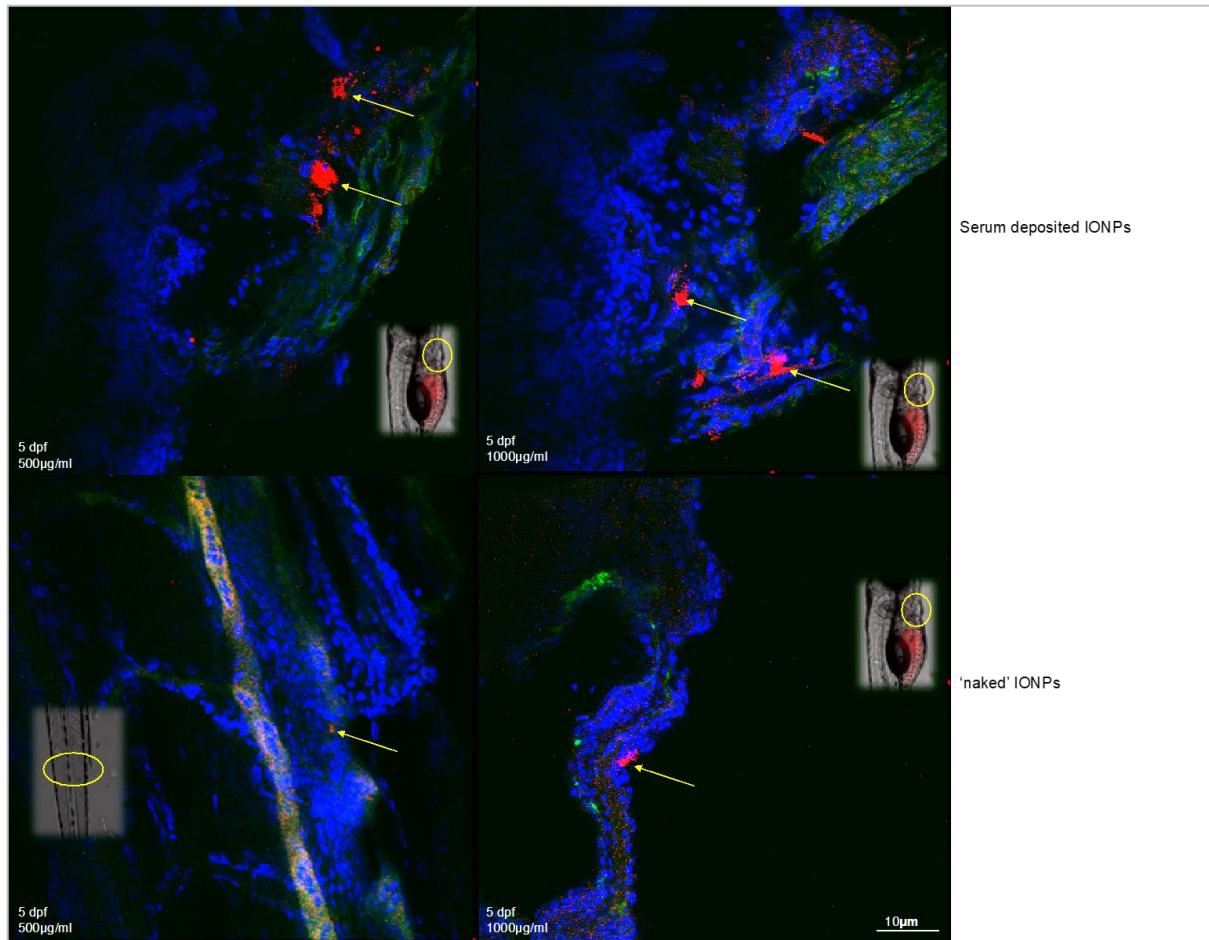


Figure 5.21. **Dextran injected in yolk sac.** The above images show the localisation of IONPs using confocal microscopy. Dextran 2,000,000 (green) was injected into the yolk sac at the 1-cell stage followed by IONPs injections (500ug/ml and 100ug/ml (red)) at 2dpf. Zebrafish embryos at 5 dpf were fixed and stained with Hoechst 33342 to reveal cell nuclei (blue) before imaging with a *Nikon Eclipse TE2000-S Confocal Microscope* with a x60 oil lens. Yellow arrows point to IONP clusters. Images were taken at the positions indicated in the grey insets and single sections of a z-stack where IONPs were visible are displayed. Scale bar 10um. Representative image of 2 imaged embryos, 30 per group.

IONP accumulation was again seen in the same area, with a small cluster seen near the cloaca (figure 5.21, bottom left), which indicates that these IONPs were very likely to be excreted shortly after. Injecting Dextran 2,000,000 into the yolk sac labelled some macrophages in and around the yolk sac, as expected as this shows that some primitive macrophages might have migrated to the yolk sac to differentiate, as stated by Herbomel, Thisse and Thisse (1999). Very little (figure 5.18) to almost no colocalisation was seen between IONPs and dextran, suggesting that the yolk sac macrophages are not recruited to sites of IONPs accumulation and remain in the yolk

sac. Instead, the IONPs remain in the heart or liver until they are excreted at a later stage. The images below show zebrafish larvae with Dextran 2,000,000 injected into the blastomere.

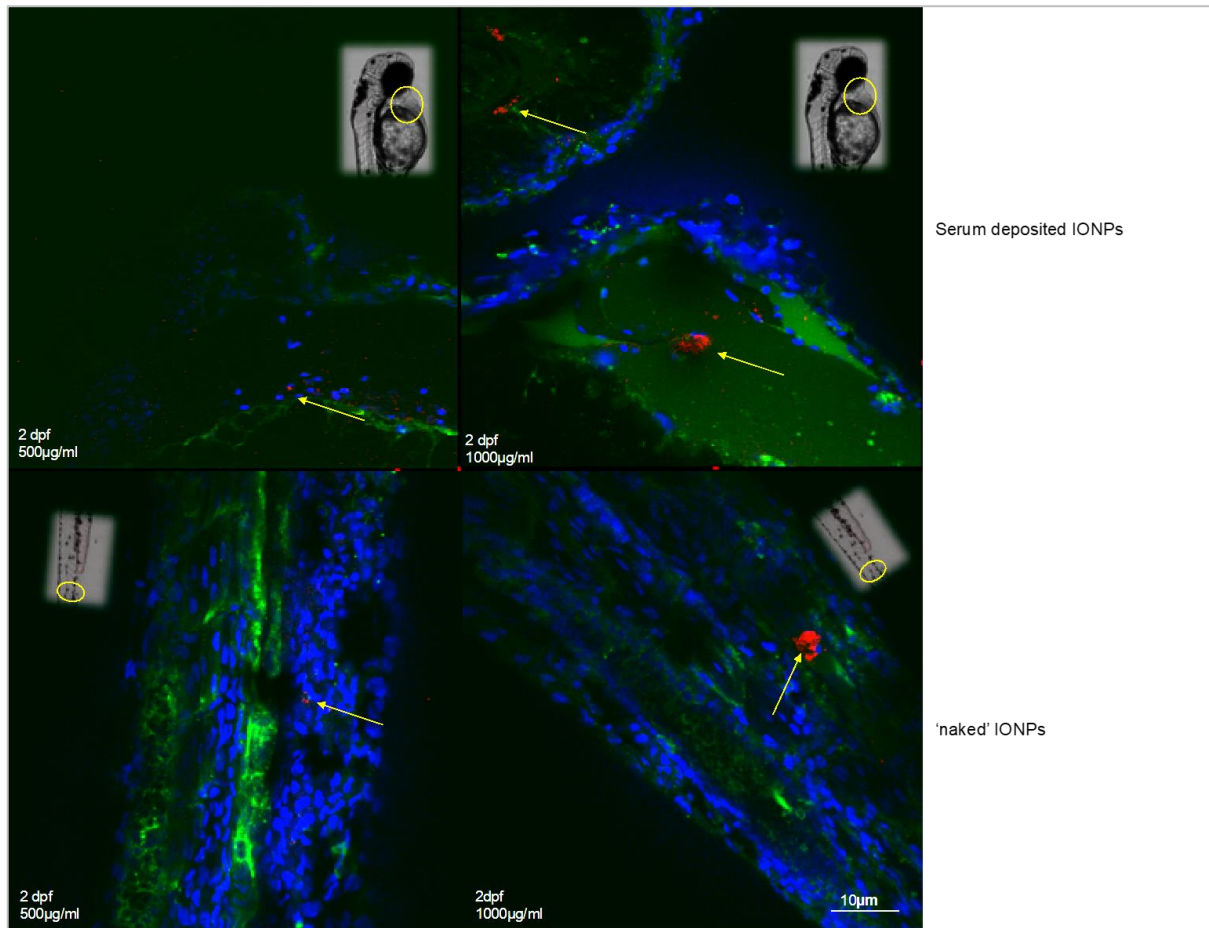


Figure 5.22. **Dextran injected in blastomere.** The above images show the localisation of IONPs using confocal microscopy. Dextran 2,000,000 (green) was injected into the blastomere at the 16-cell stage followed by IONPs injections (500ug/ml and 100ug/ml (red)) at 2dpf. Zebrafish embryos at 2 dpf, on the day of the IONP injections, were fixed and stained with Hoechst 33342 to reveal cell nuclei (blue) before imaging with a *Nikon Eclipse TE2000-S Confocal Microscope* with a x60 oil lens. Yellow arrows point to IONP clusters. Images were taken at the positions indicated in the grey insets and single sections of a z-stack where IONPs were visible are displayed. Scale bar 10um. Representative image of 2 imaged embryos, 29 per group.

The images above (figure 5.22) show IONPs localisation following IONPs microinjections on the same day. A few clusters can be seen accumulating in the pericardium and excretory routes in the tail.

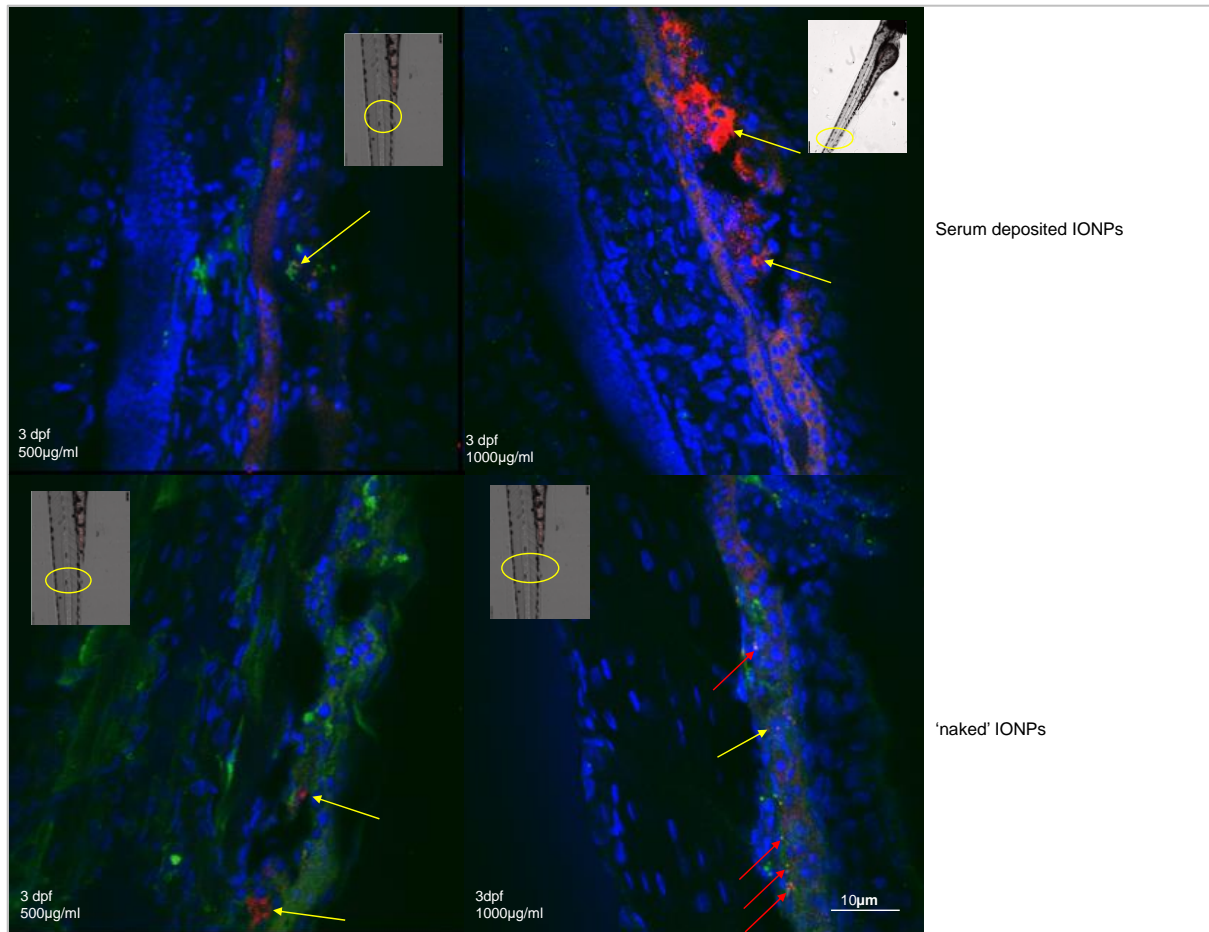


Figure 5.23. **Dextran injected in blastomere.** The above images show the localisation of IONPs using confocal microscopy. Dextran 2,000,000 (green) was injected into the blastomere at the 16-cell stage followed by IONPs injections (500ug/ml and 100ug/ml (red)) at 2dpf. Zebrafish embryos at 3 dpf were fixed and stained with Hoechst 33342 to reveal cell nuclei (blue) before imaging with a *Nikon Eclipse TE2000-S Confocal Microscope* with a x60 oil lens. Yellow arrows point to IONP clusters and red arrows indicated colocalization of IONPs with dextran 2,000,000. Images were taken at the positions indicated in the grey insets and single sections of a z-stack where IONPs were visible are displayed. The top left image does not show colocalisation however, shows the recruitment of macrophages around the IONPs. The top right image shows significant accumulation of IONPs in the caudal vein in the tail IONPs were still seen accumulated near the heart and liver. Scale bar 10um. Representative image of 2 imaged embryos, 30 per group.

From 3 dpf, more IONPs start to be visible in the tail showing that the embryo is likely processing the IONPs to be excreted. IONPs were still seen in the pericardium and liver at this stage, where they may remain for longer before excretion. Some colocalisation between IONPs and dextran was also seen, suggesting successful macrophage labelling (denoted by red arrows in the above figure).

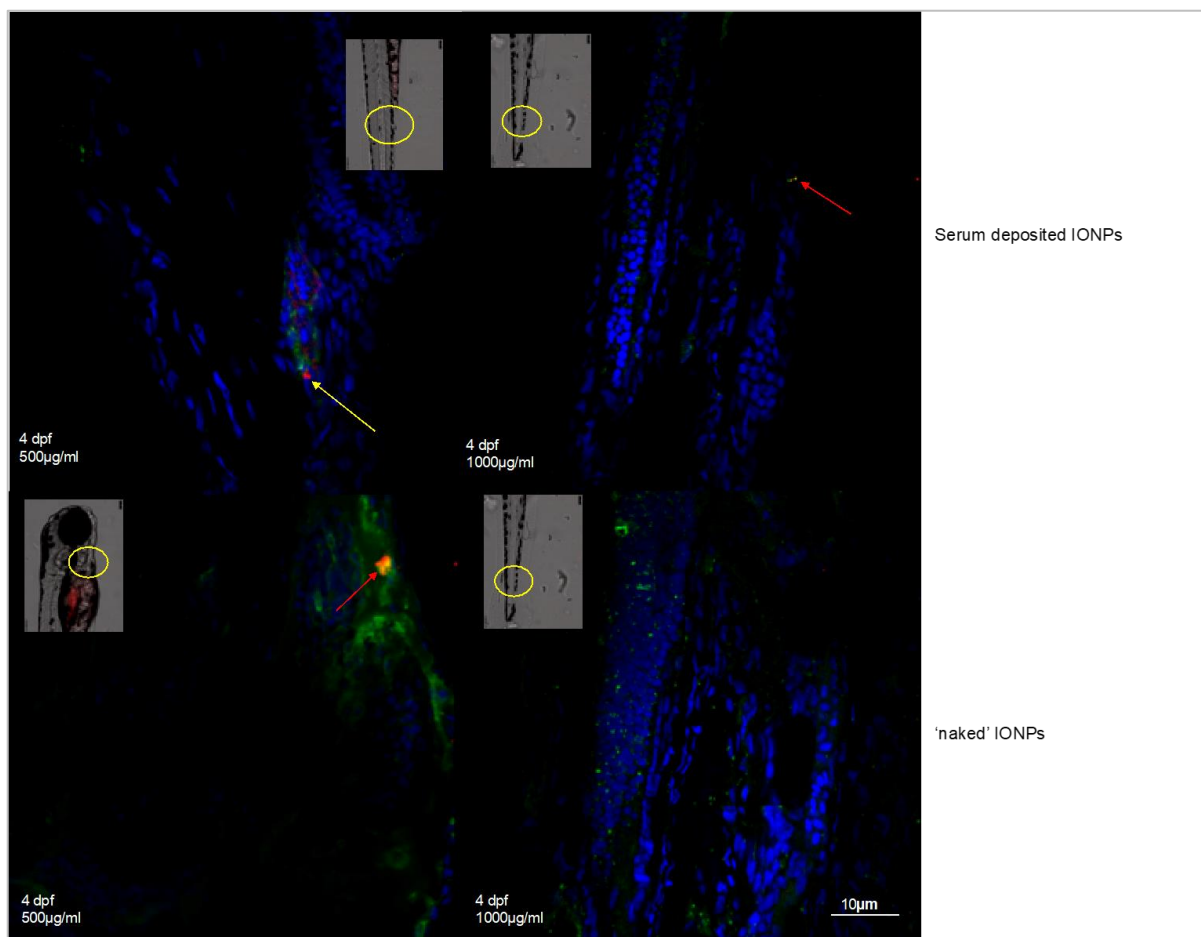


Figure 5.24. **Dextran injected in blastomere.** The above images show the localisation of IONPs using confocal microscopy. Dextran 2,000,000 (green) was injected into the blastomere at the 16-cell stage followed by IONPs injections (500ug/ml and 100ug/ml (red)) at 2dpf. Zebrafish embryos at 4 dpf were fixed and stained with Hoechst 33342 to reveal cell nuclei (blue) before imaging with a *Nikon Eclipse TE2000-S Confocal Microscope* with a x60 oil lens. Yellow arrows point to IONP clusters and red arrows indicated colocalization of IONPs with dextran 70,000. Images were taken at the positions indicated in the grey insets and single sections of a z-stack where IONPs were visible are displayed. Scale bar 10um. Representative image of 2 imaged embryos, 30 per group.

The above images (figure 5.24) show 4 day old zebrafish larvae imaged following IONPs microinjections at day 2 dpf. Colocalisation between IONPs and dextran can be seen in the pericardium in figure 5.24 (bottom left). Less IONP accumulation is seen here compared to the 3 dpf zebrafish larvae (figure 5.23).

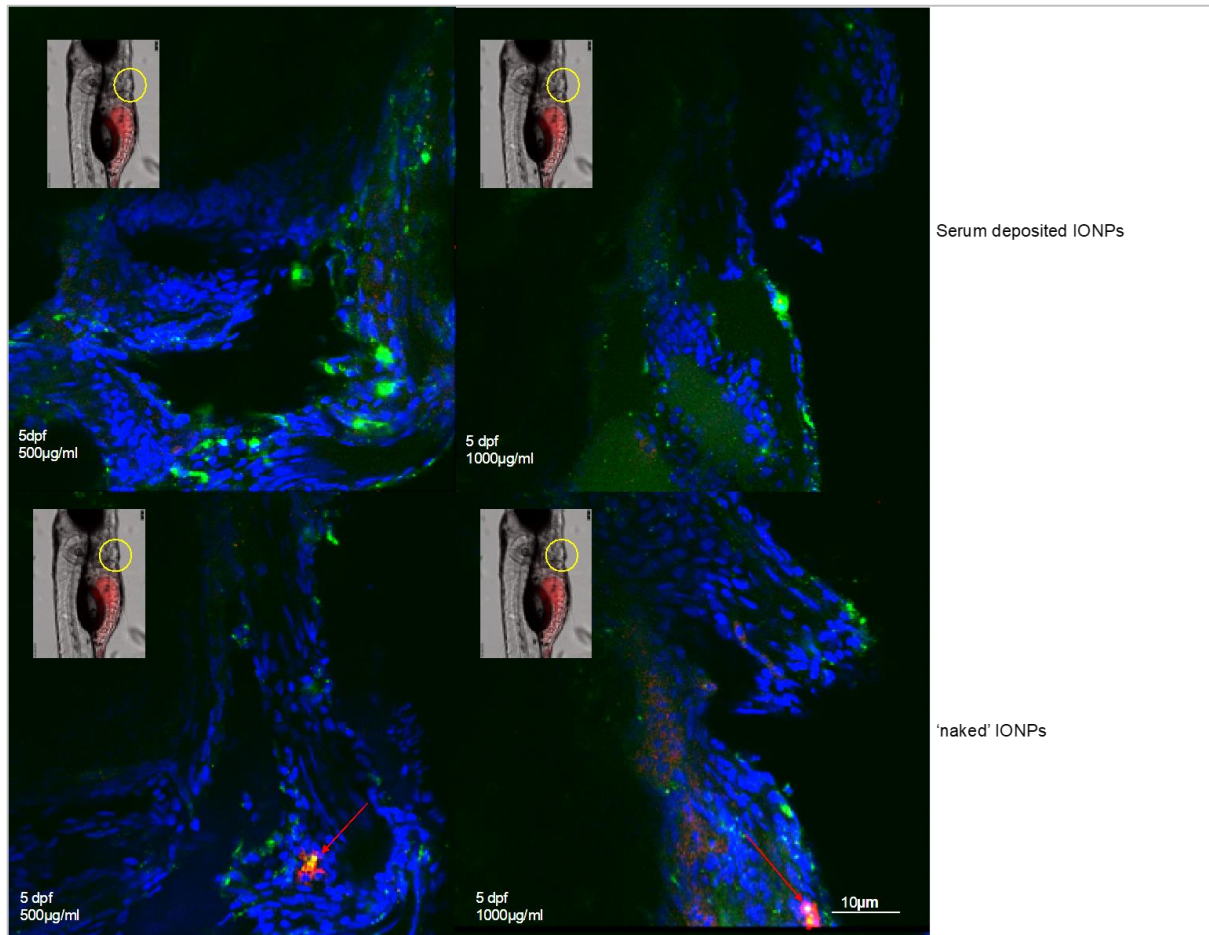


Figure 5.25. **Dextran injected in blastomere.** The above images show the localisation of IONPs using confocal microscopy. Dextran 2,000,000 (green) was injected into the blastomere at the 16-cell stage followed by IONPs injections (500ug/ml and 100ug/ml (red)) at 2dpf. Zebrafish embryos at 5 dpf were fixed and stained with Hoechst 33342 to reveal cell nuclei (blue) before imaging with a *Nikon Eclipse TE2000-S Confocal Microscope* with a x60 oil lens. Yellow arrows point to IONP clusters and red arrows indicated colocalization of IONPs with dextran 70,000. Images were taken at the positions indicated in the grey insets and single sections of a z-stack where IONPs were visible are displayed. Scale bar 10um. Representative image of 2 imaged embryos, 30 per group.

The above images (figure 5.25) show strong colocalisation between IONPs and dextran, suggesting that macrophages may have been recruited to the sites of IONP accumulation in the pericardium. The results overall show that macrophage labelling was much more successful by injecting dextran into the blastomere compared to the yolk sac. Although colocalisation between dextran and IONPs was seen in some cases, overall no significant colocalisation between macrophages and IONPs could be observed, suggesting phagocytosis by macrophages was not a major route of clearance for IONPs.

### 5.3 Discussion

The aim of this study was to investigate the biosafety and biodistribution of IONPs using zebrafish embryos as an animal model of innate immunity. The data obtained suggests that although the survival rates are relatively high, there are some toxicity issues to look out for such as pericardial oedema, which was seen at least once in most experiments conducted. Pericardial oedema is a typical manifestation of defective cardiac function in zebrafish embryos (Miura and Yelon, 2011). Hence it is important to highlight the developmental defects relating to cardiac function in response to IONPs, even if the overall risk of developing pericardial oedema was relatively low.

To investigate the effect of serum proteins on the biodistribution of IONPs, serum-deposited and 'naked' IONPs were studied. Even though the sites of IONP accumulation were very similar for both, there were some signs of different residence times in the zebrafish embryos. In some cases, 'naked' IONPs were seen near the cloaca and other excretory routes a day earlier (at 4 dpf) than serum-deposited IONPs (at 5 dpf). This suggests that serum deposition on IONPs may play a role in their uptake and distribution. Despite the slightly different clearance times, both types of IONPs accumulate in the pericardium and the liver where they may remain before being excreted. Additionally, it is important to note that the resolution of the microscopy would not allow for individual IONPs to be visualised and hence IONPs would only be seen if they are in small or large clusters. Different microscopy techniques such as TEM or SEM can be used to image samples at a much higher magnification where NPs can be seen. The residence time of IONPs in zebrafish larvae could be further studied by taking samples of the surrounding medium of the embryos/larvae at regular time points to measure the presence of IONPs in the medium either through

microscopy or by isolating the IONPs in a magnetic field before quantification. The accumulation of IONPs in the pericardium as seen in our results is quite new and at the time of writing, there were no published literature that reported similar observations with IONPs in zebrafish embryos. The mortality rate seen in our studies may not represent a true assessment of cardiotoxicity as zebrafish embryos do not need a functioning cardiovascular system to survive (Miura and Yelon, 2011). Exposure to certain chemicals including NPs can cause cardiotoxicity in zebrafish. The heart rate may be affected, thus inadequately pumping blood around the body and if severe, it can lead to cardiac muscle dysfunction in zebrafish (Zakaria *et al.*, 2018). Furthermore, gold and silver NPs were shown to change the heart morphology in zebrafish at high concentrations (Zakaria *et al.*, 2018). Thus, it is important to study any effects of cardiotoxicity following exposure to IONPs beyond 5dpf. However studies carried out in different animal models have shown that the accumulation of NPs in the pericardial space did not pose a safety concern and did not affect heart rate or cardiac function in mice (Kermorgant *et al.*, 2019).

Functional innate immunity, consisting of immune cells, chemokines and cytokines similar to those present in humans, is established in zebrafish embryos at 2 dpf (Cha *et al.*, 2018). Thus, inflammation in response to IONPs in zebrafish embryos/larvae can be studied by generating cytokine profiles using qPCR. For example, in different fish, gilthead sea bream (*S. aurata*), gold NP exposure after 4 days resulted in upregulation of pro-inflammatory cytokines such as TNF- $\alpha$  and IL-1 $\beta$  (Teles *et al.*, 2017). Another study showed that palmitate (a fatty acid) triggers an inflammatory response in zebrafish embryos which was characterised by the upregulation of NF- $\kappa$ B, IL-1 $\beta$ , TNF- $\alpha$  and COX-2 (Cha *et al.*, 2018). Taken together, these results demonstrate that exposure to NP can generate an inflammatory response in fish,

which can be measured using cytokines as biomarkers. To further study the effects of serum proteins adsorbed on IONPs, cytokine expression levels could be studied at 4 dpf and 5 dpf to identify any inflammatory responses triggered.

As mentioned in section 5.1, zebrafish and humans have a lot in common, including metabolism of drugs by the liver, hence zebrafish are promising models in the study of drug toxicity (Vliegenthart *et al.*, 2014). When designing nanotherapeutics, circulation time is an important factor to be considered. For instance, if nanotherapeutics designed for the treatment of cancer have a low circulation time, it is deemed undesirable as there is a decreased chance of nanotherapeutic accumulation at the target tumour sites (Dal *et al.*, 2020). Reduced nanoparticle circulation times in zebrafish embryos can be a direct consequence of uptake of NPs by macrophages (Dal *et al.*, 2020). Hence the next subject of investigation was to label macrophages in zebrafish embryos using a high molecular weight dextran and investigating colocalisation between dextran and IONPs, which would give a good indication of IONP uptake by macrophages. One study demonstrated the successful labelling of dextran coated NPs (13nm) in mouse models to study tumour associated macrophages and the same group also showed that dextran coated IONPs have higher macrophage avidity *in vitro* (Keliher *et al.*, 2011). Our study does not employ the use of dextran coated IONPs, however due to the fact that macrophages readily internalise dextran molecules, we aimed to use dextran as a fluorescent imaging probe *in vivo*. Another study successfully labelled tumour-associated macrophages in mice by injecting Texas red-dextran and macrophages were successfully visualised through microscopy due to their ability to phagocytose the injected dextran (Wyckoff *et al.*, 2007). Although only a handful of published literature have employed this method of macrophage labelling, other researchers have used other fluorescent imaging probes



for macrophage labelling such as GFP (green fluorescent protein), mCherry and EGFP, amongst others, where GFP seems to be the most commonly used (Li and Liu, 2018).

Our results demonstrate some successful labelling of macrophages with dextran when it was injected into one of the blastomeres at the 16-cell stage (1.5 hpf). However, the majority of IONPs did not colocalise with dextran indicating absence of phagocytosis of IONPs at the time points investigated. However, we cannot rule out that the IONP concentration in tissue macrophages was too low for detection. Although it is not clear if Kupffer cells (liver macrophages) of the embryos were also successfully labelled by dextran, different methods of macrophage labelling can be carried out to confirm our results. A study has shown that murine Kupffer cells have high dextran-endocytic activity using a dextran of molecular weight 40,000 (Movita *et al.*, 2012). Furthermore, to reinforce our results, the experiment can be repeated using other methods of macrophage tracking to rule out the possibility of dextran uptake by other innate immune cells and investigate whether Kupffer cells are labelled by those methods. For example, large doses of live fluorescent bacteria can be injected into the embryos and imaged to visualise phagocytosis by macrophages (Herbomel, Thisse and Thisse, 1999). Alternatively, a transgenic zebrafish strain, such as MPEG1.4:mCherry zebrafish, which expresses the macrophage-expressed gene 1 (MPEG1) labelled with mCherry can be used and macrophages can be visualised using fluorescence microscopy (van Pomeran *et al.*, 2019). Taking our study forward, the IONPs used in could be pre-coated with the dextran prior to injecting into embryos to observe differences in biodistribution and macrophage labelling. To further study whether IONP uptake occurs at different time points to those studied here, the embryos/larvae can be imaged at more regular time points. In our study, confocal microscopy was mainly

used to obtain images of the cross-section (by taking a z-stack) that were analysed to establish where IONPs accumulated in the embryos. However, one disadvantage of this technique was that it is time consuming and therefore allows fewer embryos/larvae to be analysed.

As mentioned previously, nanoparticle size and shape can greatly influence the bioavailability and toxic effects induced by IONPs. For example, gold NPs of size 60nm were found to be phagocytosed and efficiently cleared from the body by macrophages in zebrafish embryos (van Pomeran *et al.*, 2019). This is different to what our results suggest and one of the main reasons for this difference could be the size of IONPs used (100 nm). Another study also showed faster clearance of nanospheres compared to rod-shaped NPs, the nanospheres were found to accumulate mostly in the liver compared to NPs of different shapes (Truong *et al.*, 2015).

In this study, we have successfully shown the biodistribution of IONPs in zebrafish embryos and larvae up to 5 dpf, as well as any developmental defects induced by IONPs toxicity. Due to a limited amount of IONPs available, only a few concentrations, up to 1000 µg/ml, were studied. Higher IONPs doses to further study dose-dependent toxicity of IONPs can add to our current findings. Furthermore, some initial experiments consisted of 1 hour incubation time of IONPs with serum compared to other experiments where IONPs were incubated with serum overnight. Although, experiments were carried out to ensure that the protein amount remains unaffected on the surface of the IONPs, protein corona is a dynamic structure that is subject to change over time, which may influence their biodistribution *in vivo*. Another limitation to this study was that the zebrafish larvae were only monitored and imaged up to 5 dpf due to the lack of a project license. However, this study has a promising scope for further studies of IONP related toxicity and developmental defects. Coupled with

behavioural studies (swimming, feeding, response to stimuli) beyond 5 dpf into the juvenile and adult stage would be beneficial to contribute to our IONPs toxicity studies.

---

## **6. General Discussion**

---

Recent decades have seen a sharp increase in NP research especially for therapeutic and diagnostic purposes with growing optimism of breakthrough discoveries in the field of targeted therapy. NPs, in conjunction with therapeutic drugs, can change pharmacokinetic properties resulting in a greater therapeutic efficiency, controlled drug release and reduced side effects (Abdifetah and Na-Bangchang, 2019). NPs as drug delivery carriers are of interest in the treatment of diseases such as cancer, where patients can benefit greatly from targeted therapy. Despite being such promising agents, many NPs based drug delivery strategies are still being investigated due to toxicity concerns. Before the design and administration of NP-based drug carriers, it is vital to investigate and understand the biosafety of NPs so that strategies to overcome any toxicity issues can be developed.

Administered NPs will inevitably come into contact with serum proteins and cells of the innate immune system such as macrophages and understanding these interactions and effects is crucial to determine NP toxicity. In this thesis we studied the toxicity of IONPs on a cellular level as well as a whole organism level. We first investigated the intracellular uptake and fate of 100nm IONPs in macrophages, which seemed to localise in the late endosomes/lysosomes for likely degradation after 24 hours and also showed evidence of endocytosis by macropinocytosis. To study the immunotoxicity of IONPs, cytokines were used as biomarkers of inflammation. Transcriptome analysis was also used to identify differentially expressed genes that relate to the innate immune system to identify changes in gene expression in response to IONP exposure that can lead to unwanted pathologies. Finally, we used zebrafish embryos as a model organism to further study toxic effects of IONPs on the innate immune response in a physiological setting.

We first set out to investigate the intracellular uptake and fate of IONPs in macrophages. Our results show that serum deposition on IONPs, forming a 'protein corona', enhances the uptake of IONPs compared to 'naked' IONPs without adsorbed serum proteins. This suggests that endocytosis of serum deposited IONPs could be receptor-mediated. Studies have shown that the presence of a protein corona on NPs can result in receptor mediated endocytosis. For example, nanoceria (CeO<sub>2</sub> NPs) deposited with a protein corona were shown to be taken up after interaction with specific receptors through clathrin-mediated endocytosis (Mazzolini *et al.*, 2016). Although serum deposition may play a role in uptake patterns seen, the intracellular fate of IONPs did not seem to depend on the presence of a protein corona since there were no obvious differences in the localisation of serum-deposited IONPs and 'naked' IONPs in our results. Although, differences in uptake and colocalisation of serum-deposited IONPs with Rab 7, seen between human serum and mouse serum samples, show evidence that the IONPs with different serum coatings may be trafficked differently. Recent studies have shown the formation of an intracellular protein corona whereby intracellular proteins adsorb on the surface of NPs (Qin *et al.*, 2020) which can affect the intracellular trafficking of NPs, thus possibly resulting in a similar intracellular fate irrespective of the presence of an extracellular protein corona. Our results also show differences in uptake patterns when human serum or mouse serum proteins are adsorbed to the IONP surface. This indicates that specific differences between the two sera played a role in mediating the uptake of IONPs into the cells. A study has shown that different serum compositions in the protein corona can affect the endocytic pathways of NPs, irrespective of size and cell type (Francia *et al.*, 2019).

We also used different sized dextrans as markers of endocytosis, which showed strong evidence of IONP uptake by macropinocytosis at 24 hours. However, this result differed when mouse serum was adsorbed onto the IONPs, again suggesting that the different serum compositions can affect endocytosis. Furthermore, studies have shown that dextran coated superparamagnetic iron oxide nanoworms (SPOI NW) activated complement in human serum via the alternative and lectin pathways whereas the same nanoworms activated complement via the lectin pathway in mouse serum (Wang *et al.*, 2016). This could explain the differences seen in our results using dextran as endocytic markers. When IONP surface was deposited with human serum, strong colocalisation with dextran and uptake of IONPs was seen. For these experiments, veronal buffers were not used so we were unable to distinguish between the classical or complement pathways. Hence, as the existing literature above suggests, it is most likely that proteins associated with the alternative pathway were adsorbed onto the IONPs resulting in their uptake and the colocalisation seen. On the other hand, when IONP surfaces were deposited with mouse serum, different veronal buffers (DGVB<sup>++</sup> and EGTA) were used to favour adsorption of complement proteins of the classical and alternative pathways respectively. Based on the study carried out by Wang *et al.* (2016), and assuming that the IONPs are likely to activate complement in mouse serum via the lectin pathway could explain the decrease in IONP uptake observed. Although the lectin pathway can also be activated using DGVB<sup>++</sup>, it is believed that the classical pathway will be preferably activated with this buffer since lectin pathway activation requires the presence of higher serum concentrations (Okroj *et al.*, 2012). To further study this effect seen, a cytokine profile associated with different uptake mechanisms could be investigated to link the use of different sera with different endocytic pathways which can provide further insight on the uptake and

intracellular trafficking of these IONPs and cellular responses. Furthermore, cellular fractionation techniques can also be investigated to isolate and separate organelles following treatment with IONPs to confirm our results that suggest accumulation in late endosomes/lysosomes.

We have seen that the presence and composition of a protein coating on IONPs can have different effects on the uptake of IONPs. However, to see how this translates on an immunotoxic level and what cytokines the macrophages may secrete as an inflammation response upon exposure to IONPs, we used common pro-inflammatory and anti-inflammatory cytokines as biomarkers of inflammation reactions. Upregulation of pro-inflammatory cytokines such as IL-1 $\beta$  and IL-16 was most altered when the cells were exposed to 'naked' IONPs in EGTA buffer. Furthermore, through gene ontology analysis, the 'naked' IONPs in EGTA buffer sample showed upregulation of a significant number of genes involved in inflammatory responses. These results strongly suggest that the hydrophilic starch coating on the IONPs in conjunction with EGTA buffer stimulates a significant inflammatory response that is not seen with the other samples. This effect could be due to possibly the calcium chelating agent EGTA removing bound ions from the starch, which could alter its structural properties so that is a 'red flag' for the cell triggering an inflammatory response. EGTA is a commonly used metal-chelating agent and clinically used in patients with metal poisoning due to its affinity to bind metal ions (Finnegan and Percival, 2015). This raises the question whether it is able to bind to the iron part of the IONPs causing a displacement in the ions, resulting in cytotoxicity in the absence of a protein corona on the IONPs. Additionally EGTA is known to have a high binding affinity for Fe<sup>3+</sup> (García-Casal, Leets and Layrisse, 2004), which does make our



hypothesis stronger, however the reactions with the hydrophilic starch coating is still unclear and not well characterised. Nevertheless, our data does provide evidence that there are some interactions between the starch coating on IONPs and components of EGTA buffer, which needs further investigating.

Unlike the 'naked' IONPs in EGTA buffer, for both mouse serum deposited IONPs samples less genes associated with inflammatory responses were identified in the gene ontology analysis. Instead, upregulation of IL-10, an anti-inflammatory cytokine, was observed suggesting a suppressed macrophage activity. Hence, this could be a plausible explanation of why lower IONP uptake was seen in experiments with these IONPs (chapter 3). IL-10 was also upregulated by the 'naked' IONPs in DGVB<sup>++</sup>, which was also associated with lower IONP uptake (chapter 3.3.1).

Gene ontology investigation identified other pathways that were upregulated in addition to the innate immunity response related ones. However, analysis of these pathways is beyond the scope of this thesis. Therefore, the data presented here is only part of the genotoxic effects exhibited by IONPs and other pathways should be explored to fully understand the effects of IONPs on a cellular level, as this will contribute to the understanding of the biosafety of IONPs to be used in a physiological setting. Furthermore, due to costs, RNA-seq was not carried out on the samples that were exposed to human serum deposited IONP but it would be beneficial to sequence these samples to fully understand the differences observed between human serum and mouse serum complement activation, as laid out in chapter 3.

As part of the immunotoxicity studies, zebrafish embryos up to 5dpf were used to assess the toxicity of IONPs in a whole organism model. We have successfully demonstrated the biodistribution of IONPs in the larvae through microscopy and also successfully labelled macrophages using a high molecular weight dextran. Low colocalisation of IONPs and dextran suggested that the IONPs were not phagocytosed at the time points investigated. They were rather either cleared from the body, accumulated in the liver for likely clearance at a later stage or accumulated in the pericardium. The results showed a low mortality rate overall, although some larvae displayed symptoms of pericardial oedema, which is an indication of abnormal cardiac function. One of the main limitations of this project was that the embryos were only studied up to 5dpf, and although some toxicity was seen in the cardiovascular system, it may not translate into a true mortality rate as a result of IONPs toxicity since zebrafish embryos do not need a functioning cardiovascular system to survive (Miura and Yelon, 2011). Thus, for further studies of IONP toxicity in zebrafish embryos, it is important to study the larvae beyond 5dpf. Additionally, at 5df, the larvae still retained IONPs, hence it would be beneficial to study the residence times of IONPs beyond 5dpf. Moreover, IONP toxicity can also be assessed at a molecular level through qPCR reactions. For instance, a study used specific biomarker genes for metal toxicity, oxidative stress and inflammation reactions to assess toxicity of silver NPs in zebrafish embryos (Olasagasti *et al.*, 2014).

The IONPs studied in this thesis had a 100nm diameter and a hydrophilic starch coating around the magnetite core. It is well known that different sizes, shapes and chemical properties of NPs influence their uptake in cells and their immunotoxicity (Hoshyar *et al.*, 2016). For instance, a study showed that different shapes of gold

nanomaterials were internalised in different amounts in RAW264.7 cells because they were internalised through different endocytic pathways (Xie *et al.*, 2017). Furthermore, in the development of therapeutic and diagnostic approaches, the size of NPs can greatly influence their half-life in blood circulation, specific targeting, tumour penetration as well as cellular uptake as discussed previously (Hoshyar *et al.*, 2016). The positive uptake of IONPs seen in macrophages could be exploited in future to target tumour-associated macrophages in the tumour microenvironment to increase the efficacy of new cancer immunotherapies. Our results also show the accumulation of IONPs in lysosomes which can be exploited to make the IONPs a favourable drug delivery vehicle for targeted drug delivery to lysosomes where the low acidic pH feature can be employed to release their content.

Additionally, the cytokine profiles produced in chapter 4, in particular IL-10, could be studied as an immunomodulatory molecule when designing new drug delivery vehicles in order to suppress/avoid unwanted recognition by immune cells. To further assess toxicity of IONPs *in vitro*, techniques such as dynamic light scattering (DLS) and zeta potential (ZP) analysis can be useful. Furthermore, the *in vitro* work carried out in mouse macrophages should be carried out in primary human cells and mammalian *in vivo* models such as rodents to link the relevance of this study to humans and further assess the biosafety of IONPs and identify other toxicity issues that may arise.

Overall, we believe that the results and data generated within this thesis have contributed greatly to the study and understanding of IONP toxicity at a cellular level as well as in an organism model and provides a good building foundation to further investigate the toxic effects of IONPs and establish their biosafety as drug delivery vehicles.

---

## **7. References**

---

Abdifetah, O. and Na-Bangchang, K. (2019) 'Pharmacokinetic studies of nanoparticles as a delivery system for conventional drugs and herb-derived compounds for cancer therapy: a systematic review.', *International journal of nanomedicine*. Dove Press, 14, pp. 5659–5677. doi: 10.2147/IJN.S213229.

Abend, J. R., Uldrick, T. and Ziegelbauer, J. M. (2010) 'Regulation of tumor necrosis factor-like weak inducer of apoptosis receptor protein (TWEAKR) expression by Kaposi's sarcoma-associated herpesvirus microRNA prevents TWEAK-induced apoptosis and inflammatory cytokine expression.', *Journal of virology*. American Society for Microbiology Journals, 84(23), pp. 12139–51. doi: 10.1128/JVI.00884-10.

Aderem, A. and Underhill, D. M. (1999) 'MECHANISMS OF PHAGOCYTOSIS IN MACROPHAGES', *Annual Review of Immunology*. Annual Reviews 4139 El Camino Way, P.O. Box 10139, Palo Alto, CA 94303-0139, USA , 17(1), pp. 593–623. doi: 10.1146/annurev.immunol.17.1.593.

Al-Halifa S., Gauthier L., Arpin D., Bourgault S. and Archambault D. (2019) 'Nanoparticle-Based Vaccines Against Respiratory Viruses', *Frontiers in Immunology*. Frontiers, 10, p. 22. doi: 10.3389/fimmu.2019.00022.

Al-Mossawi, H., Yager, N., Taylor, C.A., Lau, E., Danielli, S., de Wit, J., Gilchrist, J., Nassiri, I., Mahe, E.A., Lee, W., Rizvi, L., Makino, S., Cheeseman, J., Neville, M., Knight, J.C., Bowness, P. and Fairfax, B.P. (2019) 'Context-specific regulation of surface and soluble IL7R expression by an autoimmune risk allele', *Nature Communications*. Nature Publishing Group, 10(1), p. 4575. doi: 10.1038/s41467-019-12393-1.

Albanese, A., Sykes, E. A. and Chan, W. C. W. (2010) 'Rough around the Edges: The Inflammatory Response of Microglial Cells to Spiky Nanoparticles', *ACS Nano*. American Chemical Society, 4(5), pp. 2490–2493. doi: 10.1021/nn100776z.

Alberts, B., Johnson, A., Lewis, J., Raff, M., Roberts, K. and Walter, P. (2002) 'The Adaptive Immune System'. Garland Science.

Ali, A., Zafar, H., Zia, M., Haq, I., Phull, A.R., Ali, J.S and Hussain, A. (2016) 'Synthesis, characterization, applications, and challenges of iron oxide nanoparticles', *Nanotechnology, Science and Applications*. Dove Press, 9, p. 49. doi: 10.2147/NSA.S99986.

Alkilany, A. M. and Murphy, C. J. (2010) 'Toxicity and cellular uptake of gold nanoparticles: what we have learned so far?', *Journal of nanoparticle research: an interdisciplinary forum for nanoscale science and technology*, 12(7), pp. 2313–2333. doi: 10.1007/s11051-010-9911-8.

Allen, T. C. and Kurdowska, A. (2014) 'Interleukin 8 and Acute Lung Injury', *Archives of Pathology & Laboratory Medicine*. Allen Press, 138(2), pp. 266–269. doi: 10.5858/ARPA.2013-0182-RA.

Altevogt, P., Michaelis, M. and Kyewski, B. (1989) 'Identical forms of the CD2 antigen expressed by mouse T and B lymphocytes', *European Journal of Immunology*. John Wiley & Sons, Ltd, 19(8), pp. 1509–1512. doi: 10.1002/eji.1830190826.

Ara, A., Ahmed, K. A. and Xiang, J. (2018) 'Multiple effects of CD40–CD40L axis in immunity against infection and cancer', *ImmunoTargets and Therapy*. Dove Press, Volume 7, pp. 55–61. doi: 10.2147/ITT.S163614.

Arango Duque, G. and Descoteaux, A. (2014) 'Macrophage cytokines: involvement in immunity and infectious diseases.', *Frontiers in immunology*. Frontiers Media SA, 5, p. 491. doi: 10.3389/fimmu.2014.00491.

Armstrong, A.J., Li, X., Tucker, M., Li, S., Mu, X.J., Eng, K.W., Sboner, A., Rubin, M. and Gerstein, M. (2021) 'Molecular medicine tumor board: whole-genome sequencing to inform on personalized medicine for a man with advanced prostate cancer', *Prostate Cancer and Prostatic Diseases*. Nature Publishing Group, pp. 1–8. doi: 10.1038/s41391-021-00324-5.

Auerbach, M. and Ballard, H. (2010) 'Clinical Use of Intravenous Iron: Administration, Efficacy, and Safety', *Hematology*. American Society of Hematology, 2010(1), pp. 338–347. doi: 10.1182/ASHEDUCATION-2010.1.338.

Bala Tannan, N., Manzari, M.T., Herviou, L., Ferreira, M.D.S., Hagen, C., Kiguchi, H., Manpva-Todorova, K., Seshan, V., de Stranchina, E., Heller, D.A. and Younes, A. (2020) 'Tumour Targeted Nanoparticles Improve Therapeutic Index of BCL1 and MCL1 dual Inhibition'. Anas Younes. doi: 10.1182/blood.2020008017/1790375/blood.2020008017.pdf.

Balogh, L. Nigavekar, S.S., Nair, B.M., Lesniak, W., Zhang, C., Sung, L.Y., Kariapper, M.S.T., El-Jawahri, A., Llanes, M., Bolton, B., Mamou, F., Tan, W., Hutson, A., Minc, L. and Khan, M.K. (2007) 'Significant effect of size on the in vivo biodistribution of gold composite nanodevices in mouse tumor models', *Nanomedicine: Nanotechnology, Biology and Medicine*. Elsevier, 3(4), pp. 281–296. doi: 10.1016/J.NANO.2007.09.001.

Barkal, A.A., Brewer, R.E., Markovic, M., Kowarsky, M., Barkal, S.A., Zaro, B.W., Krishnan, V., Hatakeyama, J., Dorigo, O., Barkal, L.J. and Weissman, I.L. (2019) 'CD24 signalling through macrophage Siglec-10 is a target for cancer immunotherapy.', *Nature*. NIH Public Access, 572(7769), pp. 392–396. doi: 10.1038/s41586-019-1456-0.

Behzadi, S., Serpooshan, V., Tao, W., Hamaly, M.A., Alkawareek, M.Y., Dreaden, E.C., Brown, D., Alkilany, A.M., Farokhzad, O.C. and Mahmoudi, M. (2017) 'Cellular Uptake of Nanoparticles: Journey Inside the Cell', *Chemical Society reviews*. NIH Public Access, 46(14), p. 4218. doi: 10.1039/C6CS00636A.

Benard, E.L., van der Sar, A.M., Ellett, F., Lieschke, G.J., Spaink, H.P. and Meijer, A.H. (2012) 'Infection of Zebrafish Embryos with Intracellular Bacterial Pathogens', *Journal of Visualized Experiments*, (61), p. e3781. doi: 10.3791/3781.

Binder, C., Cvetkovski, F., Sellberg, F., Berg, S., Paternina Visbal, H., Sachs, D.H., Berglund, E. and Berglund, D. (2020) 'CD2 Immunobiology', *Frontiers in Immunology*. Frontiers, 11, p. 1090. doi: 10.3389/fimmu.2020.01090.

BJ, S. and RD, H. (2011) 'Physiological effects of nanoparticles on fish: a comparison of nanometals versus metal ions', *Environment international*. Environ Int, 37(6), pp. 1083–1097. doi: 10.1016/J.ENVINT.2011.03.009.

Borgognoni, C.F., Kim, J.H., Zucolotto, V., Fuchs, H. and Riehemann, K. (2018) 'Human macrophage responses to metal-oxide nanoparticles: a review', Taylor & Francis, 46(sup2), pp. 694–703. doi: 10.1080/21691401.2018.1468767.

Bucci, C., Bakke, O. and Progida, C. (2010) 'Rab7b and receptors trafficking.', *Communicative & integrative biology*. Taylor & Francis, 3(5), pp. 401–4. doi: 10.4161/cib.3.5.12341.

Cardelli, J. (2001) 'Phagocytosis and Macropinocytosis in Dictyostelium: Phosphoinositide-Based Processes, Biochemically Distinct', *Traffic*. Blackwell Publishing Ltd, 2(5), pp. 311–320. doi: 10.1034/j.1600-0854.2001.002005311.x.

Carrow, J.K, Cross, L.M, Reese, R.W, Jaiswal, M.K, Gregory, C.A, Kaunas, R., Singh, I. and Gaharwar, A.K.(2018) 'Widespread changes in transcriptome profile of human mesenchymal stem cells induced by two-dimensional nanosilicates.', *Proceedings of the National Academy of Sciences of the United States of America*. National Academy of Sciences, 115(17), pp. E3905–E3913. doi: 10.1073/pnas.1716164115.

Cassar, S., Adatto, I., Freeman, J.L, Gamse, J.T, Iturria, I., Lawrence, C., Muriana, A., Peterson, R.T., Van Cruchten, S. and Zon, L.I. (2020) 'Use of Zebrafish in Drug Discovery Toxicology.', *Chemical research in toxicology*. NIH Public Access, 33(1), pp. 95–118. doi: 10.1021/acs.chemrestox.9b00335.

Ceresa, B. P. and Bahr, S. J. (2006) 'rab7 activity affects epidermal growth factor:epidermal growth factor receptor degradation by regulating endocytic trafficking from the late endosome.', *The Journal of biological chemistry*. American Society for Biochemistry and Molecular Biology, 281(2), pp. 1099–106. doi: 10.1074/jbc.M504175200.

Borgognoni, C.F., Mormann, M., Qu, Y., Schäfer, M., Langer, L., Öztürk, C., Wagner, S., Chen, C., Zhao, Y., Fuchs, H. and Riehemann, K. (2015) 'Reaction of human macrophages on protein corona covered TiO<sub>2</sub> nanoparticles', *Nanomedicine : nanotechnology, biology, and medicine*. Nanomedicine, 11(2), pp. 275–282. doi: 10.1016/J.NANO.2014.10.001.

Cha, S.H., Hwang, Y., Kim, K.N. and Jun, H.S. (2018) 'Palmitate induces nitric oxide production and inflammatory cytokine expression in zebrafish', *Fish & Shellfish Immunology*. Academic Press, 79, pp. 163–167. doi: 10.1016/J.FSI.2018.05.025.

Chahardehi, A. M., Arsad, H. and Lim, V. (2020) 'Zebrafish as a Successful Animal Model for Screening Toxicity of Medicinal Plants.', *Plants (Basel, Switzerland)*.

Multidisciplinary Digital Publishing Institute (MDPI), 9(10). doi: 10.3390/plants9101345.

Chakraborty, C., Sharma, A.R., Sharma, G. and Lee, S.S. (2016) 'Zebrafish: A complete animal model to enumerate the nanoparticle toxicity', *Journal of Nanobiotechnology*. BioMed Central, 14(1), p. 65. doi: 10.1186/s12951-016-0217-6.

Champion, J. A. and Mitragotri, S. (2009) 'Shape induced inhibition of phagocytosis of polymer particles.', *Pharmaceutical research*. NIH Public Access, 26(1), pp. 244–9. doi: 10.1007/s11095-008-9626-z.

Chaplin, D. D. (2010) 'Overview of the immune response.', *The Journal of allergy and clinical immunology*. NIH Public Access, 125(2 Suppl 2), pp. S3-23. doi: 10.1016/j.jaci.2009.12.980.

Charles A.J.J., Travers, P., Walport, M. and Shlomchik, M.J. (2001) 'Principles of innate and adaptive immunity'. Garland Science.

Chatterjee, P., Chiasson, V.L., Bounds, K.R. and Mitchell, B.M. (2014) 'Regulation of the Anti-Inflammatory Cytokines Interleukin-4 and Interleukin-10 during Pregnancy', *Frontiers in Immunology*. Frontiers, 5, p. 253. doi: 10.3389/fimmu.2014.00253.

Chen, P., Kanehira, K. and Taniguchi, A. (2013) 'Role of toll-like receptors 3, 4 and 7 in cellular uptake and response to titanium dioxide nanoparticles', *Science and Technology of Advanced Materials*. Taylor & Francis, 14(1), p. 015008. doi: 10.1088/1468-6996/14/1/015008.

Cohen, A.W., Hnasko, R., Schubert, W. and Lisanti, M.P. (2004) 'Role of Caveolae and Caveolins in Health and Disease', *Physiological Reviews*, 84(4).

Cooper, G. M. (2000) 'The Golgi Apparatus'. Sinauer Associates.

Coornaert, B., Carpentier, I. and Beyaert, R. (2009) 'A20: central gatekeeper in inflammation and immunity.', *The Journal of biological chemistry*. American Society for Biochemistry and Molecular Biology, 284(13), pp. 8217–21. doi: 10.1074/jbc.R800032200.

Dai, K., Huang, L., Huang, Y.B., Chen, Z.B., Yang, L.H. and Jiang, Y.A. (2017) '1810011o10 Rik Inhibits the Antitumor Effect of Intratumoral CD8+ T Cells through Suppression of Notch2 Pathway in a Murine Hepatocellular Carcinoma Model.', *Frontiers in immunology*. Frontiers Media SA, 8, p. 320. doi: 10.3389/fimmu.2017.00320.

Dal, N.K., Kocere, A., Wohlmann, J., Van Herck, S., Bauer, T.A., Resseguier, J., Bagherifam, S., Hyldmo, H., Barz, M., De Geest, B.G. and Fenaroli, F. (2020) 'Zebrafish Embryos Allow Prediction of Nanoparticle Circulation Times in Mice and Facilitate Quantification of Nanoparticle–Cell Interactions', *Small*. John Wiley & Sons, Ltd, 16(5), p. 1906719. doi: 10.1002/smll.201906719.



Daldrup-Link, H.E., Rydland, J., Helbich, T.H., Bjørnerud, A., Turetschek, K., Kvistad, K.A., Kaindl, E., Link, T.M., Staudacher, K., Shames, D., Brasch, R.C., Haraldseth, O. and Rummeny, E.J. (2003) 'Quantification of Breast Tumor Microvascular Permeability with Feruglose-enhanced MR Imaging: Initial Phase II Multicenter Trial', *Radiology*, 229(3), pp. 885–892. doi: 10.1148/RADIOL.2293021045.

Di Dalmazi, G., Hirshberg, J., Lyle, D., Freij, J.B. and Caturegli, P. (2016) 'Reactive oxygen species in organ-specific autoimmunity.', *Auto- immunity highlights*. BioMed Central, 7(1), p. 11. doi: 10.1007/s13317-016-0083-0.

DeDiego, M.L., Nogales, A., Martinez-Sobrido, L. and Topham, D.J. (2019) 'Interferon-Induced Protein 44 Interacts with Cellular FK506-Binding Protein 5, Negatively Regulates Host Antiviral Responses, and Supports Virus Replication.', *mBio*. American Society for Microbiology, 10(4). doi: 10.1128/mBio.01839-19.

Dejonghe, W., Sharma, I., Denoo, B., De Munck, S., Lu, Q., Mishev, K., Bulut, H., Mylle, E., De Rycke, R., Vasileva, M., Savatin, D.V., Nerinckx, W., Staes, A., Drozdzecki, A., Audenaert, D., Yperman, K., Maddar, A., Friml, J., Van Damme, D., Gevaert, K., Haucke, V., Savvides, S.N., Winne, J. and Russinova, E. (2019) 'Disruption of endocytosis through chemical inhibition of clathrin heavy chain function', *Nature Chemical Biology*. Nature Publishing Group, 15(6), pp. 641–649. doi: 10.1038/s41589-019-0262-1.

Denner, J., Eschricht, M., Lauck, M., Semaan, M., Schlaermann, P., Ryu, H. and Akyüz, L. (2013) 'Modulation of cytokine release and gene expression by the immunosuppressive domain of gp41 of HIV-1.', *PloS one*. Public Library of Science, 8(1), p. e55199. doi: 10.1371/journal.pone.0055199.

Desai, A. S., Hunter, M. R. and Kapustin, A. N. (2019) 'Using macropinocytosis for intracellular delivery of therapeutic nucleic acids to tumour cells.', *Philosophical transactions of the Royal Society of London. Series B, Biological sciences*. The Royal Society, 374(1765), p. 20180156. doi: 10.1098/rstb.2018.0156.

Dharmadhikari, B., Wu, M., Abdullah, N.S., Rajendran, S., Ishak, N.D., Nickles, E., Harfuddin, Z. and Schwarz, H. (2016) 'CD137 and CD137L signals are main drivers of type 1, cell-mediated immune responses.', *Oncoimmunology*. Taylor & Francis, 5(4), p. e1113367. doi: 10.1080/2162402X.2015.1113367.

Díaz-Muñoz, M. D. and Turner, M. (2018) 'Uncovering the Role of RNA-Binding Proteins in Gene Expression in the Immune System', *Frontiers in Immunology*. Frontiers, 0(MAY), p. 1094. doi: 10.3389/FIMMU.2018.01094.

Dobrovolskaia, M.A., Aggarwal, P., Hall, J.B. and McNeil, S.E. (2008) 'Preclinical studies to understand nanoparticle interaction with the immune system and its potential effects on nanoparticle biodistribution.', *Molecular pharmaceuticals*. NIH Public Access, 5(4), pp. 487–95. doi: 10.1021/mp800032f.

Dobrovolskaia, M. A., Germolec, D. R. and Weaver, J. L. (2009) 'Evaluation of nanoparticle immunotoxicity', *Nature Nanotechnology*. Nature Publishing Group, 4(7), pp. 411–414. doi: 10.1038/NNANO.2009.175.

Dobrovolskaia, M. A., Shurin, M. and Shvedova, A. A. (2016) 'Current understanding of interactions between nanoparticles and the immune system.', *Toxicology and applied pharmacology*. NIH Public Access, 299, pp. 78–89. doi: 10.1016/j.taap.2015.12.022.

Dutta, D., Sundaram, S.K., Teegarden, J.G., Riley, B.J., Fifield, L.S., Jacobs, J.M., Addleman, S.R., Kaysen, G.A., Moudgil, B.M. and Weber, T.J. (2007) 'Adsorbed Proteins Influence the Biological Activity and Molecular Targeting of Nanomaterials', *Toxicological Sciences*. Academic Press, San Diego, CA, 100(1), pp. 303–315. doi: 10.1093/toxsci/kfm217.

Echeverry, S., Shi, X.Q., Haw, A., Liu, H., Zhang, Z. and Zhang, J. (2009) 'Transforming growth factor-beta1 impairs neuropathic pain through pleiotropic effects.', *Molecular pain*. SAGE Publications, 5, p. 16. doi: 10.1186/1744-8069-5-16.

Eldor, R., Klieger, Y., Sade-Feldman, M., Vaknin, I., Varfolomeev, I., Fuchs, C. and Baniyash, M. (2015) 'CD247, a novel T cell-derived diagnostic and prognostic biomarker for detecting disease progression and severity in patients with type 2 diabetes.', *Diabetes care*. American Diabetes Association, 38(1), pp. 113–8. doi: 10.2337/dc14-1544.

Ellsworth, R.E., Decewicz, D.J., Shriver, C.D. and Ellsworth, D.L. (2010) 'Breast cancer in the personal genomics era.', *Current genomics*. Bentham Science Publishers, 11(3), pp. 146–61. doi: 10.2174/138920210791110951.

Elsabahy, M. and Wooley, K. L. (2013) 'Cytokines as biomarkers of nanoparticle immunotoxicity.', *Chemical Society reviews*. NIH Public Access, 42(12), pp. 5552–76. doi: 10.1039/c3cs60064e.

Engel, E., Michiardi, A., Navarro, M., Lacroix, D. and Planell, J.A. (2008) 'Nanotechnology in regenerative medicine: the materials side', *Trends in Biotechnology*, 26(1), pp. 39–47. doi: 10.1016/j.tibtech.2007.10.005.

England, S. J. and Adams, R. J. (2011) 'Blastomere Injection of Cleavage-Stage Zebrafish Embryos and Imaging of Labeled Cells', *Cold Spring Harbor Protocols*, 2011(8), p. pdb.prot5654-pdb.prot5654. doi: 10.1101/pdb.prot5654.

Etheridge, M.L., Campbell, S.A., Erdman, A.G., Haynes, C.L., Wolf, S.M. and McCullough, J. (2013) 'The big picture on nanomedicine: the state of investigational and approved nanomedicine products.', *Nanomedicine : nanotechnology, biology, and medicine*. NIH Public Access, 9(1), pp. 1–14. doi: 10.1016/j.nano.2012.05.013.

Ethuin, F., Delarche, C., Benslama, S., Gougerot-Pocidallo, M.A., Jacob, L. and Chollet-Martin, S. (2001) 'Interleukin-12 increases interleukin 8 production and release by human polymorphonuclear neutrophils', *Journal of Leukocyte Biology*. John Wiley & Sons, Ltd, 70(3), pp. 439–446. doi: 10.1189/JLB.70.3.439.

Fabbi, M., Carbotti, G. and Ferrini, S. (2017) 'Dual Roles of IL-27 in Cancer Biology and Immunotherapy', *Mediators of Inflammation*, 2017, pp. 1–14. doi: 10.1155/2017/3958069

Fenaroli, F., Westmoreland, D., Benjaminsen, J., Kolstad, T., Skjeldal, F.M., Meijer, A.H., van der Vaart, M., Ulanova, L., Roos, N., Nyström, B., Hildahl, J. and Griffiths, G. (2014) 'Nanoparticles as Drug Delivery System against Tuberculosis in Zebrafish Embryos: Direct Visualization and Treatment', *ACS Nano*. American Chemical Society, 8(7), pp. 7014–7026. doi: 10.1021/nn5019126.

Fernando, L.P., Kandel, P.K., Yu, J., McNeill, J., Ackroyd, P.C. and Christensen, K.A. (2010) 'Mechanism of cellular uptake of highly fluorescent conjugated polymer nanoparticles.', *Biomacromolecules*. NIH Public Access, 11(10), pp. 2675–82. doi: 10.1021/bm1007103.

Finnegan, S. and Percival, S. L. (2015) 'EDTA: An Antimicrobial and Antibiofilm Agent for Use in Wound Care.', *Advances in wound care*. Mary Ann Liebert, Inc., 4(7), pp. 415–421. doi: 10.1089/wound.2014.0577.

Fogel, J. L., Thein, T. Z. T. and Mariani, F. V (2012) 'Use of LysoTracker to detect programmed cell death in embryos and differentiating embryonic stem cells.', *Journal of visualized experiments : JoVE*. MyJoVE Corporation, (68). doi: 10.3791/4254.

Foroozandeh, P. and Aziz, A. A. (2018) 'Insight into Cellular Uptake and Intracellular Trafficking of Nanoparticles.', *Nanoscale research letters*. Springer, 13(1), p. 339. doi: 10.1186/s11671-018-2728-6.

Francia, V., Yang, K., Deville, S., Reker-Smit, C., Nelissen, I. and Salvati, A. (2019) 'Corona Composition Can Affect the Mechanisms Cells Use to Internalize Nanoparticles', *ACS Nano*. American Chemical Society, 13(10), pp. 11107–11121. doi: 10.1021/acsnano.9b03824.

Friedman, J. R. and Nunnari, J. (2014) 'Mitochondrial form and function.', *Nature*. NIH Public Access, 505(7483), pp. 335–43. doi: 10.1038/nature12985.

Ganapathy, V., Moghe, P. V. and Roth, C. M. (2015) 'Targeting tumor metastases: drug delivery mechanisms and technologies', *Journal of controlled release : official journal of the Controlled Release Society*. NIH Public Access, 219, p. 215. doi: 10.1016/J.JCONREL.2015.09.042.

Garaiova, Z., Strand, S.P., Reitan, N.K., Lelu, S., Storset, S., Berg, K., Malmo, J., Folasire, O., Bjorkoy, A. and de L. Davies, C. (2012) 'Cellular uptake of DNA - chitosan nanoparticles: The role of clathrin- and caveolae-mediated pathways', *International Journal of Biological Macromolecules*, 51(5), pp. 1043–1051. doi: 10.1016/j.ijbiomac.2012.08.016.

García-Casal, M. N., Leets, I. and Layrisse, M. (2004) 'Ethylenediaminetetraacetic acid (EDTA) does not increase iron uptake or ferritin synthesis by Caco-2 cells.', *The Journal of nutritional biochemistry*. J Nutr Biochem, 15(5), pp. 261–6. doi: 10.1016/j.jnutbio.2003.10.004.

Gibson, A.W., Edberg, J.C., Wu, J. and Kimberly, R.P. (2013) 'The Role of IL-10 in Autoimmune Pathology'. Landes Bioscience.

Gil-Yarom, N., Radomir, L., Sever, L., Kramer, M.P., Lewinsky, H., Bornstein, C., Blecher-Gonen, R., Barnett-Itzhaki, Z., Mirkin, V., Friedlander, G., Shvidel, L., Herishanu, Y., Lolis, E.J., Becker-Herman, S., Amit, I. and Shachar, I. (2017) 'CD74 is a novel transcription regulator.', *Proceedings of the National Academy of Sciences of the United States of America*. National Academy of Sciences, 114(3), pp. 562–567. doi: 10.1073/pnas.1612195114.

Goldenring, J. R. (2015) 'Recycling endosomes.', *Current opinion in cell biology*. NIH Public Access, 35, pp. 117–22. doi: 10.1016/j.ceb.2015.04.018.

Gratton, S.E.A., Ropp, P.A., Pohlhaus, P.D., Luft, J.C., Madden, V.J., Napier, M.E. and DeSimone, J.M. (2008) 'The effect of particle design on cellular internalization pathways.', *Proceedings of the National Academy of Sciences of the United States of America*. National Academy of Sciences, 105(33), pp. 11613–8. doi: 10.1073/pnas.0801763105.

Grauer, O., Jaber, M., Hess, K., Weckesser, M., Schwindt, W., Maring, S., Wölfer, J. and Stummer, W. (2019) 'Combined intracavitary thermotherapy with iron oxide nanoparticles and radiotherapy as local treatment modality in recurrent glioblastoma patients', *Journal of Neuro-Oncology*. Springer, 141(1), p. 83. doi: 10.1007/S11060-018-03005-X.

Grimes, D.T., Boswell, C.W., Morante, N.F.C., Henkelman, R.M., Burdine, R.D. and Ciruna, B. (2016) 'Zebrafish models of idiopathic scoliosis link cerebrospinal fluid flow defects to spine curvature.', *Science (New York, N. Y.)*. NIH Public Access, 352(6291), pp. 1341–4. doi: 10.1126/science.aaf6419.

Gustafson, H.H., Holt-Casper, D., Grainger, D.W. and Ghandehari, H. (2015) 'Nanoparticle Uptake: The Phagocyte Problem.', *Nano today*. NIH Public Access, 10(4), pp. 487–510. doi: 10.1016/j.nantod.2015.06.006.

Hannon, G., Lysaght, J., Liptrott, N.J. and Prina-Mello, A. (2019) 'Immunotoxicity Considerations for Next Generation Cancer Nanomedicines', *Advanced Science*. John Wiley & Sons, Ltd, 6(19), p. 1900133. doi: 10.1002/advs.201900133.

Hansen, C. G. and Nichols, B. J. (2009) 'Molecular mechanisms of clathrin-independent endocytosis.', *Journal of cell science*. Company of Biologists, 122(Pt 11), pp. 1713–21. doi: 10.1242/jcs.033951.

Harisinghani, M.G., Saksena, M.A., Hahn, P.F., King, B., Kim, J., Torabi, M.T. and Weissleder, R. (2006) 'Ferumoxtran-10-Enhanced MR Lymphangiography: Does Contrast-Enhanced Imaging Alone Suffice for Accurate Lymph Node Characterization?', <http://dx.doi.org/10.2214/AJR.04.1287>. American Roentgen Ray Society, 186(1), pp. 144–148. doi: 10.2214/AJR.04.1287.

Harush-Frenkel, O., Debotton, N., Benita, S. and Altschuler, Y. (2007) 'Targeting of nanoparticles to the clathrin-mediated endocytic pathway', *Biochemical and Biophysical Research Communications*, 353(1), pp. 26–32. doi: 10.1016/j.bbrc.2006.11.135.

He, J.-Q. *et al.* (2008) 'Association of genetic variations in the CSF2 and CSF3 genes with lung function in smoking-induced COPD.', *The European respiratory journal*. European Respiratory Society, 32(1), pp. 25–34. doi: 10.1183/09031936.00040307.

He, S., Deng, Y., Liao, Y., Li, X., Liu, J. and Yao, S. (2017) 'CREB5 promotes tumor cell invasion and correlates with poor prognosis in epithelial ovarian cancer.', *Oncology letters*. Spandidos Publications, 14(6), pp. 8156–8161. doi: 10.3892/ol.2017.7234.

von Hellfeld, R., Brotzmann, K., Baumann, L., Strecker, R. and Braunbeck, T. (2020) 'Adverse effects in the fish embryo acute toxicity (FET) test: a catalogue of unspecific morphological changes versus more specific effects in zebrafish (*Danio rerio*) embryos', *Environmental Sciences Europe*. SpringerOpen, 32(1), p. 122. doi: 10.1186/s12302-020-00398-3.

Herbomel, P., Thisse, B. and Thisse, C. (1999) *Early macrophages in zebrafish*. Hildebrandt, B. (2002) 'The cellular and molecular basis of hyperthermia', *Critical Reviews in Oncology/Hematology*, 43(1), pp. 33–56. doi: 10.1016/S1040-8428(01)00179-2.

Hoshyar, N., Gray, S., Han, H. and Bao, G. (2016) 'The effect of nanoparticle size on in vivo pharmacokinetics and cellular interaction.', *Nanomedicine (London, England)*. Future Science Group, 11(6), pp. 673–92. doi: 10.2217/nnm.16.5.

Howe, K., Clark, M.D., Torroja, C.F., Torrance, J., Berthelot, C., Muffato, M., Collins, J.E., Humphray, S., McLaren, K., Matthews, L., McLaren, S., Sealy, I. and Caccamo, M. (2013) 'The zebrafish reference genome sequence and its relationship to the human genome', *Nature*. Nature Publishing Group, 496(7446), pp. 498–503. doi: 10.1038/nature12111.

Huotari, J. and Helenius, A. (2011) 'Endosome maturation.', *The EMBO journal*. European Molecular Biology Organization, 30(17), pp. 3481–500. doi: 10.1038/emboj.2011.286.

Ilinskaya, A. N. and Dobrovolskaia, M. A. (2014) 'Immunosuppressive and anti-inflammatory properties of engineered nanomaterials', *British Journal of Pharmacology*. John Wiley & Sons, Ltd, 171(17), pp. 3988–4000. doi: 10.1111/bph.12722.

Iversen, T. G., Frerker, N. and Sandvig, K. (2012) 'Uptake of ricinB-quantum dot nanoparticles by a macropinocytosis-like mechanism', *Journal of Nanobiotechnology 2012 10:1*. BioMed Central, 10(1), pp. 1–11. doi: 10.1186/1477-3155-10-33.

Iyer, S. S. and Cheng, G. (2012) 'Role of interleukin 10 transcriptional regulation in inflammation and autoimmune disease.', *Critical reviews in immunology*. NIH Public Access, 32(1), pp. 23–63. doi: 10.1615/critrevimmunol.v32.i1.30.

Jackson, S. E. and Chester, J. D. (2015) 'Personalised cancer medicine', *International Journal of Cancer*, 137(2), pp. 262–266. doi: 10.1002/ijc.28940.

Jain, S., Hirst, D. G. and O'Sullivan, J. M. (2012) 'Gold nanoparticles as novel agents for cancer therapy.', *The British journal of radiology*. British Institute of Radiology, 85(1010), pp. 101–13. doi: 10.1259/bjr/59448833.

Jain, S.K., Gupta, Y., Jain, A., Saxena, A.R., Khare, P. and Jain, A. (2008) 'Mannosylated gelatin nanoparticles bearing an anti-HIV drug didanosine for site-specific delivery', *Nanomedicine: Nanotechnology, Biology and Medicine*. Elsevier, 4(1), pp. 41–48. doi: 10.1016/J.NANO.2007.11.004.

Jamur, M. C. and Oliver, C. (2010) 'Permeabilization of Cell Membranes', in, pp. 63–66. doi: 10.1007/978-1-59745-324-0\_9.

Jones, C. V and Ricardo, S. D. (2013) 'Macrophages and CSF-1: implications for development and beyond.', *Organogenesis*. Taylor & Francis, 9(4), pp. 249–60. doi: 10.4161/org.25676.

Jordens, I., Fernandez-Borja, M., Marsman, M., Dusseljee, S., Janssen, L., Calafat, J., Janssen, H., Wubbolts, R. and Neefjes, J. (2001) 'The Rab7 effector protein RILP controls lysosomal transport by inducing the recruitment of dynein-dynactin motors', *Current Biology*, 11(21), pp. 1680–1685. doi: 10.1016/S0960-9822(01)00531-0.

Jovic, M., Sharma, M., Rahajeng, J. and Caplan, S. (2010) 'The early endosome: a busy sorting station for proteins at the crossroads.', *Histology and histopathology*. NIH Public Access, 25(1), pp. 99–112. doi: 10.14670/HH-25.99.

Kaiserman, D. and Bird, P. I. (2010) 'Control of granzymes by serpins', *Cell Death & Differentiation*. Nature Publishing Group, 17(4), pp. 586–595. doi: 10.1038/cdd.2009.169.

Kany, S., Vollrath, J. T. and Relja, B. (2019) 'Cytokines in Inflammatory Disease.', *International journal of molecular sciences*. Multidisciplinary Digital Publishing Institute (MDPI), 20(23). doi: 10.3390/ijms20236008.

Karavitis, J. and Kovacs, E. J. (2011) 'Macrophage phagocytosis: effects of environmental pollutants, alcohol, cigarette smoke, and other external factors.', *Journal of leukocyte biology*. The Society for Leukocyte Biology, 90(6), pp. 1065–78. doi: 10.1189/jlb.0311114.

Kaur, G. and Lakkaraju, A. (2018) 'Early Endosome Morphology in Health and Disease.', *Advances in experimental medicine and biology*. NIH Public Access, 1074, pp. 335–343. doi: 10.1007/978-3-319-75402-4\_41.

Keliher, E.J., Yoo, J., Nahrendorf, M., Lewis, J., Marinelli, B., Newton, A., Pittet, M. and Weissleder, R. (2011) '89Zr Labeled Dextran Nanoparticles Enable in vivo Macrophage Imaging', *Bioconjugate chemistry*. NIH Public Access, 22(12), p. 2383. doi: 10.1021/BC200405D.

Kelley, N., Jeltema, D., Duan, Y. and He, Y. (2019) 'The NLRP3 Inflammasome: An Overview of Mechanisms of Activation and Regulation.', *International journal of molecular sciences*. Multidisciplinary Digital Publishing Institute (MDPI), 20(13). doi: 10.3390/ijms20133328.

Kermorgant, M., Ben Salem, J., Santelli, J., Calise, D., Oster, A.C., Lairez, O., Coudret, C., Verelst, M., Gales, C., Sénard, J.M. and Evalu-, A. (2019) 'Evaluation of upconverting nanoparticles towards heart theranostics', *Science*, 14(12). doi: 10.1371/journal.pone.0225729i.

Kerr, M. C. and Teasdale, R. D. (2009) 'Defining Macropinocytosis', *Traffic*. Blackwell Publishing Ltd, 10(4), pp. 364–371. doi: 10.1111/j.1600-0854.2009.00878.x.

Khan, H.A., Alamery, S., Ibrahim, K.E., El-Nagar, D.M., Al-Harbi, N., Rusop, M. and Alrokayan, S.H. (2019) 'Size and time-dependent induction of proinflammatory cytokines expression in brains of mice treated with gold nanoparticles', *Saudi Journal of Biological Sciences*. Elsevier, 26(3), pp. 625–631. doi: 10.1016/J.SJBS.2018.09.012.

Kimmel, C. B. *et al.* (1995) *Stages of Embryonic Development of the Zebrafish*.

Kirchhausen, T. (2000) 'Clathrin', *Annual Review of Biochemistry*. Annual Reviews 4139 El Camino Way, P.O. Box 10139, Palo Alto, CA 94303-0139, USA , 69(1), pp. 699–727. doi: 10.1146/annurev.biochem.69.1.699.

Kiss, A. L. and Botos, E. (2009) 'Endocytosis via caveolae: alternative pathway with distinct cellular compartments to avoid lysosomal degradation?', *Journal of cellular and molecular medicine*. Wiley-Blackwell, 13(7), pp. 1228–37. doi: 10.1111/j.1582-4934.2009.00754.x.

Kocere, A., Resseguier, J., Wohlmann, J., Skjeldal, F.M., Khan, S., Speth, M., Dal, N-J.K, Ng, M.Y.W., Alonso-Rodriguez, N., Scarpa, E., Rizzello, L., Battaglia, G., Griffiths, G. and Fenaroli, F. (2020) 'Real-time imaging of polymersome nanoparticles in zebrafish embryos engrafted with melanoma cancer cells: Localization, toxicity and treatment analysis.', *EBioMedicine*. Elsevier, 58, p. 102902. doi: 10.1016/j.ebiom.2020.102902.

Kolaczowska, E. and Kubes, P. (2013) 'Neutrophil recruitment and function in health and inflammation', *Nature Reviews Immunology*. Nature Publishing Group, 13(3), pp. 159–175. doi: 10.1038/nri3399.

Kononenko, V., Narat, M. and Drobne, D. (2015) 'Nanoparticle interaction with the immune system', *Archives of Industrial Hygiene and Toxicology*, 66(2). doi: 10.1515/aiht-2015-66-2582.

Kourko, O., Seaver, K., Odoardi, N., Basta, S. and Gee, K. (2019) 'IL-27, IL-30, and IL-35: A Cytokine Triumvirate in Cancer', *Frontiers in Oncology*. Frontiers, 9, p. 969. doi: 10.3389/fonc.2019.00969.

Kouser, L., Paudyal, B., Kaur, A., Stenbeck, G., Jones, L.A., Abozaid, S.M., Stover, C.M., Flahaut, E., Sim, R.B. and Kishore, U. (2018) 'Human Properdin Oponizes Nanoparticles and Triggers a Potent Pro-inflammatory Response by Macrophages without Involving Complement Activation', *Frontiers in Immunology*. Frontiers Media SA, 9(FEB), p. 12. doi: 10.3389/FIMMU.2018.00131.

Kraft, M. L. (2013) 'Plasma membrane organization and function: moving past lipid rafts.', *Molecular biology of the cell*. American Society for Cell Biology, 24(18), pp. 2765–8. doi: 10.1091/mbc.E13-03-0165.

Kreuter, J. (2007) 'Nanoparticles—a historical perspective', *International Journal of Pharmaceutics*, 331(1), pp. 1–10. doi: 10.1016/j.ijpharm.2006.10.021.

Krzyszczyk, P., Acevedo, A., Davidoff, E.J., Timmins, L.M., Marrero-Berrios, I., Patel, M., White, C., Lowe, C., Sherba, J., Hartmanshenn, C., O'Neill, K.M., Balter, M.L., Fritz, Z.R., Androulakis, I.P., Schloss, R.S. and Yarmush, M.L. (2018) 'The growing role of precision and personalized medicine for cancer treatment.', *Technology*. NIH Public Access, 6(3–4), pp. 79–100. doi: 10.1142/S2339547818300020.

Kucera, A., Bakke, O. and Progida, C. (2016) 'The multiple roles of Rab9 in the endolysosomal system.', *Communicative & integrative biology*. Taylor & Francis, 9(4), p. e1204498. doi: 10.1080/19420889.2016.1204498.

Kuhn, D.A., Vanhecke, D., Michen, B., Blank, F., Gehr, P., Petri-Fink, A. and Rothen-Rutishauser, B. (2014) 'Different endocytotic uptake mechanisms for nanoparticles in epithelial cells and macrophages.', *Beilstein journal of nanotechnology*. Beilstein-Institut, 5, pp. 1625–36. doi: 10.3762/bjnano.5.174.

Kumari, S., MG, S. and Mayor, S. (2010) 'Endocytosis unplugged: multiple ways to enter the cell', *Cell Research*. Nature Publishing Group, 20(3), pp. 256–275. doi: 10.1038/cr.2010.19.

Lam, S.H, Chua, H.L, Gong, Z, Lam, T.J and Sin, Y.M (2004) 'Development and maturation of the immune system in zebrafish, *Danio rerio*: a gene expression profiling, in situ hybridization and immunological study', *Developmental & Comparative Immunology*. Pergamon, 28(1), pp. 9–28. doi: 10.1016/S0145-305X(03)00103-4.

Lawrence, T. (2009) 'The nuclear factor NF-kappaB pathway in inflammation.', *Cold Spring Harbor perspectives in biology*. Cold Spring Harbor Laboratory Press, 1(6), p. a001651. doi: 10.1101/cshperspect.a001651.

Lee, E.G., Boone, D.L., Chai, S., Libby, S.L., Chien, M., Lodolce, J.P. and Ma, A.(2000) 'Failure to regulate TNF-induced NF-kappaB and cell death responses in A20-deficient mice.', *Science (New York, N.Y.)*. NIH Public Access, 289(5488), pp. 2350–4. doi: 10.1126/science.289.5488.2350.

Leeman, M., Choi, J., Hansson, S., Storm, M.U. and Nilsson, L. (2018) 'Proteins and antibodies in serum, plasma, and whole blood—size characterization using asymmetrical flow field-flow fractionation (AF4)', *Analytical and Bioanalytical Chemistry*. Springer, 410(20), p. 4867. doi: 10.1007/S00216-018-1127-2.



van Leeuwen, L. M., van der Sar, A. M. and Bitter, W. (2014) 'Animal models of tuberculosis: zebrafish.', *Cold Spring Harbor perspectives in medicine*. Cold Spring Harbor Laboratory Press, 5(3), p. a018580. doi: 10.1101/cshperspect.a018580.

LI, J., DU, Y., YAN, Z., YAN, J., ZHUANSUN, Y., CHEN, R., ZHANG, W., FENG, S. and RAN, P. (2016) 'CD80 and CD86 knockdown in dendritic cells regulates Th1/Th2 cytokine production in asthmatic mice', *Experimental and Therapeutic Medicine*. Spandidos Publications, 11(3), pp. 878–884. doi: 10.3892/etm.2016.2989.

Li, L., Wan, T., Wan, M., Liu, B., Cheng, R. and Zhang, R. (2015) 'The effect of the size of fluorescent dextran on its endocytic pathway', *Cell Biology International*. John Wiley & Sons, Ltd, 39(5), pp. 531–539. doi: 10.1002/cbin.10424.

Li, X., Lalic, J., Baeza-Centurion, P., Dhar, R. and Lehner, B. (2019) 'Changes in gene expression shift and switch genetic interactions', *bioRxiv*. Cold Spring Harbor Laboratory, p. 578419. doi: 10.1101/578419.

Li, Y. and Liu, T.-M. (2018) 'Discovering Macrophage Functions Using In Vivo Optical Imaging Techniques', *Frontiers in Immunology*. Frontiers Media SA, 9(MAR), p. 502. doi: 10.3389/FIMMU.2018.00502.

Lim, J. P. and Gleeson, P. A. (2011) 'Macropinocytosis: an endocytic pathway for internalising large gulps', *Immunology and Cell Biology*. Nature Publishing Group, 89(8), pp. 836–843. doi: 10.1038/icb.2011.20.

Lin, X., Wen, Z. and Xu, J. (2019) 'Tissue-resident macrophages: from zebrafish to mouse', *Blood Science*, 1(1), pp. 57–60. doi: 10.1097/BS9.0000000000000013.

Liu, S. (2012) 'Epigenetics advancing personalized nanomedicine in cancer therapy.', *Advanced drug delivery reviews*. NIH Public Access, 64(13), pp. 1532–43. doi: 10.1016/j.addr.2012.08.004.

Lopez-Castejon, G. and Brough, D. (2011) 'Understanding the mechanism of IL-1 $\beta$  secretion.', *Cytokine & growth factor reviews*. Elsevier, 22(4), pp. 189–95. doi: 10.1016/j.cytogfr.2011.10.001.

Lundholm, M., Mayans, S., Motta, V., Löfgren-Burström, A., Danska, J. and Holmberg, D. (2010) 'Variation in the Cd3 zeta (Cd247) gene correlates with altered T cell activation and is associated with autoimmune diabetes.', *Journal of immunology (Baltimore, Md. : 1950)*. American Association of Immunologists, 184(10), pp. 5537–44. doi: 10.4049/jimmunol.0904012.

Lundqvist, M., Stigler, J., Elia, G., Lynch, I., Cedervall, T. and Dawson, K.A. (2008) 'Nanoparticle size and surface properties determine the protein corona with possible implications for biological impacts', *Proceedings of the National Academy of Sciences of the United States of America*. National Academy of Sciences, 105(38), p. 14265. doi: 10.1073/PNAS.0805135105.

Luzio, J. P., Pryor, P. R. and Bright, N. A. (2007) 'Lysosomes: fusion and function', *Nature Reviews Molecular Cell Biology*. Nature Publishing Group, 8(8), pp. 622–632. doi: 10.1038/nrm2217.

M Samarasinghe, R., K Kanwar, R. and R Kanwar, J. (2012) 'The role of nanomedicine in cell based therapeutics in cancer and inflammation.', *International journal of molecular and cellular medicine*. Babol University of Medical Sciences, 1(3), pp. 133–44.

Ma, X., Gong, N., Zhong, L., Sun, J. and Liang, X. (2016) 'Future of nanotherapeutics: Targeting the cellular sub-organelles.', *Biomaterials*. Biomaterials, 97, pp. 10–21. doi: 10.1016/j.biomaterials.2016.04.026.

Macro, L., Jaiswal, J. K. and Simon, S. M. (2012) 'Dynamics of clathrin-mediated endocytosis and its requirement for organelle biogenesis in Dictyostelium.', *Journal of cell science*. Company of Biologists, 125(Pt 23), pp. 5721–32. doi: 10.1242/jcs.108837.

Maier-Hauff, K., Ulrich, F., Nestler, D., Niehoff, H., Wust, P. Thiesen, B., Orawa, H., Budach, V. and Jordan, A. (2011) 'Efficacy and safety of intratumoral thermotherapy using magnetic iron-oxide nanoparticles combined with external beam radiotherapy on patients with recurrent glioblastoma multiforme', *Journal of Neuro-Oncology*. Springer, 103(2), p. 317. doi: 10.1007/S11060-010-0389-0.

Marcos, V., Latzin, P., Hector, A., Sonanini, S., Hoffmann, F., Lacher, M., Koller, B., Bufler, P., Nicolai, T., Hartl, D. and Griese, M. (2010) 'Expression, regulation and clinical significance of soluble and membrane CD14 receptors in pediatric inflammatory lung diseases', *Respiratory Research*. BioMed Central, 11(1), p. 32. doi: 10.1186/1465-9921-11-32.

Martens, T.F., Remaut, K., Demeester, J., De Smedt, S.C. and Braeckmans, K. (2014) 'Intracellular delivery of nanomaterials: How to catch endosomal escape in the act', *Nano Today*. Elsevier, 9(3), pp. 344–364. doi: 10.1016/J.NANTOD.2014.04.011.

Martinez, F. O. and Gordon, S. (2014) 'The M1 and M2 paradigm of macrophage activation: time for reassessment.', *F1000prime reports*. Faculty of 1000 Ltd, 6, p. 13. doi: 10.12703/P6-13.

Martinez, V.G., Escoda-Ferran, C., Tadeu Simões, I., Arai, S., Orta Mascaró, M., Carreras, E., Martínez-Florensa, M., Yelamos, J., Miyazaki, T. and Lozano, F.(2014) 'The macrophage soluble receptor AIM/Ap16/CD5L displays a broad pathogen recognition spectrum and is involved in early response to microbial aggression', *Cellular & Molecular Immunology*. Nature Publishing Group, 11(4), pp. 343–354. doi: 10.1038/cmi.2014.12.

Mayadas, T. N., Cullere, X. and Lowell, C. A. (2014) 'The multifaceted functions of neutrophils.', *Annual review of pathology*. NIH Public Access, 9, pp. 181–218. doi: 10.1146/annurev-pathol-020712-164023.

Mayor, S. and Pagano, R. E. (2007) 'Pathways of clathrin-independent endocytosis', *Nature Reviews Molecular Cell Biology*. Nature Publishing Group, 8(8), pp. 603–612. doi: 10.1038/nrm2216.

Mayor, S., Parton, R. G. and Donaldson, J. G. (2014) 'Clathrin-independent pathways of endocytosis.', *Cold Spring Harbor perspectives in biology*. Cold Spring Harbor Laboratory Press, 6(6). doi: 10.1101/cshperspect.a016758.

Mazzolini, J., Weber, R.J.M., Chen, H., Khan, A., Guggenheim, E., Shaw, R.K., Chipman, J.K., Viant, M.R. and Rappoport, J.Z. (2016) 'Protein Corona Modulates Uptake and Toxicity of Nanoceria via Clathrin-Mediated Endocytosis', *The Biological Bulletin*. University of Chicago Press Chicago, IL, 231(1), pp. 40–60. doi: 10.1086/689590.

McCormack, R.M., de Armas, L.R., Shiratsuchi, M., Fiorentino, D.G., Olsson, M.L., Lichtenheld, M.G., Morales, A., Lyapichev, K., Gonzalez, L.E., Strbo, N., Sukumar, N., Stojadinovic, O., Plano, G.V., Munson, G.P., Tomic-Canic, M., Kirsner, R.S., Russell, D.G. and Podack, E.R. (2015) 'Perforin-2 is essential for intracellular defense of parenchymal cells and phagocytes against pathogenic bacteria.', *eLife*. eLife Sciences Publications, Ltd, 4. doi: 10.7554/eLife.06508.

Medepalli, K., Alphenaar, B.W., Keynton, R.S. and Sethu, P. (2013) 'A new technique for reversible permeabilization of live cells for intracellular delivery of quantum dots', *NANOTECHNOLOGY*, 24, pp. 205101–205114. doi: 10.1088/0957-4484/24/20/205101.

Merle, N.S., Church, S.E., Fremeaux-Bacchi, V. and Roumenina, L.T (2015) 'Complement System Part I - Molecular Mechanisms of Activation and Regulation.', *Frontiers in immunology*. Frontiers Media SA, 6, p. 262. doi: 10.3389/fimmu.2015.00262.

Michel, N. A., Zirlik, A. and Wolf, D. (2017) 'CD40L and Its Receptors in Atherothrombosis—An Update', *Frontiers in Cardiovascular Medicine*. Frontiers, 4, p. 40. doi: 10.3389/fcvm.2017.00040.

Michelucci, A., Cordes, T., Ghelfi, J., Pailot, A., Reiling, N., Goldmann, O., Binz, T., Wegner, A., Tallam, A., Rausell, A., Buttini, M., Linster, C.L., Medina, E., Balling, R. and Hiller, K. (2013) 'Immune-responsive gene 1 protein links metabolism to immunity by catalyzing itaconic acid production.', *Proceedings of the National Academy of Sciences of the United States of America*. National Academy of Sciences, 110(19), pp. 7820–5. doi: 10.1073/pnas.1218599110.

Mitchell, L.A., Lauer, F.T., Burchiel, S.W. and McDonald, J.D. (2009) 'Mechanisms for how inhaled multiwalled carbon nanotubes suppress systemic immune function in mice.', *Nature nanotechnology*. NIH Public Access, 4(7), pp. 451–6. doi: 10.1038/nnano.2009.151.

Miura, G. I. and Yelon, D. (2011) 'A guide to analysis of cardiac phenotypes in the zebrafish embryo.', *Methods in cell biology*. NIH Public Access, 101, pp. 161–80. doi: 10.1016/B978-0-12-387036-0.00007-4.

Mo, J., Sun, N., Yang, B., Li, S. and Wang, L. (2020) 'The nervous system is the major target for Gold nanoparticles: Evidence from RNA sequencing data of *C. elegans*', *bioRxiv*. Cold Spring Harbor Laboratory, p. 699785. doi: 10.1101/699785.

Mogensen, T. H. (2009) 'Pathogen recognition and inflammatory signaling in innate immune defenses.', *Clinical microbiology reviews*. American Society for Microbiology (ASM), 22(2), pp. 240–73, Table of Contents. doi: 10.1128/CMR.00046-08.

Moghimi, S. M. and Simberg, D. (2017) 'Complement activation turnover on surfaces of nanoparticles.', *Nano today*. NIH Public Access, 15, pp. 8–10. doi: 10.1016/j.nantod.2017.03.001.

Moreno-Indias, I., Dodds, A.W., Argüello, A., Castro, N. and Sim, R.B. (2012) 'The complement system of the goat: haemolytic assays and isolation of major proteins.', *BMC veterinary research*. BioMed Central, 8, p. 91. doi: 10.1186/1746-6148-8-91.

Mosser, D. M. and Edwards, J. P. (2008) 'Exploring the full spectrum of macrophage activation.', *Nature reviews. Immunology*. NIH Public Access, 8(12), pp. 958–69. doi: 10.1038/nri2448.

Movita, D., Kreefft, K., Biesta, P., van Oudenaren, A., Leenen, P.J.M., Janssen, H.L.A. and Boonstra, A. (2012) 'Kupffer cells express a unique combination of phenotypic and functional characteristics compared with splenic and peritoneal macrophages', *Journal of Leukocyte Biology*. John Wiley & Sons, Ltd, 92(4), pp. 723–733. doi: 10.1189/jlb.1111566.

Muehe, A.M., Feng, D., Eyben, R.V., Luna-Fineman, S., Link, M.P., Muthig, T., Huddleston, A.E., Neuwelt, E.A. and Daldrop-Link, H. (2016) 'Safety Report of Ferumoxytol for Magnetic Resonance Imaging in Children and Young Adults', *Investigative radiology*. NIH Public Access, 51(4), p. 221. doi: 10.1097/RLI.0000000000000230.

Nam, H.Y., Kwon, S.M., Chung, H., Lee, S.Y., Kwon, S.H., Jeon, H., Kim, Y., Park, J.H., Kim, J., Her, S., Oh, Y.K., Kwon, I.C., Kim, K. and Jeong, S.Y. (2009) 'Cellular uptake mechanism and intracellular fate of hydrophobically modified glycol chitosan nanoparticles', *Journal of Controlled Release*. Elsevier, 135(3), pp. 259–267. doi: 10.1016/J.JCONREL.2009.01.018.

Naqvi, S., Samim, M., Abdin, M., Ahmed, F.J., Maitra, A.N., Prashant, C.K. and Dinda, A.K. (2010) 'Concentration-dependent toxicity of iron oxide nanoparticles mediated by increased oxidative stress', *International Journal of Nanomedicine*. Dove Press, 5(1), p. 983. doi: 10.2147/IJN.S13244.

Natarajan, S., Harini, K., Gajula, G.P., Sarmiento, B., Neves-Petersen, M.T. AND Thiagarajan, V. (2019) 'Multifunctional magnetic iron oxide nanoparticles: diverse synthetic approaches, surface modifications, cytotoxicity towards biomedical and industrial applications', *BMC Materials 2019 1:1*. BioMed Central, 1(1), pp. 1–22. doi: 10.1186/S42833-019-0002-6.

Nesargikar, P. N., Spiller, B. and Chavez, R. (2012) 'The complement system: history, pathways, cascade and inhibitors.', *European journal of microbiology & immunology*. Akadémiai Kiadó, 2(2), pp. 103–11. doi: 10.1556/EuJMI.2.2012.2.2.

Ngobili, T. A. and Daniele, M. A. (2016) 'Nanoparticles and direct immunosuppression.', *Experimental biology and medicine (Maywood, N.J.)*. SAGE Publications, 241(10), pp. 1064–73. doi: 10.1177/1535370216650053.

Nimmerjahn, F. and Ravetch, J. V. (2007) 'Fc-Receptors as Regulators of Immunity', *Advances in Immunology*. Academic Press, 96, pp. 179–204. doi: 10.1016/S0065-2776(07)96005-8.

Nishimoto, N. and Kishimoto, T. (2004) 'Inhibition of IL-6 for the treatment of inflammatory diseases', *Current Opinion in Pharmacology*. Elsevier, 4(4), pp. 386–391. doi: 10.1016/J.COPH.2004.03.005.

Noris, M. and Remuzzi, G. (2013) 'Overview of complement activation and regulation.', *Seminars in nephrology*. Elsevier, 33(6), pp. 479–92. doi: 10.1016/j.semnephrol.2013.08.001.

Noubade, R., Wong, K., Ota, N., Rutz, S., Eidenschenk, C., Valdez, P.A., Ding, J., Peng, I., Sebrell, A., Caplazi, P., DeVoss, J., Soriano, R.H., Sai, T., Lu, R., Modrusan, Z., Hackney, J. AND Ouyang, W. (2014) 'NRRSOS negatively regulates reactive oxygen species during host defence and autoimmunity', *Nature*. Nature Publishing Group, 509(7499), pp. 235–239. doi: 10.1038/nature13152.

Oh, J.Y., Kim, H.S., Palanikumar, L., Go, E.M., Jana, B., Park, S.A., Kim, H.Y., Kim, K., Seo, J.K., Kwak, S.K., Kim, C., Kang, S. and Ryu, J.H. (2018) 'Cloaking nanoparticles with protein corona shield for targeted drug delivery', *Nature Communications*. Nature Publishing Group, 9(1), p. 4548. doi: 10.1038/s41467-018-06979-4.

Okroj, M., Holmquist, E., King, B.C. and Blom, A.M. (2012) 'Functional Analyses of Complement Convertases Using C3 and C5-Depleted Sera', *PLoS ONE*. Edited by A. I. den Hollander. Public Library of Science, 7(10), p. e47245. doi: 10.1371/journal.pone.0047245.

Olasagasti, M., Gatti, A.M., Capitani, F., Barranco, A., Pardo, M.A., Escuredo, K. and Rainieri, S. (2014) 'Toxic effects of colloidal nanosilver in zebrafish embryos', *Journal of Applied Toxicology*. John Wiley & Sons, Ltd, 34(5), pp. 562–575. doi: 10.1002/jat.2975.

Opal, S. M. and DePalo, V. A. (2000) 'Anti-Inflammatory Cytokines', *Chest*. Elsevier, 117(4), pp. 1162–1172. doi: 10.1378/CHEST.117.4.1162.

Opferman, J. T. (2008) 'Apoptosis in the development of the immune system', *Cell Death & Differentiation*. Nature Publishing Group, 15(2), pp. 234–242. doi: 10.1038/sj.cdd.4402182.

Orecchioni, M., Ghosheh, Y., Pramod, A.B. and Ley, K. (2019) 'Macrophage Polarization: Different Gene Signatures in M1(LPS+) vs. Classically and M2(LPS-) vs. Alternatively Activated Macrophages', *Frontiers in Immunology*. Frontiers, 10, p. 1084. doi: 10.3389/fimmu.2019.01084.

Paatero, I., Casals, E., Niemi, R., Özliseli, E., Rosenholm, J.M. and Sahlgren, C. (2017) 'Analyses in zebrafish embryos reveal that nanotoxicity profiles are dependent on surface-functionalization controlled penetrance of biological membranes OPEN', *Nature*. doi: 10.1038/s41598-017-09312-z.

Parichy, D.M., Elizondo, M.R., Mills, M.G., Gordon, T.N. and Engeszer, R.E. (2009) 'Normal table of postembryonic zebrafish development: staging by externally visible anatomy of the living fish.', *Developmental dynamics: an official publication of the American Association of Anatomists*. NIH Public Access, 238(12), pp. 2975–3015. doi: 10.1002/dvdy.22113.

Park, E.J., Kim, H., Kim, Y., Yi, J., Choi, K. and Park, K. (2010) 'Inflammatory responses may be induced by a single intratracheal instillation of iron nanoparticles in mice', *Toxicology*. Elsevier, 275(1–3), pp. 65–71. doi: 10.1016/J.TOX.2010.06.002.

Park, J.H., von Maltzahn, G., Ruoslahti, E., Bhatia, S.N. and Sailor, M.J. (2008) 'Micellar hybrid nanoparticles for simultaneous magnetofluorescent imaging and drug delivery.', *Angewandte Chemie (International ed. in English)*. NIH Public Access, 47(38), pp. 7284–8. doi: 10.1002/anie.200801810.

Parton, R. G. and del Pozo, M. A. (2013) 'Caveolae as plasma membrane sensors, protectors and organizers', *Nature Reviews Molecular Cell Biology*. Nature Publishing Group, 14(2), pp. 98–112. doi: 10.1038/nrm3512.

Parton, R. G. and Simons, K. (2007) 'The multiple faces of caveolae', *Nature Reviews Molecular Cell Biology*. Nature Publishing Group, 8(3), pp. 185–194. doi: 10.1038/nrm2122.

Passtoors, W.M., van den Akker, E.B., Deelen, J., Maier, A.B., van der Breggen, R., Jansen, R., Trompet, S., van Heemst, D., Derhovanessian, E., Pawelec, G., van Ommen, G.J.B., Slagboom, P.E. and Beekman, M. (2015) 'IL7R gene expression network associates with human healthy ageing', *Immunity & Ageing*. BioMed Central, 12(1), p. 21. doi: 10.1186/s12979-015-0048-6.

Pathak, R. K., Kolishetti, N. and Dhar, S. (2015) 'Targeted nanoparticles in mitochondrial medicine.', *Wiley interdisciplinary reviews. Nanomedicine and nanobiotechnology*. NIH Public Access, 7(3), pp. 315–29. doi: 10.1002/wnan.1305.

Patra, C.R., Bhattacharya, R., Mukhopadhyay, D. and Mukherjee, P. (2010) 'Fabrication of gold nanoparticles for targeted therapy in pancreatic cancer.', *Advanced drug delivery reviews*. NIH Public Access, 62(3), pp. 346–61. doi: 10.1016/j.addr.2009.11.007.

Pawde, D.M., Viswanadh, M.K., Mehata, A.K., Sonkar, R., Narendra, Poddar, S., Burande, A.S., Jha, A., Vajanthri, K.Y., Mahto, S.K., Azger Dustakeer, V.N. and Muthu, M.S. (2020) 'Mannose receptor targeted bioadhesive chitosan nanoparticles of clofazimine for effective therapy of tuberculosis', *Saudi Pharmaceutical Journal*. Elsevier, 28(12), pp. 1616–1625. doi: 10.1016/J.JSPS.2020.10.008.

Peñaloza, J.P., Márquez-Miranda, V., Cabaña-Brunod, M., Reyes-Ramírez, R., Llancalahuen, F.M., Vilos, C., Maldonado-Biermann, F., Velásquez, L.A., Fuentes, J.A., González-Nilo, F.D., Rodríguez-Díaz, M. and Otero, C. (2017) 'Intracellular trafficking and cellular uptake mechanism of PHBV nanoparticles for targeted delivery in epithelial cell lines', *Journal of Nanobiotechnology*. BioMed Central, 15(1), p. 1. doi: 10.1186/s12951-016-0241-6.

Petty, R.D., Samuel, L.M., Murray, G.I., MacDonald, G., O'Kelly, T., Loudon, M., Binnie, N., Aly, E., McKinlay, A., Wang, W., Gilbert, F., Semple, S. and Collie-Duguid, E.S.R. (2009) 'APRIL is a novel clinical chemo-resistance biomarker in colorectal adenocarcinoma identified by gene expression profiling.', *BMC cancer*. BioMed Central, 9, p. 434. doi: 10.1186/1471-2407-9-434.

Polack, F.P., Thomas, S.J., Kitchin, N., Absalon, J., Gurtman, A., Lockhart, S., Perez, J.L., Pérez Marc, G., Moreira, E.D., Zerbini, C., Bailey, R., Swanson, K.A., Roychoudhury, S., Koury, K., Li, P., Kalina, W.V., Cooper, D., Frenck, R.W., Hammitt, L.L., Türeci, Ö., Nell, H., Schaefer, A., Ünal, S., Tresnan, D.B., Mather, S., Dormitzer, P.R., Şahin, U., Jansen, K.U. and Gruber, W.C. (2020) 'Safety and Efficacy of the BNT162b2 mRNA Covid-19 Vaccine', *New England Journal of Medicine*. Massachusetts Medical Society, 383(27), pp. 2603–2615. doi: 10.1056/NEJMoa2034577.

van Pomerén, M., Peijnenburg, W.J.G.M., Vlieg, R.C., van Noort, S.J.T. and Vijver, M.G. (2019) 'The biodistribution and immuno-responses of differently shaped non-modified gold particles in zebrafish embryos', *Nanotoxicology*. Taylor & Francis, 13(4), pp. 558–571. doi: 10.1080/17435390.2018.1564079.

Pondman, K.M., Sobik, M., Nayak, A., Tsolaki, A.G., Jäkel, A., Flahaut, E., Hampel, S., ten Haken, B., Sim, R.B. and Kishore, U. (2014) 'Complement activation by carbon nanotubes and its influence on the phagocytosis and cytokine response by macrophages', *Nanomedicine: Nanotechnology, Biology and Medicine*. Elsevier, 10(6), pp. 1287–1299. doi: 10.1016/J.NANO.2014.02.010.

Pondman, K.M., Tsolaki, A.G., Paudyal, B., Shamji, M.H., Switzer, A., Pathan, A.A., Abozaid, S.M., Haken, B.T., Stenbeck, G., Sim, R.B. and Kishore, U. (2016) 'Complement deposition on nanoparticles can modulate immune responses by macrophage, B and T cells', *Journal of Biomedical Nanotechnology*. American Scientific Publishers, 12(1), pp. 197–216. doi: 10.1166/JBN.2016.2124.

Pontes, K.C.S., Groenewoud, A., Cao, J., Ataide, L.M.S., Snaar-Jagalska, E. and Jager, M.J. (2017) 'Evaluation of (*fli:GFP*) Casper Zebrafish Embryos as a Model for Human Conjunctival Melanoma', *Investigative Ophthalmology & Visual Science*. The Association for Research in Vision and Ophthalmology, 58(14), p. 6065. doi: 10.1167/iovs.17-22023.

Popova, N. V, Deyev, I. E. and Petrenko, A. G. (2013) 'Clathrin-mediated endocytosis and adaptor proteins.', *Acta naturae*. Park Media, 5(3), pp. 62–73.

Progida, C., Cogli, L., Piro, F., De Luca, A., Bakke, O., Bucci, C. and Figura, K.v. (2010) 'Rab7b controls trafficking from endosomes to the TGN.', *Journal of cell science*. The Company of Biologists Ltd, 123(Pt 9), pp. 1480–91. doi: 10.1242/jcs.051474.

Pujalté, I., Passagne, I., Brouillaud, B., Tréguer, M., Durand, E., Ohayon-Courtès, C. and L'Azou, B. (2011) 'Cytotoxicity and oxidative stress induced by different metallic nanoparticles on human kidney cells', *Particle and Fibre Toxicology* 2011 8:1. BioMed Central, 8(1), pp. 1–16. doi: 10.1186/1743-8977-8-10.

Qian, Z., Qingshan, C., Chun, J., Huijun, Z., Feng, L., Qiang, W., Qiang, X. and Min, Z. (2014) 'High Expression of TNFSF13 in Tumor Cells and Fibroblasts Is Associated With Poor Prognosis in Non-Small Cell Lung Cancer', *American Journal of Clinical Pathology*. Oxford Academic, 141(2), pp. 226–233. doi: 10.1309/AJCP4JP8BZOMHEAW.

Qiang, L., Arabeyyat, Z.H., Xin, Q., Paunov, V.N., Dale, I.J.F., Lloyd Mills, R.I., Rotchell, J.M. and Cheng, J. (2020) 'Silver Nanoparticles in Zebrafish (*Danio rerio*) Embryos: Uptake, Growth and Molecular Responses.', *International journal of molecular sciences*. Multidisciplinary Digital Publishing Institute (MDPI), 21(5). doi: 10.3390/ijms21051876.

Qin, M., Zhang, J., Li, M., Yang, D., Liu, D., Song, S., Fu, J., Zhang, H., Dai, W., Wang, X., Wang, Y., He, B. and Zhang, Q. (2020) 'Proteomic analysis of intracellular protein corona of nanoparticles elucidates nano-trafficking network and nano-bio interactions.', *Theranostics*. Ivyspring International Publisher, 10(3), pp. 1213–1229. doi: 10.7150/thno.38900.

Rampado, R., Crotti, S., Caliceti, P., Pucciarelli, S. and Agostini, M. (2020) 'Recent Advances in Understanding the Protein Corona of Nanoparticles and in the Formulation of "Stealthy" Nanomaterials', *Frontiers in Bioengineering and Biotechnology*. Frontiers Media SA, 8, p. 166. doi: 10.3389/FBIOE.2020.00166.

Rao, X., Huang, X., Zhou, Z. and Lin, X. (2013) 'An improvement of the 2<sup>-ΔΔCT</sup> method for quantitative real-time polymerase chain reaction data analysis.', *Biostatistics, bioinformatics and biomathematics*. NIH Public Access, 3(3), pp. 71–85.

Ray, A. (2016) 'Cytokines and their Role in Health and Disease: A Brief Overview', *MOJ Immunology*. MedCrave Publishing, 4(2). doi: 10.15406/moji.2016.04.00121.

Rejman, J., Oberle, V., Zuhorn, I.S. and Hoekstra, D. (2004) 'Size-dependent internalization of particles via the pathways of clathrin- and caveolae-mediated endocytosis.', *The Biochemical journal*. Portland Press Ltd, 377(Pt 1), pp. 159–69. doi: 10.1042/BJ20031253.



Rennick, J. J., Johnston, A. P. R. and Parton, R. G. (2021) 'Key principles and methods for studying the endocytosis of biological and nanoparticle therapeutics', *Nature Nanotechnology* 2021 16:3. Nature Publishing Group, 16(3), pp. 266–276. doi: 10.1038/s41565-021-00858-8.

Richards, D. M. and Endres, R. G. (2014) 'The mechanism of phagocytosis: two stages of engulfment.', *Biophysical journal*. The Biophysical Society, 107(7), pp. 1542–53. doi: 10.1016/j.bpj.2014.07.070.

Rizzo, L.Y., Theek, B., Storm, G., Kiessling, F. and Lammers, T. (2013) 'Recent progress in nanomedicine: therapeutic, diagnostic and theranostic applications.', *Current opinion in biotechnology*. Europe PMC Funders, 24(6), pp. 1159–66. doi: 10.1016/j.cobio.2013.02.020.

Saha, K., Kim, S.T., Yan, B., Miranda, O.R., Alfonso, F.S., Shlosman, D. and Rotello, V.M. (2013) 'Surface functionality of nanoparticles determines cellular uptake mechanisms in mammalian cells.', *Small (Weinheim an der Bergstrasse, Germany)*. NIH Public Access, 9(2), pp. 300–305. doi: 10.1002/sml.201201129.

Saheki, Y. and De Camilli, P. (2012) 'Synaptic vesicle endocytosis.', *Cold Spring Harbor perspectives in biology*. Cold Spring Harbor Laboratory Press, 4(9), p. a005645. doi: 10.1101/cshperspect.a005645.

Sallusto, F., Cella, M., Danieli, C. and Lanzavecchia, A. (1995) 'Dendritic cells use macropinocytosis and the mannose receptor to concentrate macromolecules in the major histocompatibility complex class II compartment: downregulation by cytokines and bacterial products.', *The Journal of experimental medicine*. The Rockefeller University Press, 182(2), pp. 389–400.

Salnikov, V., Lukyánenko, Y.O., Frederick, C.A., Lederer, W.J. and Lukyánenko, V. (2007) 'Probing the outer mitochondrial membrane in cardiac mitochondria with nanoparticles.', *Biophysical journal*. The Biophysical Society, 92(3), pp. 1058–71. doi: 10.1529/biophysj.106.094318.

Sandin, P., Fitzpatrick, L.W., Simpson, J.C. and Dawson, K.A. (2012) 'High-Speed Imaging of Rab Family Small GTPases Reveals Rare Events in Nanoparticle Trafficking in Living Cells'. doi: 10.1021/nn204448x.

Sandvig, K., Torgersen, M.L., Raa, H.A. and van Deurs, B. (2008) 'Clathrin-independent endocytosis: from nonexistent to an extreme degree of complexity.', *Histochemistry and cell biology*. Springer, 129(3), pp. 267–76. doi: 10.1007/s00418-007-0376-5.

Sanjurjo, L., Aran, G., Téllez, É., Amézaga, N., Armengol, C., López, D., Prats, C. and Sarrias, M.R. (2018) 'CD5L Promotes M2 Macrophage Polarization through Autophagy-Mediated Upregulation of ID3', *Frontiers in Immunology*. Frontiers, 9, p. 480. doi: 10.3389/fimmu.2018.00480.

Saraceni, P.R., Romero, A., Figueras, A. and Novoa, B. (2016) 'Establishment of Infection Models in Zebrafish Larvae (*Danio rerio*) to Study the Pathogenesis of

*Aeromonas hydrophila*, *Frontiers in Microbiology*. Frontiers, 7, p. 1219. doi: 10.3389/fmicb.2016.01219.

Sarma, J. V. and Ward, P. A. (2011) 'The complement system.', *Cell and tissue research*. NIH Public Access, 343(1), pp. 227–35. doi: 10.1007/s00441-010-1034-0.

Savina, A. and Amigorena, S. (2007) 'Phagocytosis and antigen presentation in dendritic cells', *Immunological Reviews*. Blackwell Publishing Ltd, 219(1), pp. 143–156. doi: 10.1111/j.1600-065X.2007.00552.x.

Schmieder, A.H., Winter, P.M., Caruthers, S.D., Harris, T.D., Williams, T.A., Allen, J.S., Lacy, E.K., Zhang, H., Scott, M.J., Hu, G., Robertson, J. D., Wickline, S.A. and Lanza, G.M. (2005) 'Molecular MR imaging of melanoma angiogenesis with  $\alpha\beta 3$ -targeted paramagnetic nanoparticles', *Magnetic Resonance in Medicine*. Wiley Subscription Services, Inc., A Wiley Company, 53(3), pp. 621–627. doi: 10.1002/mrm.20391.

Schröder, B. (2016) 'The multifaceted roles of the invariant chain CD74 — More than just a chaperone', *Biochimica et Biophysica Acta (BBA) - Molecular Cell Research*. Elsevier, 1863(6), pp. 1269–1281. doi: 10.1016/J.BBAMCR.2016.03.026.

Schuster, M., Annemann, M., Plaza-Sirvent, C. and Schmitz, I. (2013) 'Atypical I $\kappa$ B proteins - nuclear modulators of NF- $\kappa$ B signaling.', *Cell communication and signaling : CCS*. BioMed Central, 11(1), p. 23. doi: 10.1186/1478-811X-11-23.

Schwarz, D. S. and Blower, M. D. (2016) 'The endoplasmic reticulum: structure, function and response to cellular signaling.', *Cellular and molecular life sciences : CMLS*. Springer, 73(1), pp. 79–94. doi: 10.1007/s00018-015-2052-6.

Scott, C. C., Vacca, F. and Gruenberg, J. (2014) 'Endosome maturation, transport and functions', *Seminars in Cell & Developmental Biology*, 31, pp. 2–10. doi: 10.1016/j.semcd.2014.03.034.

Semete, B., Booyen, L., Lemmer, Y., Kalombo, L., Katata, L., Verschoor, J. and Swai, H.S. (2010) 'In vivo evaluation of the biodistribution and safety of PLGA nanoparticles as drug delivery systems', *Nanomedicine: Nanotechnology, Biology and Medicine*, 6(5), pp. 662–671. doi: 10.1016/j.nano.2010.02.002.

Seth, A., Stemple, D. L. and Barroso, I. (2013) 'The emerging use of zebrafish to model metabolic disease.', *Disease models & mechanisms*. Company of Biologists, 6(5), pp. 1080–8. doi: 10.1242/dmm.011346.

Shannahan, J. H., Bai, W. and Brown, J. M. (2015) 'Implications of scavenger receptors in the safe development of nanotherapeutics.', *Receptors & clinical investigation*. NIH Public Access, 2(3), p. e811. doi: 10.14800/rci.811.

Shi, J., Kantoff, P.W., Wooster, R. and Farokhzad, O.C. (2016) 'Cancer nanomedicine: progress, challenges and opportunities', *Nature Reviews Cancer*. Nature Research, 17(1), pp. 20–37. doi: 10.1038/nrc.2016.108.

Shi, M., Shi, C. and Xu, Y. (2017) 'Rab GTPases: The Key Players in the Molecular Pathway of Parkinson's Disease', *Frontiers in Cellular Neuroscience*. Frontiers, 11, p. 81. doi: 10.3389/fncel.2017.00081.

SHIIBA, M., SAITO, K., YAMAGAMI, H., NAKASHIMA, D., HIGO, M., KASAMATSU, A., SAKAMOTO, Y., OGAWARA, K., UZAWA, K., TAKIGUCHI, Y. and TANZAWA, H. (2015) 'Interleukin-1 receptor antagonist (IL1RN) is associated with suppression of early carcinogenic events in human oral malignancies', *International Journal of Oncology*. Spandidos Publications, 46(5), pp. 1978–1984. doi: 10.3892/ijo.2015.2917.

Silke, J. and Meier, P. (2013) 'Inhibitor of apoptosis (IAP) proteins-modulators of cell death and inflammation.', *Cold Spring Harbor perspectives in biology*. Cold Spring Harbor Laboratory Press, 5(2). doi: 10.1101/cshperspect.a008730.

Singh, S. and Singh, A. (2013) 'Current status of nanomedicine and nanosurgery.', *Anesthesia, essays and researches*. Medknow Publications, 7(2), pp. 237–42. doi: 10.4103/0259-1162.118976.

Slauch, J. M. (2011) 'How does the oxidative burst of macrophages kill bacteria? Still an open question.', *Molecular microbiology*. NIH Public Access, 80(3), pp. 580–3. doi: 10.1111/j.1365-2958.2011.07612.x.

Smith, C., McColl, B.W., Patir, A., Barrington, J., Armishaw, J., Clarke, A., Eaton, J., Hobbs, V., Mansour, S., Nolan, M., Rice, G.I., Rodero, M.P., Seabra, L., Uggenti, C., Livingston, J.H., Bridges, L.R., Jeffrey, I.J.M. and Crow, Y.J. (2020) 'Biallelic mutations in NRROS cause an early onset lethal microgliopathy', *Acta Neuropathologica*. Springer, 139(5), pp. 947–951. doi: 10.1007/s00401-020-02137-7.

Soetaert, F., Korangath, P., Serantes, D., Fiering, S. and Ivkov, R. (2020) 'Cancer therapy with iron oxide nanoparticles: Agents of thermal and immune therapies', *Advanced Drug Delivery Reviews*. Elsevier, 163–164, pp. 65–83. doi: 10.1016/J.ADDR.2020.06.025.

Sola, F., Canonico, B., Montanari, M., Volpe, A., Barattini, C., Pellegrino, C., Cesarini, E., Guescini, M., Battistelli, M., Ortolani, C., Ventola, A. and Papa, S. (2021) 'Uptake and Intracellular Trafficking Studies of Multiple Dye-Doped Core-Shell Silica Nanoparticles in Lymphoid and Myeloid Cells', *Nanotechnology, Science and Applications*. Dove Press, 14, pp. 29–48. doi: 10.2147/NSA.S290867.

Stolyar, S. V., Krasitskaya, V. V., Frank, L. A., Yaroslavtsev, R. N., Chekanova, L. A., Gerasimova, Y. V., Volochaev, M. N., Bairmani, M. Sh and Velikanov, D. A. (2021) 'Polysaccharide-coated iron oxide nanoparticles: Synthesis, properties, surface modification', *Materials Letters*. North-Holland, 284, p. 128920. doi: 10.1016/J.MATLET.2020.128920.

Stone, M., Jia, S., Heo, W.D., Meyer, T. and Konan, K.V. (2007) 'Participation of rab5, an early endosome protein, in hepatitis C virus RNA replication machinery.', *Journal of virology*. American Society for Microbiology, 81(9), pp. 4551–63. doi: 10.1128/JVI.01366-06.

Strähle, U., Geisler, R., Greiner, P., Hollert, H., Rastegar, S., Schumacher, A., Selderslaghs, I., Weiss, C., Witters, H. and Braunbeck, T. (2012) 'Zebrafish embryos as an alternative to animal experiments—A commentary on the definition of the onset of protected life stages in animal welfare regulations', *Reproductive Toxicology*. Pergamon, 33(2), pp. 128–132. doi: 10.1016/J.REPROTOX.2011.06.121.

Su, H., Lei, C.-T. and Zhang, C. (2017) 'Interleukin-6 Signaling Pathway and Its Role in Kidney Disease: An Update', *Frontiers in Immunology*. Frontiers, 8, p. 405. doi: 10.3389/fimmu.2017.00405.

Sun, D., Gong, L., Xie, J., He, X., Chen, S., A, L., Li, Q., Gu, Z. and Xu, H. (2017) 'Evaluating the toxicity of silicon dioxide nanoparticles on neural stem cells using RNA-Seq', *RSC Adv*. Royal Society of Chemistry, 7(75), pp. 47552–47564. doi: 10.1039/C7RA09512K.

Sun, Y., Zhang, G., He, Z., Wang, Y., Cui, J. and Li, Y. (2016) 'Effects of copper oxide nanoparticles on developing zebrafish embryos and larvae.', *International journal of nanomedicine*. Dove Press, 11, pp. 905–18. doi: 10.2147/IJN.S100350.

Szebeni, J. (2014) 'Complement activation-related pseudoallergy: A stress reaction in blood triggered by nanomedicines and biologicals', *Molecular Immunology*. Pergamon, 61(2), pp. 163–173. doi: 10.1016/J.MOLIMM.2014.06.038.

Taciak, B., Białasek, M., Braniewska, A., Sas, Z., Sawicka, P., Kiraga, Ł., Rygiel, T. and Król, M. (2018) 'Evaluation of phenotypic and functional stability of RAW 264.7 cell line through serial passages', *PLoS ONE*. Public Library of Science, 13(6). doi: 10.1371/JOURNAL.PONE.0198943.

Taylor, P.R., Martinez-Pomares, L., Stacey, M., Lin, H-H., Brown, G.D. and Gordon, S. (2005) 'MACROPHAGE RECEPTORS AND IMMUNE RECOGNITION', *Annual Review of Immunology*. Annual Reviews, 23(1), pp. 901–944. doi: 10.1146/annurev.immunol.23.021704.115816.

Teles, M., Soares, A.M.V.M., Tort, L., Guimarães, L. and Oliveira, M. (2017) 'Linking cortisol response with gene expression in fish exposed to gold nanoparticles', *Science of The Total Environment*. Elsevier, 584–585, pp. 1004–1011. doi: 10.1016/J.SCITOTENV.2017.01.153.

Tessadori, F., Rehman, A.U., Giltay, J.C., Xia, F., Streff, H., Duran, K., Bakkers, J., Lalani, S.R. and van Haaften, G. (2020) 'A de novo variant in the human HIST1H4J gene causes a syndrome analogous to the HIST1H4C-associated neurodevelopmental disorder', *European Journal of Human Genetics*. Nature Publishing Group, 28(5), pp. 674–678. doi: 10.1038/s41431-019-0552-9.

Tonelli, F., Bek, J.W., Besio, R., De Clercq, A., Leoni, L., Salmon, P., Coucke, P.J., Willaert, A. and Forlino, A. (2020) 'Zebrafish: A Resourceful Vertebrate Model to Investigate Skeletal Disorders', *Frontiers in Endocrinology*. Frontiers, 0, p. 489. doi: 10.3389/FENDO.2020.00489.

Torraca, V., Masud, S., Spaink, H. P. and Meijer, A. H. (2014) 'Macrophage-pathogen interactions in infectious diseases: new therapeutic insights from the zebrafish host model', *Disease Models & Mechanisms*. The Company of Biologists Ltd, 7(7), pp. 785–797. doi: 10.1242/dmm.015594.

Traub, L. M. and Bonifacino, J. S. (2013) 'Cargo recognition in clathrin-mediated endocytosis.', *Cold Spring Harbor perspectives in biology*. Cold Spring Harbor Laboratory Press, 5(11), p. a016790. doi: 10.1101/cshperspect.a016790.

Trede, N.S., Langenau, D.M., Traver, D., Look, A.T. and Zon, L.I. (2004) 'The Use of Zebrafish to Understand Immunity', *Immunity*. Cell Press, 20(4), pp. 367–379. doi: 10.1016/S1074-7613(04)00084-6.

Truong, N.P., Whittaker, M.R., Mak, C.W. and Davis, T.P. (2015) 'The importance of nanoparticle shape in cancer drug delivery', *Expert Opinion on Drug Delivery*. Informa Healthcare, 12(1), pp. 129–142. doi: 10.1517/17425247.2014.950564.

Tsukumo, S.-I. and Yasutomo, K. (2018) 'Regulation of CD8+ T Cells and Antitumor Immunity by Notch Signaling.', *Frontiers in immunology*. Frontiers Media SA, 9, p. 101. doi: 10.3389/fimmu.2018.00101.

Tu, S., Bhagat, G., Cui, G., Takaishi, S., Kurt-Jones, E.A., Rickman, B., Betz, K.S., Penz-Oesterreicher, M., Bjorkdahl, O., Fox, J.G. and Wang, T.C. (2008) 'Overexpression of interleukin-1beta induces gastric inflammation and cancer and mobilizes myeloid-derived suppressor cells in mice.', *Cancer cell*. NIH Public Access, 14(5), pp. 408–19. doi: 10.1016/j.ccr.2008.10.011.

Turrina, C., Berensmeier, S. and Schwaminger, S. P. (2021) 'Bare iron oxide nanoparticles as drug delivery carrier for the short cationic peptide lasioglossin', *Pharmaceuticals*, 14(5). doi: 10.3390/ph14050405.

Vallabani, N. V. S. and Singh, S. (2018) 'Recent advances and future prospects of iron oxide nanoparticles in biomedicine and diagnostics', *3 Biotech*. Springer, 8(6), p. 279. doi: 10.1007/S13205-018-1286-Z.

Vasir, J. K. and Labhasetwar, V. (2008) 'Quantification of the force of nanoparticle-cell membrane interactions and its influence on intracellular trafficking of nanoparticles.', *Biomaterials*. NIH Public Access, 29(31), pp. 4244–52. doi: 10.1016/j.biomaterials.2008.07.020.

Velazquez-Salinas, L., Verdugo-Rodriguez, A., Rodriguez, L.L. and Borca, M.V. (2019) 'The Role of Interleukin 6 During Viral Infections', *Frontiers in Microbiology*. Frontiers, 10, p. 1057. doi: 10.3389/fmicb.2019.01057.

Vellinga, M.M., Vrenken, H., Hulst, H.E., Polman, C.H., Uitdehaag, B.M.J., Pouwels, P.J.W., Barkhof, F. and Geurts, J.J.G. (2009) 'Use of ultrasmall superparamagnetic particles of iron oxide (USPIO)-enhanced MRI to demonstrate diffuse inflammation in the normal-appearing white matter (NAWM) of multiple sclerosis (MS) patients: An exploratory study', *Journal of Magnetic Resonance Imaging*. John Wiley & Sons, Ltd, 29(4), pp. 774–779. doi: 10.1002/JMRI.21678.

Ventola, C. L. (2012) 'The nanomedicine revolution: part 1: emerging concepts.', *P & T: a peer-reviewed journal for formulary management*. MediMedia, USA, 37(9), pp. 512–25.

Villarino, A. V, Huang, E. and Hunter, C. A. (2004) 'Understanding the pro- and anti-inflammatory properties of IL-27.', *Journal of immunology (Baltimore, Md. : 1950)*. American Association of Immunologists, 173(2), pp. 715–20. doi: 10.4049/jimmunol.173.2.715.

Vliegenthart, A.D.B., Tucker, C.S., Del Pozo, J. and Dear, J.W. (2014) 'Zebrafish as model organisms for studying drug-induced liver injury.', *British journal of clinical pharmacology*. Wiley-Blackwell, 78(6), pp. 1217–27. doi: 10.1111/bcp.12408.

Vllasaliu, D., Alexander, C., Garnett, M., Eaton, M. and Stolnik, S. (2012) 'Fc-mediated transport of nanoparticles across airway epithelial cell layers', *Journal of Controlled Release*. Elsevier, 158(3), pp. 479–486. doi: 10.1016/J.JCONREL.2011.12.009.

Vranic, S., Shimada, Y., Ichihara, S., Kimata, M., Wu, W., Tanaka, T., Boland, S., Tran, L. and Ichihara, G. (2019) 'Toxicological Evaluation of SiO<sub>2</sub> Nanoparticles by Zebrafish Embryo Toxicity Test.', *International journal of molecular sciences*. Multidisciplinary Digital Publishing Institute (MDPI), 20(4). doi: 10.3390/ijms20040882.

Wahajuddin and Arora, S. (2012) 'Superparamagnetic iron oxide nanoparticles: magnetic nanoplatforms as drug carriers.', *International journal of nanomedicine*, 7, pp. 3445–71. doi: 10.2147/IJN.S30320.

Wan, C., Liu, X., Bai, B., Cao, H., Li, H and Zhang, Q. (2018) 'Regulation of the expression of tumor necrosis factor-related genes by abnormal histone H3K27 acetylation: Implications for neural tube defects', *Molecular Medicine Reports*. Spandidos Publications, 17(6), pp. 8031–8038. doi: 10.3892/mmr.2018.8900.

Wang, G., Chen, F., Banda, N.K., Holers, V.M., Wu, L., Moghimi, S.M. and Simberg, D. (2016) 'Activation of Human Complement System by Dextran-Coated Iron Oxide Nanoparticles Is Not Affected by Dextran/Fe Ratio, Hydroxyl Modifications, and Crosslinking', *Frontiers in Immunology*. Frontiers, 7, p. 418. doi: 10.3389/fimmu.2016.00418.

Wang, J., Yu, Y., Lu, K., Yang, M., Li, Y., Zhou, X. and Sun, Z. (2017) 'Silica nanoparticles induce autophagy dysfunction via lysosomal impairment and inhibition of autophagosome degradation in hepatocytes', *International Journal of Nanomedicine*. Dove Press, Volume 12, pp. 809–825. doi: 10.2147/IJN.S123596.

Wang, J. T. H., Teasdale, R. D. and Liebl, D. (2014) 'Macropinosome quantitation assay', *MethodsX*, 1, pp. 36–41. doi: 10.1016/j.mex.2014.05.002.

Wang, S., Qiu, J., Liu, L., Su, C., Qi, L., Huang, C., Chen, X., Zhang, Y., Ye, Y., Ding, Y., Liang, L. and Liao, W. (2020) 'CREB5 promotes invasiveness and metastasis in colorectal cancer by directly activating MET', *Journal of Experimental & Clinical Cancer Research*. BioMed Central, 39(1), p. 168. doi: 10.1186/s13046-020-01673-0.

Wang, W., Wyckoff, J.B., Frohlich, V.C., Oleynikov, Y., Hüttelmaier, S., Zavadil, J., Cermak, L., Bottinger, E.P., Singer, R.H., White, J.G., Segall, J.E. and Condeelis, J.S. (2002) 'Single cell behavior in metastatic primary mammary tumors correlated with gene expression patterns revealed by molecular profiling.', *Cancer research*. American Association for Cancer Research, 62(21), pp. 6278–88. doi: 10.1158/0008-5472.can-06-1823.

Wang, Y.-X. J. (2011) 'Superparamagnetic iron oxide based MRI contrast agents: Current status of clinical application', *Quantitative Imaging in Medicine and Surgery*. AME Publications, 1(1), p. 35. doi: 10.3978/J.ISSN.2223-4292.2011.08.03.

Wang, Z., Tiruppathi, C., Minshall, R.D. and Malik, A.B. (2009) 'Size and dynamics of caveolae studied using nanoparticles in living endothelial cells.', *ACS nano*. NIH Public Access, 3(12), pp. 4110–6. doi: 10.1021/nn9012274.

Wei, H.-X., Wang, B. and Li, B. (2020) 'IL-10 and IL-22 in Mucosal Immunity: Driving Protection and Pathology', *Frontiers in Immunology*. Frontiers, 11, p. 1315. doi: 10.3389/fimmu.2020.01315.

Weissleder, R., Nahrendorf, M. and Pittet, M. J. (2014) 'Imaging macrophages with nanoparticles', *Nature Materials*. Nature Research, 13(2), pp. 125–138. doi: 10.1038/nmat3780.

Win, K. Y. and Feng, S.-S. (2006) 'In vitro and in vivo studies on vitamin E TPGS-emulsified poly(D,L-lactic-co-glycolic acid) nanoparticles for paclitaxel formulation', *Biomaterials*, 27(10), pp. 2285–2291. doi: 10.1016/j.biomaterials.2005.11.008.

Wongrakpanich, A., Geary, S.M., Joiner, M.A., Anderson, M.E. and Salem, A.K. (2014) 'Mitochondria-targeting particles.', *Nanomedicine (London, England)*. NIH Public Access, 9(16), pp. 2531–43. doi: 10.2217/nnm.14.161.

Wu, M., Guo, H., Liu, L., Liu, Y. and Xie, L. (2019) 'Size-dependent cellular uptake and localization profiles of silver nanoparticles', *International Journal of Nanomedicine*. Dove Press, 14, p. 4247. doi: 10.2147/IJN.S201107.

Wu, R., Chen, F., Wang, N., Tang, D. and Kang, R. (2020) 'ACOD1 in immunometabolism and disease', *Cellular & Molecular Immunology*. Nature Publishing Group, 17(8), pp. 822–833. doi: 10.1038/s41423-020-0489-5.

Wu, S.-M., Su, C.-K. and Shu, L.-H. (2018) 'Effects of calcium and estrogen on the development of the ceratohyal cartilage in zebrafish (*Danio rerio*) larvae upon embryo and maternal cadmium exposure', *Comparative Biochemistry and Physiology Part C: Toxicology & Pharmacology*. Elsevier, 213, pp. 47–54. doi: 10.1016/J.CBPC.2018.07.006.

Wu, W., He, Q. and Jiang, C. (2008) 'Magnetic iron oxide nanoparticles: synthesis and surface functionalization strategies.', *Nanoscale research letters*. Springer, 3(11), pp. 397–415. doi: 10.1007/s11671-008-9174-9.

Wyckoff, J.B., Wang, Y., Lin, E.Y., Li, J., Goswami, S., Stanley, E.R., Segall, J.E., Pollard, J.W. and Condeelis, J. (2007) 'Direct Visualization of Macrophage-Assisted Tumor Cell Intravasation in Mammary Tumors', *Cancer Research*. American Association for Cancer Research, 67(6), pp. 2649–2656. doi: 10.1158/0008-5472.CAN-06-1823.

Xia, T., Wang, J., Wu, C., Meng, F., Shi, Z., Lian, J., Feng, J. and Meng, J. (2012) 'Novel complex-coprecipitation route to form high quality triethanolamine-coated Fe<sub>3</sub>O<sub>4</sub> nanocrystals: Their high saturation magnetizations and excellent water treatment properties', *CrystEngComm*. The Royal Society of Chemistry, 14(18), pp. 5741–5744. doi: 10.1039/C2CE25813G.

Xie, X., Liao, J., Shao, X., Li, Q. and Lin, Y. (2017) 'The Effect of shape on Cellular Uptake of Gold Nanoparticles in the forms of Stars, Rods, and Triangles', *Scientific Reports*. Nature Publishing Group, 7(1), p. 3827. doi: 10.1038/s41598-017-04229-z.

Xu, X., Li, H., Zhang, Z. and Qi, X. (2009) 'Hydrodynamic properties of aqueous dextran solutions', *Journal of Applied Polymer Science*, 111(3), pp. 1523–1529. doi: 10.1002/app.29043.

Yameen, B., Choi, W. II, Vilos, C., Swami, A., Shi, J. and Farokhzad, Omid C (2014) 'Insight into nanoparticle cellular uptake and intracellular targeting.', *Journal of controlled release: official journal of the Controlled Release Society*. NIH Public Access, 190, pp. 485–99. doi: 10.1016/j.jconrel.2014.06.038.

Yang, X., Kui, L., Tang, M., Li, D., Wei, K., Chen, W., Miao, J. and Dong, Y. (2020) 'High-Throughput Transcriptome Profiling in Drug and Biomarker Discovery.', *Frontiers in genetics*. Frontiers Media SA, 11, p. 19. doi: 10.3389/fgene.2020.00019.

Yazdi, A.S., Guarda, G., Riteau, N., Drexler, S.K., Tardivel, A., Couillin, I. and Tschopp, J. (2010) 'Nanoparticles activate the NLR pyrin domain containing 3 (Nlrp3) inflammasome and cause pulmonary inflammation through release of IL-1 $\alpha$  and IL-1 $\beta$ ', *Proceedings of the National Academy of Sciences of the United States of America*. Proc Natl Acad Sci U S A, 107(45), pp. 19449–19454. doi: 10.1073/PNAS.1008155107.

Yilmaz, D. and Culha, M. (2021) 'Investigation of the pathway dependent endocytosis of gold nanoparticles by surface-enhanced Raman scattering', *Talanta*. Elsevier, 225, p. 122071. doi: 10.1016/J.TALANTA.2020.122071.

Yue, X., Wu, L. and Hu, W. (2015) 'The regulation of leukemia inhibitory factor.', *Cancer cell & microenvironment*. NIH Public Access, 2(3). doi: 10.14800/ccm.877.

Zahid, A., Li, B., Kombe, A.J.K., Jin, T. and Tao, J. (2019) 'Pharmacological Inhibitors of the NLRP3 Inflammasome', *Frontiers in Immunology*. Frontiers, 10, p. 2538. doi: 10.3389/fimmu.2019.02538.



Zakaria, Z.Z., Benslimane, F.M., Nasrallah, G.K., Shurbaji, S., Younes, N.N., Mraiche, F., Da'As, S.I. and Yalcin, H.C. (2018) 'Using Zebrafish for Investigating the Molecular Mechanisms of Drug-Induced Cardiotoxicity', *BioMed Research International*. Hindawi Limited, 2018. doi: 10.1155/2018/1642684.

Zeineddine, R. and Yerbury, J. J. (2015) 'The role of macropinocytosis in the propagation of protein aggregation associated with neurodegenerative diseases.', *Frontiers in physiology*. Frontiers Media SA, 6, p. 277. doi: 10.3389/fphys.2015.00277.

Zerial, M. and McBride, H. (2001) 'Rab proteins as membrane organizers', *Nature Reviews Molecular Cell Biology*. Nature Publishing Group, 2(2), pp. 107–117. doi: 10.1038/35052055.

Zhang, J.-M. and An, J. (2007) 'Cytokines, inflammation, and pain.', *International anesthesiology clinics*. NIH Public Access, 45(2), pp. 27–37. doi: 10.1097/AIA.0b013e318034194e.

Zhang, M., Li, Y., Wang, H., Yu, W., Lin, S. and Guo, J. (2019) 'LncRNA SNHG5 affects cell proliferation, metastasis and migration of colorectal cancer through regulating miR-132-3p/ CREB5', *Cancer Biology & Therapy*. Taylor & Francis, 20(4), pp. 524–536. doi: 10.1080/15384047.2018.1537579.

Zhang, S. and Cui, P. (2014) 'Complement system in zebrafish', *Developmental & Comparative Immunology*. Pergamon, 46(1), pp. 3–10. doi: 10.1016/J.DCI.2014.01.010.

Zheng, M., Lu, J. and Zhao, D. (2018) 'Toxicity and Transcriptome Sequencing (RNA-seq) Analyses of Adult Zebrafish in Response to Exposure Carboxymethyl Cellulose Stabilized Iron Sulfide Nanoparticles', *Scientific Reports*. Nature Publishing Group, 8(1), p. 8083. doi: 10.1038/s41598-018-26499-x.

Zolnik, B.S., González-Fernández, A., Sadrieh, N. and Dobrovolskaia, M.A. (2010) 'Nanoparticles and the immune system.', *Endocrinology*. The Endocrine Society, 151(2), pp. 458–65. doi: 10.1210/en.2009-1082.